

**ADVERTIMENT.** L'accés als continguts d'aquesta tesi queda condicionat a l'acceptació de les condicions d'ús establertes per la següent llicència Creative Commons:  <https://creativecommons.org/licenses/?lang=ca>

**ADVERTENCIA.** El acceso a los contenidos de esta tesis queda condicionado a la aceptación de las condiciones de uso establecidas por la siguiente licencia Creative Commons:  <https://creativecommons.org/licenses/?lang=es>

**WARNING.** The access to the contents of this doctoral thesis it is limited to the acceptance of the use conditions set by the following Creative Commons license:  <https://creativecommons.org/licenses/?lang=en>

A wireframe mesh of a rodent skull, showing the intricate structure of the bones. The mesh is composed of numerous small triangles, creating a detailed 3D representation of the skull's surface. The skull is oriented horizontally, with the snout pointing to the left.

**UAB**

**Universitat Autònoma  
de Barcelona**

Departament de Biologia Animal, de Biologia Vegetal i d'Ecologia  
PhD program in Biodiversity

**Evolutionary and functional patterns of the  
mandible and appendicular skeleton in *Arvicola*  
(Mammalia: Rodentia)**

**Ana Filipa Lopes Durão**

Supervisors

**Jacint Ventura Queija**

**Francesc Muñoz Muñoz**

**PhD thesis  
2023**





Facultat de Biociències  
Departament de Biologia Animal, de Biologia Vegetal i d'Ecologia  
Universitat Autònoma de Barcelona

PhD thesis

**Evolutionary and functional patterns of the  
mandible and appendicular skeleton in *Arvicola*  
(Mammalia: Rodentia)**

Ana Filipa Lopes Durão

Thesis submitted for the degree of Doctor of Philosophy in Biodiversity  
under the supervision of Dr. Jacint Ventura Queija and Dr. Francesc Muñoz  
Muñoz.

Supervisor  
Dr. Jacint Ventura Queija

Supervisor  
Dr. Francesc Muñoz Muñoz

PhD candidate  
Ana Filipa Lopes Durão

Bellaterra, 2023



*"Does the road wind up-hill all the way?  
Yes, to the very end.  
Will the day's journey take the whole long day?  
From morn to night, my friend".*

Up-Hill by Christina Rossetti

*"continua tot recte  
i ja et trobaràs el trencall.  
pren-lo, segueix-lo.  
després d'un petit desert,  
veuràs que comencen  
a canviar els decorats.  
s' afanyen també  
a donar-te les regnes.  
sí, la senda era ben bé aquesta".*

Senderi by Eduard Escoffet



## AGRADECIMIENTOS

---

Una tesis doctoral es un viaje sinuoso, lleno de altibajos, con momentos de alegría e ilusión, así como momentos de frustración y desafío. En este camino he aprendido habilidades importantes como la perseverancia, la paciencia y la capacidad de superar obstáculos aparentemente insuperables. Son muchas las personas (e instituciones) a las que me gustaría agradecerles su apoyo y contribución y que sin ellos no sería posible la realización de este proyecto:

- A la Universidad Autònoma de Barcelona por haber financiado la presente tesis a través del contrato predoctoral Personal Investigador en Formació (PIF), así como haber subvencionado mi estancia en el extranjero (Hard Tissue Research Unit - New York University).

- A mis directores de tesis, Dr. Jacint Ventura y Dr. Francesc Muñoz por compartir sus conocimientos y experiencias conmigo. Me gustaría agradecerlos la oportunidad que me habéis dado de realizar este proyecto con vosotros. También el apoyo y el compromiso que me habéis ofrecido desde el principio de mi formación académica. Moltes gràcies pels moments compartits i per poder comptar amb vosaltres fins al final d'aquesta etapa.

- A los coautores, Dra. Jessica Martínez Vargas y Dra. Cayetana Martínez Maza. Jessica, me gustaría agradecerle el tiempo y el apoyo que me has dedicado. Cayetana, gracias por tu tiempo y por la confianza que me has transmitido en el trabajo de histología.

- A los numerosos revisores anónimos que, por amor a la investigación, han contribuido a mejorar la calidad de los artículos publicados, lo que me ha permitido avanzar en mi formación como investigadora.

- Al Dr. David Galicia, por garantizarme el acceso al material del Museo de Ciencias Naturales de la Universidad de Navarra, así como por su disponibilidad y amabilidad durante mi visita a la universidad.

- To Professor Tim Bromage, for introducing me to the world of digital photomicrography. My sincere gratitude for the opportunity to carry out my research stay in your lab. From the very first day, you welcomed me as a valued member of your team and provided me with an unforgettable experience. Thank you very much Professor Bromage.

- To Dr. Johanna Warshaw, for kindly teaching me how to create the histological maps.

- To the research team of Professor Bromage Lab. Especially to Dr. Bin Hu, for kindly teaching me how to perform all the histology protocols and to Dra. Paola Cerrito for the good times spent both in the laboratory and in New York City.

- A la Unitat de Zoologia, a todas las personas que a lo largo de los años han formado parte del departamento y con quienes he vivido buenos momentos.



- A la Dra. Anna Soler, per tota l'energia positiva i l'alegria contagiosa que sempre m'ha encomanat, així com tota l'ajuda, tant acadèmica com personal.
- A la Dra. Ana Morton, por toda la flexibilidad y facilidad a la hora de realizar las prácticas docentes.
- A las coordinadoras del programa doctoral de Biodiversidad (Dra. Assumpció Malgosa y Dra. Gemma Armengol), por contestar tan amablemente a mis preguntas.
- Al tribunal de comisión de seguimiento (Dra. Asumpció Malgosa, Dra. Ana Morton y Dra. Judith Marigó), por sus interesantes aportaciones a esta tesis doctoral.
- A todos los miembros de la secretaría del departamento, que amablemente respondieron a mis consultas.
- A los técnicos de laboratorio (Manolo y a la Encarna), por su gran ayuda en la preparación del material para las actividades docentes.
- A los "PIFs" (Anna, Ester y Oriol), con quien compartí parte del camino y momentos de compañerismo.
- A la Dra. Ana Quina y la Dra. Silvina Van der Molen, que amablemente evaluaron mi tesis doctoral como expertas externas. Me gustaría agradecer vuestro tiempo y consideración al evaluar el trabajo. En especial a la Dra. Ana Quina con quien di mis primeros pasos en el mundo de la investigación y quien me animó a empezar este proyecto.
- A todos los amigos que de una forma u otra han estado presentes a lo largo de este viaje y que, a través de su amistad, me han animado a seguir adelante. En especial, me gustaría agradecer a mi amiga Elena por estar siempre ahí, por compartir conmigo todo lo que implica escribir una tesis doctoral. Gracias por nuestras caminatas, por la alegría, por comprender mis ausencias y por los abrazos llenos de ánimo. A Julia y a la pequeñita June que siempre han estado pendientes de mí y me han hecho sonreír. A Graciela que desde lejos siempre me ha animado y se ha alegrado de mis victorias.
- A Lorena, mi psicóloga, que me ha armado de herramientas para superar obstáculos y así poder gestionar mis emociones. De todo corazón, muchas gracias.
- A la familia que he formado aquí. A Fabi y Juan, por el apoyo incondicional que siempre me han dado. Por todo el cariño, motivación y ánimo. No tengo palabras para agradecer todo lo que hacen por mí. Os aprecio mucho. A Sònia, Felip, Júlia, Neus y Richard por el apoyo y por ser las personas maravillosas que son.
- Aos meus pais, ao meu irmão e à Cláudia. A vida já nos deu alguns sustos, perdemos pessoas que amamos e superamos obstáculos. Obrigada por poder contar sempre convosco, pelo amor incondicional e pelas encomendas cheias de recordações doces de Portugal.
- Por fin, un agradecimiento muy especial a Joan. Gracias por haber entrado en mi vida sin previo aviso y por haberme dejado ser parte de la tuya. Gracias por nunca soltar mi mano, por cuidarme,

por ayudarme a levantarme cuando carecía de fuerzas y por estar ahí en cada peldaño subido. Gracias por las horas que me escuchaste hablar interminablemente de la tesis o simplemente por respetar mi ausencia. Gracias por tooda la ayuda técnica y por la fantástica portada. Como dice la canción” mi persona favorita, tiene una cara bonita, tiene un ángel en su sonrisa, tiene un corazón (...)“ (aquí la cambio) de oro. Gracias por ser mi persona favorita.

Por último, quisiera dedicar este trabajo a todos aquellos que, al igual que yo, se han enfrentado a los desafíos de realizar una tesis doctoral.

¡Gracias a todos y cada uno por contribuir a este logro!



# TABLE OF CONTENTS

---

<b>ABSTRACT .....</b>	<b>v</b>
<b>ABBREVIATIONS .....</b>	<b>vii</b>
<b>CHAPTER 1. General Introduction .....</b>	<b>9</b>
1.1. Influence of locomotion on bone morphology .....	11
1.2. Ontogenetic changes in the bone morphology .....	12
1.3. Modes of locomotion in rodents .....	12
1.4. <i>Arvicola</i> .....	14
1.4.1. <i>Arvicola scherman</i> .....	15
1.4.2. <i>Arvicola sapidus</i> .....	16
1.5. Structures involved in <i>Arvicola</i> locomotion .....	17
1.5.1. Fossorial locomotion .....	17
1.5.2. Aquatic locomotion .....	18
1.6. Techniques to analyse morphological variation .....	19
1.6.1. The geometric morphometrics method .....	19
1.6.2. Bone histology .....	20
<b>CHAPTER 2. Objectives .....</b>	<b>23</b>
2.1. General objectives .....	25
2.2. Objective and hypotheses by chapters .....	26
2.2.1. Chapter 4 .....	26
2.2.2. Chapter 5 .....	26
2.2.3. Chapter 6 and 7 .....	26
2.2.4. Chapter 8 .....	27
<b>CHAPTER 3. Materials and Methods .....</b>	<b>29</b>
3.1. Sample .....	31
3.2. Geometric morphometrics .....	32
3.2.1. Preliminary analyses .....	32
3.2.2. Shape changes along postnatal ontogeny .....	33
3.2.3. Allometry .....	34
3.2.4. Phenotypic trajectory analysis .....	35
3.2.5. Interpretation and visualization of shape variation .....	36
3.3. Histology .....	36
<b>CHAPTER 4. Comparative Postweaning Ontogeny of the Mandible in Fossorial and Semiaquatic Water Voles</b> <b>.....</b>	<b>37</b>
4.1. Introduction .....	39
4.2. Materials and methods .....	41
4.2.1. Sample and data acquisition .....	41
4.2.2. Analyses of size and allometry .....	43
4.2.3. Shape variation and phenotypic trajectory analyses .....	44
4.2.4. Estimated bite force .....	45
4.3. Results .....	46
4.3.1. Analyses of size and allometry .....	46

4.3.2. Shape variation and phenotypic trajectory analyses .....	47
4.3.3. Estimated bite force .....	50
4.4. Discussion .....	51
4.4.1. Common ontogenetic phenotypic changes in the mandible of semiaquatic and fossorial water voles .....	51
4.4.2. Differences in the postweaning growth of the mandible between semiaquatic and fossorial water voles .....	52
4.5. Conclusion .....	55
4.6. Supplementary information .....	56
<b>CHAPTER 5. Obtaining Three-Dimensional Models of Limb Long Bones From Small Mammals: A Photogrammetric Approach .....</b>	<b>59</b>
5.1. Background .....	61
5.1.1. 2D vs 3D landmark data in form studies .....	61
5.1.2. The particular case of small mammals .....	62
5.1.3. Photogrammetry: An affordable and versatile solution.....	63
5.2. The equipment .....	65
5.2.1. The camera and the lens .....	65
5.2.2. The tripod and the remote trigger .....	67
5.2.3. Lighting.....	67
5.2.4. The “turntable” .....	67
5.2.5. The software.....	68
5.3. The imaging protocol.....	68
5.4. Applying the protocol to the study of the humerus form in fossorial and semiaquatic water voles (genus <i>Arvicola</i> ).....	70
5.4.1. Introduction.....	70
5.4.2. Data .....	70
5.4.3. Statistics .....	72
5.4.4. Results and Discussion .....	73
5.5. Conclusions.....	75
<b>CHAPTER 6. Three-Dimensional Geometric Morphometric Analysis of the Humerus: Comparative Postweaning Ontogeny Between Fossorial and Semiaquatic Water Voles (<i>Arvicola</i>).....</b>	<b>77</b>
6.1. Introduction .....	79
6.2. Materials and methods.....	82
6.2.1. Samples .....	82
6.2.2. Morphometric data acquisition.....	83
6.2.3. Statistical analyses.....	84
6.3. Results .....	86
6.3.1. Analyses of size and allometry .....	86
6.3.2. Shape variation and phenotypic trajectory analyses .....	88
6.4. Discussion .....	92
6.4.1. Common ontogenetic phenotypic changes in the humerus of semiaquatic and fossorial water voles .....	92
6.4.2. Differences in the postweaning growth of the humerus between semiaquatic and fossorial water voles .....	93
6.4.3. Biomechanical consequences of humerus shape.....	96
6.5. Conclusions.....	97
6.6. Supplementary information .....	99

<b>CHAPTER 7. Postnatal Ontogeny of the Femur in Fossorial and Semiaquatic Water Voles in the 3D-Shape Space .....</b>	<b>105</b>
7.1. Introduction .....	107
7.2. Materials and methods.....	109
7.2.1. Study specimens.....	109
7.2.2. Femur form.....	110
7.2.3. Statistical analyses.....	111
7.3. Results .....	113
7.3.1. Size and allometry .....	113
7.3.2. Variation in femur shape and phenotypic trajectories analyses .....	115
7.4. Discussion .....	119
7.4.1. Common ontogenetic phenotypic changes in the femur of semiaquatic and fossorial water voles	119
7.4.2. Differences in the postweaning growth of the femur between semiaquatic and fossorial water voles	119
7.4.3. Biomechanical consequences of femur shape .....	121
7.5. Conclusions .....	124
7.6. Supplementary Information .....	125
 <b>CHAPTER 8. Comparative Ontogenetic Histology of Long Bones Between Fossorial and Semiaquatic Water Voles .....</b>	 <b>131</b>
8.1. Introduction .....	133
8.2. Materials and methods.....	135
8.2.1. Sample.....	135
8.2.2. Histological sections and image acquisition.....	136
8.2.3. Image Processing.....	137
8.2.4. Tissue type classification .....	138
8.3. Results .....	140
8.3.1. Ontogenetic changes in the humerus histology.....	140
8.3.2. Ontogenetic changes in the femur histology .....	147
8.4. Discussion .....	154
8.4.1. Histology.....	154
8.4.2. Histology and macrostructure.....	157
8.4.3. Bone microstructure .....	157
8.4.4. Bone modelling .....	159
8.4.5. Cross-section shape.....	162
8.4.6. Ontogenetic trajectories .....	163
8.5. Conclusions.....	166
8.6. Supplementary information .....	167
 <b>CHAPTER 9. General Discussion .....</b>	 <b>169</b>
9.1. General context .....	171
9.2. Common ontogenetic phenotypic changes in the mandible, humerus, and femur of semiaquatic and fossorial water voles .....	172
9.3. Differences in the postweaning growth of the mandible, humerus, and femur between semiaquatic and fossorial water voles .....	173
 <b>CHAPTER 10. General Conclusions .....</b>	 <b>181</b>
<b>CHAPTER 11. References .....</b>	<b>185</b>
<b>Appendixes .....</b>	<b>213</b>



## ABSTRACT

---

Comparative ontogenetic studies between phylogenetically close species with different types of locomotion are essential to understand to which extent function can affect the different stages of development of an organism and its evolutionary implications. Several morpho-functional studies on the skeleton of rodents have reported many traits related to the mode of locomotion. Nevertheless, as regard to wild populations, most of these works are focused on adult individuals so that the extent to which functional factors affect the growth patterns is relatively poorly known. With this in mind, the main aims of the present thesis are to find phylogenetic and functional signals in the postnatal ontogeny of several bones involved in two specific modes of locomotion (digging and swimming), and to ascertain to which extent the functional pressures act in these structures. For this purpose, two representatives of the genus *Arvicola* were selected, the montane water vole, *A. scherman* (fossorial) and the Southwestern water vole, *A. sapidus* (semiaquatic). The postweaning growth patterns of the mandible, humerus and femur has been determined and their corresponding ontogenetic trajectories compared by using two-dimensional (mandible) or three-dimensional (humerus and femur) landmarks-based geometric morphometrics. To obtain appropriate 3D models of the limb long bones a protocol based on photogrammetry is proposed. Additionally, to complement the morphometric results obtained for the humerus and the femur, histological analyses of their midshaft cross-sections has been performed.

Results revealed that, in *A. scherman* and *A. sapidus*, the three bones studied underwent considerable morphological changes during the postweaning ontogeny but with a similar variation pattern. In the mandible, the juvenile individuals of both species showed important shape changes in the angular and condylar processes, maybe to an adaptation to the new food needs. In the case of the humerus and femur, juvenile voles showed externally more robust bones than adult ones. Likely, this is a compensatory response to their thin cortical walls and intracortical porosity of the cortex to reduce the fracture risk during initial locomotor efforts. Histologically, both species also showed a similar variation pattern of the cortex during postweaning ontogeny.

Significant interspecific differences were observed in the mandible, humerus, and femur size and shape of adult specimens, as well as in the corresponding postnatal allometric and phenotypic trajectories, probably because of different functional pressures exerted on these bones. Of all structures analysed, the humerus showed the most marked shape changes during growth, as well as greater microanatomical alterations, coinciding with the preponderant role it plays in the digging activity. Important differences in the shape of the adult bones between taxa were also found, particularly in the muscle insertion zones. In comparison to *A. sapidus*, fossorial water voles



showed: in the mandible, more compact ramus, and more pronounced curvature of the angular process; in the humerus, more expanded epicondylar and deltoid crests; and in the femur, a wider third and lesser trochanters, and greater bone robustness. These characteristics are similar to those described for other fossorial mammals, namely scratch-digger species, and are associated with burrowing. In relation to swimming, the femur of *A. sapidus* displays a slight increase of the greater trochanter than that of *A. scherman*, which is seemingly an adaptive response for enhancing propulsion through the water.

In the light of the results obtained here, it is concluded that the locomotion type is an important modeler of the ontogenetic trajectories of the mandible, humerus, and femur in *Arvicola*. Accordingly, this indicates that function has the potential to affect morphological evolution of these bones by inducing changes in their respective growth patterns.

## ABBREVIATIONS

---

2D - Two-dimensional

3D - Three-dimensional

ANOVA - Analysis of variance

bgPCA - Between-group PCA

CCA - Calcified cartilage areas

CPL - Circularly polarized light

CS - Centroid size

CTL - Conventional transmitted light

CVA - Canonical variate analysis

CVC - Circular vascular canal

DA - Discriminant analyses (or DFA - Discriminant function analysis)

DBR - Disorganized bone region

*df* - Degrees of freedom

F - *F* statistic

FLB - Fibrolamellar bone

GPA - Generalized Procrustes analysis

HB - Hybrid bone

HS - Homogeneity of slopes

LB - Lamellar bone

LCS - Logarithm of centroid size

MC - Medullary cavity

MD - Mahalanobis distance

ME - Measurement error

MMA - Methyl methacrylate

MS - Mean squares

*p* - *p*-value.

PC - Principal component

PCA - Principal component analysis

PFB - Parallel-fibered bone

PO - Primary osteons

PTA - Phenotypic trajectory analysis

RC - Resorption cavity

RL - Resorption lines (or reversal lines)

RRPP - Randomization permutation procedure

Rsq - R squared values

RVC - Radial vascular canals

*SDs* - Standard deviations

SS - Sum of squares

TB - Trabecular bone.

UV light - Ultraviolet light

VC - Vascular canals

Z - Effect-size

Zi - Index of strength

---

# CHAPTER 1

## GENERAL INTRODUCTION



## CHAPTER 1. GENERAL INTRODUCTION

---

### 1.1. INFLUENCE OF LOCOMOTION ON BONE MORPHOLOGY

Understanding the factors that drive phenotypic diversity has been a topic of discussion since Darwin. Most studies propose adaptive explanations for morphological variation and the relevant role that natural selection plays in its formation (Salazar-Ciudad, 2006). Morphological variation is mainly influenced by two factors: evolutionary history and ecology (e.g., mechanical demand imposed by ecological features). Evolutionary history contributes to phylogenetically close species being more like each other than would be expected by chance under homogeneous conditions (Caumul & Polly, 2005; Renaud et al., 2007). Conversely, mechanical demands imposed by ecological traits can be reflected in morphological changes, as adaptive specifications for a given environment (Hildebrand, 1985; Lehmann, 1963; Lessa & Stein, 1992; Stein, 2000). An example is when species that have the same lifestyle share similar anatomical traits regardless of phylogenetic relationship. These two factors cannot be seen as separate since functional morphology results from a compromise between the adaptive form and the possible form given by evolutionary history (Ord & Summers, 2015).

The relationships between ecology and function can be addressed by studying ecologically relevant functions of organisms. Locomotion has been considered an important driving function of phenotypic traits. Several comparative studies between rodent species have shown diverse osteological and muscular characteristics related to the different types of locomotion (Verde Arregoitia et al., 2017; Candela & Picasso, 2008; Elissamburu & de Santis, 2011; Lessa & Stein, 1992; Marcy et al., 2016; Morgan & Verzi, 2006; Samuels & Valkenburgh, 2008; Thorington & Santana, 2007). Similar traits associated with locomotion have been described in distantly related families suggesting an evolutionary convergence or parallelism (Verde Arregoitia et al., 2017; Samuels & Valkenburgh, 2008; Stein, 2000). Traditionally, this morpho-functional relationships in rodents have been analysed using bone linear measurements, although in more recent studies 2D or 3D geometric morphometrics has been applied (e.g., Hedrick et al., 2020; Marcy et al., 2016).

Despite extensive work on the external morphological variations associated with locomotion, less research has been carried out on the histological and internal geometry of bones. Although several histological studies have shown morphological features linked to the type of locomotion (Fish & Stein, 1991; Houssaye et al., 2016; Laurin et al., 2011; Wall, 1983), there are few descriptive or quantitative works focused on functional topics, in particular on the link between external morphological variation and bone microstructure (Hedrick et al., 2020; Legendre & Botha-Brink, 2018; Montoya-Sanhueza & Chinsamy, 2017; Montoya-Sanhueza et al., 2020).

### 1.2. ONTOGENETIC CHANGES IN THE BONE MORPHOLOGY

As noted above, phenotypic variation is often attributed to adaptation as it is shaped by natural selection. However, there are structural mechanisms such as organism-specific growth and development processes (ontogeny) (Salazar-Ciudad, 2006) that can influence the degree to which selection acts and alter both the direction and magnitude of changes (e.g., Klingenberg, 1998, 2016). Thus, variations in the attributes of ontogenetic patterns are important in the evolutionary processes (Klingenberg, 2016; Wilson & Sánchez-Villagra, 2011). Recent studies in phylogenetically related species have shown that, under certain circumstances (different niches, evolutionary adaptations, and behaviours), selection can rapidly modify postnatal growth patterns (Esquerré et al., 2017; Gray et al., 2019; Wilson et al., 2011).

Morpho-functional ontogenetic studies on rodent bones are relatively scarce (e.g., Cubo et al., 2006; Echeverría et al., 2014; Vassallo et al., 2016; Ventura & Casado-Cruz, 2011; Montoya-Sanhueza et al., 2019). These kinds of works are important to understand the contribution of the different stages of development of these structures to adulthood morphology, at what point in the postnatal ontogeny morphological changes appear or if these ones are maintained throughout development (Adams & Nistri, 2010; Echeverría et al., 2014). Furthermore, they permit to achieve a global view of which forces may have shaped the pattern of morphological evolution.

There are several studies on the postnatal ontogeny of different elements of the rodent skeleton at the microstructural level (e.g., Enlow, 1962; Singh et al., 1974; Sontag, 1986; Smith, 1960; García-Martínez et al., 2011). Most of these works are descriptive, having been useful to know the distribution of tissues and histological characteristics throughout ontogeny, as well as the general growth pattern of some bone structures. However, the functional link between bone microstructure and lifestyle throughout ontogeny has received little attention in the literature. In particular, postnatal growth of long bones in fossorial rodents has only recently been investigated in a functional context (Montoya-Sanhueza & Chinsamy, 2017; Montoya-Sanhueza et al., 2020). These studies have shown that the growth patterns of long bones can be influenced in part by burrowing behaviour, thus highlighting the lack of understanding of the skeletal dynamics in small mammals both during the ontogeny and in a functional perspective.

### 1.3. MODES OF LOCOMOTION IN RODENTS

With approximately 35 extant families and 2600 species, Rodents are the most diverse order of mammals (Burgin et al., 2018). Its members occupy virtually every terrestrial habitat, having developed numerous locomotion modes. This feature makes this group an excellent model to understand the emergence of morphological variations related to locomotion and how this can

influence evolution. Below is a brief summary of the different types of locomotion described in rodents.

**Terrestrial locomotion.** The most common forms of terrestrial locomotion in rodents are walking and quadrupedal running (i.e., use of all four limbs), although quadrupedal or bipedal jumping can also occur. Gait is commonly characterized by a lateral sequence i.e., a hindlimb step followed by a forelimb step on the same side (ipsilateral). Usually, the movements of the hind and fore limbs are asynchronous. In contrast, in running, three members are off the ground at every step. The bipedal jump (sometimes called ricochet) consists of the simultaneous use of the hind legs followed by an aerial phase in which the animal is not in contact with the ground (McGowan & Collins, 2018). Few rodents have this type of primary locomotion, being more related to animals that live in the desert as is the case of the kangaroo rats (*Dipodomys*).

**Arboreal locomotion.** Animals with this type of locomotion are capable of regularly climbing trees or different vertical profiles. Several rodents such as tree squirrels (*Sciurus griseus*), woodrats (*Neotoma* spp.) or porcupines (Erethizontidae) use this mode as an escape, shelter, or quick and silent movement between spaces (Montgomery, 1980). Due to the numerous mechanical challenges of this mode of locomotion, such as variation in the tree substrate, climbing, slope, balance or unpredictability of obstacles, rodents have developed both morphological (such as claws or prehensile extremities) and behavioural adaptations (Karantanis et al., 2017; Wölfer et al., 2021; Schmidt & Fischer, 2011). As in terrestrials, arboreal rodents use lateral sequencing for static stability, however asymmetrical gaits (i.e., when a pair of limbs are equally shifted in time) has been described as advantageous for increasing dynamic stability (Wölfer et al., 2021).

**Gliding locomotion.** Some species of rodents have the ability to glide through the use of a patagium, i.e., an extension of skin from the abdomen that extends to the ends of the fingers, as is the case with flying squirrels. It is a very efficient way to travel from tree to tree because although the animal expends metabolic energy due to the increase of its body surface area, little or no mechanical energy is generated by its muscles (Biewener & Patek, 2018). The displacement basically consists of a jump from a tall tree extending the patagium, in such a way that as the gravitational force acts, the speed increases and so do the aerodynamic forces. During gliding, lift and drag forces acting on the body surface balance the animal's weight, allowing it to travel long horizontal distances at constant speeds (Biewener & Patek, 2018).

**Aquatic locomotion.** Semiaquatic rodents exhibit both terrestrial and aquatic locomotion. These spend long periods in the water using swimming as a means of dispersion. The muskrat (*Ondatra zibethicus*), the capybara (*Hydrochoerus hydrochaeris*) or the southern water vole (*Arvicola sapidus*) are examples of semiaquatic species. Most of them employ simultaneous or alternating



paddling movements in which the limbs can be located close to the body or in the parasagittal plane, known as drag-based paddling propulsion (Fish, 1993). The type of paddling can be bipedal (i.e., alternating movement of the hind limbs in which the forelimbs are extended in front of the head) or quadrupedal (i.e., alternating movement of all four limbs) (Santori et al., 2008).

**Fossorial locomotion.** Fossorial rodents regularly dig extensive tunnels as shelter or to forage underground; for example, tuco-tucos (*Ctenomys* spp.), the naked mole-rat (*Heterocephalus glaber*) or the montane water voles (*Arvicola scherman*). In order to standardize the activity of all fossorial rodents, Gambaryan & Gasc (1993) classified the digging process into four cyclical steps: i) the soil is broken; ii) the loose earth is stored on or near the body; iii) the accumulated earth is moved posteriorly through 5 to 6 kicks; iv) the animal deposits the debris outside its tunnel. Three techniques for breaking soil are used by fossorial rodents (see e.g., Stein, 2000; and references therein). Most species are scratch diggers, i.e., they use alternate movements of the forelimbs in which claws break and release the soil, as has been observed, for example, in the pocket gophers (*Geomys*), *Ctenomys* or dune mole rats (*Bathyergus*). Rodents that use protruding incisors to break through the ground are called chisel-tooth diggers, such as coruros (*Spalacopus* spp.), the naked mole rat or the montane water vole. Lastly, and least common among fossorial species, is the head-lift digger, which uses its head through the neck muscles to lift the earth and thus dig, as is the case with the mole rats of genus *Nannospalax* spp. Regardless of the digging method, all fossorial rodents exhibit some morphological modifications in the teeth, neck, and forelimbs due to the high demand of this activity (Stein, 2000).

### 1.4. *ARVICOLA*

The genus *Arvicola* Lacépède, 1799 is a group of Eurasian rodents with a great number of morphotypes, including semiaquatic and fossorial forms, and exceptional ecological versatility. For this reason, this genus provides an excellent opportunity to analyse the relationship between form and mode of locomotion (function). Its taxonomy has been the subject of an intense debate that is still unresolved. Classically two species within this genus were recognized (see e.g., Reichstein, 1963, 1982): *A. sapidus*, which comprises semiaquatic populations, and *A. terrestris*, with fossorial and/or semiaquatic representatives. In the taxonomic review of this genus by Musser and Carleton (2005) three species were accepted: the southwestern water vole, *A. sapidus* Miller, 1908 (semiaquatic); the montane water vole, *A. scherman* (Shaw, 1801) (fossorial); and the European water vole, *A. amphibius* (Linnaeus, 1758) (semiaquatic or mostly semiaquatic). The southwestern water vole, *A. sapidus* Miller, 1908, constitutes a basal lineage and is the only species of the genus whose validity is not in question due to its relatively high divergence from the others (Centeno-Cuadros et al., 2009). The taxonomy of the other populations of *Arvicola* recognized by

Musser and Carleton (2005) is more problematic. They have recently been considered as belonging to two or more species, whose names vary according to different works: *A. italicus* and *A. amphibius* (Chevret et al., 2020); *A. amphibius*, *A. italicus*, *A. monticola* (formerly *scherman*) and *A. persicus* (Pardiñas et al., 2017; Mahmoudi et al., 2020). In particular, by using mitochondrial cytochrome b gene sequences, it has been argued that *A. scherman* is not a monophyletic group (Kryštufek et al., 2015), proposal that has not been supported in other molecular analyses (Balmori-de la Puente et al., 2022). As for the Iberian population considered in the current research, according to the information reported in all these works, fossorial water voles from the Pyrenees (formerly *A. terrestris monticola*) could be attributed to *A. scherman* (Musser & Carleton, 2005); *A. amphibius* sensu lato (Kryštufek et al., 2015), *A. monticola* (Mahmoudi et al., 2020; Pardiñas et al., 2017) or *A. amphibius* (Chevret et al., 2020). Until these taxonomic uncertainties are resolved, the reference of Musser and Carleton (2005) has been followed here to clearly distinguish between the two typical ecological forms of *Arvicola*, the fossorial (*A. scherman*) and the semiaquatic (*A. sapidus*).

#### 1.4.1. *Arvicola scherman*

The montane water vole (*A. scherman*) is a hypogeal rodent that perform its main biological functions underground. It has a small size body length from 12 to 18 cm and ranges from 80 to 183 g, body dimensions smaller than *A. sapidus* (Ventura, 1993). *Arvicola scherman* is a chisel-tooth digger that build complex and extensive tunnels in harder soils (Airoid, 1976; Airoidi & de Werra, 1993). In general, these tunnels are made up of superficial galleries (between 7 and 20 cm) for obtaining food, and deep galleries (between 30 and 60 cm deep) where voles store food and build its nests. Its digging mode is characterized by three phases, as shown is Fig. 1-1 (Airoidi et al., 1976; Laville, 1989; Laville et al., 1989). The first phase is biting, in which the lower and then the upper incisors bore into the earth due to the dorsoventral movement of the head. The second phase is accumulation, in which through quick and alternating movements, the forelimbs slide the ground under the abdominal area. The third phase is removal, in which the animal, with 1 to 3 kicks, expels the soil from the tunnel. The first and second phases can be repeated between 2 and 11 times before the removal phase occurs. Although the animal may stop during the digging process, it is never interrupted between the biting and accumulation phases. The cycle ends with the compaction of the walls with the muzzle and the mouth half-open like a backhoe.

This species lives in family groups composed of an adult couple and its offspring (Morel, 1981), although more complex associations have been described (Morel, 1981). Both males and females are responsible for maintaining and defending the galleries (Meylon, 1977; Morel, 1981). Its diet is herbivorous, consuming roots and bulbs as well as aerial parts of plants (Kopp, 1993; Airoidi,

1976). Due to the high energy demand resulting from underground life, each specimen consumes daily an amount of food equivalent of to its body mass (Quéré, 2009).

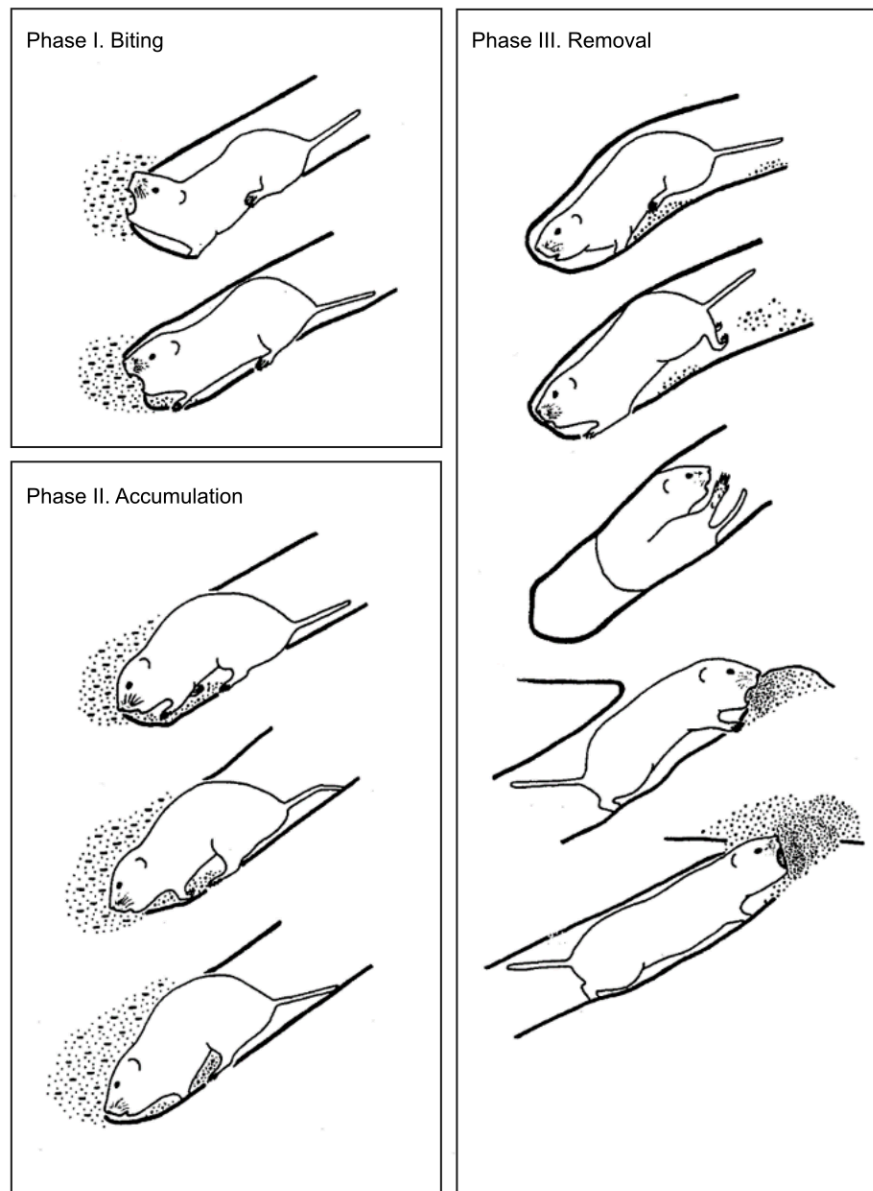


Fig. 1-1 Phases of the digging process of the underground galleries of the montane water vole (*Arvicola scherman*) (image adapted from Airoidi, 1976)

#### 1.4.2. *Arvicola sapidus*

The southern water vole (*A. sapidus*) is an endemic semiaquatic species to southwestern Europe with a medium size body length from 17 to 23 cm and range from 140 to 310 g (Ventura, 2007). It is a species that preferentially lives close to watercourse and waterbodies, with abundant herbaceous vegetation (Ventura, 2007; Mate et al., 2013). On the banks of the watercourses with low slopes and soft substrate, it builds burrows and simple galleries with two entries (Gosàlbez, 1987; Rigaux et al., 2008). Its diet is herbivorous and consists mainly of stalks and leaves of plants

that grow along the watercourse (Garde & Escala, 2000). The population from the Ebro Delta (where the sample analysed in the present work comes from) has a stenophagous diet (i.e., that feeds on a limited variety of predominant resources) of Typhaceae, Poaceae and Cyperaceae (Ventura, 2007). Currently, it is considered a vulnerable species due to its geographic limitation and low population density (Rigaux et al., 2008). As far as we know, there are no descriptive works about the swimming mode of *A. sapidus*, although probably (J. Ventura, personal observations) it has a drag-based paddling propulsion (Santori et al., 2008; Fish, 1993; Stein, 1988).

## 1.5. STRUCTURES INVOLVED IN *ARVICOLA* LOCOMOTION

The fossorial behaviour of *A. scherman* is well known through the studies conducted by Airoidi et al. (1976), Laville, (1989) and Laville et al. (1989). These works constituted the starting point to begin studying the locomotor skeleton of this species under a functional point of view. Further, comparative studies between *A. scherman* and other burrowing species (the Middle East blind mole rats, *Spalax ehrenbergi*) (Laville, 1989b; Laville et al., 1989) or the semiaquatic *A. sapidus* (Cubo et al., 2006; Ventura & Casado-Cruz, 2011) have identified diverse characteristics of the musculoskeletal system associated with the function of digging and the challenges of the hypogeal lifestyle. Main findings of these and other related studies are summarized below.

### 1.5.1. Fossorial locomotion

**Skull.** Several morphological changes in the skull have been interpreted as burrowing adaptations. One of the most marked characteristics of *A. scherman* is having protruding incisors, a physical feature distinct from other non-fossorial Arvicolidae (Laville, 1989b). This typical trait of chisel-tooth diggers allows a favourable orientation of the frontal attack on the substrate. Laville et al. (1989) showed that *A. scherman* and *Spalax ehrenbergi* share adaptive similarities related to digging, such as increased surface of masticatory muscles, increase surface of squamous bone, as well as pronounced insertion crests that improve the biting power of masticatory muscles. An increase in the insertion surface of the mastication muscles (mainly the temporal ones) has also been reported in *A. scherman* in relation to *A. sapidus* (Ventura & Casado-Cruz, 2001), providing to the former species a greater mandibular stability (Laville, 1989b). Modifications in the occipital region and on the frontal and lateral surface of the braincase have also been reported in the montane water vole (Laville, 1989b; Laville et al., 1989). Hence, for example, the greater efficiency of the muscles of the nape responsible for dorsi-flexion of the head (Laville, 1989). These morphological changes coincide with the fundamental role that the head plays in the biting phase in *A. scherman*, increasing both the biting power and the force of insertion of the lower incisors into the ground. Moreover, allometric analysis showed that ontogenetic

## GENERAL INTRODUCTION

exponents of traits linked to burrowing (zygomatic width and incisive prodomia) are significantly higher in the montane water vole than in *A. sapidus* (Cubo et al., 2006).

**Spine.** Another morphological feature observed in *A. scherman* probably related to the digging behaviour, is bifid morphology of the neural spine of the axis. This characteristic has been interpreted as an increase in the attachment area of neck muscles with a relevant role in the biting phase (Laville, 1989). The cervical vertebrae constitute an extension of the rigid transmission of movements integral with the occipital joint. During the digging process, the vertebral axis undergoes a horizontal forward translation, while the thoracolumbar region bends. Conversely, the cervical are highly mobile, which allows the head to extract substrate in different directions in space (Laville, 1989).

**Appendicular skeleton.** The anterior appendicular skeleton is involved in all phases of the digging process (Laville, 1988). In the biting phase (see 1.4.1. *Arvicola scherman*), the forelimbs serve as support and accompany the dorsoventral movements of the head through flexion and extension of the elbow joints. In the accumulation phase, it is the alternating and rapid movements of the forelimbs that pile loose debris under the animal's body. Finally, in the removal phase, the hands resist the ground support while the shoulders and elbows balance the body in the moment of the kick (hind limbs). Distancing of the deltopectoral crest in relation to the shoulder joint, elongation of the olecranon and reduction of the pelvic limb have been described in *A. scherman* in relation to other Arvicolidae as an adaptive tendency to dig (Laville, 1989). These morphological changes seem to be associated both with the pushing movement of the head during soil biting and in the accumulation phase. An increase in the diameter of the diaphysis of some limb long bones (humerus, ulna, and femur) of *A. scherman* compared to *A. sapidus* has also been described, namely in juvenile individuals (Cubo et al., 2006; Ventura, 1992). This feature is a clear adaptation of increased bone resistance to bending and torsional loads during digging (e.g., Casinos et al., 1993; Hildebrand, 1985, Montoya-Sanhueza et al., 2019). In fact, values of flexion and torsion of the ulna, humerus, and femur higher than expected in relation to the body weight of *A. scherman* were reported by Laville (1989), indicating a great bone resistance and an adaptive advantage to burrow.

### 1.5.2. Aquatic locomotion

In semiaquatic populations of *Arvicola* few studies have been performed with the purpose of identifying morphological changes associated with semiaquatic life (Stein, 1989; Samuels & Valkenburgh, 2008). These studies did not show anatomical characteristics associated with swimming. However, a comparative study between fossorial and semiaquatic populations of *Arvicola* showed that *A. sapidus* has relatively longer zeugopodium than fossorial water voles (see

Cubo et al., 2006; and references therein). This trait may be related in part to swimming, since this locomotion is favoured by the length of the paddling limb (Samuels & Valkenburgh, 2008).

## 1.6. TECHNIQUES TO ANALYSE MORPHOLOGICAL VARIATION

The identification of morphological variation between species associated with function has been recurrently approached through geometric morphometrics methods. This procedure permits the quantification of subtle phenotypic variations between species, as well as conceiving strong evidence of the contribution that certain selective pressures have in directing morphological change (e.g., Adams & Nistri, 2010). Another method with a long history in comparative studies of bone structures is the histological analysis. The combination of these two information sources contributes to have a holistic approach to bone changes related to function.

### 1.6.1. *The geometric morphometrics method*

Morphometry (or morphometrics) has been widely used to solve questions related to morphological variation that require the characterization of form and the quantification of phenotypic variation. In the 1960s and 1970s, multivariate statistical methods began to be applied to a set of morphological variables (mainly linear measurements) to quantify the shape variation within and among species; now called traditional morphometrics (Adams et al., 2004). However, this approach provides limited knowledge about shape changes, since this type of measurements lacks spatial relationships, does not capture the complete shape of the structure, and does not allow an effective separation of size and shape components. During the 1980s and early 1990s, the geometric morphometrics method (GMM) emerged, a new branch of morphometrics, in which a series of geometric and statistical tools were developed to analyse form (Bookstein, 1991). Contrary to traditional morphometry that uses linear, area or volumetric variables, this new method studies the relationship between scale and shape of structures by Cartesian geometric coordinates. Structures are represented by two- or three-dimensional points, so called landmarks. Landmarks are particular anatomical points of interest that can be recognized on all species in the study (Bookstein, 1991; Dryden & Mardia, 1998). To choose wisely a set of landmarks to include in a study, several aspects should be considered (Zelditch et al., 2012): 1) each landmark must be a homologous anatomical locus recognizable on each specimen; 2) the set of landmarks should provide adequate coverage of the structure's morphology; 3) the landmarks must be found repeatedly and reliably (i.e., the landmarks must be easily located); 4) the landmark should have conserve topological position in relation to other landmarks; and 5) specific to 2D landmarks, the landmarks should be in the same plane (coplanarity), to minimize the distortion caused by the projection of a 3D organism into a 2D plane. In landmark-based geometric morphometrics, each

specimen has a form that is summarized by configuration of landmarks. This configuration is described by  $nD$  variables, where  $n$  is the number of landmarks and  $D$  the number of dimensions (2 or 3 dimensions). With the introduction of landmark configuration, size and shape can now be parameterized separately. Shape refers to the geometric information of a structure that does not change with scaling, translation, or rotation; size refers to the scale of the structure and form to the shape and size set, since it is only invariant for translation and rotation. The shape variation between specimens is studied from the displacement between homologous landmarks.

Currently, due to statistical rigor and the ease of interpreting shape changes between species (Adams et al., 2013), landmark-based geometric morphometrics is widely applied in comparative morphological studies, namely in studies of biological development, such as growth patterns between species (e.g., Adams & Nistri, 2010; Esquerré et al., 2017; Gray et al., 2019; Wilson & Sánchez-Villagra, 2010; Zelditch et al., 2004).

### 1.6.2. *Bone histology*

At the beginning of the 20th century, many comparative studies on bone histology appeared with the purpose of analysing taxonomy, since it was thought that histology could be used for fossil specimens' identification, which otherwise would not be possible (e.g., Foote, 1913). Half a century later, with greater understanding of bone growth and larger sample sizes, publications emerged that emphasized the diversity of tissue types that could be observed in vertebrates and the first histological convergences between different groups began to appear (de Ricqlès, 1993; Warshaw et al., 2017, for review). As the bone grows, information about its pattern of growth and development is recorded in its cortical tissue, such as changes in length, diameter, shape, and anatomical spatial displacements. These recordings are microscopically visible through histological cross-sections (e.g., Enlow, 1962; Sontag, 1986). Furthermore, considering that the main function of bone is mechanical support, its micro and macro structures also partly reflected adaptations to functional demands. Currently, histological analysis is considered a potential source of information on ontogenetic, functional, and phylogenetic factors (e.g., Enlow, 1963; Currey, 2002; de Ricqlès, 1993).

Bones and other morphological elements of the skeleton are formed by tissues (Francillon-Vieillot et al., 1990). These are more or less complex associations of group of cells with similar structure that are organized to perform a given function. In the case of bone, in descriptive terms it is more appropriate to speak of tissue types, which are stereotypical patterns of anatomical organization formed by the combination of cells, vascular canals, and collagen fibres, according to certain criteria (Enlow, 1963; Francillon-Vieillot et al., 1990). Knowing the distribution and histodiversity (i.e., the wide variety of tissue types) that comprise the cortex, amplifies the knowledge of the bone growth patterns of the species, since it has been observed that species that

differ in time and in the succession of tissue types across ontogeny may have different growth rates and patterns (Amprino, 1947).

Another parameter to be considered in histology is bone modelling. The adult bone morphology is obtained by a sequence of modelling changes at the microstructural level (originally termed “growth remodelling”) (Enlow, 1963). This process results from the spatial and temporal coordination of bone tissue resorption and formation during growth. When the coordinated patterns of bone deposition and resorption on complementary endosteal and periosteal surfaces change the relative position of bone tissue within a previously established cortex, it can result in a cortical drift. This is usually related to development, for example, the curvature of long bone diaphysis. Several studies have shown that bone modelling can be influenced by phylogenetic, biomechanical, environmental, and hormonal factors (see e.g., Enlow, 1963; Currey, 2002; Cubo et al., 2005; Parfitt, 1994).





---

# CHAPTER 2

## OBJECTIVES



## CHAPTER 2. OBJECTIVES

---

### 2.1. GENERAL OBJECTIVES

Rodents are the most diverse group of living mammals, showing a great variety of locomotor strategies. Previous studies have identified several skeletal and muscular adaptations related to locomotion (e.g., Samuels & Valkenburgh, 2008), as a result of their ecomorphological diversification (Verde Arregoitia et al., 2017). These extraordinary explorative and adaptive abilities make rodents an exceptional model to assess different evolutionary processes (Cox & Hautier, 2015). However, as regard to wild species, most morpho-functional studies have been performed in adult individuals (e.g., Candela & Picasso, 2008; Morgan & Verzi, 2006; Samuels & Valkenburgh, 2008), which generates a lack of knowledge about the morphological changes of bone structures that occur throughout ontogeny and their relationships with function. Furthermore, recent investigations on insects (Frankino, 2005), amphibians (Adams & Nistri, 2010), reptiles (Esquerré et al., 2017; Gray et al., 2019; Urošević et al., 2013; Wilson & Sánchez-Villagra, 2011) and mammals (Wilson, 2018) have shown that changes in ontogenetic trajectories can occur between phylogenetically close species due to the action of extrinsic forces, resulting in interplay between selective forces and the developmental process. This issue has been scarcely addressed in rodents (e.g., Verzi et al., 2010; Wilson & Sánchez-Villagra, 2010), and therefore, little is known about the extent to which functional factors affect growth patterns in this group of mammals. As for the analytical method, morpho-functional studies on rodent bones have been carried out using traditional morphometry, i.e., based on linear measurements (e.g., Cubo et al., 2006; Echeverría et al., 2014; Montoya-Sanhueza et al., 2019). However, the current trend is to perform this kind of works by applying the landmark-based geometric morphometrics (e.g., Esquerré et al., 2017; Gray et al., 2019; Wilson & Sánchez-Villagra, 2010) which permit deeper analyses of the shape changes that occur during postnatal ontogeny. Nevertheless, relatively few comparative works have been focused on the microstructural changes during growth on bones involved in locomotion in wild rodent species (Montoya-Sanhueza & Chinsamy, 2017, Montoya-Sanhueza et al., 2020). Definitely, multivariate approach of different dimensions, such as the use of 2D and 3D geometric morphometrics (external morphology), and the study of the microanatomy of cortical bone must contribute to better understanding the postnatal ontogeny of bones and its functional adaptation.

Given this background information and using *Arvicola* as a model, the current thesis has two main aims. The first one is to find phylogenetic and functional signals in the growth patterns of several bones involved in digging and swimming. For this purpose, two representatives of this genus were selected, the fossorial *A. scherman* and the semiaquatic *A. sapidus*. The second aim is

## OBJECTIVES

to ascertain to which extent the functional pressures act in the different bones considered. In order to reach these main goals, the following specific objectives have been delineated: i) to determine the postweaning ontogenetic patterns of the mandible, the humerus, and the femur in fossorial and semiaquatic water voles, and ii) to assess the phylogenetic and functional factors involved in the phenotypic variation of these bones in both ecotypes by comparing the corresponding ontogenetic trajectories.

## 2.2. OBJECTIVE AND HYPOTHESES BY CHAPTERS

### 2.2.1. Chapter 4

This chapter focuses on comparing the postnatal ontogenetic patterns of the mandible in *A. scherman* and *A. sapidus* by means of 2D geometric morphometry and integrating multivariate techniques to detect possible phylogenetic and functional signals. A further objective is to explore indirectly the relationship between the design of the jaw-cranial system and the bite-force.

**Hypotheses:** i) due to their close phylogenetic relationship, both species show certain common features in the postnatal ontogeny of the mandible; ii) considering that the mandible is an essential structure in the digging process in *A. scherman*, even in the early postweaning, *A. scherman* shows particular changes in the mandibular shape during the postnatal ontogeny associated with this digging activity, as well as greater bite force than *A. sapidus*, especially in the adulthood; iii) as a result of differences in the functional role of the mandible in fossorial and semiaquatic water voles, significant interspecific differences between the corresponding ontogenetic trajectories are expected.

### 2.2.2. Chapter 5

This chapter focuses on establishing a photogrammetry-based protocol that permits the construction of 3D models of limb long bones of small mammals that are appropriate for geometric morphometric analyses.

### 2.2.3. Chapter 6 and 7

These chapters focus on comparing the postnatal ontogenetic patterns of long bones (Humerus – Chapter 6 and Femur – Chapter 7) in *A. scherman* and *A. sapidus* using 3D geometric morphometry and integrating multivariate techniques to detect possible phylogenetic and functional signals.

**Hypotheses:** i) due to their close phylogenetic relationship, *A. scherman* and *A. sapidus* share several features in the postnatal ontogeny of these long bones; ii) taking into account the

involvement of the humerus in the digging process and of the femur in swimming activity, significant interspecific differences in the ontogenetic trajectories are expected.

#### 2.2.4. Chapter 8

This chapter focuses on describe and compare the bone microstructure observed in the middle diaphyseal section of long bones (humerus and femur) in *A. sapidus* and *A. scherman* during postnatal ontogeny. This permitted to determine the patterns of bone modelling between species and the relationship between bone microstructure and function.

**Hypotheses:** i) histological features are shared between these species due to their phylogenetic relationships; in particular, throughout the ontogenetic stages, the long bones of water voles show a more organized matrix related to a decrease in composition of tissue types; ii) since there are interspecific differences in the external morphology of long bones related to the lifestyle, species show microstructural specializations to different habits; iii) due to burrowing represents a stronger functional pressure on bone morphology than swimming and that the humerus is a relevant structure in the digging process in *A. scherman*, this bone exhibits more marked microstructural changes than the femur during postnatal ontogeny.



---

# CHAPTER 3

## MATERIALS AND METHODS





## CHAPTER 3. MATERIALS AND METHODS

### 3.1. SAMPLE

Postnatal ontogenetic series from the mandible, humerus, and femur of two *Arvicola* species (*A. scherman* and *A. sapidus*) were analysed. The sample studied for each of these bones included a balanced number of males and females. A total of 699 bones belonging to 334 individuals of *A. scherman* (145) and *A. sapidus* (189) were used. Table 3-1 indicates the origin of the specimens examined. Most individuals (82%) were provisionally housed in the collection from the Mammalian Biology Research Group of the Universitat Autònoma de Barcelona (UAB, Bellaterra, Spain). Individuals of *A. scherman* (Aran Valley, Lleida, Spain) and *A. sapidus* (Delta de Ebro, Tarragona, Spain) were obtained between 1983 and 1984 (Ventura, 1988). All specimens had already been skeletonized and classified according to their sex and relative age class (0-5). The assignment of age classes was carried out through relationships between moulting phase, sexual stage, and skull morphology (for details, see Garde et al., 1993; Ventura & Gosálbez, 1992). The sample size of juveniles (age classes 0-2) was complemented with juvenile individuals from Mélida (Navarra, Spain) collected in 1990, and Banyoles (Girona, Spain) and Rieutort (Pyrénées Orientales, France) obtained in 1994. Results of previous studies showed no significant morphometric differences between these populations (Garde, 1992; Ventura, 1988). The sample from Melida are housed in the Museo de Ciencias of the Universidad de Navarra (UNAV, Pamplona, Spain).

Before the histological study, 3D models of right femora and left humeri of each specimen were obtained by means of photogrammetric techniques according to the protocol established in Chapter 5.

Table 3-1 Sample size analysed by location and age class.

Species	Location	Age class						Total
		0	1	2	3	4	5	
<i>Arvicola scherman</i>	Aran Valley	10	12	33	28	29	33	145
	Ebro Delta	3	7	13	27	42	32	124
<i>Arvicola sapidus</i>	Melida	10	23	26				59
	Banyoles			1				1
	Rieutort	4		1				5
Total		27	42	74	55	71	65	334

### 3.2. GEOMETRIC MORPHOMETRICS

Landmark-based geometric morphometrics method is a technique that uses landmark data combined with statistical analysis to quantify and analyse shape variation between species. In the present thesis two-dimensional (mandible) or three-dimensional (humerus and femur) landmark-based geometric morphometrics were applied. The two-dimensional landmarks were digitized with TpsDig in photographs obtained with a digital camera (Nikon COOLPIX P90) and the three-dimensional landmarks with Photomodeler in 3D models obtained by photogrammetry (Chapter 5). In the current research the landmarks were chosen considering its relevance to determine functional aspects of the form. The analyses were fundamentally carried out with the program MorphoJ (Klingenberg, 2011) and several functions from packages in R (Adams et al., 2017; Collyer & Adams, 2018).

The geometric morphometric method used here to analyse landmark data is Procrustes analysis, which permits separating size and shape components of form variation. In multiple landmark configurations a generalized Procrustes analysis (GPA; also called Procrustes superimposition) is applied so that landmark configurations can be superimposed in an optimal way. Thereby the shape coordinates (so called Procrustes coordinates) are calculated by scaling each landmark configuration to centroid size and minimizing translation and rotation differences of the structure of all specimens (Dryden & Mardia, 1998). Centroid size corresponds to the dispersion of the landmarks calculated as the square root of the summed squared distances of each landmark from the centroid of the landmark configuration (i.e., centre of gravity obtained by averaging the coordinates of all landmarks) (Bookstein, 1991). When performing the GPA in MorphoJ, the size and the shape coordinates projected in a Euclidean space tangent to the Procrustes shape space were obtained separately. Because most of the statistical methods used in morphometric analyses require the data to be in a flat Euclidean space and the Procrustes shape space (morphometric space generated after the GPA) is curved, coordinates must be projected to a tangent Euclidean space (Viscosi & Cardini, 2011).

#### 3.2.1. Preliminary analyses

Before starting the data analysis, some preliminary analyses were carried out. The first one was to inspect the existence of outliers (for shape) through two exploratory methods. The first approach was through the inspection of bones with bigger Mahalanobis distances from the average shape of the entire sample (Find outliers in MorphoJ). This method compares the multivariate normal distribution fitted to the data with the distribution of distances in the dataset. Depending on the relationship between the dimensionality of the data and the number of specimens in the dataset, either the Procrustes distance or the squared Mahalanobis distance is

used (e.g., Klingenberg & Monteiro, 2005). In our analyses, the Mahalanobis distance (large sample size) was used, which indicates how unusual the bone of an individual is in relation to the mean shape of the sample. When the data are grouped by species, this method also permits observing which landmarks deviate strongly from the average shape, being a guide for the quality of the data. The second method was the observation of individual points separated from the points cloud in the principal component analysis (PCA).

Since the sample is composed of males and females, the second preliminary analysis performed was to investigate the existence of sexual dimorphism in each species. For size, a factorial analysis of variance (ANOVA) was performed with sex and age class as categorical factors and log-transformed centroid size (LCS) as dependent variable. For shape, we used Procrustes ANOVA with shape coordinates as response variable and LCS and sex as independent variables. Centroid size was transformed to its natural logarithm to minimize large size differences between specimens. Given that species did not show significant sex differences in the bones considered, data from males and females were grouped and analysed jointly.

### 3.2.2. *Shape changes along postnatal ontogeny*

#### ***Principal component analysis (PCA)***

In order to investigate the pattern of shape changes along postnatal ontogeny in both species, a PCA was performed (Chapter 6 and 7). This is one of the most used techniques in geometric morphometry to simplify the complexity of the data and examine the patterns of shape variation among specimens in a multidimensional space (e.g., Gray et al., 2019; Esquerré et al., 2017; Viscosi & Cardini, 2011). The PCA summarizes multivariate data through linear combinations of the initial variables with maximal sample variance, maintaining trends and patterns (Jolliffe, 1986). The new variables into which the original variables are transformed are uncorrelated and are called principal components (PCs). The PCs are ordered according to the amount of explained variance. Thus, the first PC accounts for the largest variance, the second PC account for the second largest variance, and so on (Jolliffe, 1986). This has the advantage that a big amount of variation can be explained with a set of few variables (Jolliffe, 2005).

#### ***Discriminant analysis (DA)***

Discriminant analyses (DA) were carried out to visualize bone shape differences between species across ontogeny. This technique of dimensionality reduction is often used in the context of geometric morphometrics (e.g., Klingenberg & Monteiro, 2005 and references therein; Viscosi & Cardini, 2011), to find shape features that best distinguished among groups of specimens. The DA differs from a canonical variate analysis (CVA) due to only two groups being considered in the

analysis. Unlike PCA, DA considers the internal structure of the data, influencing the variation within groups and the separation between groups. For features in higher dimension space to be projected in a lower dimensional space, DA calculate the distance between the means of different groups, the distance between the mean and sample of each group and construct a new set of axes (lower dimensional space) which maximize the between groups variance and minimize the within group variance (Brown & Tinsley, 1983). Since the CVA/DA may lead to spurious results when the number of variables exceeded the number of individuals, this method can only be executed if the sample size is greater than the number of variables (Mitteroecker & Bookstein, 2011) and must be validated by cross-validation (Kovarovic et al., 2011; Viscosi & Cardini, 2011). In MorphoJ, the cross-validation is performed automatically (Klingenberg, 2011).

### ***Between-group PCA (bgPCA)***

As an interesting alternative to CVA/DA to explore group structure and summarize group differences in high-dimensional spaces, a between-group PCA (bgPCA) has been suggested (Mitteroecker & Bookstein, 2011). This type of PCA is performed on the covariance matrix based on sample  $g$  (group) means followed by the projection of the original  $n$  samples onto the principal components of the  $g$  means (Boulesteix, 2005; Mitteroecker & Bookstein, 2011). However, recently several articles have warned that like the CVA, the bgPCA can exhibit spurious groups, inflating the differences between groups when used in a small sample with a large number of variables (for more details see Bookstein, 2019; Cardini et al., 2019; Cardini & Polly, 2020). To circumvent this problem has been proposed the performance of cross-validation (Cardini & Polly, 2020; Thioulouse et al., 2021).

### ***3.2.3. Allometry***

To analyse whether allometry (i.e., shape changes due to size difference) explains a significant proportion of the morphological variation, a multivariate regression of shape (shape coordinates) onto size (LCS) was used. This technique measures the degree of linear relationship between the dependent variable (shape) and the independent variable (size). Through this method we decompose the component of variation in the dependent variable that is predicted by the independent variable, from the residual component of variation in the dependent variable, which is uncorrelated with the independent variable (Klingenberg, 2011). Thus, the residuals from this regression were considered as no allometric shape data since by using them the effect of size on shape is removed (Klingenberg, 2016). The predicted component is calculated from the slope of the regression equation and deviation of the data point from the mean in the direction of size. The residual is the difference between the total shape deviation of the data point from the mean and the value predicted from the regression line. To analyse the significance of the results, a

permutation test was performed considering the non-association between size and shape as a null hypothesis. The transformation of centroid size into natural logarithm centroid size must increase the fit to the model, which is estimated by the percentage of shape variance explained by the size. As each species has its particular slope, the regressions were performed separately.

In order to compare trajectories of ontogenetic allometry between species a Procrustes ANOVA/RRPP (randomization permutation procedure) approach was used. Procrustes ANOVA is a method adapted to the study of shape (Klingenberg & McIntyre, 1998; Klingenberg et al., 2002), which quantifies relative amounts of variation at different levels using “hierarchical sum of squares” in a linear model (Klingenberg & McIntyre, 1998; Klingenberg et al., 2002). This method is a model extended from the two factor ANOVA approach, that use Procrustes distance among specimens, instead of the covariance matrix among variables. The RRPP approach use a resampling procedure to randomize the residual shape values of a matrix of residuals from a reduced model (i.e., linear model that does not contain size\*species interaction effect) to calculate pseudo-values for estimation of effects from a full model (Adams & Collyer, 2007, 2009; Collyer & Adams, 2007; Collyer et al., 2015). For models that use more than one factor this method has shown to have higher statistical power (Anderson & terBraak, 2003). If there is a significant interaction between factors (size\*species) it is concluded that the allometric changes are not parallel, that is, they differ between species. To find out how the allometric trajectories differ between species, a pairwise comparison test was performed for the vector length (i.e., the amount of shape changes per unit change of size) and vector direction (i.e., direction of shape change associated with the size) (Collyer & Adams, 2013). Vector length is calculated from the absolute difference in vector lengths (distances), and vector direction is calculated as the inner product of the two vectors scaled to unit length. Significance was tested by permutation procedure. In the case of  $\theta = 0^\circ$  the vectors are considered parallel and if  $\theta = 90^\circ$  they are orthogonal vectors (Collyer & Adams, 2007).

#### 3.2.4. *Phenotypic trajectory analysis*

In order to compare ontogenetic trajectories of a given bone between species, a phenotypic trajectory analysis (PTA) was performed. This test is similar in concept to the allometric trajectory analysis performed previously (Adams & Collyer, 2007, 2009; Collyer & Adams, 2007, 2013). The big difference is that while in the previous test size (LCS) is used as a continuous variable, in the PTA at least one categorical variable (age class) is used as a proxy for size (Esquerré et al., 2017). Performing the two analysis provides a robust statistical framework and different perspectives on the results. The PTA procedure quantifies phenotypic shape change trajectories from a set of specimens and assesses the variation of different attributes (size, orientation, and shape) of these trajectories via RRPP (Adams & Collyer, 2007, 2009; Collyer & Adams, 2007, 2013; Collyer et al.,

## MATERIALS AND METHODS

2015). Trajectory analysis was computed by a linear model including the age class (shape coordinates ~ species\*age class). In two-factor factorial model, the first factor defines the group and the second trajectory points.

### 3.2.5. *Interpretation and visualization of shape variation*

To visualize the relative differences between species we used in Chapter 4 to 7 displacement vectors (called “lollipops” in Morphoj). These are arrows that connect landmarks in starting shape with the same destination landmark. Transformation grids were also used in the Chapter 4 and 5 to illustrate shape changes. These are observed through a deformation grid using thin-plate spline (i.e., a technique for interpolating and smoothing data). In 3D models (Chapter 6 and 7) both the PCA and PTA related shape changes were performed involving a reference specimen (the general mean shape, i.e., consensus shape) onto which the shape changes were projected.

## 3.3. HISTOLOGY

In order to obtain microanatomical information from the humerus and femur throughout the postnatal ontogeny, histological analyses were used (detailed information in the Chapter 8). For this purpose, an invasive method was applied to obtain and examine thin histological cross-sections of these bones. Cross-sections were prepared from mid-diaphysis and their examination performed under conventional transmitted light (CTL) and circularly polarized light (CPL) using a Leica-Leitz DMRXE Universal microscope, configured with a Marzhauser motorized stage. Transmitted light images were used to identify the spatial distribution of bone tissues while CPL images the collagen fibre orientation (Bromage et al., 2003). Collagen fibres are anisotropic i.e., light propagation varies according to the direction in which they are examined. Under polarized light, collagen fibres that are perfectly aligned transversely to the propagation direction have an intense glow, while fibres that are aligned to the light propagation axis appear dark (Bromage et al., 2003). The fact that an intense glow occurs in the first case is due to the light coming out of the sample being refracted, which does not occur in the second one. To highlight the calcified cartilage areas as well as cement lines (resting and resorption lines) and vascular spaces, all bone sections were stained with toluidine blue and subsequently visualized under CTL. Using the Syncroscopy Automontage software, a real-time montage of the images observed under the microscope was obtained. All histological section preparation and imaging was performed at the Hard Tissue Research Unit located at the New York University, College of Dentistry. The sections resulting from this investigation were provisionally housed in the Mammalian Biology Research Group of the Universitat Autònoma de Barcelona (UAB, Bellaterra, Spain).

---

# CHAPTER 4

COMPARATIVE POSTWEANING ONTOGENY OF THE  
MANDIBLE IN FOSSORIAL AND SEMIAQUATIC WATER  
VOLES

**Ana Filipa Durão, Jacint Ventura, Francesc Muñoz-Muñoz**

---

The content of this chapter is part of an article published in:

Mammalian Biology (2019) 97, 95-103

DOI: [10.1016/j.mambio.2019.05.004](https://doi.org/10.1016/j.mambio.2019.05.004)

---





## CHAPTER 4. COMPARATIVE POSTWEANING ONTOGENY OF THE MANDIBLE IN FOSSORIAL AND SEMIAQUATIC WATER VOLES

---

### 4.1. INTRODUCTION

Water voles of genus *Arvicola* exhibit noticeable morphological variation associated, at least in part, with the colonization of semiaquatic and/or underground habitats (Hewitt, 1999; Taberlet et al., 1998). In fact, the presence of two ecological forms (semiaquatic and fossorial) within this genus has generated considerable taxonomical controversies. During the second half of the past century, two extant species of *Arvicola* were recognized (see, e.g., Kratochvíl, 1983; Reichstein, 1982, 1963): the southern water vole, *Arvicola sapidus* (formed exclusively by semiaquatic populations distributed in the Iberian Peninsula and much of France), and the northern water vole, *Arvicola terrestris*, (that included both semiaquatic and/or fossorial populations widely distributed in the Palearctic region). More recently, Musser & Carleton (2005), following the reviews by Panteleyev (2001) and Zagorodniuk (2001), modified that taxonomic configuration and recognized three full species of *Arvicola*: *A. sapidus*, *A. amphibius* (European water vole), and *A. scherman* (montane water vole). *Arvicola amphibius* includes semiaquatic (or mostly semiaquatic) water voles formerly assigned to *A. terrestris*, and *A. scherman* (montane water vole), comprises exclusively the fossorial morphotypes previously attributed to *A. terrestris* (Musser & Carleton, 2005). Nevertheless, it must be pointed out that several previous and subsequent studies do not support this taxonomic pattern (Bernard, 1961; Kryštufek et al., 2015; Piertney et al., 2005; Taberlet et al., 1998). Since this problem seems to be far from being fully solved, in the present study, we assigned fossorial populations to *A. scherman* to clearly distinguish them from semiaquatic water voles. This taxon occurs in mountain areas of southern and central Europe (Musser & Carleton, 2005), living underground and constructing extensive burrow systems in grasslands, pastures, and orchards (Airoldi et al., 1976; Meylan, 1977).

Because of the colonization of very different habitats, the genus *Arvicola* constitutes an excellent study case to unravel the effect of the type of locomotion on the phenotypic variation (see Cubo et al., 2006 and references therein). In particular, adult fossorial and semiaquatic water voles show noticeable differences in skeletal morphology. Thus, when compared with *A. sapidus*, *A. scherman* shows an increased zygomatic width, incisor proodontia, increased diaphyseal diameter of some limb long bones and shorter zeugopodium (Cubo et al., 2006; Ventura, 2001). While both species can swim and dig, these distinguishing features seem to be associated with different habitats and the prevalence of different types of locomotion.

*Arvicola sapidus* is an active swimmer that also exhibits the capacity to dive (Mate et al., 2013). Although it does not show marked adaptive characteristics to swimming, such as interdigital membranes or a flattened tail, it has a relatively fusiform body shape that allows using the limbs and tail to tilt, dive and float as observed in other rodent species (Cook et al., 2001). During swimming, both semiaquatic and terrestrial rodents employ bipedal paddling, where limbs may be oriented vertically in the parasagittal plane or horizontally and can be used simultaneously or alternately (Dagg & Windsor, 1972; Santori et al., 2008). The locomotor cycle of bipedal paddling is divided into two phases: a power phase where the hind limbs generate propulsion, and a recovery phase where they return to the original position to begin a new cycle (Santori et al., 2008). While semiaquatic and terrestrial species swim similarly, the former shows a more hydrodynamic body posture (Santori et al., 2008).

Out of water, southwestern water voles build galleries to connect areas, breed and escape predators. These galleries are relatively simple with two entrances, one at the water level and the other below (Gosàlbez, 1987; Rigaux et al., 2008), and are preferably constructed on easily penetrable soils (Strachan et al., 2011).

Conversely to *A. sapidus*, *A. scherman* live mostly underground and build complex networks of underground galleries in harder soils (Airoidi, 1976). The digging activity of these voles is based on a strict pattern of stereotyped cyclic events (Airoidi et al., 1976; Laville, 1989; Laville et al., 1989). First, the animal digs its incisors into the ground (first the lower and then the upper incisors) and with successive head movements loose the soil. With fast and alternating movements of the fore and hind limbs, progressively evacuates the earth that remains inside the gallery. The digging cycle ends with the compaction of the gallery walls using the muzzle and incisors (Airoidi et al., 1976; Laville, 1989; Laville et al., 1989). It is important to note that the mandible plays an essential role in the digging process, in particular during its first and final phases (Laville, 1989; Laville et al., 1989).

In vertebrates, bite force is usually used as a measure of mandible performance because it is related to numerous types of functional demands, such as feeding, mating, and antipredation (Anderson et al., 2008). In studies, like the present one, where it is not possible to directly measure bite force because live animals are not available, this variable can be estimated by an index of strength (Zi) based on mandible measurements (Borges et al., 2017; Freeman & Lemen, 2008). In particular, Freeman and Lemen (2008), by using this index on several rodent species, showed that estimated bite force might be related to fossoriality and durophagy. In fact, bite force is assumed to be tightly linked to design features of the jaw-cranial system (Anderson et al., 2008). In the light of these results, it seems likely that *A. scherman* shows higher values of estimated bite force with respect to *A. sapidus* since digging is a biomechanically demanding mode of locomotion (Stein, 2000).

Ontogenetic analysis of a species allows one to determine the relative contribution of different development stages to adult shape (Young, 2008). Although closely related species may tend to conserve certain aspects of the ontogenetic trajectory (e.g., Moyano & Giannini, 2017; Scott et al., 2014), it has been found that different niches (Esquerré et al., 2017; Gray et al., 2019; Urošević et al., 2013), behaviours (Wilson, 2018) and evolutionary adaptations (Adams & Nistri, 2010; Frankino, 2005) may introduce modification in the ontogenetic pattern (e.g., Esquerré et al., 2017; Zelditch et al., 2016). Thus, given the different ecologies of *A. sapidus* and *A. scherman* and, particularly, the importance of the mandible for digging in *A. scherman*, the existence of significant differences in the species' respective ontogenetic trajectories cannot be ruled out.

The main aim of this study is to investigate whether evolved functional differences in the mandible are associated with different ontogenetic trajectories in two phylogenetically close species with very different ecologies and types of locomotion, such as the semiaquatic *A. sapidus* and the fossorial *A. scherman*. In the light of the information presented above, we hypothesise that significant interspecific differences exist in the allometric and ontogenetic trajectories of *A. sapidus* and *A. scherman*, as well as in the estimated bite force of their mandibles, as a result of differences in the functional role of the mandible in these species. Although some general aspects of the postweaning growth of the mandible in fossorial water voles are already known (Ventura & Casado-Cruz, 2011), in the present study we explore, for the first time, this developmental process in *A. sapidus* and compare it between semiaquatic and fossorial water voles applying geometric morphometric methods.

## 4.2. MATERIALS AND METHODS

### 4.2.1. Sample and data acquisition

The sample analysed consisted of 271 left mandibles distributed across two ontogenetic series, one for *A. scherman* and the other for *A. sapidus* (Table 4-1). These mandibles correspond to collection specimens of *A. scherman* (n = 118), obtained between 1983 and 1984 in the Aran Valley (Lleida, Spain), and of *A. sapidus* (n = 153) collected between 1983 and 1990 in the Ebro Delta (Tarragona, Spain) and Mélida (Navarra, Spain). Specimens of *A. sapidus* from the Ebro Delta and *A. scherman* are provisionally deposited in the collection of the Mammalian Biology Research Group of the Universitat Autònoma de Barcelona (UAB, Bellaterra, Spain). Specimens of *A. sapidus* from Navarra belong to the collection of the Museo de Ciencias of the Universidad de Navarra (UNAV, Pamplona, Spain).

All individuals were categorized into six classes of relative age (0-5) based on the relationships between molting phase, sexual stage, and skull morphology as established by Ventura and Gosálbez (1992) and Garde et al., (1993) for *A. scherman* and *A. sapidus*, respectively. For both

## POSTNATAL ONTOGENY OF THE MANDIBLE

species the age range assigned to each age class was as follows (see Ventura & Gosálbez, 1992; Garde et al., 1993): class 0, three weeks maximum; class 1, between three and six weeks; class 2, between six and ten weeks; class 3, between ten and fourteen weeks; class 4, voles older than fourteen weeks that either have not or have recently lived through their first winter; and class 5, individuals that have lived longer than one winter.

Table 4-1 Sample size for each species, age class and sex.

Species	Sex	Age class					Total	
		0	1	2	3	4		5
<i>Arvicola sapidus</i>	F	6	11	20	8	15	10	70
	M	6	10	15	18	14	15	78
	I	1	1	3	-	-	-	5
<i>Arvicola scherman</i>	F	3	4	18	9	17	11	62
	M	3	5	11	12	12	13	56
Total		19	31	67	47	58	49	271

The sample of *A. sapidus* from the Universidad de Navarra collection used in the present study, was comprised only of mandibles of specimens of age classes 0-2. These mandibles were used to increase the relatively small number of juvenile specimens in the sample of the Ebro Delta. Water voles of these two populations do not differ significantly in the morphometric characteristics of the skull (Garde, 1992).

To analyse the ontogenetic variation of mandible form in *A. sapidus* and *A. scherman*, we used landmark-based geometric morphometrics. Mandibles were photographed from the external side along with a scale bar with a digital camera (Nikon COOLPIX P90) by the same person (A. F. D.) under standardized conditions. To ensure that the lens and the specimen plane were parallel, a spirit level was used. Each mandible was positioned in the center of the optical field, focusing in the region of the alveolus of m1 and at a distance that minimized and standardized photographic distortion. Fifteen two-dimensional landmarks were digitized in each scaled image by the same person (A. F. D.) with tpsDig2.26 (Rohlf, 2010) (Fig. 4-1 and Supplementary Information, Table S4-1). The size of the mandibles was estimated by its centroid size (CS), calculated as the square root of the summed squared distances of each landmark from their centroid (Bookstein, 1991). To obtain shape variation, landmark configurations were superimposed through a generalized Procrustes fit conducted on all specimens together, which removes the variation of size, position, and orientation from the landmark coordinates (Rohlf & Slice, 1990). Afterward, landmark configurations were projected onto a linear shape tangent space (Dryden & Mardia, 1998; Goodall, 1991). The resulting landmark coordinates (i.e., Procrustes coordinates) only account for shape variation and can be analysed with multivariate statistics (Klingenberg et al., 2003).

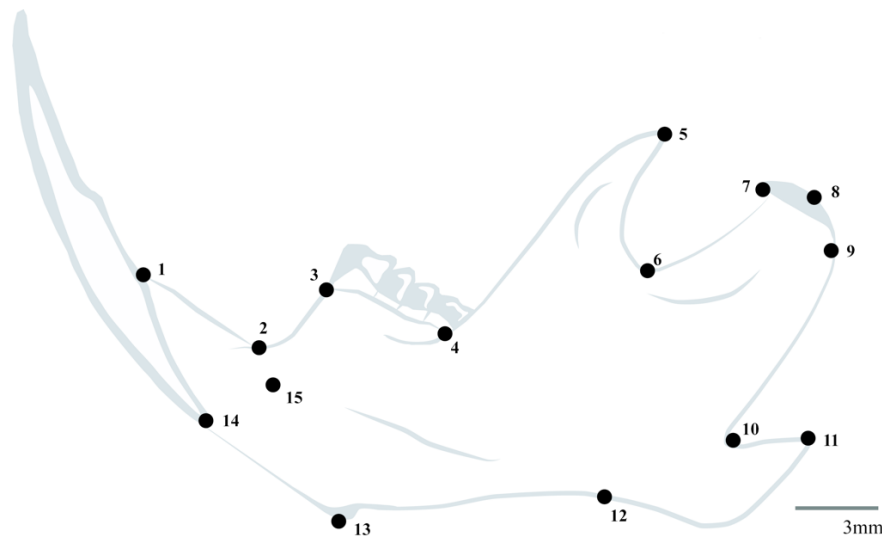


Fig. 4-1 Labial view of the left mandible with the layout of the landmarks used in the geometric morphometric analyses.

In order to evaluate the presence of sexual dimorphism on mandible size, a factorial ANOVA with sex and age class as categorical variables and logarithm of centroid size (LCS) as the dependent variable was conducted separately in each species. The presence of sexual dimorphism in mandible shape was tested separately in each species by performing a Procrustes ANOVA with sex and the LCS as categorical and continuous variables respectively. Although in *A. scherman* sexual differences were negligible both for size and shape (Supplementary Information, Table S4-2 and S4-3), in *A. sapidus* significant differences were found in size but not in shape (Supplementary Information, Table S4-4 and S4-5). After applying the Tukey HSD post-hoc test considering the age classes in *A. sapidus* in no case differences were significant. Thus, we assumed that sexual dimorphism was negligible in the mandible of *A. sapidus*, which is concordant with the results found in previous studies (Garde, 1992; Ventura, 1993; Ventura & Casado-Cruz, 2011). Consequently, data of both sexes were grouped in subsequent analyses. Geometric morphometric analyses were conducted with MorphoJ v.1.06d (Klingenberg, 2011) and statistical analyses using STATISTICA v.12 software (StatSoft, 2014).

#### 4.2.2. Analyses of size and allometry

Mean CS and the corresponding standard deviations were calculated between specimens of the same age class for each species. To assess the effect of age class and species on mandible size a factorial ANOVA with LCS as dependent variable was conducted. To evaluate if size was significantly different between species in each age class a Post Hoc Test (Tukey HSD test) was performed. All these analyses were carried out using STATISTICA v.12 software. To limit the occurrence of Type-I error (i.e., “false” positive) in sets of related tests, the sequential Bonferroni correction was systematically conducted (Rice, 1989).

To study allometric shape variation (i.e., shape change associated with size), a multivariate regression of shape onto the LCS was conducted in each species. Statistical significance of regressions was obtained through permutation tests with 10,000 iterations under the null hypothesis of independence between size and shape (Klingenberg, 2011). These analyses were achieved with MorphoJ v.1.06d. To investigate whether the species differ in their ontogenetic allometric trajectories, a Procrustes ANOVA, with the shape as the response variable, species as a categorical predictor, and LCS as a covariate was conducted (Goodall, 1991; Klingenberg et al., 2002; Klingenberg & McIntyre, 1998). Interspecific differences between allometric trajectories can be inferred when the interaction term (Species x LCS) from this ANOVA is significant (Zelditch et al., 2016). A randomized residual permutation procedure (RRPP) was conducted to generate statistical distributions and effect sizes (Adams & Collyer, 2009, 2007; Collyer & Adams, 2013, 2007). Because a significant interaction term was obtained in this ANOVA (see Results), further analyses were performed to test for differences in vectors of allometric coefficients. As vectors, they may differ in two geometric attributes, orientation, and length. Differences between the two species in the length and orientation of vectors of allometric coefficients were tested, respectively, by calculating the absolute difference in vector lengths (distances) and the angle between vectors (Collyer & Adams, 2007). The angle was computed considering that the cosine of the angle is the correlation between two vectors, which is calculated as the inner product between normalized vectors (Sheets & Zelditch, 2013). To test the null hypothesis that the observed angle between trajectories is no larger than might be expected by chance, a permutation test of the residuals of the reduced model with 10,000 iterations was applied (Sheets & Zelditch, 2013). These statistical analyses were carried out using the “advanced.procD.lm” function in the geomorph package (Adams et al., 2017) in R v 3.5.1 (R Development Core Team, 2016).

#### 4.2.3. *Shape variation and phenotypic trajectory analyses*

To uncover a common pattern of shape changes through the ontogeny of the two species, a between-group principal component analysis (PCA) averaging by age class was performed. This method projects data of individual specimens onto the principal components of the group averages and allows to examine the axis of greater shape variation and visualize potential separation between age groups (Boulesteix, 2005; Mitteroecker & Bookstein, 2011). A second between-group PCA was performed with the aim to reveal differences between both species in the pattern of shape changes through ontogeny. This PCA was conducted on the covariance matrix of the averages of Procrustes coordinates from specimens of the same species and age class. Procrustes distance between species were calculated from shape data and non-allometric shape data (i.e., allometric shape removed) in order to assess which shape change is not linked to size, in each age

class. All analyses were performed using MorphJ v.1.06d. In these analyses, the sequential Bonferroni correction was also conducted.

To compare mandible shape changes throughout ontogeny between the two species a phenotypic trajectory analysis approach was used (Adams & Collyer, 2009, 2007; Collyer & Adams, 2013, 2007). This approach quantifies phenotypic change from a sequence of two or multiple points of trajectory and dissects these patterns into their fundamental components: size, shape, and direction of the trajectory (Adams & Collyer, 2009; Collyer & Adams, 2013). Trajectory size is defined as the length of the trajectory through the morphospace, calculated as the sum of the distances between levels. Trajectory orientation corresponds to the general covariation of shape variables associated with a change in a variable (e.g., age), measured as an angle in degrees. Trajectory shape, which corresponds to gradual phenotypic changes over time, was measured from the deviations between the adjacent multiple points in Procrustes distances (Adams & Collyer, 2009; Collyer & Adams, 2013). In the present study a two-factor factorial model was performed, with species as groups and age classes (second factor) as trajectory points, in which the trajectories were estimated from a linear model. To compare the attributes of the trajectory (i.e., size, shape, and direction), a permutation test by residual randomization with 10,000 iterations was conducted (Adams & Collyer, 2009, 2007; Collyer & Adams, 2013, 2007). To quantify shape change trajectories, assess the variation in attributes of the trajectories via permutation, and visualize a PC scatter plot, the “trajectory.analysis” function in the R package geomorph was used (Adams et al., 2017).

#### 4.2.4. *Estimated bite force*

The bite force of each species was estimated by the index of strength ( $Z_i$ ) proposed by Freeman and Lemen (2008). This index has shown to be directly related to bite force, and it has been suggested as a surrogate when direct measurement is not possible. The incisor strength was calculated using the following formula:

$$Z_i = \frac{(\text{cranial-caudal incisive length})^2 \times (\text{medial-lateral incisive width})}{6}$$

To transform the values of  $Z_i$  to newton (N), and thus to obtain an estimated bite force, the following regression equation was used:

$$\log_{10}(\text{estimated bite force}) = 0.566 \times \log_{10}(Z_i) + 1.432$$

The cranial-caudal length and the medial-lateral width were obtained with a Mitutoyo 500-150 Digimatic Vernier Calliper (Mitutoyo America Corporation, Aurora, Illinois, USA) from a subsample of individuals that included all age classes of both species (Supplementary Information,



Table S4-6). The measurements were obtained three times, and the mean was used to reduce measurement error. The measurement of the cranial-caudal length was perpendicular to the curvature of the incisor.

Since in previous studies a dependence of estimated bite force on mandible size was detected (e.g., Borges et al., 2017; Maestri et al., 2016), a regression of  $\log_{10}$  (estimated bite force) onto the LCS was performed to assess such an association in our sample. Because estimated bite force significantly depended on mandible size (see section 4.3 Results), an ANCOVA with species as categorical factor and LCS as a continuous variable was conducted to evaluate differences in estimated bite force between species taking into account the effect of size. All analyses were performed using R v 3.5.1.

### 4.3. RESULTS

#### 4.3.1. Analyses of size and allometry

The factorial ANOVA revealed a significant effect of age class and species on mandible size, as well as a significant interaction of both factors (Supplementary Information, Table S4-7). Mandible size increased with age class in both species, being the mandibles of *A. scherman* significantly smaller than those of *A. sapidus* across all age classes (Fig. 4-2, Supplementary Information, Table S4-8).

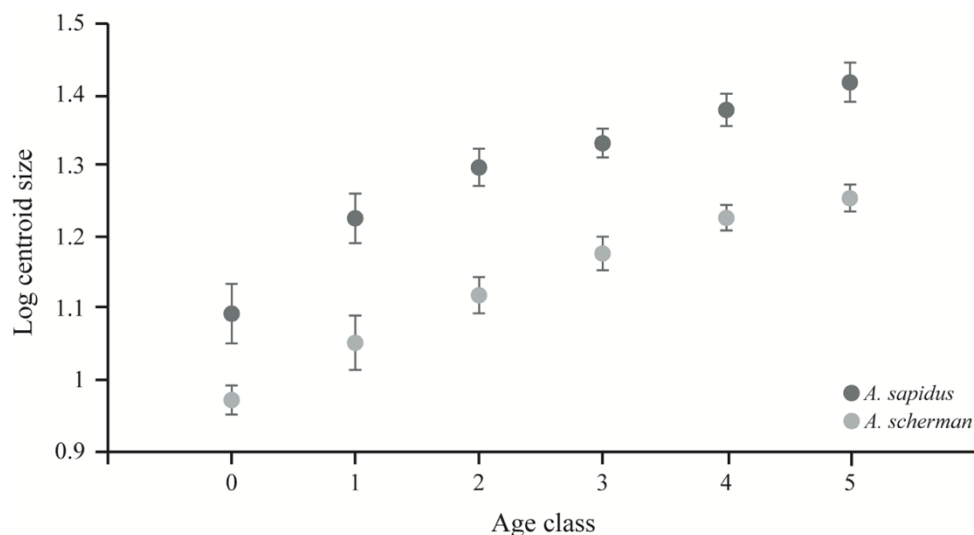


Fig. 4-2 Ontogenetic variation of the logarithm of centroid size (points: mean values, whiskers: standard deviation) of the mandible in *Arvicola sapidus* and *Arvicola scherman*.

Multivariate regressions of shape onto LCS performed within species showed a significant allometric component ( $p < 0.0001$  in both cases), with similar percentages of shape changes explained by size in both species, 26.9% and 25.7% in *A. scherman* and *A. sapidus*, respectively (Fig. 4-3). A significant effect of species, size and their interaction on mandible shape was found

in the Procrustes ANOVA (Table 4-2). The significant interaction term indicates that the shape differences between species depend on the size and suggest possible differences in the allometric trajectories. In fact, the comparison of vectors of allometric coefficients revealed significant differences in vector lengths ( $\Delta d = 0.045$ ;  $p = 0.020$ ), with *A. scherman* displaying a longer vector than *A. sapidus*, as well as in their direction ( $\theta = 35.66^\circ$ ;  $p < 0.001$ ).

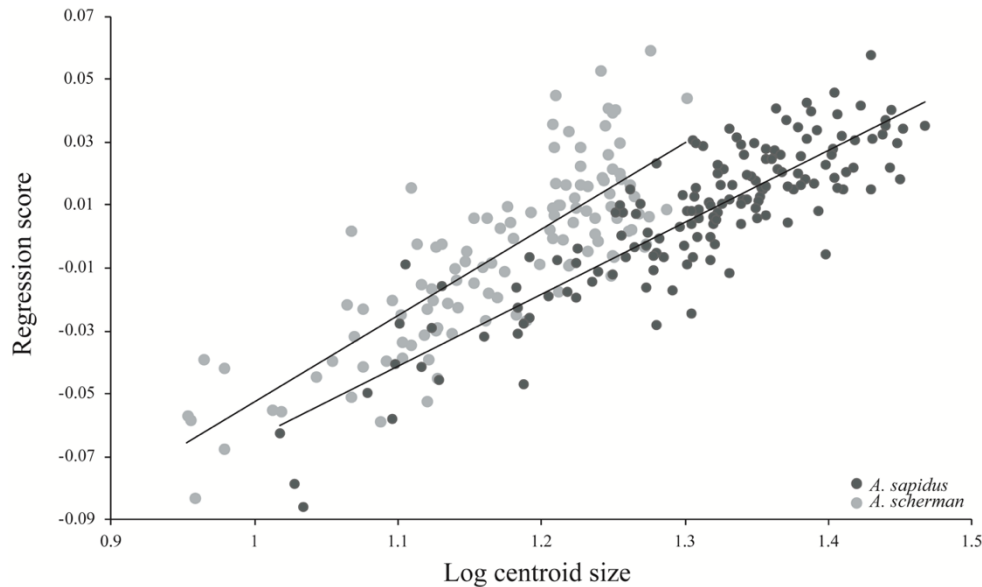


Fig. 4-3 Multivariate regression of shape onto log centroid size in *Arvicola sapidus* and *Arvicola scherman* and their respective regression lines.

Table 4-2 Results of the Procrustes ANOVA testing the effects of species, logarithm centroid size (LCS) and the interaction between them on shape conducted on the entire sample.

Effect	df	SS	MS	Rsqr	F	Z	p
Species	1	0.138	0.138	0.223	103.699	8.842	<0.001
LCS	1	0.114	0.114	0.184	85.749	8.577	<0.001
Species x LCS	1	0.012	0.012	0.020	9.300	4.482	<0.001
Residuals	267	0.356	0.001	0.573			
Total	270	0.621					

Abbreviations: *df*, degrees of freedom; *SS*, sum of squares; *MS*, mean squares; *Rsqr*, R squared values; *F*, F statistic; *Z*, effect-size; *p*, *p*-value.

#### 4.3.2. Shape variation and phenotypic trajectory analyses

The between-group PCA conducted on the covariance matrix of the Procrustes coordinates averaged by age class revealed a common pattern of shape changes associated with age class in both species. Along the first principal component (PC1), which explained 48.8% of total mandible shape variation, shape changed with age class (Fig. 4-4). On the other hand, along the second principal component (PC2), which explained 12.8% of variation, shape changed in the positive direction from age class 0 to age class 2, and then in the negative direction from age class 3 to age class 5. Shape changes along PC1 take place principally in the ventral part of the mandible, the

condylar process and the alveolar region of the incisor. Main shape variations along PC2 occurred mainly in the angular and coronoid processes, and the incisor alveolus.

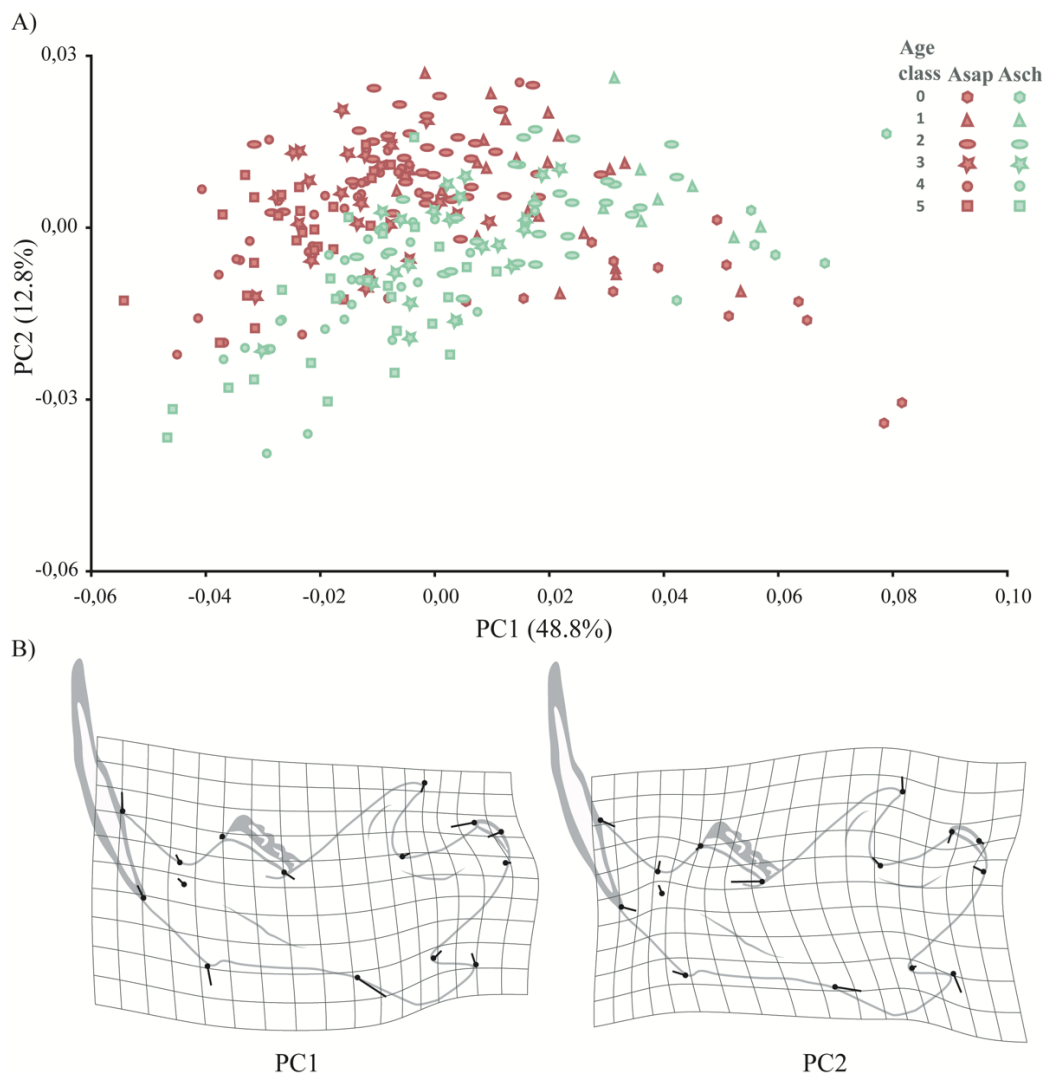


Fig. 4-4 A) Scatter plot of PC1 versus PC2 scores from PCA averaged by age class (Asap – *Arvicola sapidus*; Asch – *Arvicola scherman*). B) Displacement vectors and deformation grids of shape changes along PC1 and PC2 axes. Scale factor: 0.1 units in a positive direction from the consensus (outlines and center of coordinates).

The between-group PCA conducted on the covariance matrix of Procrustes coordinates average by species and age class, revealed a clear spatial distribution of species and gradual separation of the age classes along the first two principal components (PC1 and PC2, Fig. 4-5). PC1 accounted for 41.7% and PC2 for 23.4% of the total mandible shape variation. Shape changes along PC1 were associated with age class and consequently, coincide with the changes mentioned in the PC1 of between-group PCA average by age class. Variation along PC2 was related to interspecific differences, in which shape changes were mainly in the ventral part of the mandible, the condylar and angular processes, and the incisor alveolus. Procrustes distances between species were significant for all age classes (Table 4-3) in both shape data and non-allometric shape data.

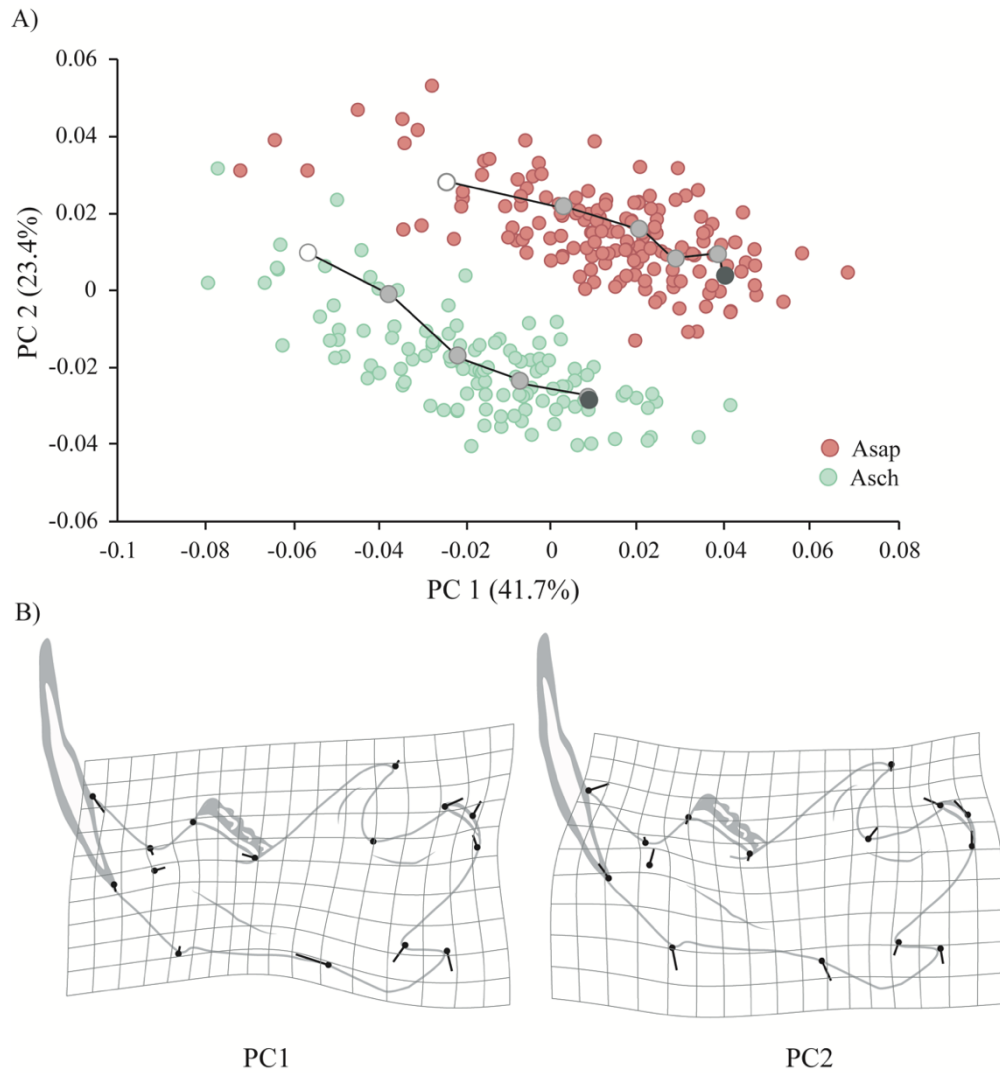


Fig. 4-5 A) Scatter plot of PC1 versus PC2 scores from PCA averaged by species and age class, according to species. The larger circles correspond to the means of each age class (Asap – *Arvicola sapidus*; Asch – *Arvicola scherman*). B) Displacement vectors and deformation grids of shape changes (eigenvectors) along PC1 and PC2 axes. Scale factor: 0.1 units in a positive direction from the consensus (outlines and center of coordinates).

Table 4-3 Procrustes distance between *Arvicola sapidus* and *Arvicola scherman* in each age class and associated *p*-values.

Age class	Procrustes distances			
	Raw data	<i>p</i> -value*	Size-corrected data	<i>p</i> -value*
0	0.045	<0.001	0.057	<0.001
1	0.050	<0.001	0.058	<0.001
2	0.054	<0.001	0.059	<0.001
3	0.049	<0.001	0.075	<0.001
4	0.050	<0.001	0.064	<0.001
5	0.049	<0.001	0.056	<0.001

\*After sequential Bonferroni correction.

In terms of phenotypic trajectories, no significant differences were found between species either in size ( $\Delta d = 0.001$ ;  $p = 0.922$ ) or shape of the trajectories ( $D_p = 0.211$ ;  $p = 0.201$ ). However, significant differences were detected in the orientation of the trajectories ( $\theta = 34.01^\circ$ ;  $p < 0.001$ ).

#### 4.3.3. Estimated bite force

The linear regression of  $\log_{10}$  (estimated bite force) onto the LCS showed that estimated bite force is significantly related to mandible size (87.9%;  $p < 0.0001$ ; Fig. 4-6). The ANCOVA confirmed this association, and highlighted significant differences between species, but not a significant interaction term (Table 4-4). Specifically, in *A. scherman* the estimated bite force was significantly higher than in *A. sapidus* (Mean *A. scherman* = 1.376 N, Mean *A. sapidus* = 1.271 N).

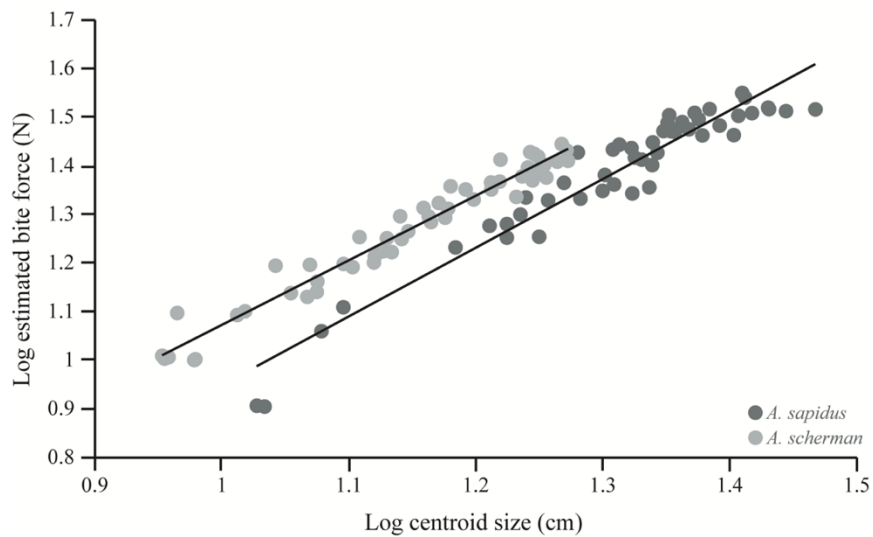


Fig. 4-6 Regression analysis between the logarithm of estimated bite force (N = newton) and the logarithm of centroid size for *Arvicola sapidus* and *Arvicola scherman* their respective regression lines.

Table 4-4 Results of the ANCOVA performed to test for the effect of logarithm centroid size (LCS) and species on log estimated bite force.

Effect	<i>df</i>	SS	MS	F	<i>p</i>
LCS	1	2.064	2.064	1779.996	<0.001
Species	1	0.166	0.166	143.226	<0.001
LCS x Species	1	0.002	0.002	1.518	0.221
Residuals	102	0.118	0.001		

Abbreviations: *df*, degrees of freedom; SS, sum of squares; MS, mean squares; F, F statistic; *p*, *p*-value

#### 4.4. DISCUSSION

##### 4.4.1. *Common ontogenetic phenotypic changes in the mandible of semiaquatic and fossorial water voles*

The mammalian mandible is a complex structure whose form changes along ontogeny are the result of complex interactions between extrinsic and intrinsic factors that can differ among species. However, conserved developmental pathways may cause different species to share similar phenotypic modifications during growth. According to our results, in spite of significant differences during the postweaning ontogeny of the mandible form between *A. sapidus* and *A. scherman*, both taxa show a similar variation pattern of this structure during this period. In particular, most important shape changes occurred during the juvenile stage, dynamics that seems to be a conservative feature in the ontogenetic development of the mammalian mandible (see e.g., Cardini & Tongiorgi, 2003; Christiansen, 2012; Fuchs et al., 2015; Martinez-Maza et al., 2012; Menegaz & Ravosa, 2017). Our analyses revealed important shape changes in the angular and condylar processes of the mandible of young individuals of *A. sapidus* and *A. scherman*, modifications that can be interpreted as an adaptation to the new post-birth food needs (Cardini & Tongiorgi, 2003; Martinez-Maza et al., 2012; Martínez-Vargas et al., 2017). In fact, mandible shape changes associated with the transition to a different type of diet in juvenile water voles were already suggested for *A. scherman* (Ventura & Casado-Cruz, 2011), and the results of the present study also support this relationship for *A. sapidus*. In rodents, this change of diet has been related to an increase in the muscular load exerted by the masticatory muscles (Enomoto et al., 2010; Menegaz & Ravosa, 2017). In this context some lines of evidence support that mechanical forces exerted by the masticatory muscles can promote significant modifications of the mandible shape (Ödman et al., 2008), and also an increase of the bite force (Cox et al., 2015). Nevertheless, the characteristics of our study do not allow us to unravel the interaction between the functional and programmed developmental factors involved in these phenotypic changes.

Another pattern of mandible shape variation shared by *A. sapidus* and *A. scherman* was observed in the between-group PCA averaged by age class. Specifically, from age classes 0 - 2 shape changes in PC2 occur in the positive direction, involving a shortening and a flattening of the diastema, a dorsal expansion of the coronoid process, a ventral expansion of the angular process and an expansion of the ventral surface; while from age class 3 - 5 the opposite changes occur. On the one hand, this pattern could be linked, at least in part, to bone histomorphogenesis. Thus, in the house mice (*Mus musculus*) it has been observed that the most rapid and active growth occurs during the first eight postnatal weeks (Martinez-Maza et al., 2012; see review Zoetis et al., 2003) and that bone resorption increases between six and eight postnatal weeks (Martínez-Vargas et al.,

2017) coinciding with age class 2. While these similarities may suggest the existence of conserved patterns of bone remodelling of the mandible, histological studies of these species and further ontogenetic analyses on other rodents are needed to test this hypothesis. On the other hand, this pattern could be due to the heterogeneous time intervals of the age classes established. Thus, whereas each time interval of the first four age classes is only of few weeks, that of the two higher classes is markedly wider and less accurate. This suggests that the shape variation during adulthood actually occurs more slowly than can be deduced, in principle, based on inspection of the PCA plot.

#### 4.4.2. Differences in the postweaning growth of the mandible between semiaquatic and fossorial water voles

##### **Size changes**

The mandible size of *A. scherman* is lower than that of *A. sapidus*, along the whole postnatal ontogeny. In the former species, small body size is associated with an adaptation to hypogeic life (Cubo et al., 2006). Large bodies lead to more substantial digging costs (Vleck, 1979), which leads to a trade-off between size increase and metabolic economy in burrowing (Borges et al., 2017). It has been suggested that the diminution of the size becomes an advantage for a fossorial animal (White, 2005). For example, in the case of pocket gophers (*Thomomys*), the reduction of body size allows minimizing the volume of soil moved (Marcy et al., 2016). The decrease of body size is associated with the consumption of energy that a fossorial animal spends to move, since this energy is much higher than that spent by an epigeic animal to travel the same distance below ground (Vleck, 1979; White et al., 2006). In the case of *A. scherman*, the energy demand resulting from underground life is so high that it leads to a daily food consumption equivalent to its body mass (Quééré, 2009). Therefore, once the energy required for locomotion in *A. scherman* is very high, the canalization of energy limits its body size.

##### **Shape changes**

Results obtained in the present study reveal significant ontogenetic differences in the mandible shape between both water vole taxa, and confirm the pattern of phenotypic variation previously described in *A. scherman* (Ventura & Casado-Cruz, 2011). The study of allometric shape changes indicate that the patterns of mandible growth differ between the two species. In particular, *A. scherman* showed a longer vector of allometric coefficients than *A. sapidus*, indicating a higher rate of allometric shape change along postnatal ontogeny in the former species. The direction of the vectors of allometric coefficients was also significantly different between the two taxa, showing that the relative covariations of shape variables per unit of change size differ between them. It is

expected that phylogenetically close and morphologically similar species have low angles and differ little in their allometric trajectories (Zelditch et al., 2016). For example, in the work by Zelditch et al. (2016) the angle found for *Callospermophilus lateralis* and *Otospermophilus variegatus*, was 16.39°. In the present study, the angle between the vectors of allometric coefficients of *A. sapidus* and *A. scherman* was of 35.66°, a relatively high value considering that both species belong to the same genus. The phenotypic trajectories of the two water vole taxa, which describe allometric and non-allometric shape changes along age classes, differed in their direction, but not in their length and shape. These results suggest that the two species differ in the type, but not in the amount, of mandible shape changes. The angle between phenotypic trajectories was very similar to that between vectors of allometric coefficients. In fact, most of the shape changes along ontogeny are allometric. In this way, differences in the allometric and phenotypic trajectories indicate that mandibles of *A. sapidus* and *A. scherman* display different size-related shape changes and different growth dynamics.

Morphological distances between *A. sapidus* and *A. scherman* were significant throughout the ontogenetic series, both shape data and non-allometric shape data analyses. Values of non-allometric shape data were greater than values obtained with shape data, which suggests that in spite of different allometric trajectories a part of allometric shape changes is shared between the two taxa. When comparing the adult mandible shape between *A. sapidus* and *A. scherman*, several differences were noted. In particular, the latter species shows a relatively longer diastema with a marked angular profile. This feature allows an increase in the contact area with the soil and a more efficiently entry of the incisor into the soil (Ventura & Casado-Cruz, 2011; and references therein). Moreover, the more compact mandibular ramus and the more pronounced curvature of the angular process in *A. scherman* seem to be concordant with a more robust and efficient structure to fix the muscle insertion (Cardini & Tongiorgi, 2003; Kesner, 1980; Stein, 2000). The elongation of the diastema is linked to the muscle attachment in the ascending ramus since the propulsive force to remove the soil results from the action of different masticatory muscles (masseter, temporalis, internal and external pterygoids). The largest masticatory muscle of rodents is the masseter, which is divided into four portions: the superficial masseter, the deeper masseter, the anterior deep masseter, and the anterior deep masseter infraorbital part (Sato, 1997). From all masticatory muscles, the deeper masseter is estimated to exert the largest force. This muscle originates along the ventral surface of the zygomatic arch and inserts into the lateral side of the angular process and the mandibular ramus. Shape changes detected in this region of the mandible in *A. scherman* could be related to the high strength of this muscle. In fact, shape variation in the angular and condylar process between semifossorial and semiaquatic rodent species have been reported in another study (Perez et al., 2009). Besides that, the increased mass of the masseteric muscle also is consistent with the widening of the zygomatic arc in *A. scherman* (see, e.g., Cubo et



al., 2006), and can explain the higher estimated bite force value found in this species respect to *A. sapidus*. In this sense, Maestri et al. (2016) noted that in small mammals a shorter coronoid process, a more extensive condyloid process, a wider and shorter angular process, and a shorter and more curved diastema might provide a stronger bite force. All these features can be observed in *A. scherman*.

Several studies have shown that the rodent mandible can be rapidly shaped by different feeding strategies and food consistency, exhibiting a strong relation between shape and diet (Anderson et al., 2014; Mavropoulos et al., 2005, 2004; Michaux et al., 2007; Renaud et al., 2010; Tanaka et al., 2007; Yamada & Kimmel, 1991). Because both *A. sapidus* and *A. scherman* are strictly herbivorous (see, e.g., Kopp, 1993; Saucy, 1999; Ventura, 2007), it can be assumed that the load exerted by the muscles in relation to the consistency of the food is similar in both species, and consequently that the diet has a negligible effect on the interspecific differences in mandible shape.

Perez et al. (2009) suggested that the shape divergence of mandible morphology between semifossorial and semiaquatic species of the family Echimyidae is significantly associated with ecological factors, namely features related to digging activities. Therefore, the environment factor may play a major role in shaping morphological variation and lead relatively close species to exhibit different phenotypic trajectories (e.g., Esquerré et al., 2017). Considering that the mandible of *A. scherman* shows similar traits to those reported for other digging rodent species (e.g., Álvarez et al., 2011; Laville et al., 1989; Nevo, 1979; Stein, 2000), and that these characteristics are not present in the mandible of *A. sapidus*, we suggest that the differences in mandible morphology between these *Arvicola* taxa are the result of adaptations to the selective pressure exerted by the subterranean life in *A. scherman* (Álvarez et al., 2011; Rodrigues et al., 2016). Whether these differences are the result of a plastic response during postnatal ontogeny to the digging process or are already genetically fixed in the developmental pattern of *A. scherman* remains to be elucidated, since soon after weaning individuals of this species show an innate digging behaviour, which in turn is identical to that in adults (Airoidi et al., 1976).

Bone morphology is not static and may change due to extrinsic stimuli throughout the life of the animal (Herring, 2003). In this way, previous results obtained in *A. scherman* seem to indicate that mandible shape changes occurring during adulthood could be related to the mechanical stress produced by persistent digging activity (Ventura & Casado-Cruz, 2011). In the present work, both results of ontogenetic trajectory and Procrustes distances do not support this hypothesis. However, a greater dispersion of shape for given size was detected in age classes 4 and 5 in *A. scherman* in relation to *A. sapidus* (Fig. 4-3). This fact may be related to the wide and not precise time intervals of age classes 4 and 5; in fact, individuals classified in different age classes may find themselves temporarily separated for a short period of time. On the other hand, the shape

dispersion found in age class 5 in multivariate regression analysis, may suggest that the most dispersed individuals correspond to the older ones. Anyway, only ontogenetic or functional studies based on a precise knowledge of the age of the individuals can really elucidate if a longer digger activity would lead to a greater change in mandibular shape in adult fossorial water voles.

#### 4.5. CONCLUSION

The comparison of postweaning ontogenetic series of closely related species with different ecology and type of locomotion is at the core of how ecological factors can influence the evolutionary process. Results here obtained reveal that semiaquatic *A. sapidus* and fossorial *A. scherman* show significant differences in the growth, phenotypic trajectories, and estimated bite force. These findings allowed us to shed light on the effect that these two different types of locomotion have on postweaning growth of the mandible in phylogenetically close species. It would be very interesting to develop further studies to assess the effect that digging and swimming might have on other bone structures that play an essential role in these functions, such as the cranium, scapula, and forelimbs (e.g., in the digging process) and the pelvic girdle and hind limbs (e.g., in swimming). Likewise, adding more *Arvicola* taxa in comparative analyses on the form variation of all these structures would be essential to detect phylogenetic and functional signals in the evolution of the locomotor skeleton in this genus.

4.6. SUPPLEMENTARY INFORMATION

Table S4-1 Description of the 15 landmarks used in the geometric morphometric analyses.

Landmark	Description
1	Dorsal-most point on incisor alveolar
2	Point of maximum curvature of incisor ramus
3	Cranial edge of the molar alveolar process
4	Intersection of molar alveolar and base of coronoid process
5	Most dorsal point of coronoid process
6	Point of maximum curvature between the coronoid and condyloid processes
7	Most cranial point of the condylar process
8	Most caudal and dorsal point of the condylar process
9	Most caudal point of the condylar process
10	Most cranial point of the angle that separates the condyloid and angular processes
11	Caudal-most point of the angular process
12	Cranial-most point of the angular process along the ventral surface of the mandible
13	Caudal-most tuberosity of the insertion site of mandibular transverse muscle
14	Ventral-most point on incisor alveolar
15	Mental foramen

Table S4-2 Factorial ANOVA statistical assessment of the effects of age class, sex and the interaction between them on mandible size conducted on the *Arvicola sherman* sample.

Effect	df	SS	MS	F	p
Age class	5	0.687	0.137	259.6	0.000
Sex	1	0.001	0.001	0.9	0.341
Age class x Sex	5	0.008	0.002	3.0	0.015
Residuals	106	0.056	0.001		

Abbreviations: *df*, degrees of freedom; SS, sum of squares; MS, mean squares; F, F statistic; Z, effect-size; *p*, *p*-value.

Table S4-3 Results of the Procrustes ANOVA performed for *Arvicola sherman* sample testing the effects of sex, logarithm centroid size (LCS) and the interaction between them on shape conducted on the entire sample.

Effect	df	SS	MS	Rsq	F	Z	p
LCS	1	0.058	0.058	0.269	42.659	5.539	0.01
Sex	1	0.001	0.001	0.007	1.052	0.549	0.29
LCS x Sex	1	0.001	0.001	0.004	0.697	-0.346	0.65
Residuals	114	0.154	0.001	0.720			
Total	117	0.214					

Abbreviations: *df*, degrees of freedom; SS, sum of squares; MS, mean squares; Rsq, R squared values; F, F statistic; Z, effect-size; *p*, *p*-value.

Table S4-4 Factorial ANOVA statistical assessment of the effects of age class, sex and the interaction between them on mandible size conducted on the *Arvicola sapidus* sample.

Effect	df	SS	MS	F	p
Age class	5	1.154	0.231	299.0	0.000
Sex	1	0.005	0.005	6.1	0.014
Age class x Sex	5	0.003	0.001	0.7	0.649
Residuals	136	0.105	0.008		

Abbreviations: *df*, degrees of freedom; SS, sum of squares; MS, mean squares; F, F statistic; *p*, *p*-value.

Table S4-5 Results of the Procrustes ANOVA performed for *Arvicola sapidus* sample testing the effects of sex, logarithm centroid size (LCS) and the interaction between them on shape conducted on the entire sample.

Effect	df	SS	MS	Rsqr	F	Z	p
LCS	1	0.066	0.066	0.253	49.822	6.203	0.01
Sex	1	0.002	0.002	0.008	1.529	1.287	0.07
LCS x Sex	1	0.002	0.002	0.009	1.785	1.200	0.14
Residuals	144	0.192	0.001	0.730			
Total	147	0.262					

Abbreviations: *df*, degrees of freedom; SS, sum of squares; MS, mean squares; Rsqr, R squared values; F, F statistic; Z, effect-size; *p*, *p*-value.

Table S4-6 The sample size used for bite force analysis by species, age class and sex.

Species	Sex	Age class						Total
		0	1	2	3	4	5	
<i>Arvicola sapidus</i>	F	2	5	5	4	5	5	26
	M	2	4	5	5	5	5	26
<i>Arvicola scherman</i>	F	3	4	5	5	5	5	27
	M	3	4	5	5	5	5	27
Total		10	17	20	19	20	20	106

Table S4-7 Factorial ANOVA statistical assessment of the effects of species, age class and the interaction between them on mandible size conducted on the whole sample.

Effect	df	SS	MS	F	p
Age class	5	1.718	0.344	485.0	<0.001
Species	1	1.273	1.273	1797.8	<0.001
Age class x Species	5	0.015	0.003	4.2	<0.001
Residuals	259	0.183	0.001		

Abbreviations: *df*, degrees of freedom; SS, sum of squares; MS, mean squares; F, F statistic; *p*, *p*-value.

POSTNATAL ONTOGENY OF THE MANDIBLE

Table S4-8 Mean centroid size and standard deviation of the mandible in *Arvicola sapidus* and *Arvicola scherman* in different age classes and associated *p*-values.

Age class	Centroid size (cm)		<i>p</i> -values*
	<i>Arvicola sapidus</i>	<i>Arvicola scherman</i>	
0	2.98 ± 0.13	2.65 ± 0.06	<0.001
1	3.41 ± 0.12	2.87 ± 0.11	<0.001
2	3.67 ± 0.09	3.06 ± 0.08	<0.001
3	3.79 ± 0.08	3.25 ± 0.08	<0.001
4	3.97 ± 0.09	3.41 ± 0.06	<0.001
5	4.13 ± 0.12	3.51 ± 0.07	<0.001
mean	3.73 ± 0.33	3.24 ± 0.25	<0.001

\*After sequential Bonferroni correction.

---

# CHAPTER 5

OBTAINING THREE-DIMENSIONAL MODELS OF LIMB  
LONG BONES FROM SMALL MAMMALS: A  
PHOTOGRAMMETRIC APPROACH

**Ana Filipa Durão, Francesc Muñoz-Muñoz,  
Jessica Martínez-Vargas, Jacint Ventura**

---

The content of this chapter is part of a book chapter in:  
Geometric morphometrics. Trends in biology, paleobiology and  
archaeology (2018), pp. 125–138  
ISBN (Electronic): 978-84-944730-3-6

---



## CHAPTER 5. OBTAINING THREE-DIMENSIONAL MODELS OF LIMB LONG BONES FROM SMALL MAMMALS: A PHOTOGRAMMETRIC APPROACH

---

### 5.1. BACKGROUND

#### 5.1.1. 2D vs 3D landmark data in form studies

Geometric morphometrics is the statistical analysis of biological form based on two-dimensional (2D) or three-dimensional (3D) Cartesian landmark coordinates (Mitteroecker & Gunz, 2009). In a morphometric context, landmarks are discrete anatomical loci that can be reliably recognised as the same loci in all specimens under study (Zelditch et al., 2004). Although some biological structures are virtually 2D (e.g., insect wings), organisms and their parts are predominantly 3D objects. Therefore, it would seem reasonable that most geometric morphometric studies should use 3D landmarks to assess form variation. In contrast, many 3D biological structures have been studied using 2D images because of the simplicity, efficiency and reduced cost of this technique (Cardini, 2014; Gould, 2014; Muñoz-Muñoz et al., 2016). This practice, however, entails some problems such as measurement error, loss of important information, and a possible misinterpretation of real shape changes (Buser et al., 2017; Cardini, 2014; Chiari et al., 2008). These drawbacks are especially remarkable in structures with an important 3D component (Cardini, 2014). In fact, while a considerable degree of concordance between 2D and 3D datasets has been detected regarding the patterns of size and shape variation of rather flat structures, such as the mandible of the marmot or the mouse, this concordance has been less evident in highly 3D structures, such as the skull of the marmot or the sculpin (Buser et al., 2017; Cardini, 2014; Navarro & Maga, 2016). These results warn about employing 2D landmarks to assess form variation of highly 3D structures, especially at the intraspecific level (Cardini, 2014).

While the use of 2D images to measure morphological variation of 3D biological structures is a widespread practice that will likely continue for several years (Cardini, 2014), the number of published studies that use 3D landmarks has increased steadily since the development of geometric morphometrics. This trend is illustrated in Fig. 5-1, which shows how the number of 3D geometric morphometric studies has evolved between the years 2000 and 2017<sup>1</sup>. The rise of 3D

---

<sup>1</sup> The graphs were constructed from the number of publications included in all databases of *Web of Science* containing as a topic “geometric morphometrics” only, and both “geometric morphometrics” and “3D” simultaneously. In order to include the maximum number of published articles on these topics, terminological variants were included in the search with the connector “or”: the variants “geometric morphometrics” and “geometric morphometric”, and “3D”, “three-dimensional”, and “three dimensional” were considered. Containing these words as a topic was regarded as indicative of the methodology followed in the article. However, it should be taken into account that a detailed analysis of the literature was not carried out to verify if the articles including these words as a topic actually used these methodologies.



geometric morphometric studies might have several reasons, among which there might be the generalised perception among researchers that using data of the proper dimensionality would improve the results. However, the increasing availability and precision of 3D technologies probably also plays a prominent role in the expansion of this approach. The first 3D geometric morphometric studies almost exclusively obtained landmarks from “big” mammalian skeletal structures, such as the skull of primates or carnivores, with the aid of 3D coordinate digitisers (e.g., O’Higgins & Jones, 1998; Reig et al., 2001). Since then, the technologies to obtain 3D landmarks directly from the object or, alternatively, to obtain 3D models from which landmarks can be recorded, have developed and diversified enormously, and at present allow us to obtain 3D landmarks from a vast array of biological structures.

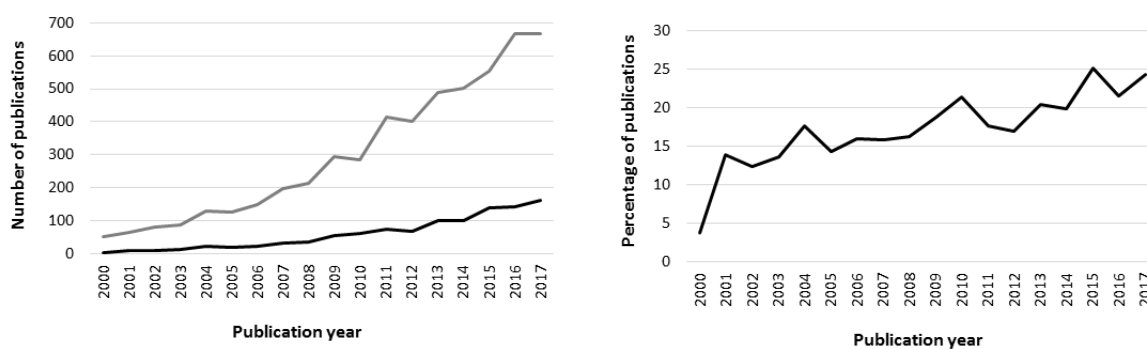


Fig. 5-1 Evolution of the number of 3D geometric morphometric studies from the year 2000 to 2017. The upper panel shows the increase in the total number of geometric morphometric studies (black line) and in the number of 3D geometric morphometric studies (grey line). The lower panel shows the change in the percentage of the latter in relation to the former.

### 5.1.2. The particular case of small mammals

Over the last two decades, the use of 3D landmarks has showed an increasing trend, becoming the standard methodology in fields such as anthropology and biomedical research. However, this tendency seems to be somewhat slower in certain groups of animals, as is the case with small mammals<sup>2</sup>. A possible explanation for this fact is that devices precise enough for accurate 3D digitization of tiny objects have a high cost (Muñoz-Muñoz et al., 2016). Nonetheless, this seems to be changing with the increasing variety and accessibility of 3D technologies. Towards the end of the twentieth century, some pioneer studies already employed sets of photographs and statistical methods to obtain 3D landmarks from skulls of small mammals (Fadda & Corti, 2001;

---

Moreover, the search was not exhaustive, and therefore these graphs should be contemplated as approximate.

<sup>2</sup> The term *small mammals* does not correspond to any taxonomic category or natural group of mammals. This term is usually used to refer to members of the orders Rodentia, Eulipotyphla and Scandentia, in which the majority of species are small-bodied as compared to most other mammals. Here we use the term *small mammal* to refer to those mammalian species whose skull length is around, or smaller than, 50 millimetres.

Fadda et al., 1997). The methodology followed in these studies involved sets of complex instruments or entailed constraints on the positioning of the objects under study. Maybe for these reasons, this methodology was not generally adopted, and studies of shape variation in small mammals conducted during the following years were mainly based on 2D landmarks recorded on different views of the structure under analysis (e.g., Fernandes et al., 2009; Kamilari et al., 2013; Monteiro et al., 2003; Sans-Fuentes et al., 2009; Wilson, 2013; Yazdi & Adriaens, 2013). More recently, a growing number of studies have employed 3D landmarks to assess form variation of the skull of small mammals (e.g., Attanasio et al., 2013; Cornette et al., 2013; Evin et al., 2011; Gomes-Rodrigues et al., 2016; Martínez-Abadías et al., 2013; McIntosh & Cox, 2016a, 2016b; Navarro & Maga, 2016; Parsons et al., 2014). Because of its complexity and biological importance, the mammalian skull (comprising the cranium and the mandible) is a model structure for the study of morphological variation. Moreover, some species of small mammals, such as the mouse or the rat, are model species in the fields of biomedical research and evolutionary biology. These two factors might explain why analyses of morphological variation of the skull of model species seem to be leading the shift from 2D to 3D. Lately, the form of post-cranial bones, such as limb long bones, of small mammals has also been analysed using 3D data (Caskenette et al., 2016). However, most of the published works analysing the form of post-cranial bones in these mammals are still mainly based on 2D pictures (e.g., Echevarría et al., 2014; Marcy et al., 2016; Morgan et al., 2017). Because of the important 3D component of these bones and the difficulty in orienting them in a plane, the use of 3D data to analyse their form seems, at least, appealing. In addition, since the high cost of the devices precise enough for 3D digitization of small objects is a possible cause of the predominance of 2D over 3D studies, the development of more affordable techniques to recover 3D shape of these bones would be of interest.

### 5.1.3. *Photogrammetry: An affordable and versatile solution*

Several technologies to obtain 3D landmarks are currently available, such as coordinate digitisers (e.g., Microscribe™ and Polhemus™), reflex microscopes, automated precision measurement systems (e.g., Micro-Vu Vertex Multisensor Measuring Center™), computed tomography, 3D scanners (including contact scanners, laser scanners, and structured light scanners), and photogrammetry. Of course, each of these techniques has its advantages and drawbacks, and the suitability of each one depends on the particular circumstances, including specific features of the object under study (e.g., the type, its size, its surface), the place where the data or the model will be obtained, or the preferences of the researcher. For example, coordinate digitisers, reflex microscope, and Micro-Vu Vertex allow 3D landmarks to be obtained directly from the object, whereas 3D scanners, computed tomography, and photogrammetry generate 3D digital models or surfaces from which landmarks can be recorded. Having *in silico* models may be interesting when

## PHOTOGRAMMETRY APPROACH

the sample is not easily accessible, as is the case with museum specimens or wild animals, because once you have obtained the model it is always available. This makes it feasible to obtain additional data or revise possible errors without the need to get back to the real specimen. Performing a detailed enumeration and analysis of the pros and cons of each of these technologies is out of the scope of this chapter. However, when the budget is limited, the choice of which technology to use in order to obtain 3D data from tiny objects depends on two main factors, namely the precision of the device and its cost, which tend to be positively associated. Of course, other factors, such as the time needed to obtain the data or the usefulness of the technology in future studies, might also be important when deciding which technology to employ. In this context, we consider photogrammetry a very interesting tool, since it is economical and versatile. Stereophotogrammetry (or photogrammetry for short) estimates 3D coordinates of points on an object using measurements made on two or more 2D images taken from different positions. Thus, the basic equipment needed for photogrammetry consists of a digital camera and specialised software. Because these components have a considerably lower cost than other devices for obtaining 3D data, photogrammetry is usually considered a low-cost method (Chiari et al., 2008; Katz & Friess, 2014; Muñoz-Muñoz et al., 2016). In fact, since some specialised software is freely available on the web and digital cameras are widely accessible, photogrammetry can be performed at virtually no cost. However, obtaining precise models of small objects requires specific photographic material, which increases the overall cost of the technique. Moreover, free software usually offers limited versions of payment software, or only perform some of the utilities of the latter, which at the end implies either using a complex set of specialised programs or buying licensed software. In this study, we used the software PhotoModeler Scanner (Eos System Inc, 2014), which is commercial software with a life-long license currently listed at \$2,995. When compared with that of other technologies, this cost is still limited (Katz & Friess, 2014). However, comparison of costs should be taken with caution since it can change considerably with time. In addition to being cost-effective, photogrammetry has other advantages. One of the most remarkable ones is its versatility. We consider photogrammetry a highly versatile tool for two main reasons. First, photogrammetry allows us to obtain precise 3D models from structures of virtually any size, from earth surface regions (e.g., Haneberg, 2008) to microscopic objects (e.g., Ball et al., 2017; Eulitz & Reiss, 2015). Second, photogrammetry can be performed in a wide range of conditions and places, from the field to the lab or the museum. As a result, we can use photogrammetry to perform studies of very different organisms only adapting the technique to the particular situation by adding or changing some specific devices to the equipment. For example, if we want to obtain the 3D model of a small object (e.g., the skull of a mouse), then a macro lens and a tripod, or another type of camera support, will be indispensable.

Photogrammetry has been widely used in disciplines such as geomorphology, architecture or archaeology. In the field of morphometrics, its possible advantages were already highlighted more than three decades ago (Jacobshagen, 1981). However, studies have only recently started using photogrammetric techniques to recreate 3D models of human (e.g., Hasset & Lewis-Bale, 2017; Katz & Friess, 2014; Quinto-Sánchez et al., 2018) or animal (e.g., Aristide et al., 2013; Chiari et al., 2008; Evin et al., 2016; Falkingham, 2012; Muñoz-Muñoz et al., 2016) phenotypes. Although it is common to combine photogrammetric techniques with macro photography to generate 3D models of small objects in disciplines such as archaeology (e.g., Gajski et al., 2016; Marziali & Dionisio, 2017; Yanagi & Chikatsu, 2010), as far as we know this approach has not been applied to the study of form variation of limb long bones in small mammals. Considering the interest in using 3D data to analyse form variation, and the advantages that photogrammetry offers in recreating small 3D objects, the aim of this study was to establish a protocol that would allow the construction of 3D models of limb long bones from small mammals being appropriate for geometric morphometric analyses. The technical details to obtain the 3D models can be found in the following two sections. In section 5.2 we present a list of the equipment employed in this study and their specific utilities in the context of macro photography, whereas in section 5.3 we perform a detailed description of the imaging protocol. In order to test the usefulness of the resulting 3D models to analyse form variation, in section 5.4 we present a practical case in which we compare the 3D form of the humerus of two different species of the genus *Arvicola*, one fossorial and one semiaquatic, by means of standard geometric morphometric analyses. This case study is performed with a small sample and does not intend to be a detailed analysis of form variation between the two species. It aims to unveil the main size and shape differences of the humerus between the two species and compare the results with previous descriptions.

## 5.2. THE EQUIPMENT

### 5.2.1. *The camera and the lens*

When performing photogrammetric 3D reconstructions, the result is entirely dependent on the quality of the photos, so choosing the right camera (or set of cameras) is essential. Almost any camera can be useful to construct 3D models of “big” objects, but when it comes to obtaining precise 3D models of tiny objects it is worth considering to use a digital single-lens reflex (DSLR) camera. The maximum resolution that can be achieved depends, among other things, directly on the number of megapixels the camera has. Professional DSLR cameras give optimal results, but they are very expensive; however, the pictures obtained with mid-priced DSLR cameras yield very good models as well. Although a high resolution is very important, other camera features are to be considered. For example, in macro photography it is crucial to avoid camera vibration during

## PHOTOGRAMMETRY APPROACH

the capture of the picture. Therefore, that a remote trigger can be connected to the camera or, alternatively, that the camera has a delayed-action shutter function, is mandatory (see section 5.2.2). Another interesting camera feature is the possibility to flip and rotate the screen, because it facilitates taking pictures with the camera in any position.

The lens is also an important component of the equipment, especially when we intend to take pictures of small objects. In such a case, the best solution is to use a macro lens. Fixed focal length lenses are preferable for photogrammetry, because they maximise the quality of the photographs and prevent any accidental variable focal lengths, which may occur with a zoom lens. As occurs with the camera, the better the lens, the better the result. Unfortunately, though, also the higher the cost. However, good macro lenses are available at a reasonable cost, being 1:1 macro lenses an interesting option. A magnification ratio of 1:1 means that when the camera is positioned at the closest focus distance, the image formed on the sensor will be the same size as the subject. This magnification is achievable only at the very closest focus distance, which might be a problem in some particular situations (for example, if we want to take photographs of free-moving animals, because they will probably escape).

It is also interesting to add a polarising filter to the lens, because it reduces reflections on shiny surfaces, which is the case with bones. In this study, we used a Canon EOS 750D DSLR camera (24.2 megapixels) equipped with a Tamron 60mm f/2.0 Di II LD macro lens and a polarising filter (Fig. 5-2).



Fig. 5-2 Photographic equipment employed to obtain the pictures of the *Arvicola* humeri. The camera with the macro lens, the polarising filter, the tripod, and the remote trigger separately (top) and mounted in front of the humerus fixed to the turntable inside the lightbox (bottom).

### 5.2.2. *The tripod and the remote trigger*

Vibration of the camera during image capture produces blurry photos, especially at low shutter speed. This is a major problem when performing photogrammetric reconstructions because image blur disturbs the visual analysis and interpretation of the data, causes errors, and can degrade the accuracy of automatic photogrammetric processing algorithms. This problem is even greater in macro photography because the depth of field decreases as magnification increases, and a shallow depth of field means that an important part of the picture will be out of focus. A way to increase the depth of field, and therefore the focused portion of the picture, is to set a large F-stop number, which actually means a small aperture of the diaphragm. Under given lighting conditions, taking photographs with large F-stop numbers results in a reduction of the light that arrives at the sensor. Decreasing the shutter speed compensates the loss of light that occurs with small diaphragm apertures, but this increases the problem of camera vibration. In these conditions, the use of a tripod or any other camera support and a remote trigger is essential to obtain focused and sharp images. The self-timer (at a position of 2 seconds), or triggering the shutter by a light touch on the screen in a touchscreen camera, can replace the remote trigger. In this study, we used a Benro Travel Angel FTA 18AB0 aluminium tripod and a Canon RC-6 P/550D remote trigger.

### 5.2.3. *Lighting*

In photogrammetric reconstruction, lighting is important for several reasons. When taking the photos, the light should be intense, diffuse, and uniform. Intense lighting allows to shoot at small diaphragm apertures and at low ISO. Closing the diaphragm increases the depth of field (as explained in section 5.2.2) whereas lowering the ISO reduces the grain and the noise, and both options together result in sharper pictures and better 3D reconstructions. More important than the intensity of light is its evenness. In fact, a soft light with no gleams is preferable to an intense but uneven light (Mallison & Wings, 2014). The uniformity of the lighting will reduce the gleams on shiny objects, and will avoid harsh changes in shadows during the rotation of the subject, which might cause the failure of photogrammetric processing. In order to have good lighting conditions, we used an Amzdeal photo lightbox equipped with a strip of 30 LED lamp beads.

### 5.2.4. *The “turntable”*

With the aim of obtaining photographs of each humerus from different perspectives, we used the “turntable method”, which consists in taking a series of photographs with the camera fixed onto a tripod by rotating the object across a small angle between shots with the aid of a turntable (section 5.3; Mallison & Wings, 2014). Although using an automatic turntable and shooting with the burst mode greatly reduces the time needed to photograph the object, this practice has the

## PHOTOGRAMMETRY APPROACH

inconvenience that some pictures may be poorly focused and that the time intervals between shots could change depending on the speed of the camera. For both reasons, we used a manual rotating device and took the photographs one by one (see section 5.3 for details). As a rotating device, we used a Petri dish with the base fixed to the floor of the lightbox and with a printed 360° ruler stuck to the internal face of the lid. As a support to hold the bones, a stick of 10 cm was fixed to the centre of the external face of the lid (Fig. 5-2). This stick was used to separate the object from the floor, which makes it easier to take the photographs and crop the bone from the background.

### 5.2.5. *The software*

Some specialised software is freely available on the web. However, as explained in section 5.1.3, free software usually offers limited versions of payment software or performs very specific functions. Therefore, working with free photogrammetric software finally comes at the price of using a complex set of specialised programs. In this study, we used the commercial software PhotoModeler Scanner (Eos System Inc, 2014).

## 5.3. THE IMAGING PROTOCOL

As explained in section 5.2.4, images were obtained with the “turntable method” (Mallison & Wings, 2014). Humeri were fixed by their proximal end onto the support with the aid of a reusable putty-like adhesive (Blu Tack™). A tripod was used to fix the camera in a portrait position at a distance of 20 cm from the surface of the lens to the humerus. In order to cover the whole surface of the bone, 33 photographs of each humerus were taken through two complete rotations of 360° with the camera placed at a different height each time (Fig. 5-3). In the first whole rotation, the camera (taking the centre of the lens as a reference) was set at the same height as the bone (the horizontal plane). At this height, 24 photographs were taken, by rotating the bone at intervals of 15°. In the second rotation, the camera was set at a height in which the axis of the lens formed an approximate angle of 20° above the horizontal plane. From this angle, nine photographs were taken by rotating the bone at intervals of 40°. Although in principle it is not necessary, the first photograph of each complete rotation was always taken with humeri placed in the same position, i.e., with the caudal surface oriented parallel to the camera lens. The focus was set to manual and adjusted for each shot, in order to get as much focused surface as possible. The camera settings (i.e., the ISO, the F-stop or diaphragm aperture, and the shutter speed) were also adjusted manually to obtain properly exposed pictures. Because we intended to obtain photographs of a small object under controlled conditions of light, the key camera setting was the F-stop. As explained in section 5.2.2, in macro photography large F-stop numbers are desirable to increase

the depth of field and consequently the focused part of the subject. However, as the F-stop number increases, so do the diffraction and the blurriness of the image; for this reason, extremely high F-stop numbers were avoided. The general rule of thumb is to use F-stop numbers of about F11 or F16, so we used F16. Because the aperture of the diaphragm was small, a high ISO and/or a low shutter speed were needed to counteract the loss of light. As previously mentioned, the noise increases with the ISO, while a low shutter speed was not a big problem in our case because the camera was fixed onto the tripod and shot with a remote trigger. Therefore, we decided to shoot at ISO 200 and at a shutter speed of 2 seconds to counteract the loss of light.

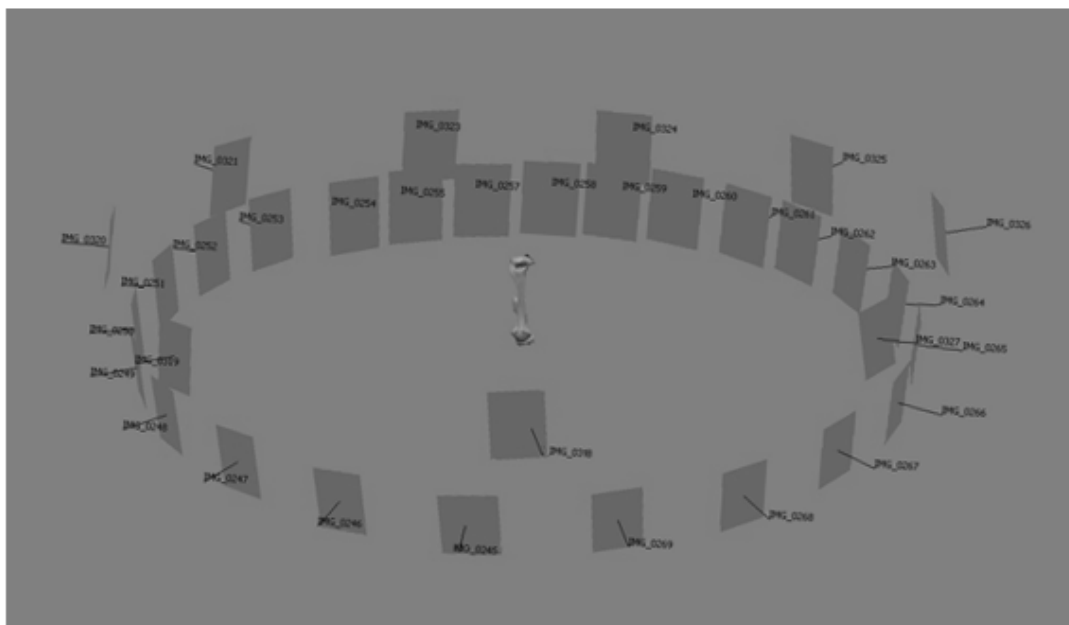
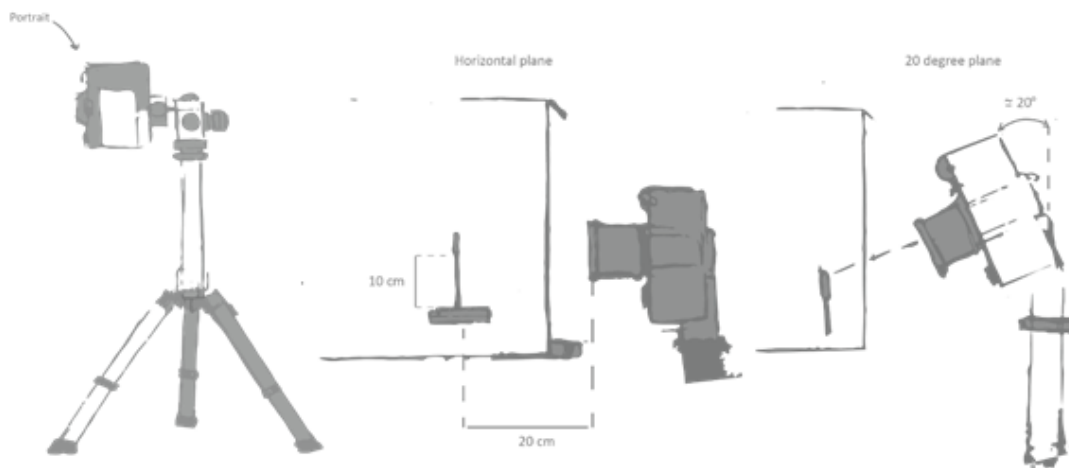


Fig. 5-3 Diagram of the position of the camera during the two complete rotations (top) and picture of the camera positions around the humerus that constitute the imaging protocol (bottom).



#### 5.4. APPLYING THE PROTOCOL TO THE STUDY OF THE HUMERUS FORM IN FOSSORIAL AND SEMIAQUATIC WATER VOLES (GENUS *ARVICOLA*)

##### 5.4.1. Introduction

With the aim of testing the method here described to analyse form variation of skeletal structures in small mammals, we selected a small sample of humeri of two rodent species. Since this bone provides important and rich functional information, we compared its form variation in two species that are phylogenetically very close but very different in their ecology and ethology. Specifically, our analyses were focused on two water vole species of the Palaearctic genus *Arvicola*: the southwestern water vole, *Arvicola sapidus*, which occurs in the Iberian Peninsula and much of France (e.g. Ventura, 2007 and references therein), and the montane water vole, *Arvicola scherman* (formerly fossorial form of *Arvicola terrestris*; for details see Musser & Carleton, 2005; but see also Kryštufek et al., 2015), which is found in mountainous areas of southern and central Europe (Musser & Carleton, 2005). While *A. sapidus* is a semiaquatic rodent, *A. scherman* is hypogeal and has a fossorial type of locomotion. Fossorial water voles construct extensive burrow systems in grasslands, pastures, and orchards (Airoldi, 1976). The digging process used by these mammals follows a strict pattern of stereotyped cyclic events; the skull is the main tool for excavation, but the limbs, and particularly the forelimbs, also play an essential role in soil removal (for details see Airoldi et al., 1976). Significant differences between fossorial and semiaquatic water voles in the skeletal structures involved in locomotion, including the humerus, have been described in the literature (e.g., Cubo et al., 2006; Laville et al., 1989; Laville, 1989b; Ventura & Casado-Cruz, 2010).

##### 5.4.2. Data

For analyses, we used the right humerus of ten adult males, five belonging to *A. sapidus* and five to *A. scherman*. In each 3D model, 18 landmarks (Fig. 5-4; Table 5-1) were collected with the command “Point Auto-detection” of the PhotoModeler Scanner software. Morphometric data are affected by measurement error (ME), which is defined as the variability of repeated measurements of a particular character taken on the same individual, relative to its variability among individuals in a particular group (Bailey & Byrnes, 1990). In order to evaluate the ME associated with the landmarking procedure, landmarks were recorded twice by the same person in two separate sessions.

The 3D models were scaled in order to study size. The linear distance between landmark 1 and 15 (ILD 1–15) directly measured on the humerus of each specimen was used to scale the 3D models. Measurements were obtained with a Mitutoyo no. 500-150 Digimatic Caliper (Mitutoyo

America Corporation, Aurora, Illinois, USA) with 0.01 mm resolution. To reduce the effect of ME in the scaling of the models, this distance was measured three times in each specimen and the mean of three replicates was used to obtain the scaling factor.

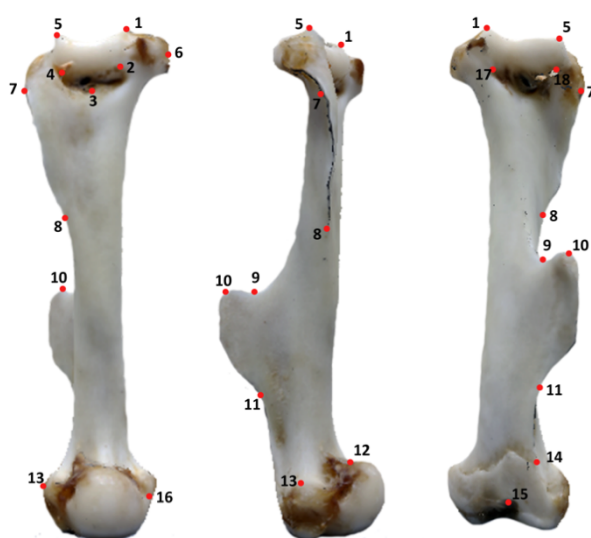


Fig. 5-4 Images of the 3D model of an *Arvicola sapidus* right humerus from caudal (left), lateral (centre), and cranial (right) views indicating the location of the 18 anatomical landmarks (see Table 5-1 for landmark definitions).

Table 5-1 Anatomical definitions of the collected landmarks displayed in Fig. 5-4.

Landmark	Description
1	Most medio-distal point of the trochlea
2	Most medio-proximal point of the caudal side of the trochlea
3	Point of maximum curvature of the olecranon fossa
4	Most latero-proximal point of the caudal side of the trochlea
5	Most distal point of contact between the trochlea and the capitulum
6	Most medial tip of the medial epicondyle
7	Most lateral point of the lateral epicondylar crest
8	Point of insertion of the lateral epicondylar crest on the diaphysis
9	Point of maximum curvature at the distal part of the deltopectoral crest between the deltoid tuberosity and the diaphysis
10	Most distal point of the deltoid tuberosity
11	Most proximal point of contact between the deltopectoral crest and the tricipital line
12	Most distal point of the union between the humerus head and the diaphysis
13	Most medio-distal point of the great tuberosity at the suture between the proximal epiphysis and the diaphysis
14	Union between the tricipital line and the greater tuberosity at the suture between the proximal epiphysis and the diaphysis
15	Most proximal point of the bicipital groove from cranial view
16	Point of maximum curvature of the suture between the proximal epiphysis and the diaphysis at the groove between the humerus head and the lesser tuberosity
17	Most medio-proximal point of the cranial side of the trochlea
18	Most latero-proximal point of the cranial side of the capitulum

### 5.4.3. *Statistics*

Geometric morphometric analyses were performed by implementing the methods included in the MorphoJ software, version 1.06d (Klingenberg, 2011). The form of the humerus was decomposed into size and shape, which were studied separately. Size was estimated through centroid size (CS), which is defined as the square root of the sum of the squared distances from each landmark to the centroid of the configuration (Rohlf & Slice, 1990). Then, the configurations of landmarks were superimposed through a generalised Procrustes analysis, and they were projected onto the tangent shape space (Dryden & Mardia, 1998). This procedure removes the variation in the landmark coordinates due to isometric size, position, and orientation, while preserving shape information (Dryden & Mardia, 1998). To assess the effect of ME on size and shape, an analysis of variance (ANOVA) was performed separately for each component of form. To assess the ME in humerus size, a nested ANOVA was conducted with CS as a dependent variable, individual as random factor, replicate as error term, and species as additional main effect (Palmer & Strobeck, 1986). The ME in humerus shape was assessed by means of a Procrustes ANOVA, which is equivalent to the two-factor ANOVA developed by Palmer and Strobeck (1986) but adapted to the study of shape (Klingenberg & McIntyre, 1998; Klingenberg et al., 2002). In this ANOVA, individual was entered as random factor, replicate as error term, species as additional main effect, and the Procrustes coordinates as dependent variables. Although these ANOVAs were originally developed for the study of asymmetry (Klingenberg & McIntyre, 1998; Klingenberg et al., 2002), they can also be used to assess the relative magnitudes of ME from repeated measurements even if structures only from one body side are measured (e.g., Morgan & Álvarez, 2013), as is the case with this study.

Allometry, i.e., size-dependent shape changes, was evaluated with a multivariate regression of shape onto the logarithm of CS (log CS). Statistical significance was calculated using a permutation test with 10,000 iterations under the null hypothesis of no allometric relationship (Monteiro, 1999). In order to visualise the whole set of form changes that allow us to compare our results with those reported in previous studies, and considering that no dependence of shape onto size was detected (see section 5.4.4), subsequent analyses were performed with raw data.

Afterwards, patterns of shape variation were explored with a principal component analysis (PCA) conducted on the variance-covariance matrix of mean individual shapes. A canonical variate analysis (CVA) and a discriminant function analysis (DFA) were conducted to examine the shape features that best distinguished between species. Mahalanobis distance (MD) between species was obtained, together with the statistical significance resulting from permutation test with 10,000 iterations.

#### 5.4.4. Results and Discussion

The ANOVA for CS revealed significant size differences between the humerus of the two species (Table 5-2), with *A. sapidus* having bigger humerus than *A. scherman* (mean CS of 41.4 and 33.5 mm, respectively). These results are completely concordant with those obtained in traditional morphometric studies performed with a sample containing the specimens used in this study (Ventura, 1990, 1992). The ANOVA also revealed that size variation among individuals was significantly larger than variation among replicates (ME), which in fact only represented 0.08% of total CS variation. The Procrustes ANOVA for shape revealed similar results (Table 5-2). Significant differences in humerus shape were also detected between species. As observed for CS, variation among individuals was significantly larger than variation among replicates (ME), although in this case ME represented a higher percentage of shape variation (Table 5-2).

Table 5-2 Results of the nested ANOVA for CS (above) and the Procrustes ANOVA for shape (below).

Effect	SS	% SS	MS	df	F	p
Species	310.388	96.35	310.388	1	216.18	< 0.0001
Individual	11.486	3.57	1.436	8	53.74	< 0.0001
Replicate	0.267	0.08	0.027	10		
Effect	SS	% SS	MS	df	F	p
Species	1.921 x 10 <sup>-2</sup>	37.07	4.087 x 10 <sup>-4</sup>	47	5.47	< 0.0001
Individual	2.807 x 10 <sup>-2</sup>	54.17	7.466 x 10 <sup>-5</sup>	376	7.73	< 0.0001
Replicate	4.538 x 10 <sup>-3</sup>	8.76	9.655 x 10 <sup>-6</sup>	470	216.18	< 0.0001

Abbreviations: SS, sum of squares; % SS, percentage of total sum of squares; *df*, degrees of freedom; MS, mean squares; F, F statistic; *p*, *p*-value.

The multivariate regression of shape onto log CS was not significant (9.9%,  $p = 0.565$ ), though this is probably due to the small sample size employed in this study.

The first two PCs resulting from the PCA performed with raw data together explained 63.1% of shape variation. The scatter plot of both PCs showed a non-overlapped arrangement of the two species along PC1, which is consistent with the differences between species detected in the Procrustes ANOVA (Fig. 5-5). Shape changes associated with PC1 indicated that, when compared with *A. sapidus*, the humerus of the fossorial species *A. scherman* shows greater distancing between the zones of muscular insertion and the articular surfaces, which is consistent with previous studies (Laville, 1989b). In particular, a relative latero-proximal and caudal displacement of the epycondilar crest, a relative distal displacement and a widening of the deltopectoral crest, and a widening of the proximal and the distal epiphyses were observed when moving from *A. sapidus* to *A. scherman* along PC1 (Fig. 5-6). The CVA and DFA analyses confirmed these results, the shape changes between species being almost identical to those associated with PC1. Moreover, despite the small sample size, Mahalanobis' distance between the two species was significant (MD = 3.381,  $p = 0.006$ ).

## PHOTOGRAMMETRY APPROACH

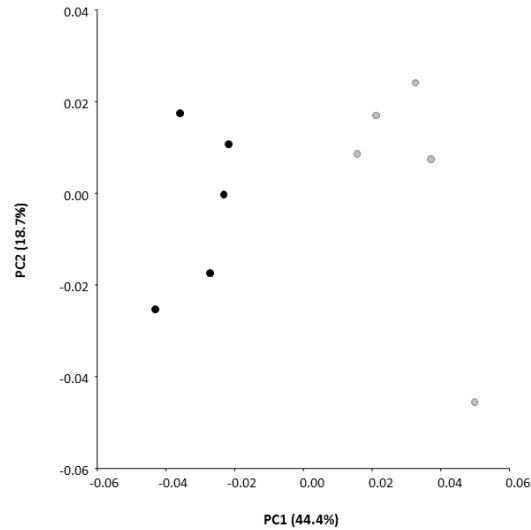


Fig. 5-5 Scatter plot of PC1 vs. PC2 obtained with raw data. Percentage of shape variation explained by each PC is indicated within parentheses.

According to Laville et al. (1989), the more distal position of the deltopectoral insertion in relation to the shoulder joint in *A. scherman* increases the efficiency of the acromiodeltoid, spinodeltoid, pectoral and latissimus dorsi muscles. Under a kinematic point of view, this efficiency can be associated with a more active action of pushing and traction of the proximal part of the forelimb during the digging phase in which the humerus is involved. Additionally, shape changes both in proximal and distal epiphyses of the humerus between fossorial and semiaquatic water voles suggest certain interspecific differences in the strength of: i) the scapular muscles involved in the extension, adduction, flexion and rotation of the humerus; ii) the brachialis muscles, and antebrachium flexor; and iii) the elbow ligaments.

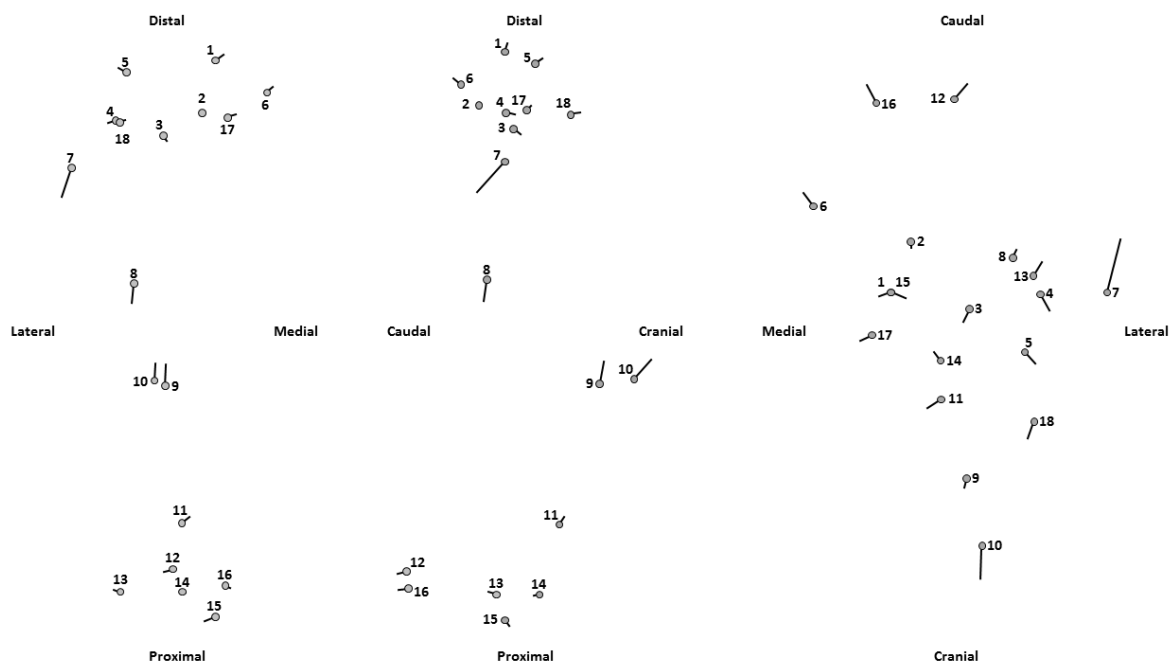


Fig. 5-6 Shape changes associated with PC1 from caudal, latero-cranial, and distal views of the humerus (left, centre, and right panels respectively). Grey circles represent the consensus configuration, and vectors represent a shape change of 0.05 units of PC score in the negative direction along the PC axis.

## 5.5. CONCLUSIONS

In our experience, an important point when performing photogrammetric reconstructions of small biological structures is to establish a specific imaging protocol for the object we intend to model. Since different biological structures differ in their form, colour, and texture, the imaging protocol (including the number and position of the photographs and the camera settings) has to be adapted to these particular traits of the object in order to be useful to obtain the 3D models. However, once the protocol has been established, the 3D models are obtained consistently and with a reasonable time investment.

Previous studies have highlighted that the 3D models obtained with photogrammetry are precise and accurate for morphometric analysis (Muñoz-Muñoz et al., 2016 and references therein). Although we have not specifically tested the accuracy of the method in obtaining 3D models of humeri from small mammals, the changes in size and shape between the two species detected in the case of study are fully consistent with those already described in the literature (Laville et al., 1989). This concordance lets us suggest that the 3D models built with the photogrammetric techniques explained in this chapter are accurate and capture actual morphological differences between the two species. The ANOVAs for size and shape indicated that variation among individuals is significantly larger than variation among replicates, which points out that the technique is precise and that ME error is not an important concern in our study. However, it should be noted that ME could especially lead to biased results in those studies

## PHOTOGRAMMETRY APPROACH

where interesting variation is subtle, like in fluctuating asymmetry analyses (Klingenberg & McIntyre, 1998; Klingenberg et al., 2002; Palmer & Strobeck, 1986). In fact, the ANOVAs employed in this study have been specifically designed to test if variation in fluctuating asymmetry is larger than ME. Since we have only analysed the right humerus, the magnitude of ME with respect to fluctuating asymmetry, which is usually lower than variation among individuals, remains to be tested. However, the percentage of sum of squares (SS) of the replicate term in our study is similar to the percentages obtained in previous studies, and the total amount of variation of the replicate term is of one order of magnitude lower (see Muñoz-Muñoz et al., 2016 for comparison).

For all these reasons, we conclude that the photogrammetric protocol described in this chapter is a useful and affordable solution to obtain 3D models of limb long bones from small mammals for morphometric analysis.

---

# CHAPTER 6

THREE-DIMENSIONAL GEOMETRIC MORPHOMETRIC  
ANALYSIS OF THE HUMERUS: COMPARATIVE  
POSTWEANING ONTOGENY BETWEEN FOSSORIAL  
AND SEMIAQUATIC WATER VOLES (*ARVICOLA*)

**Ana Filipa Durão, Francesc Muñoz-Muñoz, Jacint Ventura**

---

The content of this chapter is part of an article published in:

Journal of Morphology (2020) 281, 1679-1692

DOI: 10.1002/jmor.21278

---





## CHAPTER 6. THREE-DIMENSIONAL GEOMETRIC MORPHOMETRIC ANALYSIS OF THE HUMERUS: COMPARATIVE POSTWEANING ONTOGENY BETWEEN FOSSORIAL AND SEMIAQUATIC WATER VOLES (*ARVICOLA*)

---

### 6.1. INTRODUCTION

Locomotion plays an important role in species ecology since it allows animals to move, store food, escape from potential predators, and capture prey (Biewener & Patek, 2018; Polly 2007). Due to its physical properties, the environment may restrict locomotion (Biewener & Patek, 2018) and exert specific functional constraints (Biewener & Patek, 2018; Gillis & Blob, 2001; Houssaye & Fish, 2016). Accordingly, in mammals, the different types of locomotion are linked with distinct bone phenotypes (e.g., Botton-Divet et al., 2016; Botton-Divet et al., 2017; Hildebrand, 1985; Lessa et al., 2008; Polly, 2007; Samuels & Valkenburgh, 2008; Stein, 2000). Anatomical traits associated with locomotion may show specializations for a particular ecological niche. Thus, digging, for example, requires an ability to produce and transmit force during long periods of activity, which makes diggers tend to have a general strengthening of the musculoskeletal components involved in burrowing (e.g., Elissamburu & Vizcaíno, 2004; Fernández et al., 2000; Hildebrand, 1985; Stein, 2000). In contrast, the density and viscosity of the environment demand hydrodynamic characteristics on the musculoskeletal system of swimmers (Gillis & Blob, 2001; Gingerich, 2003; Howell, 1930; Webb & Blake, 1985). Although, digging and swimming have similar functional demands on the skeleton, the environment (water and soil) in which species moves implies different forces, and consequently a different response on the musculoskeletal system. The appendicular skeleton may have shorter and stout forelimbs in digging mammals than compared to normal epigeous forms (Casinos et al., 1993; Echeverría et al., 2014; Stein, 2000). Swimming species are characterized by stocky hindlimbs and elongate metatarsals (Samuels et al., 2013; Samuels & Valkenburgh, 2008).

Water voles of genus *Arvicola* Lacépède, 1799 constitute an excellent model to analyse the relationships between form and type of locomotion (function), because semiaquatic and/or hypogeic populations exist. The taxonomic revision by Musser and Carleton (2005) recognised the following species of *Arvicola*: the southwestern water vole, *Arvicola sapidus* Miller, 1908 (semiaquatic), the montane water vole, *Arvicola scherman* (Shaw, 1801) (fossorial), and the European water vole, *Arvicola amphibius* (Linnaeus, 1758) (semiaquatic or mostly semiaquatic). Although several studies do not support this taxonomic configuration (for details see Ventura & Casado-Cruz, 2011 and references therein; Chevret et al., 2020; Mahmoudi et al., 2020) we

followed that taxonomy in the present work in order to clearly distinguish a typical fossorial morphotype from a typical semiaquatic one (*A. sapidus*).

Among fossorial rodent species three methods of digging can be found (Stein, 2000): scratch-digging (i.e., claws of the manus are used to break up soil; e.g., *Ctenomys*, *Bathyergus*, *Geomys*); head-lift (i.e., incisors in concert with the skull form a powerful drill, that works like a spade to remove and loose the soil; e.g., *Nannospalax*, *Ellobius*) and chisel-tooth digging (i.e., incisors are used to break down the ground; e.g. *Cryptomys*). Depending on the mode of digging different adaptations of the appendicular skeleton or skull have been described (Calede et al., 2019; Hildebrand, 1988; Samuels & Valkenburgh, 2009; Stein, 2000). As for *Arvicola*, fossorial water voles (*A. scherman*) are chisel-tooth diggers that build complex burrow systems in harder soils (Airoldi, 1976; Airoldi & de Werra, 1993; Laville, 1989). The burrowing procedure is based on a strict pattern of stereotyped cyclic events, in which the animal uses the incisors to loosen the soil, and then with fast and alternative movements of fore and hind limbs remove the ground of the burrow. The cycle is concluded when the gallery walls are compacted with the muzzle and incisors (Airoldi et al., 1976; Laville, 1989; Laville et al., 1989). Instead, semiaquatic water voles, such as *A. sapidus*, build simple galleries with two entries at the level of water (Gosàlbez, 1987; Rigaux et al., 2008), and preferably in easily penetrable or silt soils (Strachan et al., 2011). Although these voles do not show conspicuous swimming adaptations, they are expert swimmers and divers (Mate et al., 2013). Their swimming method is based on rapid, successive, and alternative movements of fore and hind limbs. Like other rodent species (see, e.g., Santori et al., 2008), *A. sapidus* use the hind limbs for propulsion, which together with forelimbs movements allows it to move quickly in water.

Many bone structures in *Arvicola* exhibit a noticeable morphological variation associated, at least in part, with these different locomotor typologies (see e.g., Cubo et al., 2006 and references therein; Samuels & Valkenburgh, 2009). Most studies on this topic have interpreted intrageneric phenotypic differences in the skull and/or limb long bones under functional or evolutionary points of view (Laville et al., 1989; Laville, 1989; Cubo et al., 2006). Nevertheless, descriptive or comparative analyses of the postweaning growth of skeletal structures between *Arvicola* taxa are scarce and based mainly on linear measurements (Cubo et al., 2006; Ventura, 1988). In fact, studies on representative samples by applying landmark-based geometric morphometric methods have been performed only on the mandible (Durão et al., 2019; Ventura & Casado-Cruz, 2011). Results from these studies revealed that although particular shape changes are preserved in *A. scherman* and *A. sapidus* during postnatal ontogeny, there are significant interspecific differences in mandible size and shape, in the orientation of allometric and phenotypic trajectories, and in estimated bite force. Likewise, the mandible shape of fossorial water voles shows certain features associated with the digging activity, such as larger diastema, a lower

ramus, a ventral and caudal expansion of the condylar process, and a dorsal expansion of the angular process (Durão et al., 2019).

As mentioned above, although *A. scherman* is a chisel-tooth digger the forelimbs also play an important role in digging galleries. Indeed, in many chisel-tooth diggers the forelimbs are used a lot in bracing the body and removal of soil (Stein, 2000). In contrast, *A. sapidus* do not burrow nets of galleries and consequently, their forelimbs are not subject to such demanding biomechanical conditions. In spite of these clear ecological differences, the pattern of size and shape variation of the limb long bones along postnatal development in both semiaquatic and fossorial water voles have been scarcely studied (Cubo et al., 2006, Ventura, 1988; Ventura, 1992) and the corresponding ontogenetic phenotypic trajectories and the allometric effect on shape variation are unknown. Comparative ontogenetic studies permit to understand the processes of morphological diversification (Sheets & Zelditch, 2013) because postnatal growth may contribute significantly to adult morphology (Richtsmeier et al., 1993). Likewise, it is worth to keep in mind that closely related species may conserve common traits in early postnatal development (e.g., Sanfelice & Freitas, 2007), although different functional demands and ecological life may lead to divergent growth trajectories (e.g., Durão et al., 2019; Gray et al., 2019; Sanfelice & Freitas, 2007).

The present study is a part of a project aimed at determining, by means of three-dimensional (3D) geometric morphometrics, the postnatal ontogenetic patterns of the appendicular skeleton in *A. sapidus* and *A. scherman*, two water vole taxa with different locomotor typologies. As a first step, we compare here the corresponding postweaning growth patterns of the humerus, regarding its different locomotor implication in these species. Taking into account the involvement of this structure in the different lifestyles in *Arvicola*, we hypothesize that *A. sapidus* and *A. scherman* share ontogenetic features of this bone due to their close evolutionary relationships, but also that significant differences between them in both the allometric and phenotypic trajectories exist. As far as we are aware, the present study constitutes the first approach on the postweaning ontogeny of a limb long bone in small mammal species by using 3D geometric morphometrics. Likewise, although there is information on the postnatal development of the humerus in scratch-digger rodents (e.g., Echeverría et al., 2014; Montoya-Sanhueza et al., 2019; Vassallo, 1998), we report here the first results on this subject concerning a comparison of a chisel-digger vole with a semiaquatic morphotype. In a broader context, we aimed to determine to which extent function generates interspecific differences in the postweaning ontogeny of a limb long bone in phylogenetically close arvicoline with different lifestyles. Considering their different type of locomotion (semiaquatic and fossorial) and the well documented and significant ontogenetic series of postcranial bones available in some collections the selected taxa of *Arvicola* represent a good model to analyse this issue.

## 6.2. MATERIALS AND METHODS

### 6.2.1. Samples

We analysed 201 right humeri of two ontogenetic series belonging to *A. scherman* (Shaw, 1801) and *A. sapidus* Miller, 1908 (details in Table 6-1). All specimens of *A. scherman* were collected in the Aran Valley (Lleida, Spain), and most of *A. sapidus* in the Ebro Delta (Tarragona, Spain), between 1983 and 1984. Since the available number of juvenile specimens of *A. sapidus* from this zone was relatively low, we increased the sample size with humeri from collection specimens from Mérida (Navarra, Spain), Banyoles (Girona, Spain) and Rieutort (Lozère Department, France), captured in 1990 (Mérida) and 1994 (Banyoles and Rieutort). The morphometrical characteristic of the humerus between these populations of *A. sapidus* does not differ significantly (Garde, 1992; Ventura, 1988). Humeri analysed correspond to specimens provisionally deposited in the collection of the Mammalian Biology Research Group of the Universitat Autònoma de Barcelona (UAB, Bellaterra, Spain), excepting the individuals of *A. sapidus* from Mérida, which belong to the collection of the Museo de Ciencias of the Universidad de Navarra (UNAV, Pamplona, Spain). Catalogue numbers of museum material are in Appendix 1.

As in previous studies based on the same samples analysed here (Durão et al., 2019; Ventura & Casado-Cruz, 2011), specimens of both species were ascribed into six classes of relative age based on the relationships between moulting phase, sexual stage, and skull morphology (for details, see Ventura & Gosálbez, 1992; Garde et al., 1993). The age intervals of each class are the following: class 0, 3 weeks maximum; class 1, between 3 and 6 weeks; class 2, between 6 and 10 weeks; class 3, between 10 and 14 weeks; class 4, voles older than 14 weeks that either have not or have recently lived through their first winter; and class 5, individuals that have lived longer than one winter. All individuals from the last two age classes are considered fully adult.

Table 6-1 Sample size for each species, age class and sex.

Species	Sex	Age class						Total
		0	1	2	3	4	5	
<i>Arvicola sapidus</i>	F	4	6	11	5	12	4	42
	M	5	6	11	10	12	12	56
<i>Arvicola scherman</i>	F	2	3	9	10	11	15	50
	M	3	5	11	11	10	13	53
Total		14	20	42	36	45	44	201

### 6.2.2. Morphometric data acquisition

To analyze the ontogenetic variation of the humerus form in *A. sapidus* and *A. scherman*, we used landmark-based geometric morphometrics. 3D models of the humeri were obtained by means of photogrammetric techniques according to the protocol established by Durão et al. (2018). In brief, 33 photographs from different perspectives were taken of each humerus in two complete rotations of 360° using the “turntable method”, which consists in taking a series of photographs at small intervals, from a static camera and rotating the object placed on a turntable (Mallison & Wings, 2014). Images were obtained with a Canon EOS 750D DSLR camera equipped with a Tamron 60mm f/2.0 Di II LD macro lens and a polarizing filter. From the complete set of 33 photographs, a 3D model of each humerus was obtained, and in each model 18 landmarks (Fig. 6-1 and Supplementary Information, Table S6-1) were digitized using PhotoModeler Scanner software (EOS Systems Inc., 2015). All the models were scaled, using the linear distance between the landmarks 1 and 15. To reduce the measurement error, the measures were recorded three times and the mean value was used to scale the models. Measurements were obtained with a Mitutoyo 500-161-21 Digital Caliper (Mitutoyo America Corporation, Aurora, IL) with 0.01 mm resolution. To assess the quality of the models, internal software parameters (total error, residual values and precision values) were used. All the photographs, landmarks, and measurements were taken by the same person (A. F. D.) to avoid an interobserver error.

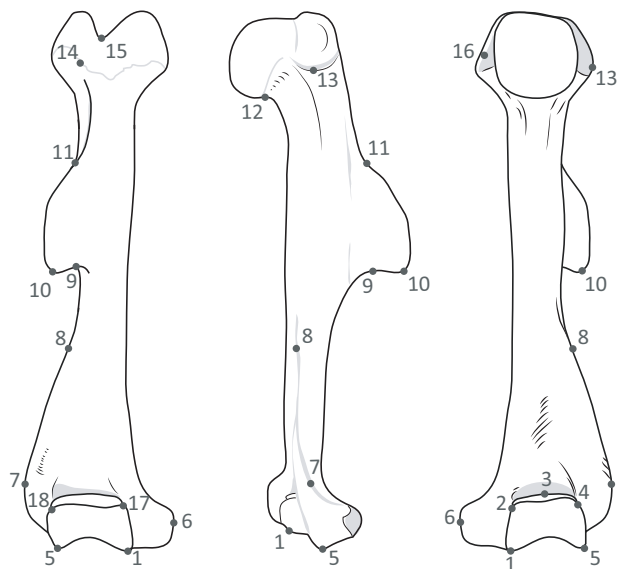


Fig. 6-1 Images of the three-dimensional (3D)-model in an *Arvicola sapidus* right humerus (from left to right: cranial, lateral and caudal views), indicating the layout of the anatomical landmarks used in the geometric morphometric analyses (see Supplementary Information, Table S6-1 for landmark definitions).

Size of each humerus was estimated as centroid size (CS), defined as the square root of the sum of squared distances of each landmark from their centroid (Bookstein, 1991). To obtain shape variables, the landmarks configurations of all specimens were superimposed with a generalized

Procrustes fit and projected onto the shape tangent space (Rohlf & Slice, 1990). The landmarks coordinates obtained after this procedure (Procrustes coordinates) only account for shape variation (Dryden & Mardia, 1998; Goodall, 1991), and therefore they were used for further analyses. Geometric morphometric analyses were performed using MorphoJ v.1.07a (Klingenberg, 2011).

### 6.2.3. Statistical analyses

#### **Sexual dimorphism**

In each taxon, to assess sexual dimorphism on humerus size and shape, a factorial analysis of variance (ANOVA) and a Procrustes ANOVA were performed, respectively. The factorial ANOVA was conducted with sex and age class as categorical variables and the logarithm of CS (LCS) as dependent variable. In the Procrustes ANOVA, sex and the LCS were entered as categorical and continuous variables respectively, and the Procrustes coordinates as dependent variables. In both species, sexual dimorphism for size and shape was negligible (Supplementary Information, Table S6-2 – S6-5), which agrees with the results obtained in previous studies (Garde, 1992; Ventura, 1988, 1993; Ventura & Casado-Cruz, 2011). Consequently, data from both sexes were grouped within each species and analysed jointly. These statistical analyses were carried out using STATISTICA v.12 software (StatSoft, 2014).

#### **Analyses of size and allometry**

For each species, the mean LCS and the corresponding *SDs* of each age class were calculated. A factorial ANOVA with the LCS as dependent variable was performed to assess the effect of age class and species on humerus size. Differences in size were tested between species in each age class performing a Tukey HSD post hoc test. In order to test if, in adult specimens (age classes 4 and 5), the humerus of *A. scherman* is smaller than that of *A. sapidus*, an analysis of covariance (ANCOVA) was carried out, with the LCS as dependent variable, species as categorical factor, and body length as continuous variable. These analyses were carried out using STATISTICA v.12 software. The sequential Bonferroni correction was systematically conducted to reduce the occurrence of a Type-I error in sets of related tests (Rice, 1989).

To study allometric shape variation (i.e., shape change associated with size) the Procrustes coordinates were regressed against the LCS (Monteiro, 1999) separately in each species. The residuals from this regression were considered as non-allometric shape data since by using them the effect of size on shape is removed (Klingenberg, 2016). Statistical significance of the results was tested against the null hypothesis of size and shape independence through a permutation test with 10,000 iterations using MorphoJ v.107a (Klingenberg, 2011). To compare the allometric

relationship between species, we performed a Procrustes ANOVA model using LCS, species, and their interaction as model effect (Goodall, 1991). This analysis was performed using the “procD.lm” function from the R v 3.5.1 (R Development Core Team, 2016) package geomorph (Adams & Otárola-Castillo, 2013), which assesses significance via distributions generated with resampling permutation (Collyer et al., 2015). Statistically significant interaction between species and the LCS (see section 6.3. Results) suggested interspecific differences in allometry. Accordingly, we compared the vectors of allometric coefficients of the two species to evaluate the differences between the two species in allometric trajectories. As vectors, they may differ in length and angle. To compare the length (amount of shape change per unit of size) and angle (direction of shape change associated with the size) of vectors of allometric coefficients between species, we performed a pairwise test for homogeneity of slopes (HS) using the “advanced.procD.lm” function in geomorph (Adams & Otárola-Castillo, 2013) in R v 3.5.1 (R Development Core Team, 2016). The angle was calculated in degrees, taking as a null hypothesis that the observed angle between trajectories is no larger than might be expected by chance. Statistical significance was evaluated from a randomized residual permutations procedure (RRPP) with 10,000 iterations (Sheets & Zelditch, 2013). To evaluate the effect of persistent digging activity, by comparing the vectors of static allometric coefficients between taxa, “procD.lm” and “advanced.procD.lm” functions (described above) were applied to adult specimens (age classes 4 and 5) only.

### ***Shape variation, morphological distance, and phenotypic trajectory analyses***

To delve into the differences between the two species in the pattern of shape changes along postnatal ontogeny, a principal component analysis (PCA) was conducted. Shape changes associated with PC axes were computed, and a warped 3D object was performed using the “plotRefToTarget” function in geomorph in R v 3.5.1. To analyse the morphological distance between species, Procrustes distance was calculated from shape data and non-allometric shape data (i.e., allometric shape removed) in each age class. Once multiple statistical tests were done, the sequential Bonferroni correction was carried out. To visualize differences of humerus shape between species across ontogeny, a discriminant analysis was carried out with specimens of age class 0 - 3 and 4 and 5 (adults). Analyses described above were performed with MorphoJ v.1.07d.

To test whether ontogenetic trajectories of humerus differ between species, a phenotypic trajectory analysis on the shape data using the “trajectory.analysis” function in geomorph was computed (Adams & Collyer, 2007, 2009; Collyer & Adams, 2007, 2013). This procedure quantifies different attributes of a shape change trajectory between two or more points (Adams & Collyer, 2009) and allows pairwise comparison of three different attributes of the trajectory: size, shape, and direction. Trajectory size describes the magnitude of phenotypic change displayed by that taxon (Collyer & Adams, 2013); trajectory direction the general orientation of phenotypic



evolution in the multivariate trait space and trajectory shape corresponds to gradual phenotypic changes over time (Adams & Collyer, 2009). We used species as groups, and age class as the trajectory points. Attribute differences were evaluated from a RRPP with 10,000 iterations (Adams & Collyer, 2007, 2009; Collyer & Adams, 2007, 2013). To visualize the phenotypic trajectories, a principal component of fitted values from linear model fit over 10,000 random permutations was performed (Adams & Collyer, 2009).

### 6.3. RESULTS

#### 6.3.1. Analyses of size and allometry

The factorial ANOVA showed a significant effect of age class and species on humerus size, as well as a significant interaction between both factors (Table 6-2). Both species displayed a progressive increase in size over ontogeny. Humerus size of *A. scherman* was significantly smaller than that of *A. sapidus* in all age classes (Fig. 6-2, Table 6-3). The ANCOVA showed a significant effect of body length on humerus LCS but neither the species factor nor the interaction were significant (Supplementary Information, Table S6-6). The results of the multivariate regressions revealed that in both species, shape changes are significantly associated with changes in size. Size explained a slightly higher percentage of shape changes in *A. scherman* (27.57%) than in *A. sapidus* (23.92%; Fig. 6-3). In the Procrustes ANOVA, size, species, and the interaction of these two terms were significant (Table 6-4). These results confirm the existence of a significant allometric component and indicate that the humerus of *A. scherman* and *A. sapidus* have different shapes. Moreover, the significant interaction term between species and size suggest that the allometric trajectories of the two species are different. In fact, pairwise test for HS showed that the vectors of allometric coefficients of the two species significantly diverge in orientation ( $\theta = 32.36^\circ$ ;  $p < 0.001$ ) and length ( $\Delta d = 0.06$ ;  $p < 0.001$ ), with *A. scherman* displaying a longer vector than *A. sapidus* ( $d_{A.scherman} = 0.24$ ;  $d_{A.sapidus} = 0.18$ ). The Procrustes ANOVA performed to assess the effect of persistent digging activity, also showed a significant interaction between species and size terms in adult specimens ( $F = 2.202$ ;  $df = 1$ ;  $p < 0.040$ ). The pairwise test showed significant differences in the orientation ( $\theta = 82.98^\circ$ ;  $p = 0.02$ ). Although the length of the vector of allometric coefficients of *A. scherman* was greater than *A. sapidus* ( $d_{A.scherman} = 0.32$ ;  $d_{A.sapidus} = 0.23$ ), this difference was not significant ( $\Delta d = 0.09$ ;  $p = 0.19$ ).

Table 6-2 Results of the factorial ANOVA testing the effects of species (*Arvicola scherman* and *Arvicola sapidus*), age class and the interaction between them on humerus size (logarithm of centroid size).

Effect	df	SS	MS	F	p
Age class	5	3.094	0.619	372	<0.001
Species	1	1.782	1.782	1072	<0.001
Age class x Species	5	0.052	0.010	6	<0.001
Residuals	189	0.314	0.002		

Abbreviations: *df*, degrees of freedom; *SS*, sum of squares; *MS*, mean squares; *F*, F statistic; *p*, *p*-value.

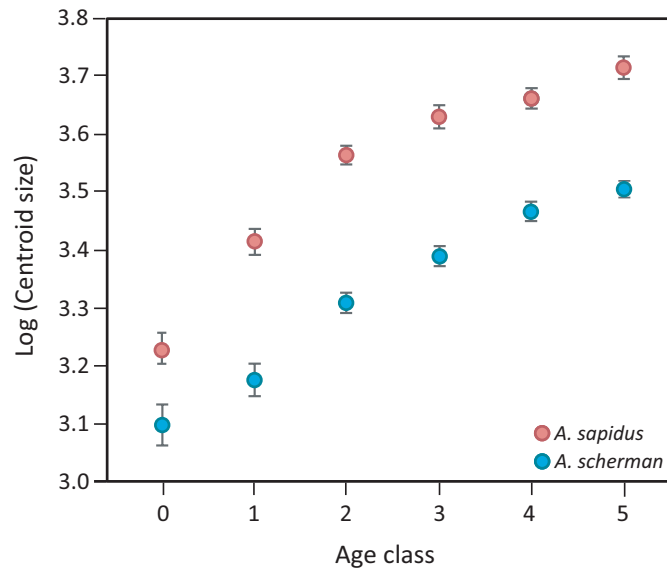


Fig. 6-2 Ontogenetic variation of the logarithm of centroid size (points, mean values; whiskers, SD) of the humerus in *Arvicola sapidus* and *Arvicola scherman*.

Table 6-3 Mean centroid size and standard deviation of the humerus in *Arvicola sapidus* and *Arvicola scherman* in different age classes and associated *p*-values.

Age class	<i>Arvicola sapidus</i>	<i>Arvicola scherman</i>	<i>p</i> *
0	25.26 ± 0.43	22.05 ± 0.57	<0.001
1	30.37 ± 0.37	23.86 ± 0.45	<0.001
2	35.21 ± 0.27	27.26 ± 0.29	<0.001
3	37.67 ± 0.33	29.55 ± 0.28	<0.001
4	38.93 ± 0.26	31.97 ± 0.28	<0.001
5	40.97 ± 0.32	33.21 ± 0.24	<0.001
mean	34.73 ± 0.14	27.98 ± 0.15	<0.001

\*After sequential Bonferroni correction.

## POSTNATAL ONTOGENY OF THE HUMERUS

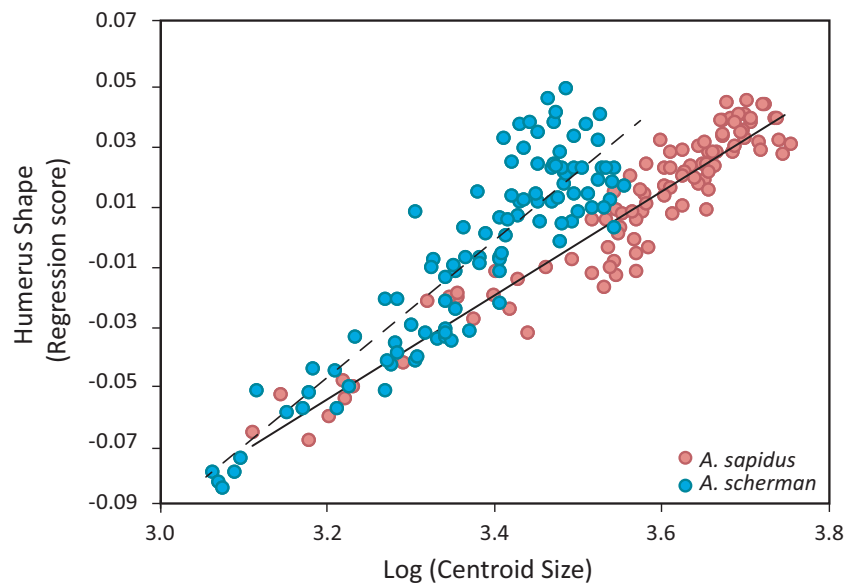


Fig. 6-3 Multivariate regression of shape onto the logarithm of centroid size in *Arvicola sapidus* and *Arvicola scherman* and their respective regression lines.

Table 6-4 Results of the Procrustes ANOVA testing the effects of species (*Arvicola scherman* and *Arvicola sapidus*), logarithm of centroid size (LCS) and the interaction between them on shape conducted on the entire sample.

Effect	<i>df</i>	SS	MS	Rs <sub>q</sub>	F	Z	<i>p</i>
Species	1	0.143	0.143	0.195	64.581	8.652	<0.01
LCS	1	0.138	0.138	0.188	62.073	8.563	<0.01
Species x LCS	1	0.015	0.015	0.020	6.728	4.154	<0.01
Residuals	197	0.437	0.002	0.596			
Total	200	0.733					

Abbreviations: *df*, degrees of freedom; SS, sum of squares; MS, mean squares; Rs<sub>q</sub>, R squared values; F, F statistic; Z, effect-size; *p*, *p*-value.

### 6.3.2. Shape variation and phenotypic trajectory analyses

In the PCA of the covariance matrix of the entire sample, the first two PCs jointly explained more than 50% of overall variance (PC1 = 31.05%; PC2 = 19.79%). Differences between species and age classes were explained by a combination of the two first PCs (Fig. 6-4a). In each species, shape changes associated with increasing age occurred in the negative direction along the two PCs.

First principal component accounted for main differences between taxa; most *A. scherman* individuals (excepting some adults) showed positive scores and most *A. sapidus* specimens (excepting some juveniles) exhibited negative ones. Shape changes along PC1 (with increasing scores) involved a distal expansion of the deltoid and epicondylar crests, a proximal expansion of the olecranon fossa, a slight torsion of the diaphysis and expansion of the medial epicondyle, evidenced through the opposite the epicondyle crest. Also, a general expansion of the distal epiphysis, which includes the trochlea and capitulum, and the medial and lateral epicondyles (Fig. 6-4b and Supplementary Information, Fig. S6-1). Shape changes along PC2 (with increasing

scores) involved a general expansion of the humerus head, the distal epiphysis, and the olecranon fossa, as well as a proximal retraction of the deltoid crest and a shortening of the proximal part of the epicondylar crest (Fig. 6-4c). Subsequent PC axes individually accounted for a very low percentage of variance (Supplementary Information, Table S6-7) and did not show clear association with factors of interest.

The DAs showed that both in juvenile-subadult (age classes 0-3) and adult stages (age classes 4 and 5) the humerus of *A. scherman* show in respect to *A. sapidus* a broader distal epiphysis due to a slight expansion of both epicondyles, a longer epicondylar crest, and a more latero-distally expanded deltoid crest (Fig. 6-5 and Supplementary Information, Fig. S6-2).

Procrustes distances between species were significant for all age classes (Table 6-5) in both shape data and non-allometric shape data. The phenotypic trajectories of the two species (Fig. 6-6) significantly differed in their orientation ( $\theta = 32.34^\circ$ ;  $p < 0.001$ ), size ( $\Delta d = 0.026$ ;  $p = 0.05$  ( $d_{A.scherman} = 0.163$ ;  $d_{A.sapidus} = 0.137$ )) and shape ( $D_p = 0.31$ ;  $p = 0.002$ ).

POSTNATAL ONTOGENY OF THE HUMERUS

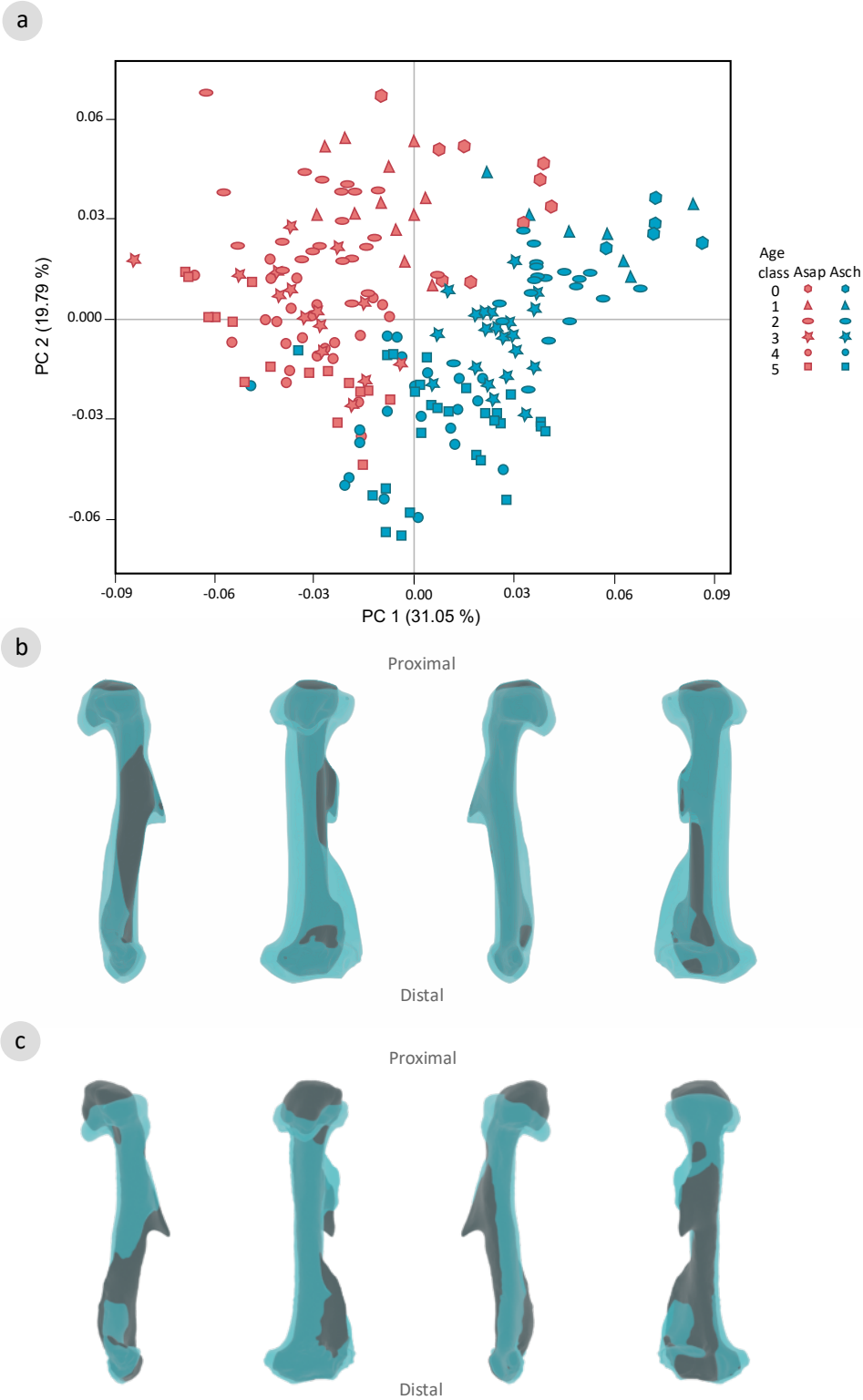


Fig. 6-4 (a) Scatterplot of PC1 versus PC2 scores from principal component analysis (PCA). (b) and (c) Shape changes associated with each extreme of the first two principal components (PC1, (b); PC2, (c)) are represented: grey, negative extreme of the axis; blue, positive extreme of the axis. Bones are represented form left to right in lateral, caudal, medial, and cranial views.

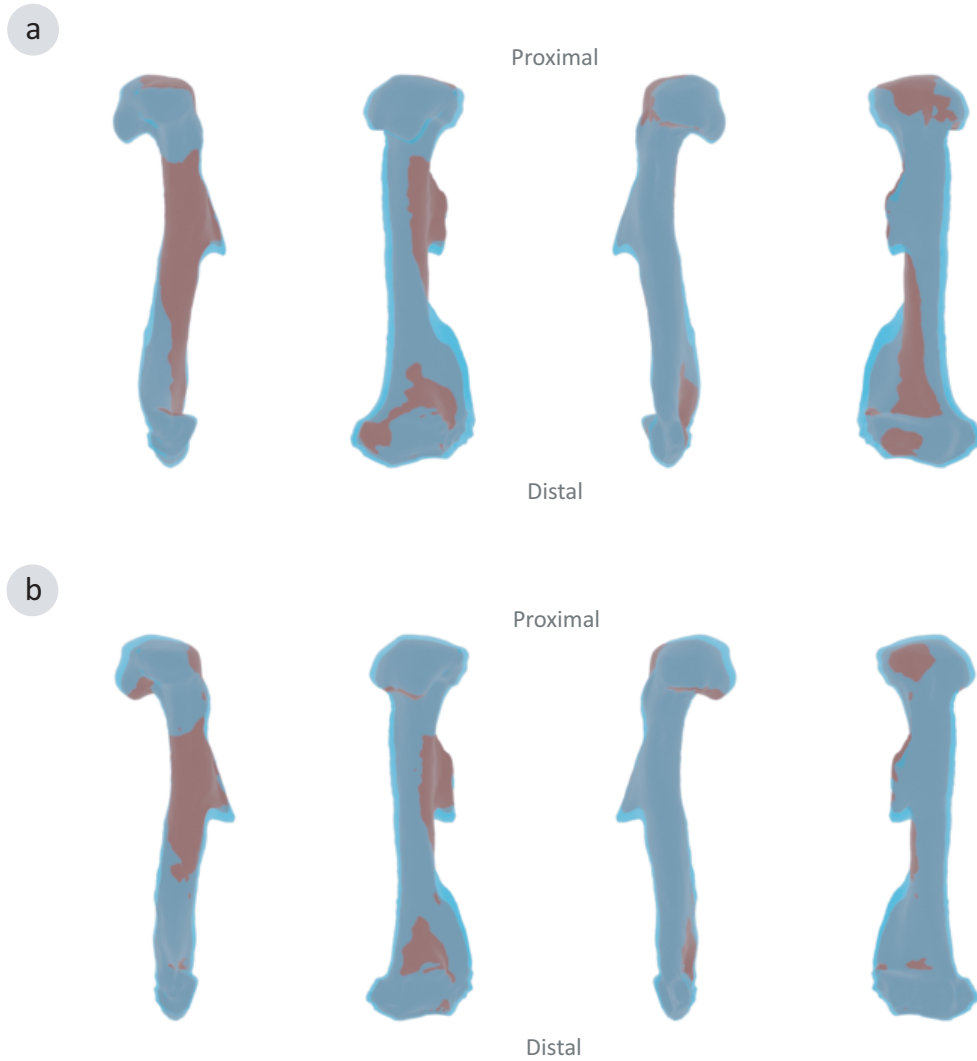


Fig. 6-5 Shape changes of the humerus between specimens of *Arvicola sapidus* (red) and *Arvicola scherman* (blue). (a) In specimens of age classes 0–3. (b) In specimens of age classes 4 and 5. Bones are represented from left to right in lateral, caudal, medial, and cranial views.

Table 6-5 Procrustes distance between *Arvicola sapidus* and *Arvicola scherman* in each age class and associated  $p$ -values.

Age class	Shape data	$p^*$	Non-allometric shape data	$p^*$
0	0.063	<0.001	0.070	<0.001
1	0.069	<0.001	0.066	<0.001
2	0.072	<0.001	0.070	<0.001
3	0.061	<0.001	0.065	<0.001
4	0.048	<0.001	0.063	<0.001
5	0.057	<0.001	0.064	<0.001

\*After sequential Bonferroni correction.

## POSTNATAL ONTOGENY OF THE HUMERUS

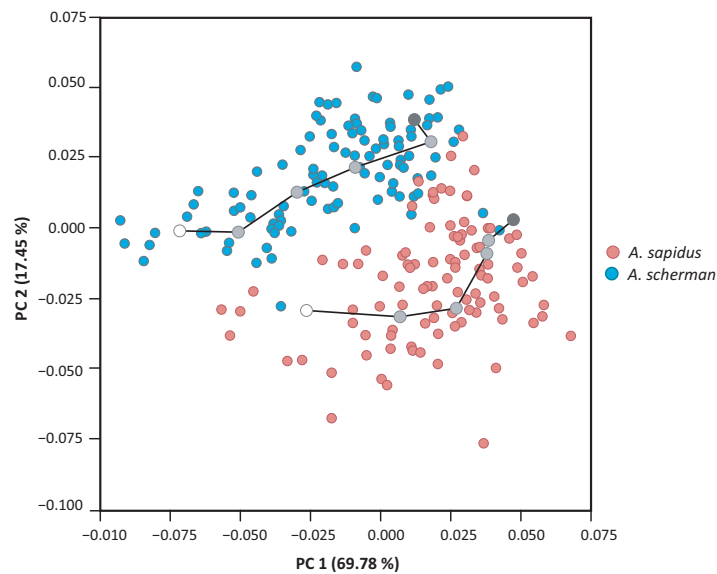


Fig. 6-6 Visualization of ontogenetic phenotypic trajectories of *Arvicola sapidus* and *Arvicola scherman*. Shape trajectories projected onto the first two PCs (based on covariance matrix of group means). Trajectories are shown as lines. The larger circles correspond to the means of each age class (from age class 0 to 5 from left to right).

### 6.4. DISCUSSION

As hypothesized, our comparative analyses between *A. scherman* and *A. sapidus* revealed shared, but also divergent, humerus form changes during the postnatal ontogeny of both species. Common traits are probably related to their close phylogenetic relationship whereas the phenotypic divergences detected may reflect functional factors. In particular, our results suggest that the type of locomotion may play a major role in shaping morphological variation within the genus *Arvicola*, which has also been reported for other mammalian taxa (Arias-Martorell et al., 2012; Botton-Divet et al., 2016, 2017; Hopkins & Davis, 2009; Kilbourne, 2017).

#### 6.4.1. Common ontogenetic phenotypic changes in the humerus of semiaquatic and fossorial water voles

The development of a functional musculoskeletal system requires muscle forces (Sharir et al., 2011). This musculoskeletal system includes muscle-induced mechanical forces that regulate morphogenesis and maintenance of skeletal tissues (Berendsen & Olsen, 2015), being essential for robust weight-bearing bones (Robling & Turner, 2009). Thus, muscle force on bone may cause changes in bone morphology. The shape changes in the humerus of *Arvicola* reported in the present study are probably due to, at least in part, to the increase of the muscular load during growth. Our PCA results revealed a similar general growth pattern in *A. sapidus* and *A. scherman*. In each species, during postweaning ontogeny, the main phenotypic changes with age correspond

to an expansion of the deltopectoral and epicondylar crests. On the deltopectoral crest inserts the deltoid muscle that contributes to forelimb retraction, and on the epicondylar crest attach the extensor carpi radialis, the ulnaris, and the brachioradialis muscles, which act on the wrist joint and on the joints of the forepaw. Additionally, in both taxa, a relative compression of the head and distal epiphysis with age was observed, specifically in the lesser and greater tuberosities, the trochlea, and the capitulum. These changes reveal that young water voles, irrespectively of their locomotor typology, have relatively more robust humeri than adult individuals. Relatively wider epicondyles have also been observed in pups of the Talas Tuco-tuco, *Ctenomys talarum* (Echeverría et al., 2014), and Cape dune mole-rat, *Bathyergus suillus* (Montoya-Sanhueza et al., 2019), both scratch-digger species. Likewise, histological studies carried out in *B. suillus* showed that juvenile specimens exhibit a thinner wall bone and higher intracortical porosity than adults (Montoya-Sanhueza et al., 2019; Montoya-Sanhueza & Chinsamy, 2018). Since a mineralization and an increase of bone and osteon density occurs during bone growth (see Hart et al., 2017 and references therein), a greater bone thickness at an early stage of ontogeny may be a compensatory response to the existence of a weaker material, which helps to maintain structural rigidity, reduce the risk of fractures, and preserve the mechanical similarity (Carrier, 1983; Echeverría et al., 2014; Montoya-Sanhueza et al., 2019). Although this hypothesis is based on results observed in scratch-digger rodents, a similar pattern could exist in fossorial water voles, since they begin to dig shortly after birth (Airoldi et al., 1976). While this pattern in early stage of ontogeny has a consequence of accommodating loads in more flexible elements, could be also linked, at least in part, to a basic developmental pathway. Nevertheless, considering that *A. scherman* is a chisel-tooth digger, certain histological differences in its humerus respect to that of *Bathyergus* can be expected. It is clear that histological studies on fossorial water voles are needed to elucidate this issue. Likewise, it would be interesting to compare some histological parameters between fossorial and semiaquatic water voles in order to determine possible differences related to the corresponding locomotor typologies. In this way, it is worth to keep in mind that many semiaquatic mammals are regular diggers and show limb morphology well-suited for both habits (Samuels & Valkenburgh, 2008).

#### 6.4.2. Differences in the postweaning growth of the humerus between semiaquatic and fossorial water voles

##### **Size change**

In all stages of the postweaning ontogeny, the humerus of *A. scherman* shows in all stages of the postweaning ontogeny a significantly smaller size than that of *A. sapidus*. However, in adult individuals, differences disappear when body size is considered, which indicates that smaller



humerus size in *A. scherman* is a consequence of reduced body size. Since larger size is linked to the primitive semiaquatic condition, the body size reduction in *A. scherman* seems to be an adaptive response to hypogeic life (Cubo et al., 2006). When comparing different rodent species of similar body mass, terrestrial locomotion and swimming are considerably less costly than the fossorial displacement (Seymour et al., 1998; Vleck, 1979; White et al., 2006). Digging requires high energy consumption so that fossorial rodents have developed ways to maximize and channel energy more efficiently (Heffner & Heffner, 1990; Lessa et al., 2008). Thus, for example, a decrease in body size becomes an advantage for a fossorial animal (White, 2005), since the reduction of the amount of soil to be burrowed leads to a substantial reduction of the locomotion costs (Vleck, 1979; White et al., 2006). In short, in *A. scherman* the relatively smaller size of the humerus is associated with its smaller body size, which seems to be an adaptation to reduce the digging cost. However, this hypothesis seems to not be supported within *A. amphibius* s.l., since clear size differences were not detected between aquatic and fossorial forms (Chevret et al., 2020). This discordance is probably linked to the greater morphological heterogeneity (morphotypes and ages) within the sample of *A. amphibius* s.l. analysed. Compared to *A. scherman*, *A. sapidus* shows larger body size at all ages, which is congruent with the pattern commonly observed in more aquatic mammals, and probably linked, at least in part, to thermoregulatory demands (Gearty et al., 2018).

One of the characteristics of fossorial rodents is having relatively short limbs (Nevo, 1979; Stein, 2000). The design of this structure, which results of selective pressures associated to the digging activity (Casinos et al., 1993; Echeverría et al., 2014), allows increasing the out-force by decreasing the out-lever of the forearm (Stein, 2000), and thus to minimize the cost of burrow construction (Nevo, 1979). It must be kept in mind that this reasoning corresponds to scratch-digger species and that fossorial water voles use a different digging procedure. The results of the ANCOVA reveal that the size of the humerus does not differ significantly between *A. scherman* and *A. sapidus* when considering body size, and therefore it can be assumed that that in both species the humerus is proportionally to the same size. However, since we have not performed comparisons of the size of the antebrachium and manus bones, we cannot corroborate statistically whether the forelimb of *A. scherman* is relatively shorter than that of *A. sapidus*.

### **Shape changes**

The comparative analysis of the lengths of the vectors of the allometric coefficients showed that in *A. scherman* humerus shape changes per size unit are larger than in *A. sapidus*. Likewise, the diverging directions of the vectors indicate that the specific shape changes associated with size are significantly different between these taxa. A similar pattern was found in the mandible (Durão et al., 2019). Since a long evolutionary time is required for allometric slopes to evolve, allowing

ontogenetic trajectories to explore new areas of morphological space, phylogenetically close and morphologically similar species, in general, tend to differ little in their allometric trajectories (Gould, 1966; Voje et al., 2013). Moreover, changing the direction of allometric trajectory has high costs to growth dynamics (Gould, 1966). In the case of the *Arvicola* taxa here studied, the noticeably divergent allometric trajectories found both in the humerus and the mandible may be attributable to the different functional pressures exerted on these bones.

Considering the essential role of the mandible in the digging process in fossorial water voles, several comparisons between the effect of burrowing on this structure and the humerus during adulthood can be made. The allometric regression revealed that in age classes 4 and 5 *A. scherman* shows an important humerus shape variation not associated with size, a fact not observed in *A. sapidus*. This pattern was also found for the mandible (Durão et al., 2019), and it was hypothesized that it could be due to the mechanical stress produced by the persistent digging activity during adulthood (Durão et al., 2019; Ventura & Casado, 2011). Interestingly, in the case of the humerus, the shape changes during adulthood seem to be more pronounced than those found in the mandible. While in the mandible neither phenotypic trajectories nor the Procrustes distances supported that assumption, in the humerus a greater divergence between phenotypic trajectory in age class 5, as well as a greater Procrustes distance shape data in the last age class, was observed. Furthermore, in the case of the humerus when comparing only age classes 4 and 5, the direction of the vectors of allometric coefficients was significantly different between both taxa, and the angle was much larger ( $90.5^\circ$ ) than when considering all age classes ( $32.8^\circ$ ). Although in *A. scherman* the mandible constitutes an essential structure to dig, it also plays an important role in obtaining food, social interactions, and, in general, in the underground lifestyle. Consequently, we suggest that the differences in the patterns of shape variation between the humerus and the mandible in the adult component (classes 4 and 5) of our samples are attributable to the differences in the remodelling patterns of both structures during adulthood. In the particular case of the mandible, the remodelling seems not depending only on the digging activity, but also to other functions associated with the hypogeal life. Thus, although both structures play an important role in burrowing, our results suggest that the pressure of this function is greater in the humerus than in the mandible.

Significant differences in the length and direction of the phenotypic trajectories were detected between fossorial and semiaquatic water voles. Length differences revealed that *A. scherman* shows larger changes in the humerus shape than *A. sapidus*. However, the magnitude of shape changes was lower than allometry vectors lengths which indicates that most major changes along ontogeny are related to size. In addition, we observed that the phenotypic trajectories have different directions in the shape space defined by PC1 and PC2. Thus, whereas in *A. scherman*, the phenotypic trajectory follows a rather constant direction (excepting shape changes occurring

between age classes 4 and 5), in *A. sapidus*, the direction of the trajectory changes substantially from age class 2 onwards. Results also revealed noticeable interspecific differences in the humerus shape in each age class. Although these divergences are probably related, to a greater or lesser extent, with the different types of locomotion of each species, our study does not allow us to determine the specific factors that shape each trajectory.

#### 6.4.3. Biomechanical consequences of humerus shape

Morphological distances between *A. sapidus* and *A. scherman* were significant across the ontogeny, both when using shape data or non-allometric shape data. Distances considering the former data were in general (except in age classes 1 and 2) lower than when using the non-allometric shape ones, which suggests that the species shared a part of allometric shape changes. Comparing the adult humerus shape between both taxa several differences were noted. In particular, *A. scherman* showed a more expanded epicondylar and deltoid crests, features that have been found in scratch-digger species (e.g., Echeverría et al., 2014; Lessa et al., 2008; Morgan & Alvarez, 2013).

In fossorial animals, one way to increase the force generated by the forelimbs is by expanding the area on the skeleton for muscle origin and insertion (Stein, 2000). Indeed, in *A. scherman* the deltopectoral crest expands distally during postnatal ontogeny, taking the deltopectoral insertion a more distal position in relation to the shoulder joint. This disposition increases a mechanical advantage by enlarging the in-lever arm (i.e., distance from muscle attachment to joint) of the deltoideus and pectoral muscles, which contribute to forelimb retraction and shoulder stabilization (Elissamburu & de Santis, 2011; Fernández et al., 2000; Hildebrand, 1985; Stein, 2000), and increase the efficiency of the deltoid scapular, acromial deltoid pectoral, and latissimus dorsi muscles (Laville, 1989). Although these features are more conspicuous in scratch-diggers, such as *Ctenomys* or *Geomys* species (Echeverría et al., 2014; Lessa et al., 2008; Morgan & Alvarez, 2013; Rose & Emry, 1983; Stein, 2000), they are probably present in chisel-tooth diggers, since also in these species the relative increase in force generated by bone modification allows the animal to use the downward pressure of their forefeet to counterbalance the upward pressure movement of the head to remove soil (Stein, 2000). Specifically, a relatively large deltopectoral crest was also observed in other chisel-tooth diggers, such as *Cryptomys hottentotus*, *Heliophobius argenteocinereus*, and *Heterocephalus glaber* (Samuels & Valkenburgh, 2008).

In addition, the epicondylar crest in *A. scherman* is longer than in *A. sapidus*. In this area, inserts the brachioradialis muscle that allows flexion of the elbow joint and assists with the pronation and supination of the forearm. Likewise, the wrist and digital flexor muscles also originate on the distal humerus and play an important role in digging. This feature was observed in scratch-digger rodents, such as *Ctenomys* species (Elissamburu & de Santis, 2011; Hildebrand, 1985). Those muscles might facilitate stabilization of the wrist and elbow joints, which would

potentially assist chisel-tooth digging behaviours. The expansion of the supracondylar ridge of the humerus suggests a greater muscular development and capacity for force production in the pronators and supinators muscles of the forearm (Elissamburu & de Santis, 2011; Hildebrand, 1985; Stein, 2000), which in the case of *A. scherman* may not only be related to dig but also to fossorial lifestyle. Besides, we detected a slight torsion of the diaphysis during postweaning ontogeny in *A. scherman*, feature that may have emerged as an advantage for digging. In fact, by changing the line of action of the diaphysis there is an increase in the effective force of the flexor muscles (Fernández et al., 2000; Hildebrand, 1988; Vassallo, 1998).

Another phenotypic difference observed between *A. scherman* and *A. sapidus* is an expansion of the great tuberosity in the former species. The great tuberosity holds the insertions of the supraspinatus, infraspinatus, and teres minor muscles, all of them involved in the stabilization of the shoulder (Polly, 2007). This condition may provide more stability in the shoulder joint of *A. scherman*, since increasing the extension area of insertion around the great tuberosity. Therefore, the larger greater tuberosity in *A. scherman* is probably associated with the continuous and fast movements involved to remove the soil of the galleries.

Swimming imposes challenges for semiaquatic species. The morphological changes exhibited by semiaquatic mammals must be related to the time and activities that the animal performs in water (Dunstone, 1979; Stein, 1988). Active swimmers require strong propulsion and ability to manoeuvre (Santori et al., 2008), which may impose constraints in the limbs. Almost all semiaquatic rodents swim with the hind limb or tail paddling locomotion (Nowak, 1999), and most morphological adaptations occur in hindlimbs (Samuels & Valkenburgh, 2008; Stein, 1988). However, there are a few semiaquatic rodents that have developed quadrupedal paddling mode of swimming, such as occurs in water voles of genus *Arvicola*. When compared with *A. scherman*, no features clearly related to swimming were found in *A. sapidus*. The low degree of specialization of the humerus for an aquatic mode of life in *A. sapidus* may be related to its great dependence on land.

## 6.5. CONCLUSIONS

Our results emphasize the importance of comparative postnatal ontogenetic studies in phylogenetically close species with a different type of locomotion to assess how ecological factors can affect the growth patterns. In addition, this study highlights the importance of using multivariate quantitative analyses to ascertain the allometric and phenotypic trajectories between species. In *Arvicola*, significant differences in allometric and phenotypic trajectories of the humerus found between *A. scherman* and *A. sapidus* are associated with their different lifestyles, suggesting that part of the morphological variation in the former species is related to

## POSTNATAL ONTOGENY OF THE HUMERUS

the digging activity. Additionally, in adult individuals of *A. scherman*, there is a certain shape variation not associated with size, fact not detected in *A. sapidus*. This difference, already observed in the mandible (Durão et al., 2019), might be due to the burrowing of galleries and other functions of the hypogeic life in fossorial water voles.

Although *A. scherman* is a chisel-tooth digger, several traits of their humerus are similar to those described in scratch-digger rodent species (Lessa & Stein, 1992; Stein, 2000). Nevertheless, these characters are less pronounced in fossorial water voles, results that are concordant with the different implications of the forelimb in the digging activity in these two types of diggers.

6.6. SUPPLEMENTARY INFORMATION

Table S6-1 Description of the 18 landmarks used in the geometric morphometric analyses.

Landmark	Description
1	Most mid-distal point of the trochlea.
2	Most mid-proximal point of the caudal side of the trochlea.
3	Point of maximum curvature of the olecranon fossa.
4	Most latero-proximal point of the caudal side of the trochlea.
5	Most distal point of contact between the trochlea and the capitulum.
6	Most medial tip of the medial epicondyle.
7	Most lateral point of the epicondylar crest.
8	Most proximal point of the epicondylar crest.
9	Point of maximum curvature at the distal part of the deltopectoral crest between the deltoid tuberosity and the diaphysis.
10	Most distal point of the deltoid tuberosity.
11	Most proximal point of contact between deltopectoral crest and tricipital line.
12	Most distal point of the union between the humerus head and the diaphysis.
13	Most mid-distal point of the great tuberosity at the suture between the proximal epiphysis and the diaphysis.
14	Union between the tricipital line and the greater tuberosity at the suture between the proximal epiphysis and the diaphysis.
15	Most proximal point of the bicipital groove from cranial view.
16	Point of maximum curvature of the suture between the proximal epiphysis and the diaphysis at the groove between the humerus head and the lesser tuberosity.
17	Most mid-proximal point of the cranial side of the trochlea.
18	Most latero-proximal point of the cranial side of the capitulum.

Table S6-2 Factorial ANOVA statistical assessment of the effects of age class, sex and the interaction between them on humerus size (logarithm of centroid size) conducted on the *Arvicola sherman* sample.

Effect	df	SS	MS	F	p
Age class	5	1.377	0.275	239.8	0.000
Sex	1	0.000	0.000	0.2	0.679
Age class x Sex	5	0.006	0.001	1.1	0.383
Residuals	91	0.104	0.001		

Abbreviations: *df*, degrees of freedom; *SS*, sum of squares; *MS*, mean squares; *F*, *F* statistic; *Z*, effect-size, *p*, *p*-value.

Table S6-3 Results of the Procrustes ANOVA performed for *Arvicola scherman* sample testing the effects of sex, logarithm of centroid size (LCS) and the interaction between them on humerus shape conducted on the entire sample.

Effect	df	SS	MS	Rsqr	F	Z	p
LCS	1	0.086	0.086	0.276	38.539	7.604	<0.001
Sex	1	0.003	0.003	0.009	1.306	0.772	0.215
LCS x Sex	1	0.002	0.002	0.006	0.768	-0.283	0.584
Residuals	99	0.222	0.002	0.709			
Total	102	0.313					

Abbreviations: *df*, degrees of freedom; *SS*, sum of squares; *MS*, mean squares; *Rsqr*, R squared values; *F*, *F* statistic; *Z*, effect-size; *p*, *p*-value.

POSTNATAL ONTOGENY OF THE HUMERUS

Table S6-4 Factorial ANOVA statistical assessment of the effects of age class, sex and the interaction between them on humerus size (logarithm of centroid size) conducted on the *Arvicola sapidus* sample.

Effect	<i>df</i>	SS	MS	F	<i>p</i>
Age class	5	1.902	0.380	179.7	0.000
Sex	1	0.000	0.000	0.0	0.856
Age class x Sex	5	0.020	0.004	1.9	0.101
Residuals	86	0.182	0.002		

Abbreviations: *df*, degrees of freedom; SS, sum of squares; MS, mean squares; F, F statistic; Z, effect-size, *p*, *p*-value.

Table S6-5 Results of the Procrustes ANOVA performed for *Arvicola sapidus* sample testing the effects of sex, logarithm of centroid size (LCS) and the interaction between them on humerus shape conducted on the entire sample.

Effect	<i>df</i>	SS	MS	Rsq	F	Z	<i>p</i>
LCS	1	0.066	0.066	0.239	30.297	7.775	<0.001
Sex	1	0.002	0.002	0.009	1.112	0.450	0.313
LCS x Sex	1	0.003	0.003	0.009	1.190	0.602	0.272
Residuals	94	0.205	0.002	0.742			
Total	97	0.276					

Abbreviations: *df*, degrees of freedom; SS, sum of squares; MS, mean squares; Rsq, R squared values; F, F statistic; Z, effect-size; *p*, *p*-value.

Table S6-6 Results of the ANCOVA testing the effects of species (*Arvicola scherman* and *Arvicola sapidus*), body length (BL) and the interaction between them on humerus size (logarithm of centroid size).

Effect	<i>df</i>	SS	MS	F	<i>p</i>
Species	1	0.000	0.000	0.035	0.852
BL	1	0.042	0.042	27.098	<0.001
Species x BL	1	0.000	0.000	0.009	0.924
Residuals	83	0.129	0.002		

Abbreviations: *df*, degrees of freedom; SS, sum of squares; MS, mean squares; F, F statistic; Z, effect-size, *p*, *p*-value.

Table S6-7 Eigenvalues and percentages of variance in the principal component analysis (PCA).

Component	Eigenvalues	% Var.	% Cum.	Component	Eigenvalues	% Var.	% Cum.
1	0.00113264	31.049	31.049	25	0.00001814	0.497	94.798
2	0.00072197	19.791	50.841	26	0.00001731	0.475	95.273
3	0.00030431	8.342	59.183	27	0.00001605	0.44	95.713
4	0.00023108	6.335	65.517	28	0.00001532	0.42	96.133
5	0.00015046	4.125	69.642	29	0.00001446	0.396	96.529
6	0.00011479	3.147	72.789	30	0.00001375	0.377	96.906
7	0.00009866	2.704	75.493	31	0.00001217	0.334	97.239
8	0.00007632	2.092	77.585	32	0.00001162	0.319	97.558
9	0.00006884	1.887	79.472	33	0.00001039	0.285	97.843
10	0.00006467	1.773	81.245	34	0.00000975	0.267	98.11
11	0.00005872	1.61	82.855	35	0.00000929	0.255	98.365
12	0.00005238	1.436	84.291	36	0.00000855	0.234	98.599
13	0.00005104	1.399	85.69	37	0.00000722	0.198	98.797
14	0.00004675	1.282	86.971	38	0.00000662	0.182	98.978
15	0.00003937	1.079	88.051	39	0.00000622	0.171	99.149
16	0.00003574	0.98	89.03	40	0.00000554	0.152	99.301
17	0.00003115	0.854	89.884	41	0.00000516	0.141	99.442
18	0.00002753	0.755	90.639	42	0.00000502	0.138	99.58
19	0.00002499	0.685	91.324	43	0.00000457	0.125	99.705
20	0.00002408	0.66	91.984	44	0.00000371	0.102	99.807
21	0.00002328	0.638	92.622	45	0.00000303	0.083	99.89
22	0.00002153	0.59	93.212	46	0.00000251	0.069	99.959
23	0.00002099	0.575	93.788	47	0.00000151	0.041	100
24	0.00001872	0.513	94.301				

Abbreviations: % Var., % Variance; %, Cum. %, Cumulative



POSTNATAL ONTOGENY OF THE HUMERUS

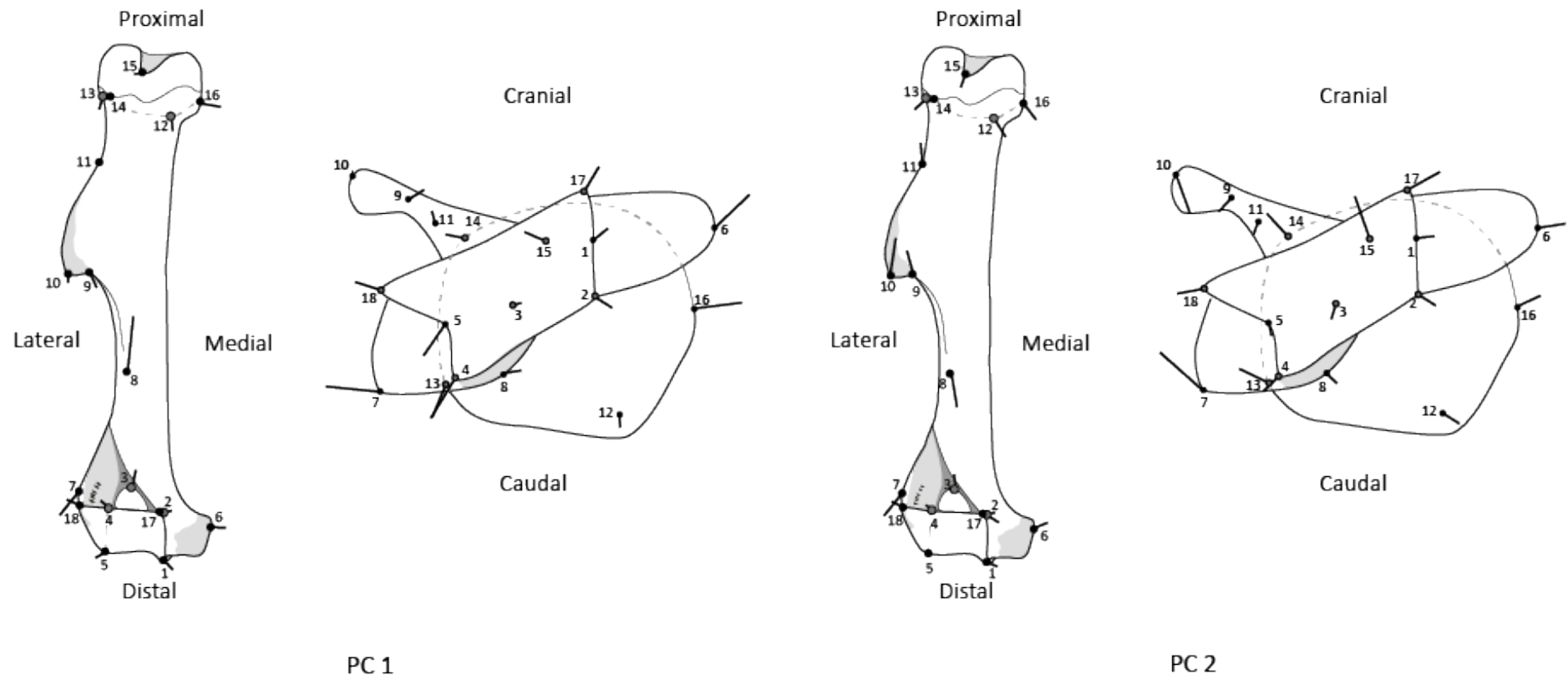


Fig. S6-1 A) Shape changes associated with each extreme of the first two principal components (0.10). The displacement vectors of shape changes are displayed into the consensus image of a right humerus in cranial and ventral view. The black dots are on the visible plane and the grey dots on the back plane.

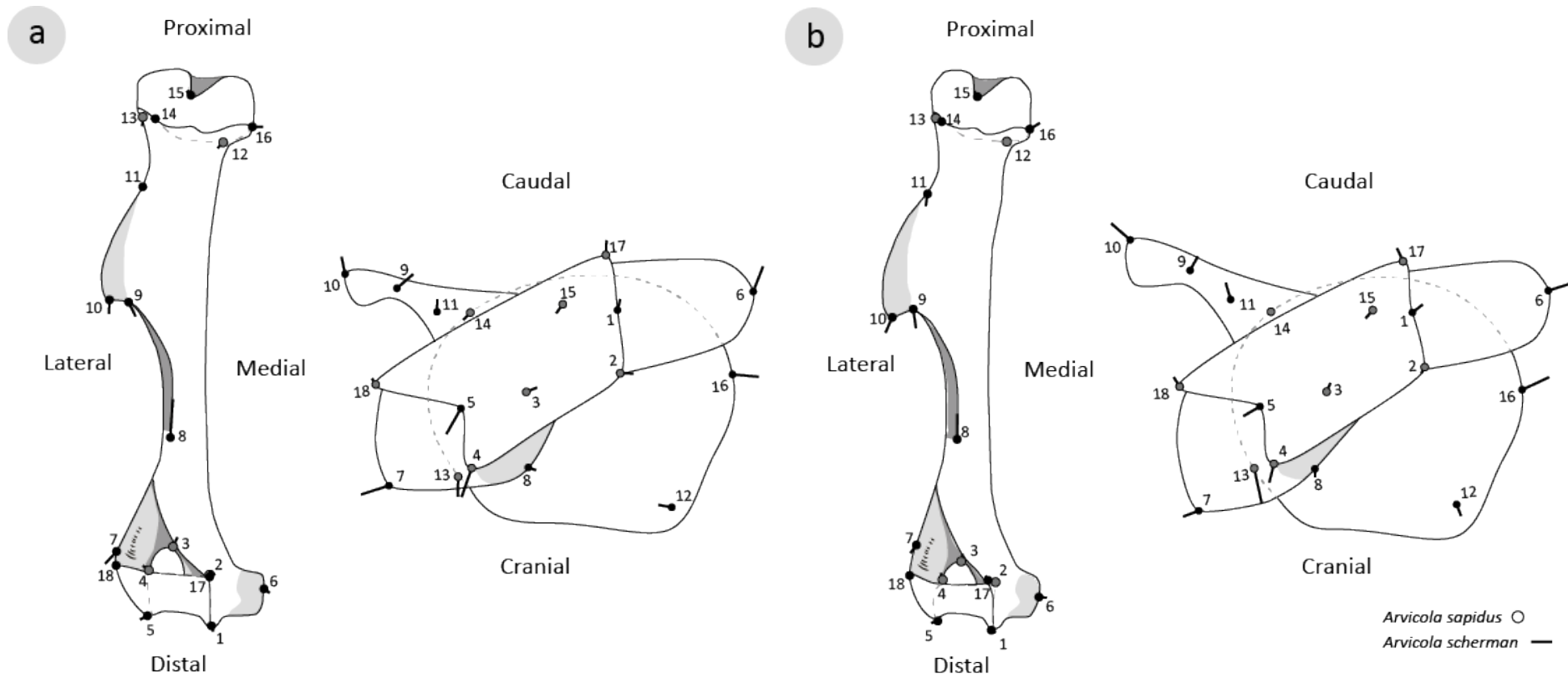


Fig. S6-2 Shape changes of the humerus between specimens of *Arvicola sapidus* (dot) and *Arvicola scherman* (line). The black dots are on the visible plane and the grey dots on the back plane. A) In specimens of age classes 0 to 3. B) In specimens of age classes 4 and 5. The displacement vectors of shape changes are displayed into the *A. sapidus* image of a right humerus in cranial and ventral view.



---

# CHAPTER 7

POSTNATAL ONTOGENY OF THE FEMUR IN FOSSORIAL  
AND SEMIAQUATIC WATER VOLES IN THE 3D-SHAPE  
SPACE

**Ana Filipa Durão, Francesc Muñoz-Muñoz, Jacint Ventura**

---

The content of this chapter is part of an article published in:

The Anatomical Record (2022) 305, 1073-1086

DOI: 10.1002/ar.24765

---



## CHAPTER 7. POSTNATAL ONTOGENY OF THE FEMUR IN FOSSORIAL AND SEMIAQUATIC WATER VOLES IN THE 3D-SHAPE SPACE

---

### 7.1. INTRODUCTION

Over the past decades, extensive work has been done on the role played by the locomotor behaviour on the phenotypic variation of limb long bones in rodents (Durão et al., 2020; García-Esponda & Candela, 2016; Hildebrand, 1985; Lehmann, 1963; Lessa et al., 2008; Samuels & Valkenburgh, 2008; Stein, 1993, 2000). Notably, it has been shown that different locomotion modes may lead to profound changes in the architecture of the myoskeletal system (Candela & Picasso, 2008; Lessa et al., 2008; Salton & Sargis, 2009; Sargis, 2002). Moreover, ecological factors, functional constraints, or evolutionary adaptations can be associated with modifications of the postnatal developmental pathways of the corresponding bone structures (Adams & Nistri, 2010; Durão et al., 2019; Durão, et al., 2020; Esquerré et al., 2017; Gray et al., 2019; Wilson & Sánchez-Villagra, 2010). In this context, a comparison of the ontogenetic trajectories of limb long bones of closely related species with different locomotor types is an excellent way to determine to which extent function affects growth patterns. Within rodents, water voles of the Palaearctic genus *Arvicola* constitute an optimal subject to explore this issue since it comprises a high number of morphotypes and two main ecological forms, semiaquatic, and fossorial.

The phylogenetic relationships of the representatives of *Arvicola* are currently under debate. Classically two species within this genus were recognized (see, e.g., Reichstein, 1963, 1982): *Arvicola sapidus*, which comprises semiaquatic populations, and *Arvicola terrestris*, with fossorial and/or semiaquatic representatives. In the taxonomic review of this genus by Musser and Carleton (2005) three species were accepted: the southwestern water vole, *A. sapidus* Miller, 1908 (semiaquatic); the montane water vole, *A. scherman* (Shaw, 1801) (fossorial); and the European water vole, *A. amphibius* (Linnaeus, 1758) (semiaquatic or mostly semiaquatic). Although *A. sapidus* is widely accepted as a valid species, recent studies based on analyses of genetic data have given rise to controversy on the taxonomy of the formerly accepted *A. terrestris* (for details, see Chevret et al., 2020; Kryštufek et al., 2015; Mahmoudi et al., 2020; Pardiñas et al., 2017; Ventura & Casado-Cruz, 2011 and references therein). As for the Iberian populations analysed in the present study, according to these new results, fossorial water voles from the Pyrenees could be attributed to *A. amphibius sensu lato* (Kryštufek et al., 2015), *A. monticola* (Mahmoudi et al., 2020; Pardiñas et al., 2017) or *A. amphibius* (Chevret et al., 2020). Since this point remains unsolved, we decided to follow the taxonomic arrangement by Musser and Carleton (2005) to clearly distinguish between typical fossorial (*A. scherman*) and semiaquatic (*A. sapidus*) morphotypes.

Fossorial water voles exhibit the so-called chisel-tooth digging, which involves the use of procumbent incisors to break the soil (Stein, 2000). The soil loosened by the incisors is removed from the tunnel through rapid and alternative movements of the fore and hind limbs, and the gallery walls are compacted by the rostrum (Airoidi et al., 1976; Laville, 1989; Laville et al., 1989). This digging process allows *A. scherman* to build extensive and complex burrow systems in hard soils (Airoidi, 1976; Airoidi & de Werra, 1993; Laville, 1989). Conversely to fossorial water voles, *A. sapidus* lives in freshwater habitats where it builds burrows on easily penetrable soils (Ventura, 2007). These rodents are excellent swimmers and divers (Mate et al., 2013; Quéré & Le Louarn, 2011) albeit they do not show marked morphological characteristics associated with these activities. During swimming, *A. sapidus* uses fore and hind limbs to move quickly in water and with hind limbs to generate propulsion. Thus, in *A. scherman* and *A. sapidus* hind legs are employed differently, according to their dominant type of locomotion. On the one hand, fossorial water voles mainly use their hindlimbs to remove the soil from the burrow (see Airoidi et al., 1976). During this phase, the animal takes a flexed posture; the pelvis is tilted forward, the angle between the femur and the pelvis diminishes, and the thigh is extended backward (Laville, 1989). On the other hand, as mentioned above, semiaquatic water voles use hind legs to generate propulsion during swimming. Specifically, *A. sapidus* places first the hind feet ventrally and then extends the hip and knee. In this process, the femur is essential to make rapid movements and to exert force during the legs' stroke.

Despite the important role that the hindlimbs play in the different locomotion modes in *Arvicola*, little is known about the postnatal development of their bones (Garde, 1992; Ventura, 1988, 1990, 1992). Surprisingly, this observation can be also extended to rodents in general (Elissamburu & Vizcaíno, 2004; Laville, 1989; Montoya-Sanhueza et al., 2019; Samuels & Valkenburgh, 2008; Stein, 1993). The present study is the third one of a series that aimed to determine the postnatal development of bone structures involved in locomotion in the two ecological forms of *Arvicola*: fossorial and semiaquatic. The main goal of this research is to compare the postnatal ontogeny of the femur in *A. scherman* (fossorial) and *A. sapidus* (semiaquatic) to detect possible phylogenetic and functional signals in this process. We compared the vectors of growth trajectories to estimate whether evolved functional differences are associated with different ontogenetic patterns. We hypothesize that these species share conserved shape changes throughout their postnatal growth. However, considering the corresponding type of locomotion, we also expect significant interspecific differences both in the allometric and phenotypic trajectories. This hypothesis is supported by our previous results obtained for the mandible (Durão et al., 2019) and humerus (Durão et al., 2020) of these taxa. It is worth mentioning that although there is available information on the postweaning development of the femur in scratch-digger rodents (Echeverría et al., 2014; Montoya-Sanhueza et al., 2019;

Vassallo, 1998), here we give the first findings on this subject concerning a chisel-tooth digger vole (*A. scherman*). The results obtained in *A. scherman* were compared, under a functional perspective, with those corresponding to a typical semiaquatic species of the same genus (*A. sapidus*).

## 7.2. MATERIALS AND METHODS

### 7.2.1. Study specimens

We studied ontogenetic series of two *Arvicola* representatives: *A. sapidus* and *A. scherman*. The analysed sample (Table 7-1) consisted of 182 right femora from museum collections, 89 belonging to *A. sapidus* from the Ebro Delta (Tarragona, Spain), and 93 to *A. scherman* from the Aran Valley (Lleida, Spain). Due to the small number of juvenile *A. sapidus* in this sample, we complemented it with femurs of juvenile individuals from Mérida (Navarra, Spain) collected in 1990, and Banyoles (Girona, Spain) and Rieutort (Lozère, France) obtained in 1994. Results of previous studies showed no significant morphometric differences between these populations (Garde, 1992; Ventura, 1988).

Table 7-1 Sample size for each species, age class and sex.

Species	Sex	Age class						Total
		0	1	2	3	4	5	
<i>Arvicola sapidus</i>	F	2	10	9	3	9	4	89
	M	3	10	8	10	9	12	
<i>Arvicola scherman</i>	F	2	5	10	10	10	10	93
	M	4	2	10	10	10	10	
Total		11	27	37	33	38	36	182

We analysed specimens belonging to the same collections examined in previous comparative studies on the ontogeny of the mandible (Durão et al., 2019; Ventura & Casado-Cruz, 2011) and humerus of these species (Durão et al., 2020). As in the case of these bones, those specimens were already distributed into six classes of relative age according to criteria based on the moulting phase, sexual stage, and skull morphology (for details see Garde et al., 1993; Ventura & Gosálbez, 1992). The age intervals corresponding to each group are the following (Garden et al., 1993; Ventura & Gosálbez, 1992): class 0, 3 weeks maximum; class 1, between 3 and 6 weeks; class 2, between 6 and 10 weeks; class 3, between 10 and 14 weeks; class 4, between 14 weeks and one winter; and class 5, individuals that have lived more than one winter. Individuals from the last two age classes were considered fully adults.

Excepting the femurs of *A. sapidus* from Mérida, all material analysed in the present study is provisionally housed in the collection from the Mammalian Biology Research Group of the Universitat Autònoma de Barcelona (UAB, Bellaterra, Spain). Specimens from Mérida belong to the



collection of the Museo de Ciencias of the Universidad de Navarra (UNAV, Pamplona, Spain). Catalogue numbers of museum material are in Appendix 2.

### 7.2.2. Femur form

#### ***Three-dimensional (3D) models***

Femur form variation was studied from 3D models obtained by the photogrammetric technique, which permits to obtain accurate and precise models of the external form of small objects from photograph sets (Durão et al., 2018). Each model was constructed from a set of 33 photographs of each femur using a Canon EOS 750D DSLR camera equipped with a Tamron 60mm f/2.0 Di II LD macro lens and a polarizing filter mounted on a tripod. The models were obtained through the “turntable method”, which consists of keeping the camera fixed at a point and taking photographs of the object while it rotates on a turntable in small intervals. All photographs were taken inside a lightbox to even out the light and reduce gleams and harsh changes in shadows during the rotation of the specimen. In order not to obstruct viewing angles and to obtain a complete digital model, the photographs were taken at intervals of 15° (Falkingham, 2012). Thus, photographs were taken in two complete rotations of 360°: the first rotation at the same height as the bone (taking 24 photos at intervals of 15°) and the second rotation at the height of bone size, positioning the lens at 20° from the horizontal plane (taking 9 photos at 40° intervals). Each photo was taken via remote trigger to reduce camera shake while capturing images and get focused and sharpened photos. Internal software parameters, such as total error and residual and precision values, were used to assess the quality of the models. For more details about the protocol, see Durão et al. (2018).

#### ***Morphometric data***

The femur form was characterised using 3D landmark-based geometric morphometrics. A set of 20 landmarks (Fig. 7-1) were digitized on the femur surface using Photomodeler Scanner software v.2015.1.1 (EOS Systems Inc. 2015). Landmark definition is available in Supplementary Information S7-1. We set the scale for each model using the mean value of the three measurements of the linear distance between points 2 and 11. Measurements were obtained with a Mitutoyo 500-161-21 Digital Caliper (Mitutoyo America Corporation, Aurora, IL) with a 0.01 mm resolution. To avoid interobserver error all femur digitalization was taken by the same person (A. F. D.). Subsequent analyses were performed using MorphoJ v.1.07a (Klingenberg, 2011) and a routine written for R statistical framework v. 4.1.0 (R Development Core Team, 2016).

Femoral form was separated into size and shape components, which were analysed separately. Centroid size, defined as the square root of the sum of the square distances of each

landmark from their centroid (Bookstein, 1991), was used as a proxy for femur size. The raw 3D landmarks coordinates were subjected to a generalised Procrustes alignment (Rohlf & Slice, 1990) to remove non-shape information (size, position, and orientation) (Dryden & Mardia, 1998; Goodall, 1991). Thus, the isometric effect of size on shape was removed but not allometry. The resulting Procrustes coordinates were used as shape variables in further analyses.

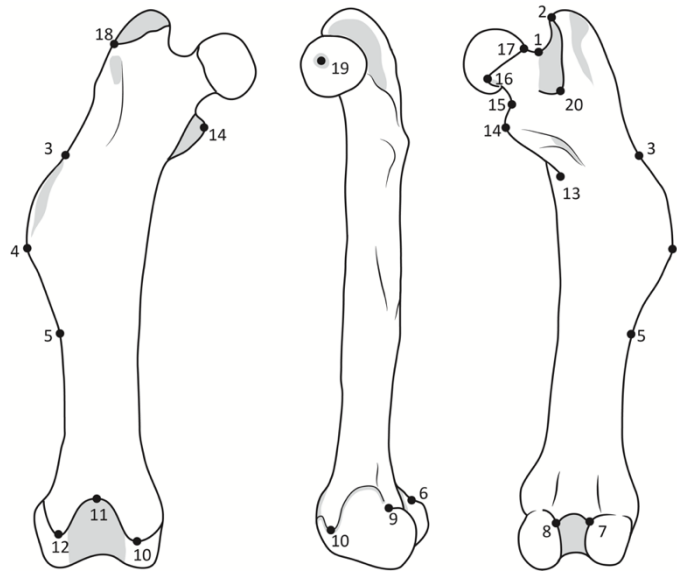


Fig. 7-1 Femur image of *Arvicola scherman* showing the position of the 20 anatomical landmarks used in the geometric morphometric analyses, from left to right: cranial, medial, and caudal. See Supplementary Information, Table S7-1 for landmark definitions.

### 7.2.3. Statistical analyses

#### **Sexual dimorphism**

We assessed the presence and magnitude of sexual dimorphism in each species on femur size and shape performing a factorial analysis of variance (ANOVA) and a Procrustes ANOVA, respectively. The factorial ANOVA was conducted with sex and age class as categorical factors and log-transformed centroid size (LCS) as dependent variable. In the case of Procrustes ANOVA, sex was introduced as categorical factor, LCS as continuous variable and Procrustes coordinates as dependent variables. No sexual dimorphism was found in any species (Supplementary Information, Table S7-2 - S7-5), which corroborates results obtained in other studies (Garde, 1992; Ventura, 1988, 1990, 1992, Ventura & Casado-Cruz, 2011). Consequently, for each species data from both sexes were analysed together.

#### **Size and allometry**

For both *A. sapidus* and *A. scherman* the mean LCS and the respective standard deviations for each age class were computed. The effects of species and age classes on femur size were tested across

the entire sample with a factorial ANOVA. To test for differences between species in each age class, a Tukey's HSD test was applied. To reduce the occurrence of a Type-I error in sets of related tests a sequential Bonferroni correction was conducted (Rice, 1989). These analyses were carried out using STATISTICA v.12 software (StatSoft, 2014).

The statistical relationship between size and shape (allometry) was assessed for each species separately by multivariate regression of Procrustes coordinates on LCS (Monteiro, 1999). Statistical significance of the results was tested under the null hypothesis of no allometric relationship through a permutation test with 10,000 iterations. These analyses were performed with MorphoJ v.1.07a. A Procrustes ANOVA model using LCS, species and their interaction as model effect (Goodall, 1991) was conducted to estimate the allometric relationship between species, by means of the "procD.lm" function from the R package geomorph (Adams et al., 2017). The statistical significance was assessed via distributions generated with resampling permutation with 10,000 iterations (Collyer et al., 2015). In this ANOVA, the significant interaction between species and LCS suggests interspecific differences in allometry. Since this was the case (see section 7.3. Results), to evaluate differences in ontogenetic allometric patterns, the attributes of the vectors of allometric coefficients, length (magnitude) and orientation (angle) were computed applying the "pairwise" function from the package RRPP (Collyer & Adams, 2018). Vector length describes the amount of shape changes per unit change of size and vector orientation indicates the relative covariations of shape variables per unit change of size (Collyer & Adams, 2013). Statistical significance of the tests was via pairwise assessments of the similarity in slopes and through 10,000 randomized residual permutations.

### **Shape variation**

A principal component analysis (PCA) on Procrustes aligned coordinates was performed to investigate the variation among landmarks in the data set. To visualize the shape differences associated with the major principal components (PCs) a warped 3D model was produced using "plotRefToTarget" function from R package geomorph (Adams et al., 2017). To measure similarity and difference between species, we calculated Procrustes distances from shape data and non-allometric shape data (allometric shape removed) in each age class. The residuals obtained from the multivariate regression of Procrustes coordinates on LCS for each age class of each species were used as non-allometric shape data (see Klingenberg, 2016). Sequential Bonferroni corrections were applied. Femur shape differences across ontogeny between *A. sapidus* and *A. scherman* were visualized by discriminant analysis (DA) performed in two separate groups of individuals: juvenile and subadult (age class 0 - 3), and adult (age class 4 and 5). All the described analyses were conducted with MorphoJ v.1.07a. The resulting coordinates of this difference were imported and used in "plotRefToTarget" function to visualize the differences between species.

To compare ontogenetic trajectories between species, a phenotypic trajectory analysis (PTA) on the Procrustes coordinates, using the “trajectory.analysis” function from the RRPP, was conducted (Adams & Collyer, 2007, 2009; Collyer & Adams, 2007, 2013). This function quantifies the attributes of the phenotypic trajectories (size, orientation and shape) for each group and compares these attributes between groups via permutation (Adams & Collyer, 2009). We used species as group and age class as the trajectory points. Attribute differences were estimated from sampling distributions generated from 10,000 random residual iterations (Adams & Collyer, 2007, 2009; Collyer & Adams, 2007, 2013). To visualize the ontogenetic phenotypic trajectories, a PC of fitted values from linear model fit over multiple random permutations was computed (Adams & Collyer, 2009). To visualise shape changes, a warped 3D model was plotted. To ensure that the low sample size of classes 0 and 1 did not influence the PTA, the same analysis was performed without these two age classes.

### 7.3. RESULTS

#### 7.3.1. Size and allometry

The factorial ANOVA indicated that femur size was significantly influenced by species, age class and the interaction of both factors (Table 7-2). Femur size increased throughout ontogeny in both species (Fig. 7-2), although it was always larger in *A. sapidus* than in *A. scherman* (Table 7-3). Multivariate regression of Procrustes coordinates on LCS for each species revealed that both species show significant shape changes, in *A. sapidus* the size explained 38.52% of the shape variation and in *A. scherman* 27.88% (Fig. 7-3).

Species, size and their interaction had a significant effect on femur shape (Table 7-4). Thus, there was allometry in femur shape and the significant interaction term suggests that the allometric slopes of these species were significantly different. Pairwise comparison of allometric trajectories confirmed that allometric slopes significantly differed between species ( $\theta = 26.02^\circ$ ;  $p < 0.001$ ). No significant pairwise difference in trajectory length was detected ( $\Delta d = 0.017$ ;  $p = 0.06$ ), but *A. sapidus* displayed a longer vector than *A. scherman* ( $d_{A. scherman} = 0.169$ ;  $d_{A. sapidus} = 0.186$ ).

Table 7-2 Results of the factorial ANOVA testing the effects of species, age class and the interaction between them on femur size (logarithm of centroid size).

Effect	<i>df</i>	SS	MS	F	<i>p</i>
Species	1	3.951	3.951	1566.2	<0.001
Age class	5	4.204	0.841	333.3	<0.001
Age class x Species	5	0.044	0.009	3.5	0.005
Residuals	170	0.429	0.003		

Abbreviations: *df*, degrees of freedom; SS, sum of squares; MS, mean squares; F, F statistic; *p*, *p*-value.

POSTNATAL ONTOGENY OF THE FEMUR

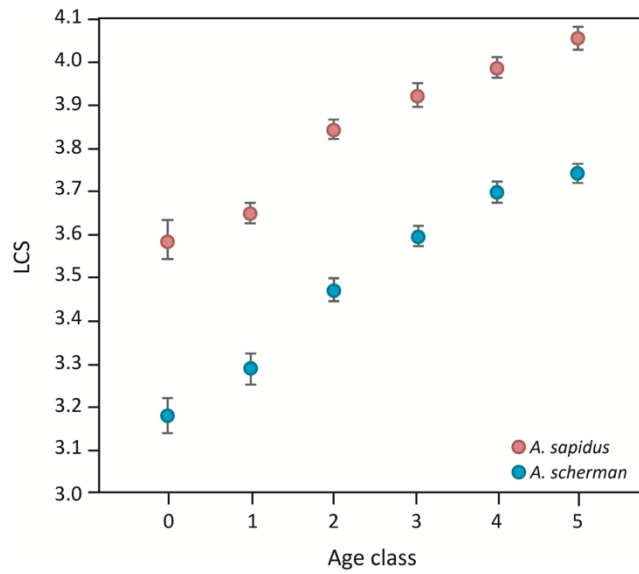


Fig. 7-2 Mean values of the logarithm of centroid size (LCS) of the femur across the ontogeny in *Arvicola sapidus* and *Arvicola scherman* (whiskers, standard deviation).

Table 7-3 Mean centroid size and standard deviation of the femur in *Arvicola sapidus* and *Arvicola scherman* in each age class and associated *p*-values.

Age class	Centroid size		<i>p</i> -values
	<i>Arvicola sapidus</i>	<i>Arvicola scherman</i>	
0	35.49 ± 0.92	24.08 ± 0.84	<0.001
1	38.64 ± 0.46	28.09 ± 0.77	<0.001
2	46.68 ± 0.50	32.25 ± 0.46	<0.001
3	50.44 ± 0.57	36.38 ± 0.46	<0.001
4	53.76 ± 0.48	40.27 ± 0.46	<0.001
5	57.56 ± 0.51	42.09 ± 0.46	<0.001
mean	47.10 ± 0.24	33.86 ± 0.24	<0.001

\*After sequential Bonferroni correction.

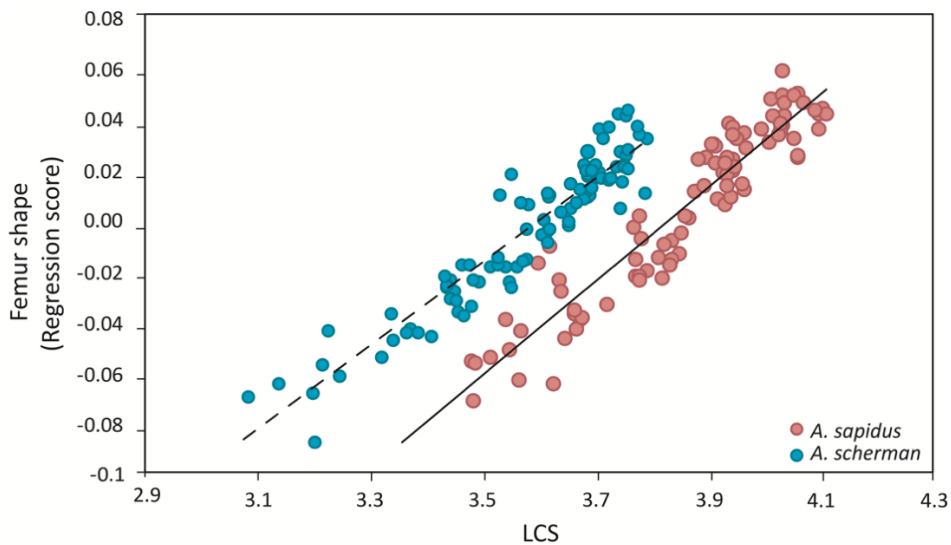


Fig. 7-3 Multivariate regression of shape onto the logarithm of centroid size (LCS) in *Arvicola sapidus* and *Arvicola scherman* and their respective regression lines.

Table 7-4 Results of the Procrustes ANOVA testing the effects of logarithm of centroid size (LCS), species and the interaction between them on shape conducted on the entire sample.

Effect	<i>df</i>	SS	MS	Rs <sub>q</sub>	F	Z	<i>p</i>
LCS	1	0.135	0.135	0.254	73.899	5.319	<0.01
Species	1	0.062	0.062	0.117	33.945	7.230	<0.01
LCS x Species	1	0.008	0.008	0.016	4.615	4.732	<0.01
Residuals	178	0.325	0.002	0.613			
Total	181	0.530					

Abbreviations: *df*, degrees of freedom; SS, sum of squares; MS, mean squares; Rs<sub>q</sub>, R squared values; F, F statistic; Z, effect-size; *p*, *p*-value.

### 7.3.2. Variation in femur shape and phenotypic trajectories analyses

In the PCA of shape data, the first two PCs jointly explained 45.62% of overall variance (PC1 = 247 34.01%, PC2 = 11.61%) (Fig. 7-4a). Each of the remaining PCs accounted for less than 6.7% of the variation (Supplementary Information, Table S7-6) and did not show a clear association with factors of interest. The shape changes explained by PC1 were mainly associated with age so that the youngest specimens showed positive values while the oldest ones showed negative values. The PCA that characterizes the general shape of the femur among specimens showed that younger individuals have high values of PC1 (Fig. 7-4a). Increasing scores of PC1 involved a medial expansion of the femur's head (verifiable by a medial shift of the *fovea capitis*), distal expansion of the lesser trochanter, lateral expansion of the greater trochanter, shortening of the third trochanter, and a general expansion of the distal epiphysis. Specifically, the latter change included a medial expansion of medial condyle and medial epicondyle, and a lateral expansion of lateral condyle and lateral epicondyle (Fig. 7-4b and Supplementary Information, Fig. S7-1). The PC2 accounted for differences between the two species, with most *A. sapidus* specimens (excepting some adults) showing positive scores and most *A. scherman* individuals (excepting certain individuals of each age class) negative ones. Most individuals of *A. sapidus* (high PC2 values) have a slight reduction of the femur head (lateral shift of the *fovea capitis*) and a narrowing of the femur's neck, slight shortening of the greater and lesser trochanters, marked shortening and narrowing of the third trochanter, and distal expansion of both condyles (Fig. 7-4c and Supplementary Information, Fig. S7-1).

The DAs showed that both juveniles-subadult (age classes 0-3) and adult (age classes 4 and 5) individuals of *A. scherman* showed a more robust femur than *A. sapidus*. This robustness is mainly due to the expansion of the lesser trochanter, a slight medial shift of the femur head, relatively longer and prominent third trochanter, and medial expansion of both the medial epicondyle and medial condyle (Figs. S7-2 and S7-3). In general, both species showed similar morphological changes between juvenile-subadult and adult stages (Figs. S7-2a and S7-2b; S7-3a and S7-3b). In all age classes, both in shape data and in non-allometric shape data, Procrustes distances between

POSTNATAL ONTOGENY OF THE FEMUR

species were significant (Table 7-5). These distances were always higher in non-allometric shape data.

Comparisons between the phenotypic trajectories (Fig. 7-5) revealed significant differences between species in the direction (angle) of shape change ( $\theta = 29.45^\circ$ ;  $p < 0.001$ ). However, neither the size (magnitude) ( $\Delta d = 0.009$ ;  $p = 0.36$  ( $d_{A.scherman} = 0.138$ ;  $d_{A.sapidus} = 0.129$ )) nor the shape of the phenotypic trajectories ( $D_p = 0.21$ ;  $p = 0.08$ ) were significantly different between taxa. For PC1, both species trajectories run from lower values as juveniles to higher values as adults. Along PC2 there is a separation between trajectories, showing *A. sapidus* the highest scores. The variation detected in shape data by a PTA without age classes 0 and 1 was similar to that observed when considering all age classes (Supplementary Information, Table S7-7).

Table 7-5 Procrustes distance between *Arvicola sapidus* and *Arvicola scherman* in each age class and associated  $p$ -values.

Age class	Procrustes distance			
	Shape data	$p$ -value*	Non-allometric shape data	$p$ -value*
0	0.036	<0.001	0.109	<0.001
1	0.036	<0.001	0.051	<0.001
2	0.037	<0.001	0.089	<0.001
3	0.040	<0.001	0.096	<0.001
4	0.037	<0.001	0.066	<0.001
5	0.048	<0.001	0.069	<0.001

\*After sequential Bonferroni correction

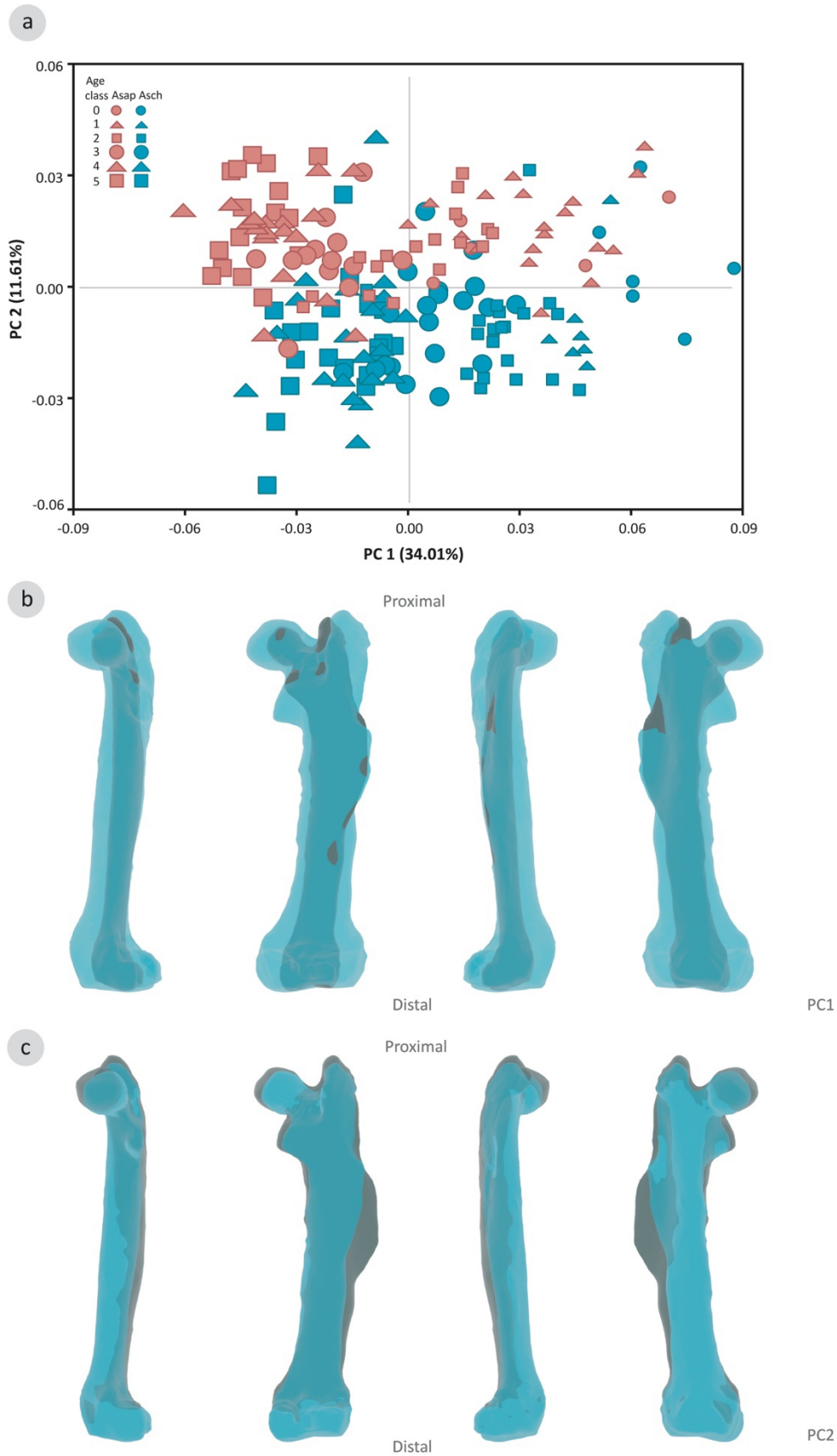


Fig. 7-4 (a) Scatterplot of the first two principal components (PC1 and PC2) from the principal component analysis performed on Procrustes coordinates. (b, c) Shape changes associated with each extreme of the first two principal components; grey, negative extreme of the axis; blue, positive extreme of the axis. Bones are represented from left to right in medial, caudal, lateral, and cranial views.



POSTNATAL ONTOGENY OF THE FEMUR

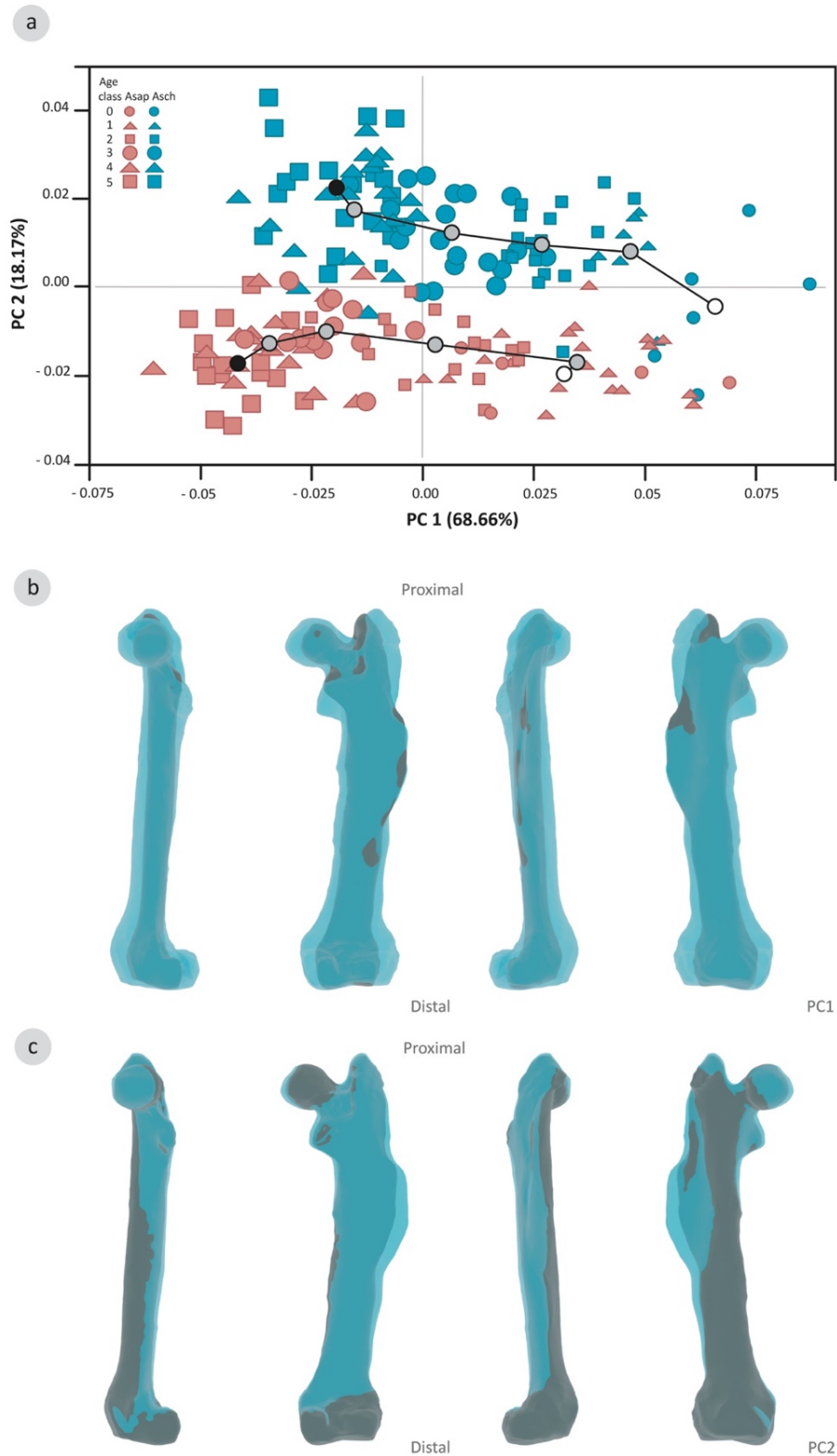


Fig. 7-5 Ontogenetic phenotypic trajectories of *Arvicola sapidus* and *Arvicola scherman* derived from the phenotypic trajectory analysis. (a) Shape trajectories projected onto the first two principal components (PC1 and PC2) (based on covariance matrix of group means). White dots represent the beginning (age class 0) and the black dots the end (age class 5) of the trajectories. The lines define the trajectories and the larger dots to the mean of each age class. (b, c) Shape changes associated with each extreme of the first two principal components; grey, negative extreme of the axis; blue, positive extreme of the axis. Bones are represented from left to right in medial, caudal, lateral, and cranial views.

## 7.4. DISCUSSION

### 7.4.1. *Common ontogenetic phenotypic changes in the femur of semiaquatic and fossorial water voles*

In concordance with our hypothesis, the PCA revealed that the general pattern of femur shape variation during postnatal ontogeny is similar in *A. sapidus* and *A. scherman*. In particular, important shared morphological changes were observed in the epiphyses. The first PC showed that the proximal and distal epiphysis are relatively larger in young individuals than in adult ones. These features likely provide a more multiaxially mobile hindlimb to juvenile voles (Salton & Sargis, 2009). Results obtained in an experimental study on mice (Serrat et al., 2007) allow us to suggest that differences in the epiphyses shape between juvenile and adult water voles could be associated to age-related differences in the expression levels of several growth factors.

In addition, the femur is more robust in juvenile than in adult individuals. This is due, at least in part, to the increase in body mass that determines higher mechanical loads on the limb long bones (García & da Silva, 2006). A similar growth pattern was reported for the postweaning ontogeny of the humerus (Durão et al., 2020), according to which, regardless of the type of locomotion, both bones are more robust in young than in adult water voles. In rodents, limb long bones of juvenile individuals are generally composed of faster deposition tissues and poorly mineralized woven (Enlow, 1962; Montoya-Sanhueza & Chinsamy, 2018). In contrast, adult specimens are characterized by having a mature compact bone, formed by lamellar bone that acts as a fiber-reinforced composite material (Enlow, 1962; Montoya-Sanhueza & Chinsamy, 2018). Since the mechanical and structural properties of the bone determine the organism's response to a mechanical load (Hart et al., 2017 and references therein), robust limb long bones in young water voles might be a compensatory response to minimize the risk of fractures during initial locomotor efforts. As pointed out for other mammal species (Carrier, 1983; Echeverría et al., 2014; Montoya-Sanhueza et al., 2019; Young, et al., 2010), this response in *Arvicola* is probably related to the weak bone matrix and lower muscular development characteristic of juvenile individuals.

### 7.4.2. *Differences in the postweaning growth of the femur between semiaquatic and fossorial water voles*

#### ***Size change***

The femur size of *A. scherman* is significantly smaller than that of *A. sapidus* across the whole postnatal ontogeny, which is congruent with the body size relationship between both taxa. The relatively smaller body size of *A. scherman* appears to be an adaptive response to hypogeic life

(Cubo et al., 2006; Durão et al., 2019, 2020). Given that the burrowing cost is proportional to the volume of soil dug (Vleck, 1979), it is usually assumed that a decrease in body size achieves a reduction in burrow cross-section, and consequently a reduction of the locomotion cost. Since the digging activity requires high energy, a decrease in body size becomes an advantage for fossorial animals (White, 2005) allowing them to channel energy more efficiently.

### **Shape change**

The analysis of allometric trajectories revealed a significant difference in the direction of the vectors of allometric coefficients between *A. sapidus* and *A. scherman*, which indicates that allometry is a significant component of the femoral shape variation. Significant interspecific differences in the direction of the vectors of allometric coefficients have been previously reported in the mandible (Durão et al., 2019) and the humerus (Durão et al., 2020) (Supplementary Information, Table S7-7). No significant difference in the length of the vectors was found, which means that the amount of shape changes per size unit is equal in both taxa. The fact that both species have a similar magnitude of allometric shape changes in the femur may be due to the important involvement of the femur in corresponding types of locomotion from an early age. Specifically, very young individuals of *A. scherman* quickly show an identical digging behaviour to adults (Airoldi et al., 1976). To our knowledge, the age at which southern water voles begin to swim has not been reported but personal observations (J. V.) suggest that this activity appears not too late after weaning. Although the mechanical action of the femur is different in digging and swimming, functional pressure can be alike (Salton & Sargis, 2009; Samuels & Valkenburgh, 2008; Samuels et al., 2013; Smith & Savage, 1956) contributing to a similar magnitude of the femoral shape change during postnatal ontogeny in these species. The fact that the mandible and humerus play a preponderant role in the digging process makes the functional pressure produce important morphological changes in these bones in a short time. Since in *A. sapidus* these structures are not subjected to the same functional pressure, their age-related changes are not so rapid. Although, in semiaquatic species, such as *A. sapidus*, the femur plays an important role in swimming, in the tibia and metatarsals there are key changes associated with the generation of propulsion during the power stroke and with paddling during swimming (Samuels & Valkenburgh, 2008). This could justify why, unlike the femur, in the mandible (Durão et al., 2019) and the humerus (Durão et al., 2020) the length of the vectors also differed significantly between species.

It has been suggested that time is needed for changes in the direction of allometric trajectories to take place (e.g., Voje et al., 2013) due to the high costs to growth dynamics (Gould, 1966). However, several works have shown that ontogenetic trajectories themselves can evolve, being prone to selection and evolutionary change (Adams & Nistri, 2010; Gray et al., 2019; Wilson & Sánchez-Villagra, 2010). Our results suggest that ontogeny may be more flexible than previously

thought and that locomotion mode is an important selective force modelling the allometric trajectory of the involved bones. The different functional pressures exerted on the femur in the two studied species may have led to phenotypic variation and consequently to differences between the corresponding allometric trajectories.

In all age classes, the shape of the femur differed significantly between *A. sapidus* and *A. scherman*. Their phenotypic trajectories showed a different direction, indicating that not only the shape of the bone differs in each age class, but also that shape changes occurring during postnatal ontogeny are not concordant in the two species. The angle between phenotypic trajectories was quite similar to that observed in the allometric trajectories, which may suggest that a significant amount of the variation in femur shape is allometric. Similar results were also reported for the mandible of these species (Durão et al., 2019). In the humerus, in addition to the interspecific differences in the direction of the corresponding phenotypic trajectories, the length of these was also significantly different between both taxa, evidencing a larger shape change during the postnatal growth of this bone in *A. scherman* than in *A. sapidus* (Durão et al., 2020). The relative amount of shape variation explained by the factor species was also greater in the humerus than in the femur (compare results from Table 7-4 with those of Table 6-4). As results of the PCAs revealed, while in the humerus, differences between species were mainly explained by PC1, which accounted for 31% of total shape variation (Durão et al., 2020) in the femur differences between species were mostly explained by PC2, which accounted for less than 12% of the total shape variation. These results seem to indicate that functional pressures are related to the type of locomotion and that, depending on the role of each bone, the shape changes occurring during ontogeny may be more or less pronounced. The more marked shape changes of the humerus during postnatal ontogeny are concurrent with the prominent action of this bone in the digging process, and with the fact that this is a biomechanically and energetically very demanding activity (White, 2005).

In semiaquatic animals, relatively major morphological changes in the distal bones of hindlimbs are expected, taking into account their involvement in producing propulsive forces during swimming (Samuels & Valkenburgh, 2008). To test this hypothesis, it would be interesting, for example, to perform comparative morphological analyses by means of geometric morphometrics on the postnatal ontogeny of the tibia in fossorial and semiaquatic water voles, especially bearing in mind that certain evolutionary changes in the form of this bone have been reported in *Arvicola* by using linear measurements (Cubo et al., 2006).

#### 7.4.3. Biomechanical consequences of femur shape

Locomotion imposes strong demands on the musculoskeletal system, which may affect bone morphology and the organization of attached musculature (Biewener & Patek, 2018). Our results

on the femur of *A. sapidus* and *A. scherman* show that the morphological distances between these species were significantly different in all age classes. Distances were greater in the non-allometric shape data than shape data, which reveals that these taxa shared part of allometric shape changes. Several interspecific differences in the adult femur shape were also observed, the most conspicuous being the extension of the greater and third trochanter, and the position of the *fovea capitis*.

### **Fossorial locomotion**

The morphology of the third trochanter is highly variable in the mammalian femur, in terms of its presence/absence, lateral expansion and proximo-distal length (Salton & Sargis, 2009). Both *A. scherman* and *A. sapidus* show this tubercle but in the former species, it is wider and much distal. As described for example in the capybara (*Hydrochoerus hydrochaeris*), in this part of the femur inserts the gluteus superficialis muscle (García-Esponda & Candela, 2016), which originates from the lumbodorsal fascia and that helps flex the hip joint. As has been reported for several mammal species, the mass of this muscle seems to have noticeable effects on the size, position and shape of the third trochanter (Anemone & Covert, 2000; García-Esponda & Candela, 2016; Salton & Sargis, 2009; Sargis, 2002; Smith & Savage, 1956). In particular, a wider third trochanter is linked to the powerful development of the gluteus superficialis muscle (Smith & Savage, 1956). This feature may provide a mechanical advantage because it increases the efficiency of the moment arm as well as provides a great lever for gluteus superficialis muscle (Salton & Sargis, 2009; Sargis, 2002). A robust third trochanter also contributes to the hip stabilization during the extension of the leg and may be reduced bending stresses. This trait has also been found in other fossorial mammals (Salton & Sargis, 2009), such as the Hispaniolan solenodon (*Solenodon paradoxus*), the mole-like rice tenrec (*Oryzoryctes hova*), the four-toed rice tenrec (*Oryzoryctes tetradactylus*) and the naked mole-rat (*Heterocephalus glaber*). As suggested by Salton and Sargis (2009), the sturdiness of this trochanter permits a powerful thigh extension with some abduction, action related to throwing back the loose earth to kicking it out of the burrow. Since in *A. scherman* the hindlimbs play a relatively important role in the digging process (Airoidi et al., 1976; Laville, 1989, 1989b), a stronger flex of the hip could be linked to the corresponding mechanical requirement.

The lesser trochanter of *A. scherman* is oriented postero-medially and is larger than in *A. sapidus*. Similar morphological features than we have observed in *A. scherman* had already been described in other diggers, such as species of the genus *Tympanoctomys*, scratch-digger/chisel-tooth diggers (Pérez et al., 2017), and representatives of the family Bathyergidae (Sahd et al., 2019). This trochanter provides the insertion site for the iliopsoas complex, the strongest flexor of the hip, that has an important function in standing, walking and running, namely in the recovery phase. In *A. scherman*, the well-developed lesser trochanter could indicate a large insertion area

for this complex. Its postero-medial protraction could be related to parasagittal movements and a strong lateral rotation of the femur considering that the medial position of the lesser trochanter increases the lever arm for the iliopsoas muscle (Argot, 2002; Taylor, 1976; Toledo et al., 2015). *Arvicola scherman* also shows a slight variation on the femur head angle in relation to *A. sapidus*, being more medially in the latter species. These differences could be linked to the restricted planes of motion (Anemone & Covert, 2000; Salton & Sargis, 2009; Szalay & Sargis, 2001) and consequently associated with differences in hip mobility between the two species. The femur of *A. scherman* exhibits a cranial-medial shift of the *fovea capitis* related to *A. sapidus*. In this dimple attach the teres femoris ligament, one of the large ligaments that connect the femoral head to the hip. The relatively great extension of the *fovea capitis* in *A. scherman* suggests a strong ligament and a greater stabilization of the hip and knee. The general morphology of the lesser trochanter in *A. scherman* is consistent with the ability for extension and flexion of the hip as well as, abduction and external rotation of the femur. These movements are favoured by the presence of a strong ligament that helps to stabilize the hip when vigorously kicks. In turn, the medial position of the femur head in *A. scherman* may limit hip mobility at parasagittal motion, while maintaining the capacity for extension and flexion. These morphological characteristics in *A. scherman* are probably related to the digging process, specifically, to the soil removal, in which the angle between the pelvis and the femur diminishes, and the hip is extended backward to sweep loose soil farther away from the burrow.

Another distinctive feature of *A. scherman* with respect to *A. sapidus* is the existence of a more robust femur, which is congruent with the results published in previous studies based on linear measurements (Cubo et al., 2006; Ventura, 1988, 1990, 1992). This typical trait of fossorial rodents (Biknevicius, 1993; Casinos et al., 1993; Samuels & Valkenburgh, 2008; Wilson & Geiger, 2015) is related to withstand the bending and torsion forces placed on the limbs during the digging process (Biknevicius, 1993; Stein, 2000). The robustness of the femur in *A. scherman* likely results from both the support that the bone needs for the development of muscles and as a response to the mechanical stress that hindlimbs are continuously subjected to. Compared to *A. sapidus*, *A. scherman* exhibits a wide distal epicondyle which provides a great surface area for the insertion of the gastrocnemius and soleus muscles, plantar flexors of the foot (García-Esponda et al., 2016). The increase in the epicondylar area may aid in resisting the tendency of the body to be pushed backward while digging, as suggested by Samuels and Valkenburgh (2008) for other chisel-tooth digger rodent species (Bathyergids and Spalacids).

### ***Aquatic locomotion***

Swimming imposes challenges for semiaquatic species because water is a dense and viscous medium that establishes a strong hydrodynamic demand on the musculoskeletal system (Gillis &

Blob, 2001). This requirement can lead to morphological changes that allow improving locomotor performance and stability, such as increased speed, drag reduction, improved thrust output, and increased manoeuvrability (Fish & Stein, 1991; Fish, 2016 and references therein). Different adaptations of the hindlimbs seem to have been developed by different quadrupedal paddling mammals with semiaquatic habits (Botton-Divet et al., 2016; García-Esponda & Candela, 2016; Stein, 1988). These morphological changes seem to be related to the amount of time spent by the animal in water, and to the activities performed there (Dunstone, 1979; Stein, 1988). Semiaquatic animals, due to their great dependence on land once compared to their terrestrial relatives, display few or absent limb specializations (García-Esponda & Candela, 2016; Thewissen & Taylor, 2007). This moderate morphological variation appears to be associated with functional needs both on land and in water (Stein, 1989). As for *Arvicola*, we observed that *A. sapidus* shows, in comparison with *A. scherman*, a slight medial-cranial extension of the greater trochanter. This tubercle provides the insertion area for the gluteus piriformis and medius muscles, both extensors and abductors of the hip joint (García-Esponda & Candela, 2016). The modest expansion of the greater trochanter in *A. sapidus* could be related to the relative size increase of the gluteus medius muscle, feature also found in other semiaquatic rodent species (Candela & Picasso, 2008; Stein, 1988). This muscle is involved in rapid movement towards the end of the stroke (Smith & Savage, 1956). As suggested by Stein (1988), the size increase of the gluteus medius muscle allows decreasing the resistance to water, maintaining the impulse after starting the power phase. This morpho-functional relationship remains to be tested in *A. sapidus*.

## 7.5. CONCLUSIONS

Results obtained in the present study reveal a combination of phylogenetic and functional signals in the postnatal growth of the femur in *A. sapidus* and *A. scherman*. On the one hand, shared common traits between these taxa were found, which can be considered traces of their common origin. On the other hand, we found evidence that certain variations in the femur shape and particular differences in allometric and phenotypic trajectories between these taxa are associated with their different types of locomotion. Our study emphasizes the importance of developing comparative studies in closely related species to assess to which extent functional and phylogenetic factors affect the growth patterns of bones involved in locomotion. As for genus *Arvicola* in particular, it would be interesting to extend this kind of studies to other semiaquatic or fossorial water vole populations, and even others that can change the type of locomotion according to the reproduction cycle and/or the environmental conditions (Barreto & MacDonald, 2000; Kratochvíl & Grulich, 1961; Potapov et al., 2012; Stewart et al., 2019; Telfer et al., 2003).

7.6. SUPPLEMENTARY INFORMATION

Table S7-1 Definition of the 20 anatomical landmarks used in the geometric morphometric analyses.

Landmark	Description
1	Most distal point of the proximal curvature of the femoral neck
2	Medio-proximal tip of the greater trochanter
3	Most proximal point of the third trochanter
4	Most lateral point of the third trochanter
5	Most distal point of the third trochanter
6	Most distal point between the diaphysis and lateral epicondyle
7	Most proximo-medial point of the intersection between the lateral condyle and the margin of the intercondylar fossa
8	Most proximo-lateral point of the intersection between the medial condyle and the margin of the intercondylar fossa
9	Most distal point of the adductor tubercle
10	Most distal point of the medial condyle at the articular capsule (patellar surface)
11	Most proximal point of the articular capsule (patellar surface)
12	Most distal point of the lateral condyle at the articular capsule (patellar surface)
13	Most distal point of the lesser trochanter
14	Most medial point of the lesser trochanter
15	Most proximal point of the lesser trochanter
16	Most internal point of the external margin of the femoral head
17	Most external point of the external margin of the femoral head
18	Most distal point of the greater trochanter
19	Central point of fovea capitis
20	Most latero-distal point of the intertrochanteric line

Table S7-2 Factorial ANOVA statistical assessment of the effects of sex, age class and the interaction between them on femur size (logarithm of centroid size) conducted on the *Arvicola scherman* sample.

Effect	df	SS	MS	F	p
Sex	1	0.001	0.001	0.5	0.462
Age class	5	2.270	0.454	310.4	<0.001
Age class x Sex	5	0.011	0.002	1.5	0.213
Residuals	81	0.119	0.002		

Abbreviations: *df*, degrees of freedom; *SS*, sum of squares; *MS*, mean squares; *F*, F statistic; *Z*, effect-size; *p*, *p*-value.

Table S7-3 Procrustes ANOVA performed for *Arvicola scherman* sample testing the effects of logarithm of centroid size (LCS), sex and the interaction between them on femur shape.

Effect	df	SS	MS	Rsqr	F	Z	p
LCS	1	0.072	0.072	0.279	35.562	8.273	<0.001
Sex	1	0.003	0.003	0.012	1.533	1.225	0.115
LCS x Sex	1	0.003	0.003	0.010	1.299	0.801	0.209
Residuals	89	0.179	0.002	0.699			
Total	92	0.256					

Abbreviations: *df*, degrees of freedom; *SS*, sum of squares; *MS*, mean squares; *Rsqr*, R squared values; *F*, F statistic; *Z*, effect-size; *p*, *p*-value.



POSTNATAL ONTOGENY OF THE FEMUR

Table S7-4 Factorial ANOVA statistical assessment of the effects of sex, age class and the interaction between them on femur size (logarithm of centroid size) conducted on the *Arvicola sapidus* sample.

Effect	<i>df</i>	SS	MS	F	<i>p</i>
Sex	1	0.011	0.011	3.0	0.087
Age class	5	2.077	0.415	118.8	<0.001
Age class x Sex	5	0.027	0.005	1.5	0.186
Residuals	77	0.269	0.004		

Abbreviations: *df*, degrees of freedom; SS, sum of squares; MS, mean squares; F, F statistic; Z, effect-size; *p*, *p*-value.

Table S7-5 Procrustes ANOVA performed for *Arvicola sapidus* sample testing the effects of logarithm of centroid size (LCS), sex and the interaction between them on femur shape.

Effect	<i>df</i>	SS	MS	Rsqr	F	Z	<i>p</i>
LCS	1	0.088	0.087	0.385	55.355	7.910	<0.001
Sex	1	0.003	0.003	0.014	2.036	1.642	0.070
LCS x Sex	1	0.002	0.002	0.008	1.268	0.743	0.213
Residuals	85	0.134	0.002	0.592			
Total	88	0.227					

Abbreviations: *df*, degrees of freedom; SS, sum of squares; MS, mean squares; Rsqr, R squared values; F, F statistic; Z, effect-size; *p*, *p*-value.

Table S7-6 Eigenvalues and percentages of variance in the principal component analysis performed on Procrustes coordinates.

Component	Eigenvalues	% Var.	% Cum.	Component	Eigenvalues	% Var.	% Cum.
1.	0.00099186	34.012	34.012	28.	0.0001359	0.466	94.944
2.	0.00033854	11.609	45.621	29.	0.0001217	0.417	95.361
3.	0.00019257	6.603	52.224	30.	0.0001183	0.406	95.767
4.	0.00014932	5.120	57.345	31.	0.0001009	0.346	96.113
5.	0.00013853	4.750	62.095	32.	0.0000960	0.329	96.442
6.	0.00010539	3.614	65.709	33.	0.0000903	0.310	96.751
7.	0.00009914	3.400	69.109	34.	0.0000849	0.291	97.042
8.	0.00008657	2.969	72.077	35.	0.0000814	0.279	97.322
9.	0.00007326	2.512	74.590	36.	0.0000764	0.262	97.583
10.	0.00006376	2.186	76.776	37.	0.0000703	0.241	97.824
11.	0.00006107	2.094	78.870	38.	0.0000614	0.211	98.035
12.	0.00005224	1.791	80.662	39.	0.0000610	0.209	98.244
13.	0.00004605	1.579	82.241	40.	0.0000577	0.198	98.442
14.	0.00004013	1.376	83.617	41.	0.0000536	0.186	98.626
15.	0.00003770	1.293	84.910	42.	0.0000512	0.176	98.802
16.	0.00003630	1.245	86.155	43.	0.0000477	0.163	98.965
17.	0.00003353	1.150	87.304	44.	0.0000424	0.146	99.111
18.	0.00003221	1.104	88.409	45.	0.0000406	0.139	99.250
19.	0.00002865	0.982	89.391	46.	0.0000388	0.133	99.383
20.	0.00002520	0.864	90.255	47.	0.0000356	0.122	99.505
21.	0.00002160	0.741	90.996	48.	0.0000317	0.109	99.614
22.	0.00002008	0.689	91.684	49.	0.0000304	0.104	99.718
23.	0.00001788	0.613	92.298	50.	0.0000251	0.086	99.804
24.	0.00001779	0.610	92.908	51.	0.0000216	0.074	99.878
25.	0.00001696	0.581	93.489	52.	0.0000196	0.067	99.945
26.	0.00001469	0.504	93.993	53.	0.0000160	0.055	100.000
27.	0.00001414	0.485	94.478				

Abbreviations: % Var., % Variance; Cum. %, Cumulative %

Table S7-7 Pairwise results in allometric trajectory and phenotypic trajectory analyses in mandible, humerus and femur without age classes 0 and 1.

	Mandible	Humerus	Femur	Femur without 0 & 1
Allometric trajectory	$\Delta d = 0.045; p = 0.020$ $\theta = 35.66^\circ; p < 0.001$	$\Delta d = 0.06; p < 0.001$ $d_{A.scherman} = 0.24;$ $d_{A.sapidus} = 0.18$ $\theta = 32.36^\circ; p < 0.001$	$\Delta d = 0.017; p = 0.067$ $d_{A.scherman} = 0.169;$ $d_{A.sapidus} = 0.186$ $\theta = 26.02^\circ; p < 0.001$	$\Delta d = 0.019; p = 0.244$ $d_{A.scherman} = 0.196;$ $d_{A.sapidus} = 0.215$ $\theta = 34.68^\circ; p < 0.001$
Phenotypic trajectory	$\Delta d = 0.001; p = 0.922$ $\theta = 34.01^\circ; p < 0.001$ $D_p = 0.211; p = 0.201$	$\Delta d = 0.026; p = 0.05$ $d_{A.scherman} = 0.163;$ $d_{A.sapidus} = 0.137$ $\theta = 32.34^\circ; p < 0.001$ $D_p = 0.31; p = 0.002$	$\Delta d = 0.009; p = 0.359$ $d_{A.scherman} = 0.138;$ $d_{A.sapidus} = 0.129$ $\theta = 29.45^\circ; p < 0.001$ $D_p = 0.209; p = 0.0752$	$\Delta d = 0.004; p = 0.601$ $d_{A.scherman} = 0.068;$ $d_{A.sapidus} = 0.064;$ $\theta = 36.96^\circ; p < 0.001$ $D_p = 0.132; p = 0.5859$

POSTNATAL ONTOGENY OF THE FEMUR

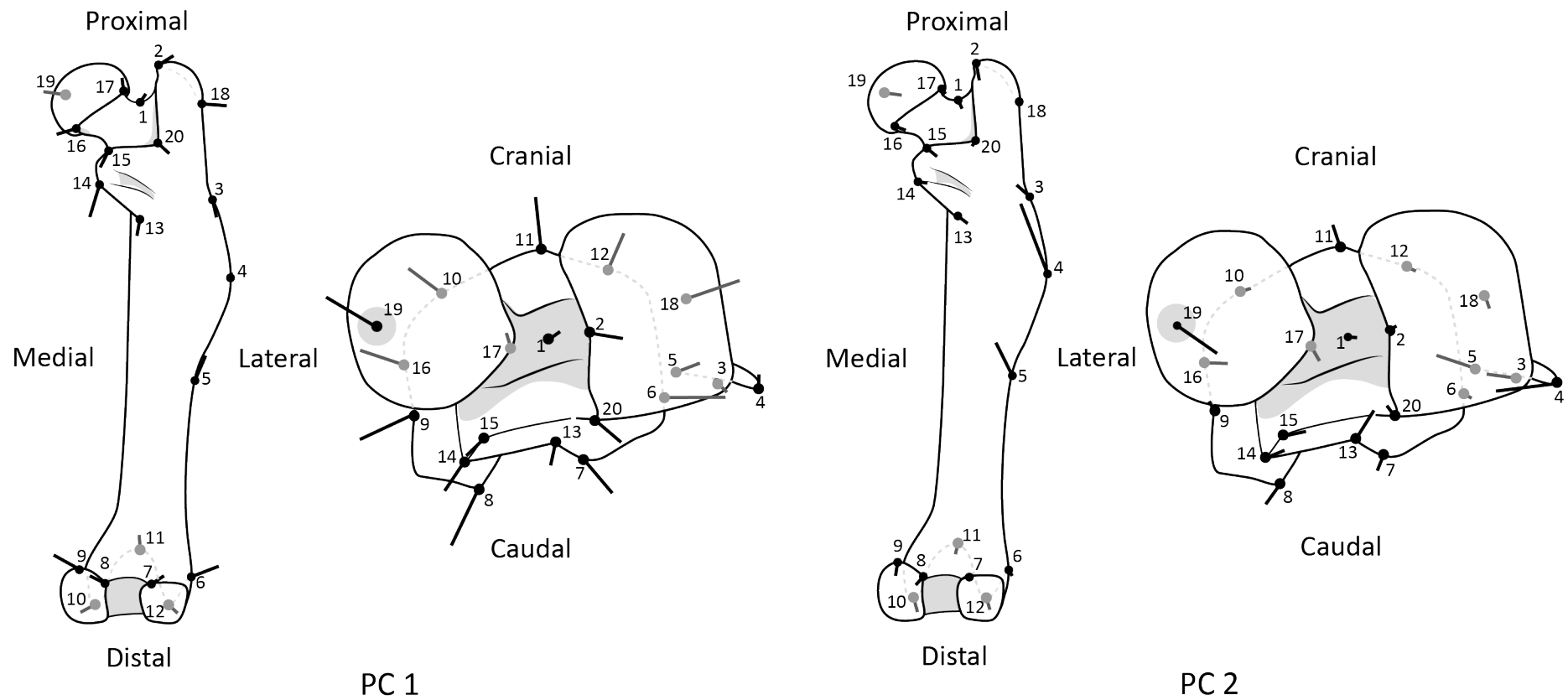


Fig. S7-1 Shape changes associated with each extreme of the first two principal components (PC1 and PC2) (0.10) from the principal component analysis. Dots represents landmarks. Black dots in the visible plan and grey dots in the back plan. The displacement vectors of shape changes are displayed into the schematic representation of the consensus of the femur in caudal and ventral view.

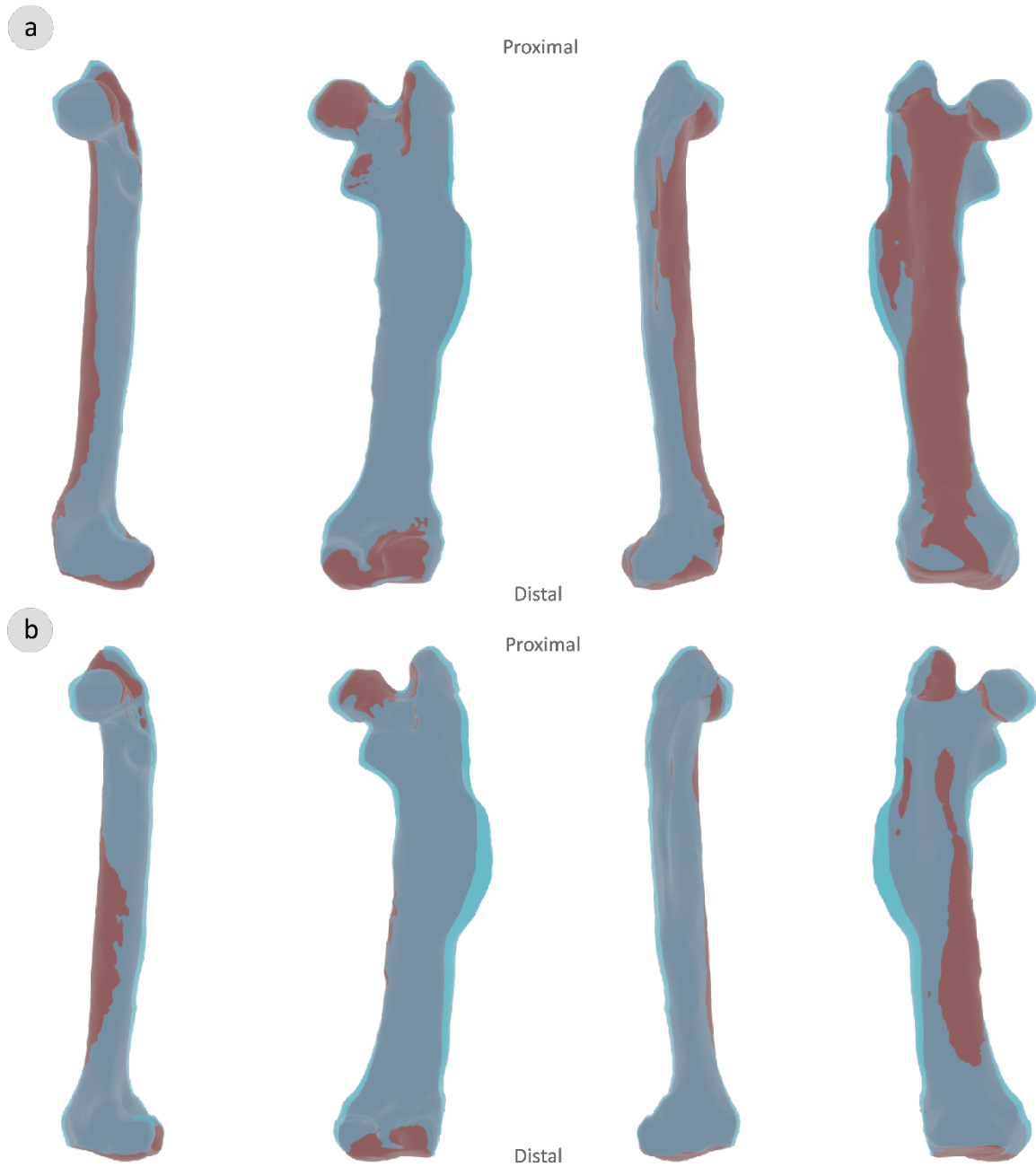


Fig. S7-2 Shape changes of the femur between specimens of *Arvicola sapidus* (red) and *Arvicola scherman* (blue). (a) In specimens of age classes 0 - 3. (b) In specimens of age classes 4 and 5. Bones are represented from left to right in medial, caudal, lateral and cranial views.

POSTNATAL ONTOGENY OF THE FEMUR

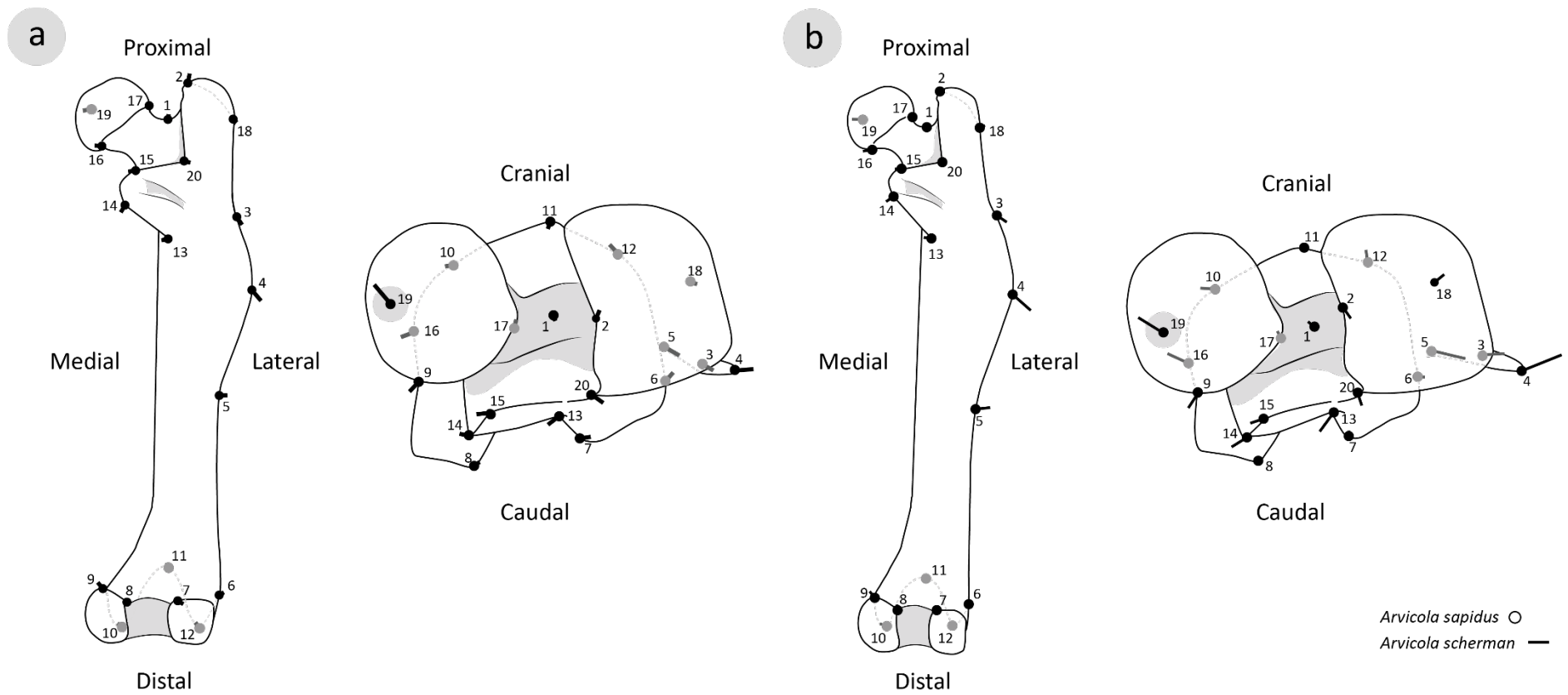


Fig. S7-3 Visualization of shape changes of the femur between specimens of *Arvicola sapidus* (dot) and *Arvicola scherman* (line). (a) In juvenile and subadult individuals (age classes 0 - 3). (b) In adult individuals (age classes 4 and 5). Black dots in the visible plan and grey dots in the back plan. The displacement vectors of shape changes are displayed into the schematic representation of *A. sapidus* femur in caudal and ventral view.

---

# CHAPTER 8

COMPARATIVE ONTOGENETIC HISTOLOGY OF LONG  
BONES BETWEEN FOSSORIAL AND SEMIAQUATIC  
WATER VOLES

**Ana Filipa Durão, Cayetana Martínez-Maza,  
Francesc Muñoz-Muñoz, Jacint Ventura**

---

The content of this chapter is part of a manuscript in preparation

---



## CHAPTER 8. COMPARATIVE ONTOGENETIC HISTOLOGY OF LONG BONES BETWEEN FOSSORIAL AND SEMIAQUATIC WATER VOLES

---

### 8.1. INTRODUCTION

The relationship between bone microanatomy and lifestyle (aquatic, semiaquatic or terrestrial) has been studied in several vertebrate taxa (e.g., Canoville & Laurin, 2010; Fish & Stein, 1991; Houssaye et al., 2013; Laurin et al., 2011; Meier et al., 2013; Stein, 1989; Wall, 1983) in order to understand the microstructural specializations associated with locomotion. In this context, the ratio between bone cortex and medullary cavity has been suggested as a biomechanical indicator of potential lifestyles (e.g., Canoville & Laurin, 2010; Laurin et al., 2011; Meier et al., 2013). For instance, long bones of aquatic vertebrates have shown massive bones with an occlusive medullary cavity and terrestrial mammals have shown a large medullary cavity associated with moderately thick compact cortex (e.g., Canoville & Laurin, 2010; de Ricqlès & Buffrènil, 2001; Fish & Stein, 1991; Laurin et al., 2004). Although the relation between inner bone structure and terrestrial and aquatic locomotion has been widely studied, there are few studies that attempt to establish this relationship in other modes of locomotion, such as fossorial (Montoya-Sanhueza & Chinsamy, 2017, 2018; Montoya-Sanhueza et al., 2020; Legendre & Botha-Brink, 2018; Walker et al., 2020). In recent years, this interest has increased and an association between subterranean life and increased cortical thickness due to the deposition of bone tissue has been proposed (Montoya-Sanhueza & Chinsamy, 2017).

Bone inner structure is an important source of information about the life of an individual since it records the development and all the constraints that the animal experiences throughout its life (e.g., Enlow, 1962; Smith, 1960; Turner, 1998). Microstructural variation and the distribution of bone tissue type has been understood as a reflection and combination of phylogenetic, ontogenetic, and functional factors (Enlow, 1962; de Ricqlès, 1993, 2007; Castanet et al., 2001; Cubo et al., 2005; Currey, 2002; Gosman, 2012; Maggiano, 2012; Martin et al., 1998; Mcfarlin et al., 2016, Pearson & Lieberman, 2004; Warshaw, 2008). Comparative ontogenetic studies between phylogenetically close species with different lifestyles are a powerful tool to understand the impact of function, recognizing phylogenetic homologies and ontogeny. The genus *Arvicola* is an excellent model to investigate the effect of lifestyle on microanatomical structure of the bone because it shows great ecological versatility, with mainly semiaquatic or fossorial populations. In the present study we used two species of *Arvicola* representative of each of these ecotypes, the Southwestern water vole, *A. sapidus* (semiaquatic) and the montane water vole, *A. scherman*



(fossorial). Here we used the taxonomic pattern by Musser and Carleton (2005) but see General Introduction (section 1.4. *Arvicola*).

Within fossorial rodent species, three digging modes have been recognized (Hildebrand, 1985; Stein, 2000): scratch (i.e., it uses the claws of the manus to break the soil: e.g., *Geomys*); head-lift (i.e., it uses the incisors together with the skull to form a powerful drill, e.g., *Nannospalax*), and chisel-tooth digging (i.e., it uses the incisors to break down the ground, e.g., *Cryptomys*). The montane water vole, *A. scherman* is a chisel-tooth digger that live underground in complex and extensive burrow systems constructed in hard soils (Airoidi, 1976; Airoidi & de Werra, 1993; Laville, 1989). This species lives mainly in meadows, pastures, and orchards (Giraudoux et al., 1997) and has a great influence on the ecosystem in which it lives due to the importance they have as prey (Giraudoux et al., 2020; Rodríguez et al., 2020; Weber et al., 2002). Its digging mode is characterized by stereotyped cyclic events, in which the incisors are driven into the ground to loosen the earth, and with quick movements of fore and hind limbs it expels the soil from the burrow. The compaction of the tunnel walls is carried out with muzzle and incisors (Airoidi et al., 1976; Laville, 1989). Several previous works have observed morphological variations partly associated with this type of locomotion (Cubo et al., 2006; Laville, 1989b; Laville et al., 1989), namely in the humerus (Durão et al., 2020), the femur (Durão et al., 2022) and the mandible (Durão et al., 2019; Ventura & Casado-Cruz, 2011), structures directly involved in the digging activity. The most recent studies were performed applying the geometric morphometrics method and associated statistics (Durão et al., 2019, 2020, 2022).

The Southern water vole, *A. sapidus* is a semiaquatic species that lives on the banks of calm courses or bodies of water with high vegetation cover. The construction of its gallery takes place on the water's edge (Gosálbez, 1987; Rigaux et al., 2008), to facilitate access to water. Expert swimmers and divers, their swimming style is characterized by drag-based paddling propulsion, i.e., alternative movements of the fore and hind limbs, obtaining propulsion through the legs. A recent study comparing postweaning ontogeny of the femur between *A. sapidus* and *A. scherman* showed that, compared to fossorial water voles, *A. sapidus* shows a slight increase in the greater trochanter, feature that has been interpreted as an adaptive response to increase propulsion through water (Durão et al., 2022).

Osteohistological studies between *A. sapidus* and *A. scherman* have been limited to the inner enamel with a skeletochronology perspective (Marcolini et al., 2011). The absence of histological information, especially from long bones, makes impossible to have a holistic approach to bone changes related to locomotion and prevents meaningful comparative studies with other groups. In this sense, the present work aims to (1) describe the histological observations in the middle diaphyseal section of the humerus and femur in *A. sapidus* and *A. scherman*, (2) compare histological features between species and bones and (3) explore the relationship between bone

inner structure and function (locomotion). Considering the involvement of these structures in locomotion and the results obtained in the macrostructure analyses (Durão et al., 2020, 2022), we hypothesize that the inner bone, especially in the humerus, will show microstructural specializations to the different lifestyles, as well as shared histological characteristics between the two species due to their close phylogenetic relationship.

Bone modelling provides direct evidence of the cellular process underlying bone growth, while results of geometric morphometric analyses inform on the direction and magnitude of bone growth. With this in mind, the growth pattern obtained at the microstructural level in the humerus and femur of these species of *Arvicola* will be contrasted with the corresponding ontogenetic trajectories described in previous studies (Durão et al., 2020, 2022).

## 8.2. MATERIALS AND METHODS

### 8.2.1. Sample

Cross-section from 42 right femora (f) and 42 left humeri (h) of *Arvicola sapidus* ( $f_n=21$ ,  $h_n= 19$ ) and *A. scherman* ( $f_n=21$ ,  $h_n= 23$ ) were studied (Table 8-1). The sample of *A. sapidus* and *A. scherman* were collected in the Ebro Delta (Tarragona, Spain), and the Aran Valley (Lleida, Spain), respectively, between 1983 and 1984. Since these populations are the same as those used in previous studies (Durão et al., 2019, 2020, 2022; Ventura, 1988; Ventura & Casado-Cruz, 2011), the specimens had already been distributed into six age classes according to moulting phase, sexual stage and skull morphology (for details, see Garde et al., 1993; Ventura & Gosálbez, 1992): class 0, 3 weeks maximum; class 1, between 3 and 6 weeks; class 2, between 6 and 10 weeks; class 3, between 10 and 14 weeks; class 4, between 14 weeks and one winter; and class 5, individuals that have lived more than one winter. Due to the histological characteristics shared among the different age classes, in the histological descriptions, the age classes were grouped in younger (age classes 0 and 1) and older juvenile individuals (age class 2); subadult individuals (age class 3) and adult individuals (age classes 4 and 5). Catalogue number of each specimen is indicated in Supplementary Information (Table S8-1).

## COMPARATIVE HISTOLOGY OF THE HUMERUS AND THE FEMUR

Table 8-1 Sample size for each species, age class, sex, and bone.

Species	Bone	Sex	Age class					Total		
			0	1	2	3	4		5	
<i>Arvicola sapidus</i>	Humerus	F	1	1	1	2	2	2	9	19
		M	2	0	2	2	2	2	10	
	Femur	F	0	1	3	2	2	2	10	21
		M	4	0	1	2	2	2	11	
<i>Arvicola scherman</i>	Humerus	F	2	2	2	2	2	2	12	23
		M	1	2	2	2	2	2	11	
	Femur	F	1	3	2	2	2	2	12	21
		M	2	1	1	2	1	2	9	

Abbreviations: F, female; M, male

### 8.2.2. Histological sections and image acquisition

Cross-sections were prepared from mid-diaphysis. In the humerus, the sections were cut below deltoid crest and in the femur below the third trochanter, as show the Fig. 8-1.

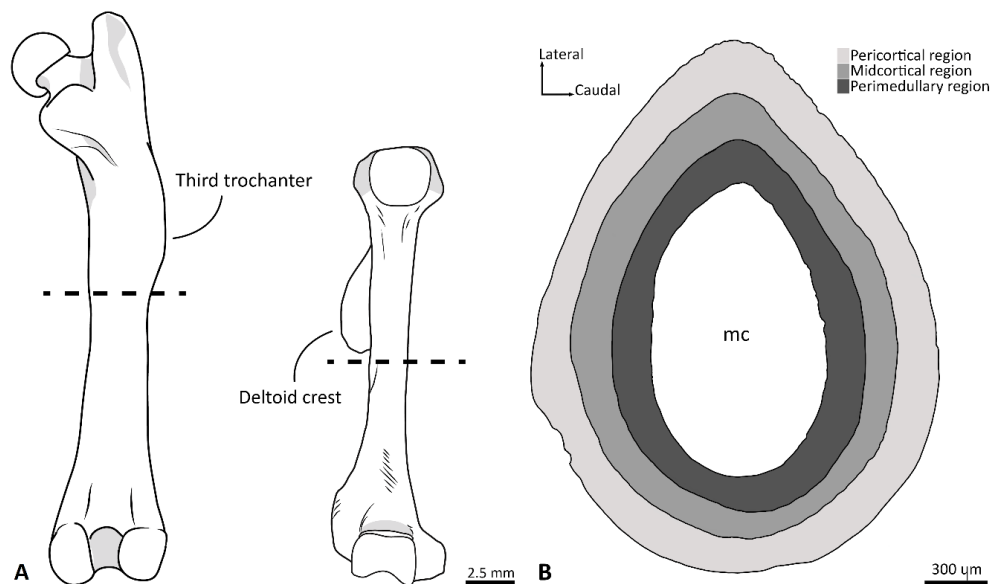


Fig. 8-1 (A) Representation of the right femur and left humerus (from left to right) of an adult (age class 5) *Arvicola sapidus* from caudal view. Dashed lines indicate the histological cross-section cut. (B) Delimitation of the cortical regions (pericortical, midcortical and perimedullary region) on a schematic humeral cross-section (mc, medullary cavity). The regions were divided proportionately.

All the cut bones were dehydrated through two successive changes of 100% ethanol at 24-h intervals, under vacuum at room temperature. As preparation for embedding, the bones were immersed in two successive changes of 100% Methyl Salicylate at 24h intervals, and in a series of infiltration solutions based on Methyl Methacrylate, n-Butyl Phthalate and Benzoyl Peroxide (MMA) that were renewed at intervals of 24h and 96h. Then, to proceed with the embedding, each bone was placed in a separate small, labelled jar in a solution MMA and cured at room temperature

in the hood. Once mostly cured, the jars were exposed to UV light overnight and stored in the oven at 37 °C for 24h (minimum).

Cured embedded bone blocks were cracked out of the jars manually with the help of a hammer, being ready for section preparation. The blocks were cut with a diamond blade at the distal end of the midshaft to expose the surface of the bone. Final polish was achieved manually on a Buehler® MetaServ™ 250 using an 800 and 1200 grit paper. To reduce the contact area with the slide, all blocks were cut. The blocks were mounted on plastic slides using EXAKT 402 together with the light cured adhesive Technovit® 7210. Mounted blocks were cut to produce thick sections of about  $120\mu\text{m} \pm 5\mu\text{m}$  and ground to  $100 \pm 5\mu\text{m}$  finishing with 1200 grit paper.

Images of the sections were obtained with a 10x objective in conventional transmitted light (CTL) and circularly polarized light (CPL) using a Leica-Leitz DMRXE Universal microscope, configured with a Marzhauser motorized stage. Real-time assembly was performed during image acquisition with the Syncroscopy Automontage software, resulting in a gigapixel image. Transmitted light images allow easier identification of osteocyte lacunae and vascular canal morphologies, while CPL images provide information on collagen fibre orientation (Bromage et al., 2003).

Some authors described the presence of calcified cartilage islands in the cortex of the rodents' long bones (Bach-Gansmo et al., 2013; Ip et al., 2016; Shipov et al., 2013). In order to visualize the calcified cartilage areas, as well as facilitate the identification of cement lines (resting and resorption lines) and vascular spaces, bone sections were stained with toluidine blue. All cross-sections were visualized under a CTL (10x) and images obtained as described above.

All histological sections were prepared at the Hard Tissue Research Unit located at the New York University College of Dentistry and are housed in the Mammalian Biology Research Group of the Universitat Autònoma de Barcelona (UAB, Bellaterra, Spain).

### 8.2.3. *Image Processing*

Each CTL and CPL image was transferred and aligned in layers into GIMP (GNU Image Manipulation Program). For a better visualization of the growth pattern in each bone, tissue type map was created in each specimen. For that, by eye and manually each tissue type category was delimited and areas with the major bone tissue were painted with an assigned colour code (see section 8.3 Results). In some cases, to clarify the tissue type observed due to the low resolution of the captured image, the sections were examined in real-time.

#### 8.2.4. Tissue type classification

Tissue types were classified based on osteocyte lacunae shape and density, mineralized collagen fiber matrix orientation and vascularity (pore orientation and density), according to criteria used by Warshaw (2008), following de Ricqlès and colleagues' method (summarized in Francillon-Vieillot et al., 1990), with some modifications. Parallel-fibered and lamellar bones were considered independent categories instead of one category (lamellar-zonal category), because has been suggest that these tissue types have different growth rates between them (e.g., Amprino, 1947). Additionally, we have identified hybrid bone as an intermediate tissue between parallel-fibered bone and lamellar bone (for more information see Warshaw, 2008). Examples and a brief description of each tissue type identified in the present study are shown in Fig. 8-2. The tissues were also designated according to their deposition rate, i.e., woven bone with the fastest deposit rate, fibrolamellar bone, parallel-fibered bone, and finally lamellar bone, as the slowest one (e.g., Amprino, 1947; de Margerie et al, 2002). Generally, faster forming tissues display less organized fibrillar structure and/or more vascularization compared to slower deposited tissues (e.g., Francillon-Vieillot et al., 1990; Warshaw et al., 2017).

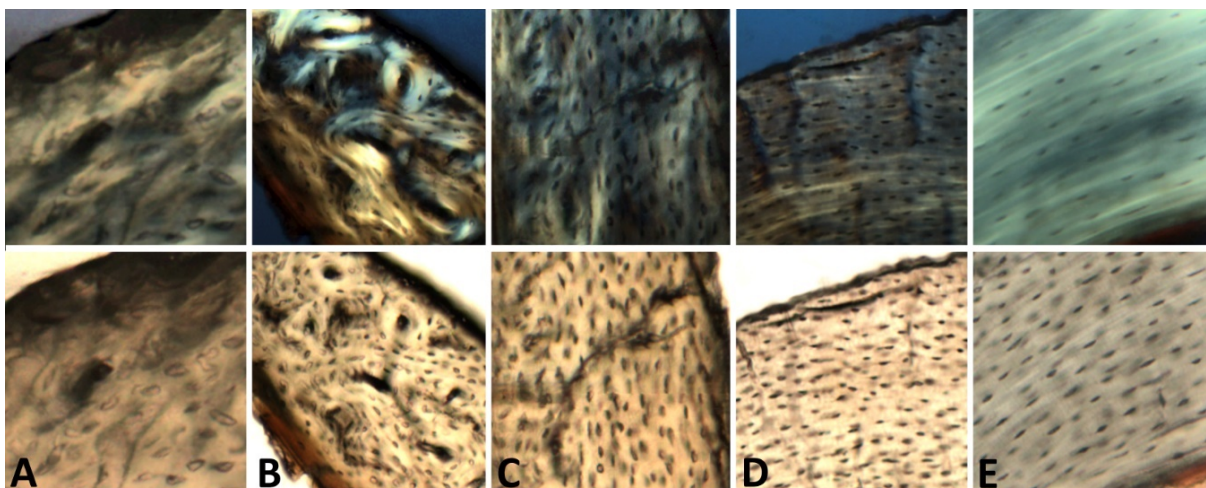


Fig. 8-2 Examples and classification of tissue types according to the definitions of de Ricqlès and colleagues (summarised in Francillon-Vieillot et al. 1990), as modified by Warshaw (2008). At the top are the images of circularly polarized light (CPL) and at the bottom the corresponding conventional transmitted light (CTL). Left to Right – (A) Woven bone is characterized by a random distribution of osteocytes with a rounded or star shape. (B) Fibrolamellar bone is initially characterized by a structure composed of fine cancellous trabeculae of woven bone. More compact tissue is established when the vascular canals are surrounded by lamellar or parallel-fibered bones, forming primary osteons. (C) Parallel-fibered bone is an intermediary tissue between woven bone and lamellar bone in relation to the organization of collagen fibers. Parallel-fibered bone is, more organized than woven bone and is identified based on rounded or more flatted osteocytes. Under CPL collagen fibers are similarly aligned. (D) Hybrid bone comprises the combination of different forms of lacunar osteocyte, which may be more rounded or flattened. These are well aligned with each other but under CPL there is no clear lamellar structure. (E) Lamellar bone is the most organized tissue type, characterized by flattened osteocyte lacunae, well-aligned with each other. Under CPL the alternation of dark and light bands is visible. In case it was not possible to observe the lamellar structure under CPL, the distribution and osteocyte lacunae shape were considered.

Based on previous works (Bach-Gansmo et al., 2013; Ip et al., 2016; Shipov et al., 2013), an additional category called disorganized bone region (DBR) was added. These regions are mostly composed of woven and parallel-fibered bone with calcified cartilage (Fig. 8-3).

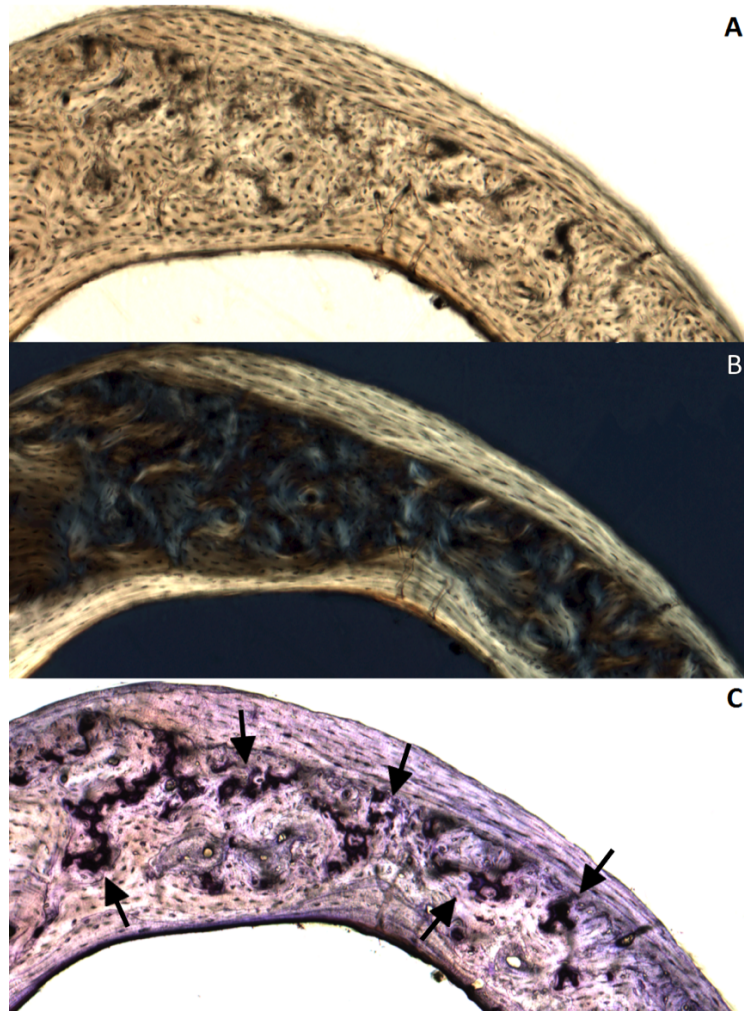


Fig. 8-3 Comparison of the visualization of disorganized bone regions (DBR) with calcified cartilage areas, in a subadult female (F3FAS84120702). (A) Under conventional transmitted light neither the DBR nor the calcified cartilage areas are easily differentiated from lamellar/hybrid bone. (B) Under circularly polarized light, alignment of collagen fibers in the lamellar region and isotropic orientation in the DBR is visible. (C) Toluidine blue staining images allow the identification of calcified cartilage areas easily (black arrows) but do not facilitate the differentiation of DBR from lamellar and hybrid bone.

For each ontogenetic stage of each species and bone we qualitatively describe the dynamics of the bone tissue following the description of Enlow (1962) and Goldman et al. (2009). These characteristics included the distribution of primary periosteal and endosteal bone tissues, deposition of new tissue, presence of resting or resorption lines, distribution of vascular canals on cortex and on margin of bone surface (as recent tissue deposition), and irregular bone surface and resorption cavities (as resorptive bone). Cortical drift pattern was determined using microstructure features, such as distribution of bone tissue types, resorption lines indicating a

change in growth direction, resorption cavities and the presence of faster periosteal tissues deposition (e.g., incorporation of vascular canals at the periosteal surface). The cortex was divided into three equal parts, as in Montoya-Sanhueza & Chinsamy (2017): perimedullary, midcortical and the pericortical region (Fig. 8-1).

### 8.3. RESULTS

Below we describe the qualitative observations of the cross-sections performed in the humerus and femur of *A. scherman* and *A. sapidus* in different age classes: juvenile individuals (younger (age classes 0 and 1) and older juvenile individuals (age class 2)), subadult individuals (age class 3) and adult individuals (age classes 4 and 5). The different tissue types and their description are shown in Fig. 8-2. Since sexual dimorphism was not observed in either of the two species, the description of tissue types was carried out jointly for males and females. Given that, no quantitative analysis was performed on the samples, all analyses referenced below were based on qualitative observation. Throughout the ontogenetic series, *A. sapidus* showed a greater cortical thickness than *A. scherman* in both the femur and humerus (Fig. 8-4 and 8-9).

#### 8.3.1. Ontogenetic changes in the humerus histology

##### ***Arvicola scherman***

The humerus of younger juvenile individuals showed a circular shape with cortical thickness quite similar between specimens, a thin cortical wall and large medullary cavity compared to other age classes. The cortex was comprised mostly of well-vascularized parallel-fibered bone via simple primary vascular canals (Fig. 8-4, 8-5A, B). Layers of hybrid or lamellar bones were mostly limited to pericortical region on the cranial and caudal sides (Fig. 8-4, 8-5C). Resorption occurred throughout the perimedullary region, with greater incidence on the lateral, cranial and craniomedial sides with trabecular bone formation (Fig. 8-5A, D). Periosteal expansion happened around the bone in age class 0, which suggests a predominant tendency of periosteal growth in the first weeks of development. In the humerus of the individuals of age class 1, the periosteal bone deposition in the pericortical region on the medial and cranial side via vascular canals (Fig. 8.5A, D) and the intensive resorption on the perimedullary region indicate bone growth in cranial direction. The humerus of two individuals (H1FAT83081106, H1FAT83112628) of this age showed a DBR on the caudal side of the perimedullary region (Fig. 8-4).

The humerus of older juvenile voles varied in its microstructural organization, while some individuals shared similar histological features with younger juvenile individuals, other specimens shared it with subadult voles (Fig. 8-4). The subperiosteal deposition seen in younger

juvenile individuals intensifies medially and cranially with vascularized parallel-fibered bone via simple primary vascular canals in juveniles of age class 2 (Fig. 8-5E). The humerus of one individual (H2MAT83081114) showed fibrolamellar bone deposition along the bone's medial side. Tissue deposited in the periosteum caused a triangular shape bone in the humerus of two individuals (H2FAT83081117, H2MAT83081114) (Fig. 8-5A). Increased perimedullar resorption on the lateral, cranial and medial sides (Fig. 8-5F, G) and endosteal lamellar bone deposition on the caudal side suggest a cranial cortical shift (Fig. 8-5A). All specimens exhibited a midcortical DBR on the caudal side (Fig. 8-4, 8-5F).

The humerus of subadult individuals showed an increase in periosteal and endosteal lamellar bone deposition in relation to older juvenile individuals, suggesting a slowing of osteogenesis rates. Bone deposited on the periosteal surface remained on the cranial and medial side. On the medial side, intracortical fibrolamellar and parallel-fiber bone deposits were also observed (Fig. 8-4, 8-5H-J). This deposition, together with the intense resorption on the medial side, caused variation in cortical thickness in this region. As in older juvenile individuals, the DBR was seen on the caudal side of the midcortical region (Fig. 8-4, 8-5H), although in most cases this region was more reduced. On cranial and craniomedial side intense resorption was detected in the perimedullary region, with trabeculae visible in one specimen (H3FAT83072827). The triangular shape bone observed in some specimens of older juvenile voles was accentuated in subadult individuals.

The humerus of adult specimens (age classes 4 and 5) showed a cortex mostly composed of lamellar bone (Fig. 8-4, 8-5A, L, M), with vascularized parallel-fiber bone on the medial and cranial side. Although the caudal side still showed DBR, it tends to become residual in specimens of age class 5 (Fig. 8-4, 8-5K, L). The triangular shape of the humerus was maintained in adult individuals. Due to the extensive endosteal resorption, evidenced by resorption cavities and trabecularization, an increase of the medullary cavity compared to subadult was observed in adult voles (Fig. 8-4 and 8-5A). Cortical thickness remained similar. The presence of resorption lines in the medial region (Fig. 8-5I, M), and endosteal lamellar bone deposition on the lateral side suggests a medial cortical shift. Primary osteons were visible on the lateral side (Fig. 8-5M).



## COMPARATIVE HISTOLOGY OF THE HUMERUS AND THE FEMUR

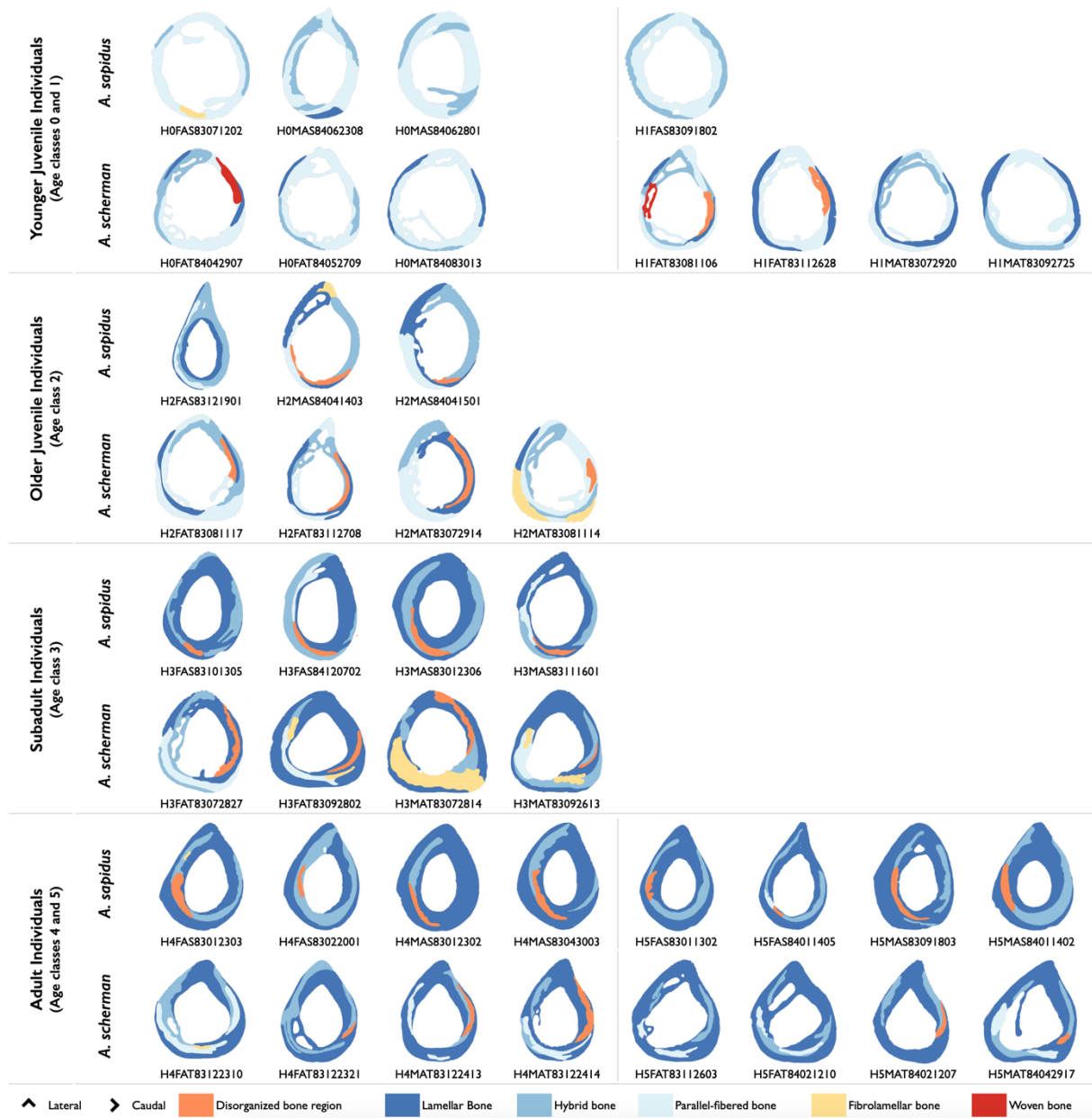


Fig. 8-4 Illustrative maps of the areas occupied by the different bone tissues in the humerus, in all specimens of *A. scherman* and *A. sapidus* used in the study. All images are scaled to the same size to facilitate comparison between specimens. Vertical lines separate age classes within each age group.

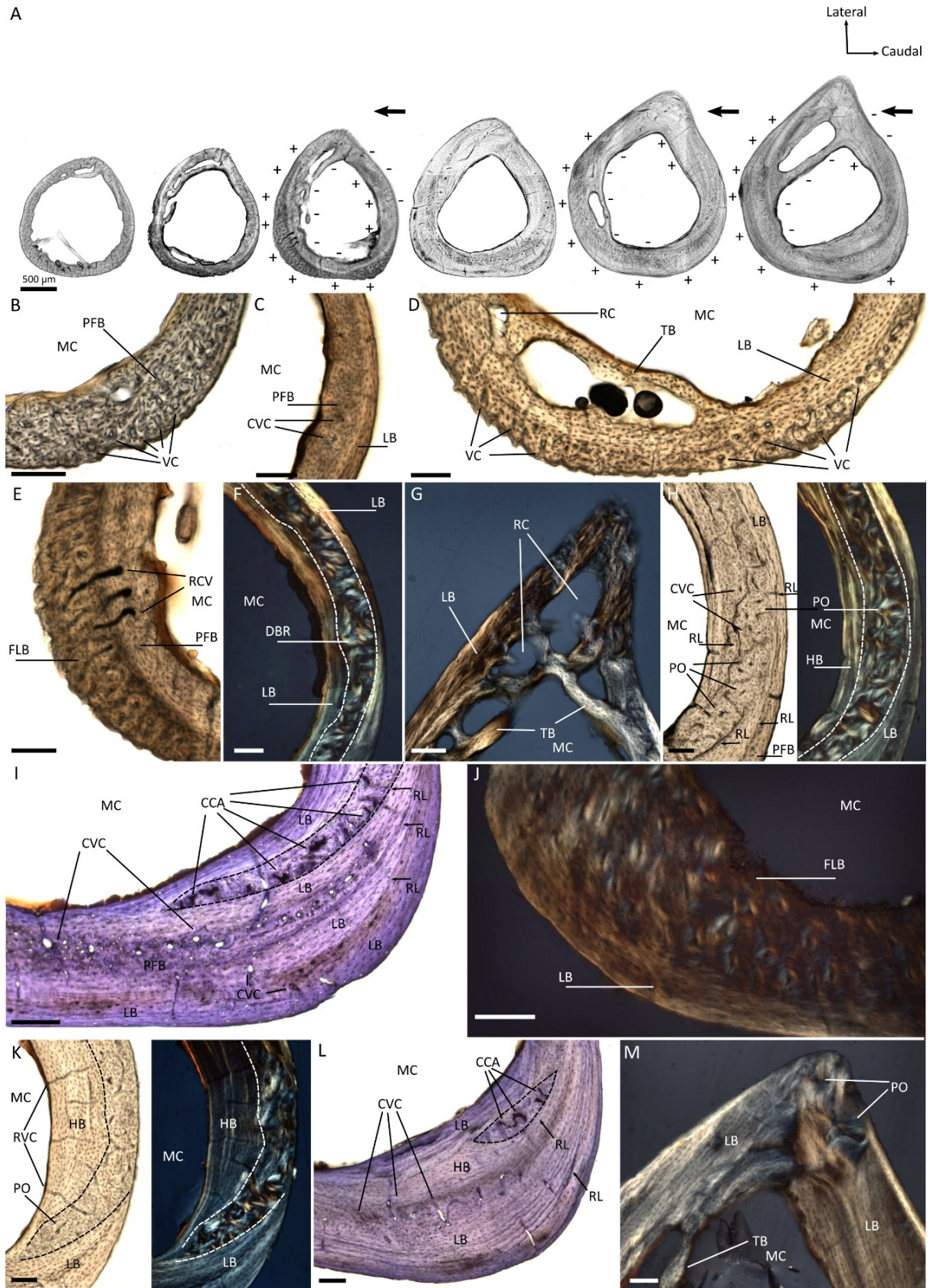


Fig. 8-5 Histological cross-sections of left humeri of *Arvicola scherman*. (A) Cross-sections of all age classes (0-5 from left to right). Scheme of the depositional (+) and resorptive (-) surface according to the characteristics described in the results, in order to reconstruct the predominance of the cortical drift direction (arrow). Scale bar: 500 µm. (B) Caudomedial cortex of a juvenile female (H0FAT84042907)

composed by vascularized parallel-fibered bone showing a depositional periosteal surface. (C) Caudal cortex of a juvenile male (H1MAT83072920). (D) Medial cortex of a juvenile female (H1FAT83081106) showing a depositional periosteal surface and a perimedullary resorption. (E) Craniomedial cortex of an older juvenile male (H2MAT83081114) showing a deposit of periosteal surface evidenced by woven bone punctuated by vascular canals surrounded by parallel-fibered bone. (F) Circularly polarized light (CPL) image of the caudal cortex of an older juvenile male (H2MAT83072914) showing a disorganized bone region (DBR) between lamellar bone (marked with dashed lines). (G) Circularly polarized light image of the lateral cortex of an older juvenile female individual (H2FAT83112708) showing trabecular network. (H) Convectional transmitting light image (left) and CPL image (right) of the caudal cortex of a subadult individuals (H3FAT83072827). Convectional transmitting light image showing in detail the distribution of vascular canals and primary osteons in the cortex, between periosteal and endosteal lamellar bone. Circularly polarized light image showing the convulsion pattern of the DBR (marked with dashed lines). (I) Toluidine blue staining images of caudomedial cortex of a subadult male (H3FAT83092802) showing vascular canals within periosteal lamellar bone, deposit of endosteal and periosteal lamellar bone and calcified cartilage within the DBR (dashed lines). (J) Circularly polarized light image of the caudal cortex of a subadult male (H3MAT83072804) showing an extensive deposit of fibrolamellar bone. (K) Convectional transmitting light image (left) and CPL image (right) of the caudal cortex of an adult male (H4MAT83122414). Under CPL is visible the convulse pattern of DBR. (L) Toluidine blue staining image of caudomedial cortex of an adult female (H5FAT84021210) showing an extensive cortical grow. (M) Circularly polarized light image of the lateral cortex of an adult male (H5MAT84042917) showing a collagen fibers orientation. Abbreviations: CCA, calcified cartilage areas; CVC, circular vascular canal; FLB, fibrolamellar bone; HB, hybrid bone; LB, lamellar bone; MC, medullary cavity; PFB, parallel-fibered bone; PO, primary osteons; RC, resorption cavity; RL, resorption lines (or reversal lines); RVC, radial vascular canals; VC, vascular canals; TB, trabecular bone. Dashed line delimited the DBR. Scale bar for B–J: 150  $\mu$ m.

### ***Arvicola sapidus***

The humerus of younger juveniles exhibited a circular shape with relatively thick cortical wall compared with other age classes and with *A. scherman* (Fig. 8-4, 8-6A), excepting one specimen (H0FAS83071202) which the cortical thickness was similar to that observed in *A. scherman* (Fig. 8-5A, 8-6A). This deviation may be related to the age class variability. The cortex was typified by parallel-fibered and hybrid bones (Fig. 8-4). This latter, limited to the craniolateral and medial side of the pericortical region (Fig. 8-4, 8-6B). Parallel fibered bone had better organized osteocytes and fewer longitudinal canals in *A. sapidus* than *A. scherman* in same age class. The specimen with the thinnest cortical region (H0FAS83071202) showed a cranial side and craniomedial periosteal deposition via simple circular canals and fibrolamellar bone (Fig. 8-6C). The single individual of age class 1 showed a humerus with primary osteons laterally and resorption cavities in the lateral and posterior sides (Fig. 8-4, 8-6A).

Juvenile specimens in age class 2 showed a large increase on humerus surface and thickness of cortical region (Fig. 8-4, 8-6A) with an elliptical shape. As well as an increase of hybrid and lamellar bone tissues on the cortex (Fig. 8-4), indicating changes in bone composition. Two specimens exhibited a DBR on the medial side. A periosteal growth on the cranial side was suggested by subperiosteal vascular canals and well-vascularized parallel-fibered (Fig. 8-6D). Perimedullary resorption occurred on the lateral and cranial side as evidenced by the resorption cavities and trabecular bone in the medullary cavity (Fig. 8-4). Exposure of the DBR to the medullary cavity may be due to extensive resorption on the medial side (Fig. 8-6E). All this

evidence, together with deposition of perimedullary lamellar endosteal bone on the caudal side, suggest a tendency of the bone to drift from caudal to cranial margins (Fig. 8-6A).

Compared to the previous ontogenetic stage, the humerus of subadult individuals had a greater cortical thickness and a well-organized cortex, composed practically of lamellar and hybrid bones (Fig. 8-4, 8-6A, F). All voles exhibited DBR, "sandwiched" between hybrid and/or lamellar bones on craniomedial side (Fig. 8-4, 8-6G), with few longitudinal primary osteons, and simple canals (Fig. 8-6G). A continued cranial drift was evidenced by endosteal lamellar deposition on the caudal side and expansion of periosteal lamellar bone on the opposite side pericortically (Fig. 8.4). In one individual (H3FAS83101305), cortical expansion showed signs of craniomedial periosteal deposition, and in another one (H3MAS83012306), an increased cortical thickness was observed due to lamellar tissue around the medullary cavity (Fig. 8-6G).

Adult voles had a humeral microstructural organization similar to that of subadults. The cortex was composed by lamellar and hybrid bones with a DBR, boundary between periosteal and endosteal tissue. Unlike subadult individuals, this region in adult voles was on the medial side (Fig. 8-4, 8-6H, I). The pattern observed in the humerus of almost all individuals suggests cranial bone drift, except for that observed in one specimen (H5FAS84011405), which suggests a craniomedial drift due to the signs of periosteal deposition (Fig. 8-4). The intensive periosteal lamellar bone deposition caused an asymmetric bone growth of the cranial region in relation to other areas of the cortex. The continuous endosteal tissue deposition around the perimedullary region triggered a decrease in the medullary cavity throughout ontogeny and an increase of cortical thickness. As in *A. scherman*, the humerus of some specimens showed primary osteons on the lateral side and a change in the main direction of the osteocytes (Fig. 8-6J).

COMPARATIVE HISTOLOGY OF THE HUMERUS AND THE FEMUR



Fig. 8-6 Histological cross-section of left humeri of *Arvicola sapidus*. (A) Cross-section of all age classes (0-5). Juvenile to adult individuals from left to right. Scheme of the depositional (+) and resorptive (-) surface according to the characteristics described in the results, in order to reconstruct the predominance of the cortical drift direction (arrow). Scale bar: 500 µm. (B) Craniolateral cortex of a juvenile male (HOMAS84062308). (C) Fibrolamellar bone in the medial cortex of a juvenile female (HOFAS83071202). (D)

Cranial cortex of an older juvenile male (H2MAS84041501) showing perimedullary resorption and a cortical composed by parallel-fibered bone with vascular canals. (E) Toluidine blue staining images of medial cortex of an older juvenile male (H2MAS84041501) composed by a disorganized bone region (DBR) (marked with dashed lines) with simple vascular canals, endosteal and periosteal lamellar bone. (F) Cranial cortex of a subadult female (H3FAS84120702). (G) Toluidine blue staining images of the medial cortex of a subadult male (H3MAS83012306). Cortical bone showing extensive endosteal lamellar and periosteal lamellar bones marked with resorption lines. Between these two surfaces is noticeable a DBR (marked with dashed lines) with longitudinal primary osteons, simple canals, and calcified cartilage area. (H) Cranial cortex of an adult male (H4MAS83012302) composed by periosteal lamellar bone, endosteal hybrid bone and a layer of hybrid bone with longitudinal primary osteons and simple vascular canals. Periosteal resorption marked with black arrows. (I) Circularly polarized light image of the lateral cortex of an adult male (H5MAS83091803) showing a convulsion pattern in the DBR between periosteal and endosteal lamellar bones (marked with dashed lines). (J) Circularly polarized light image of the lateral cortex of an adult male (H5MAS84011402) showing a collagen fibers orientation. Abbreviations: CCA, calcified cartilage areas; CVC, circular vascular canal; FLB, fibrolamellar bone; HB, hybrid bone; LB, lamellar bone; MC, medullary cavity; PFB, parallel-fibered bone; PO, primary osteons; RL, resorption lines (or reversal lines); RVC, radial vascular canals; VC, vascular canals; TB, trabecular bone. Dashed line delimited the DBR. Scale bar for B-J: 150  $\mu$ m.

### 8.3.2. Ontogenetic changes in the femur histology

#### *Arvicola scherman*

The femur of young juvenile individuals showed an elliptical shape with thin cortical wall with a large medullary cavity. The cortex was composed by fast-depositing tissues on the lateral side (Fig. 8-8A). The femur of five individuals (F0MAT84052614, F0MAT84083013, F1FAT83081106, F1FAT83092620, F1FAT83112703) showed formation of fine-cancellous, woven bone by subperiosteal deposition (Fig. 8-7, 8-8B). Between this fast-depositing tissue and parallel-fibered bone, thin bands of lamellar bone were observed, indicating changes in deposition rates (Fig. 8-8B). Three juvenile (F0FAT84052709, F0MAT84083013, F1FAT83112703) showed asymmetrical wall growth in the cranial side of the femur, suggesting an essentially periosteal growth, evidenced by the presence of vascularized parallel-fibered bone, and pericortical woven bone (Fig. 8-7). In the lateral side of the bone, some individuals showed resorption cavities forming trabeculae (Fig. 8-7, 8-8A, C). In the femur of the juvenile of age class 0, the cortex in the medial side was mostly vascularized by radial canals. In the juvenile voles of age class 1, a DBR with circular vascular canal and calcified cartilage areas, between periosteal and endosteal lamellar bone were observed (Fig. 8.7, 8.8D). Resorption occurred essentially on the endosteal side cranially, exposing the DBR to the medullary cavity in some specimens (Fig. 8-7, 8-8D). Increased periosteal deposit and endosteal resorption on the cranial side indicates a cranial-lateral cortical drift.

The femur of older juvenile individuals showed an increase in cortical thickness compared to younger ones. Unlike the humerus, the matrix of the femur was mostly composed of hybrid and lamellar bones, with DBR occupying a large portion of the cortex. Signs of cortical drift such as endosteal deposition in the perimedullary region on the caudal side (Fig. 8-7), resorption on the opposite side with bone trabecularization and exposure of the DBR to the medullary cavity (Fig.

8-7, 8-8F), and subperiosteal lamellar bone deposition on the cranial and craniolateral side (Fig. 8-8F) indicate bone growth in cranial direction. One specimen (F2FAT83081012) showed a large part of the cortex of the femur formed by fibrolamellar bone (Fig. 8-8E).

In subadult voles the cortex of the femur was slightly more organized than in individuals of the previous age class. Interestingly, an increase in DBR was observed. Namely, two individuals (F3FAT83092706, F3FAT83092802) showed an asymmetric band distributed along the femur cross-section, except in the lateral side where it is located perimedullary (Fig. 8-8G, H). The continuous perimedullar endosteal resorption observed on the lateral and cranial sides, the deposit of periosteal lamellar bone and well-vascularized parallel-fibered bone by simple canals on the same side, the deposit of endosteal hybrid bone and the exposure of the disorganized region to the pericortical region on the craniomedial side, suggests craniolateral bone growth (Fig. 8-8A, H). The femur of one individual (F3MAT83092613) showed a slightly different pattern from the other specimens, with a very thick cortical wall in the lateral side, formed by well-vascularized parallel-fibered bone (Fig. 8-7).

The femur of the adult voles, especially those of age class 4, showed an important increase in cortical thickness, and consequent decrease in the medullary cavity, compared to that of the femur of the individuals of age classes 0-3 (Fig. 8-8A). This increase in cortical thickness was due to the deposit of endosteal lamellar and hybrid bone in the medial and caudal side, as well as of periosteal lamellar bone deposit in the lateral and cranial side of the pericortical region, evidenced by the resorption lines on both sides (Fig. 8-8J). In turn, resorption cavities were observed on the lateral side, indicating intense resorption, and originating a large medullary cavity in individuals of age class 5. Signs of a craniolateral cortical drift were evidenced by deposition of periosteal lamellar bone on the craniolateral side, reduction of DBR due to intense endosteal resorption on the lateral side (Fig. 8-7, 8-8I, K), endosteal deposition on the opposite side, and disruption of the DBR interface line.

COMPARATIVE HISTOLOGY OF THE HUMERUS AND THE FEMUR

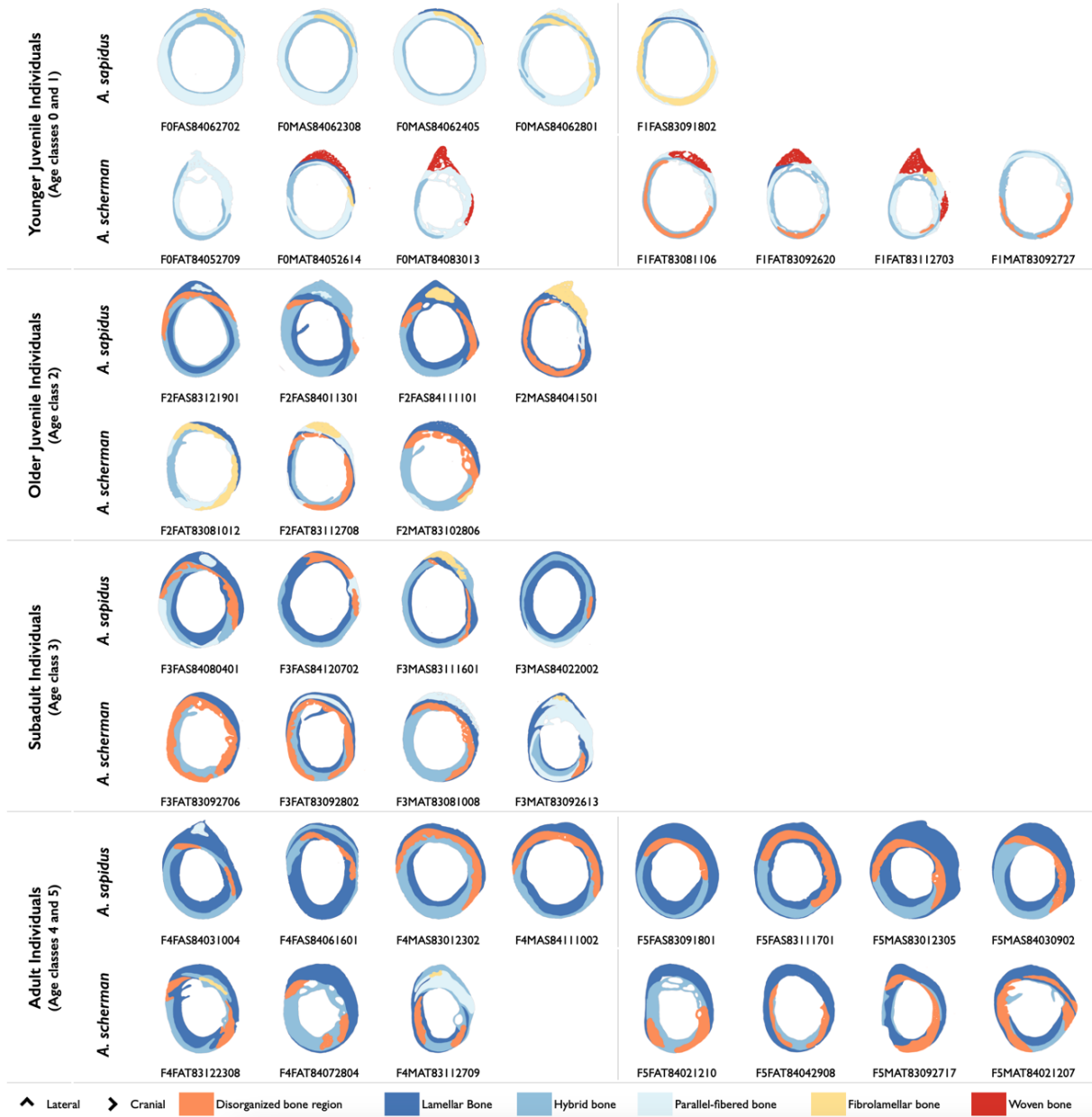


Fig. 8-7 Illustrative maps of the areas occupied by the different bone tissues in the femur, in all specimens of *A. scherman* and *A. sapidus* used in the study. All images are the same size to facilitate comparison between specimens. Vertical lines separate age classes.



COMPARATIVE HISTOLOGY OF THE HUMERUS AND THE FEMUR

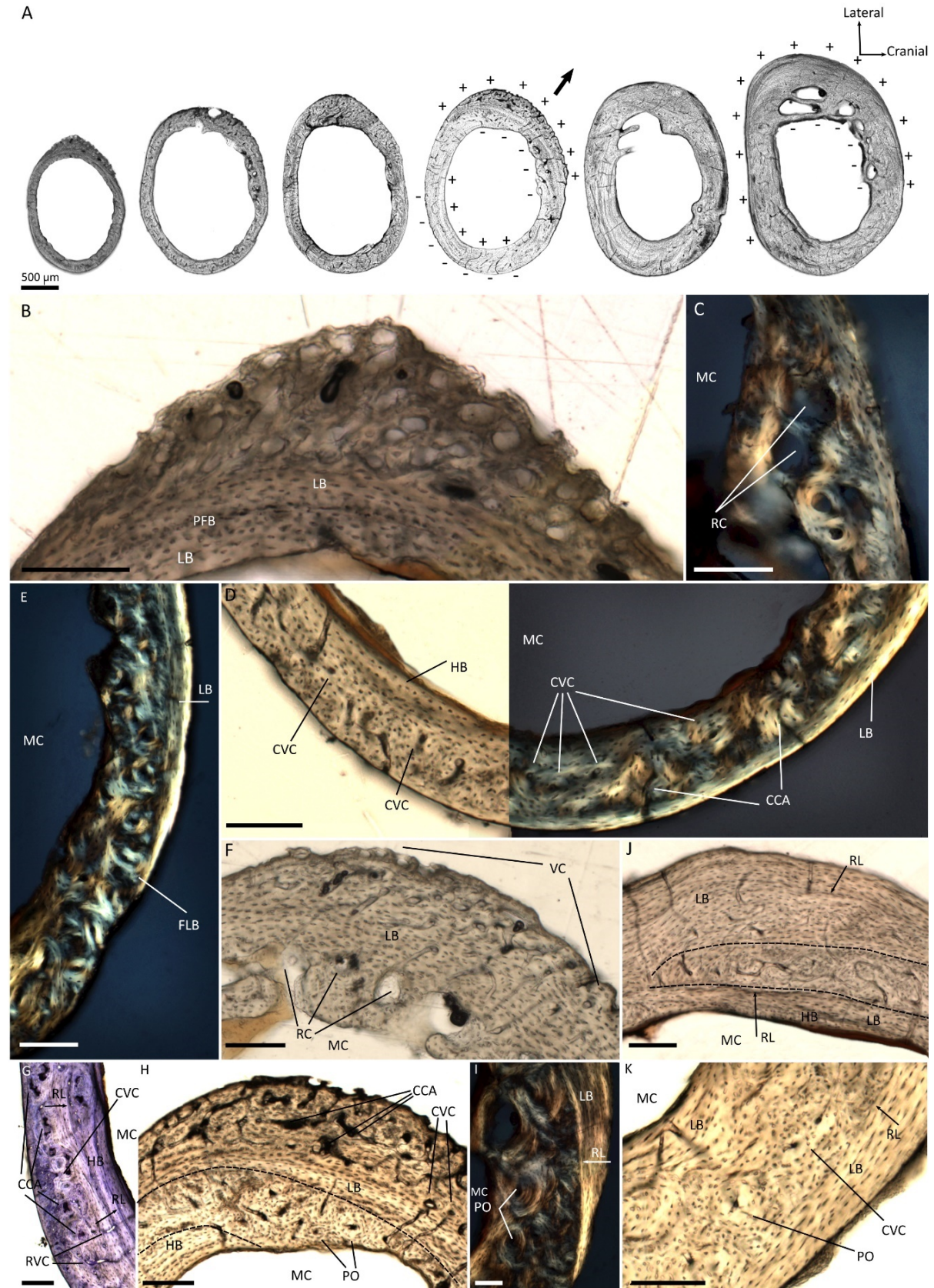


Fig. 8-8 Histological cross-section of right femora of *Arvicola scherman*. (A) Cross-section of all age classes (0-5). Juvenile to adult individuals from left to right. Scheme of the depositional (+) and resorptive (-) surface according to the characteristics described in the results, in order to reconstruct the predominance of the cortical drift direction (arrow). Scale bar: 500  $\mu$ m. (B) Lateral cortex of a juvenile male

(F0MAT84052614) showing formation of fine-cancellous, woven bone by subperiosteal deposition. (C) Cranial cortex of a juvenile female (F1MAT83092727) with resorption cavities. (D) Montage of a continuous image of medial cortex of a juvenile male (F1FAT83081106), half in conventional transmitting light (CTL) and half in circularly polarized light (CPL). The image shows vascular canals and hybrid bone (CTL), and the convulsion pattern in the disorganized bone region (CPL). (E) Circularly polarized light image of cranial cortex of an older juvenile female (F2FAT83081012) showing a dense layer of primary osteons and periosteal lamellar bone. (F) Lateral cortex of an older juvenile male (F2MAT83102806) showing endosteal resorption and subperiosteal deposition by vascularization. (G) Toluidine blue staining image of caudal cortex of a subadult female (F3FAT83092802) showing a disorganized bone region (DBR) with circular vascular canal. Deposit of endosteal hybrid bone marked with resorption lines. (H) Lateral cortex of a subadult male (F3MAT83081008) showing dense endosteal vascularization and subperiosteal deposition by vascular canals. (I) Circularly polarized light image of the caudolateral cortex of an adult female (F5FAT84021210) showing a convulsion pattern in DBR (dashed lines). (J) Lateral cortex of an adult male (F5MAT84021207). Dashed lines define the DBR. (K) Craniomedial cortex of an adult male (F5MAT83092717). Abbreviations: CCA, calcified cartilage areas; CVC, circular vascular canal; FLB, fibrolamellar bone; HB, hybrid bone; LB, lamellar bone; MC, medullary cavity; PFB, parallel-fibered bone; PO, primary osteons; RC, resorption cavity; RL, resorption lines (or reversal lines); RVC, radial vascular canals; VC, vascular canals; TB, trabecular bone. Dashed line delimited the DBR. Scale bar for B-J: 150  $\mu$ m.

### ***Arvicola sapidus***

The femur of younger juveniles showed a similar cortical thickness and the size of the medullary cavity to each other. The cortex was mainly formed by highly vascularized parallel-fibered bone with radial and circular canals (Fig. 8-9B). Endosteal hybrid bone surrounded the medullary cavity (Fig. 8-9C). Fibrolamellar bone “sandwiched” between lamellar bone or lamellar and parallel-fibered bones, as well as subperiosteal deposition by vascular canals was visible in the lateral side of the femur (Fig. 8-9D), indicating a periosteal growth. The femur of the single individual of age class 1 showed a cortical matrix formed by fibrolamellar and parallel fibered bones, except for the lateral side where lamellar bone was observed (Fig. 8-7, 8-9A, C).

Compared with younger juveniles, the femur of individuals of age class 2 showed greater cortical thickness and a more organized cortex, formed mostly by lamellar/hybrid bones (Fig. 8-9). Cross-sections had an elliptical shape, which was maintained throughout ontogeny. This increase in cortical thickness was mostly due to endosteal depositions along the cortex (Fig. 8-9A). In terms of bone increase, a large difference was also observed. Lateral side was mainly composed of lamellar/hybrid bones but showed primary osteon and vascular canals on the midcortical region (Fig. 8-9E). On the same side of the perimedullary region, resorption was evidenced by the presence of a resorption cavity. In the mid-cortical region of the craniolateral side, an asymmetric DBR band crossed the cortex, interrupted on the lateral side (Fig. 8-9E-F). The femur of one specimen (F2MAS84041501) showed a distinct histological pattern, with a cortex practically composed by DBR between lamellar bone, except for the craniolateral side, where it was formed by fibrolamellar bone (Fig. 8-9F).

Subadult individuals showed a slight increase on femur surface and thickness of cortical region compared to older juvenile voles, but with similar cortex composition. Resorption in the lateral side of perimedullary region, endosteal lamellar bone deposit around the medullary cavity

(except in craniolateral side), and periosteal lamellar bone deposition in the lateral and cranial side, suggest a craniolateral cortical drift (Fig. 8-9G, H). The femur of three individuals (F3FAT83092706, F3FAT83092802, F3MAT83081008) exhibited a thin periosteal cortex, indicating low periosteal expansion (Fig. 8-7).

The femur of adult individuals showed an increase of cortical walls thickness, and a decrease in the medullary cavity, compared to the previous ontogenetic stage (Fig. 8-9A). As in subadults, adult voles exhibited a deposit of lamellar bone along the perimedullary region, except in the craniolateral zone, where resorption occurred. Resorption lines were detected in the intracortical region of the medial side indicating lamellar bone formation. All specimens showed an increase of DBR that cross the cortex from the caudal to the cranial side passing through the lateral side (Fig. 8-9I-J). This band lies between the periosteal and endosteal bones. Periosteal expansion by lamellar bone was observed on lateral and cranial sides (Fig. 8-9A, J). The arrangement of the histological elements suggests as in subadult individuals, tendency of the bone to grow to craniolateral margins (Fig. 8-9A).

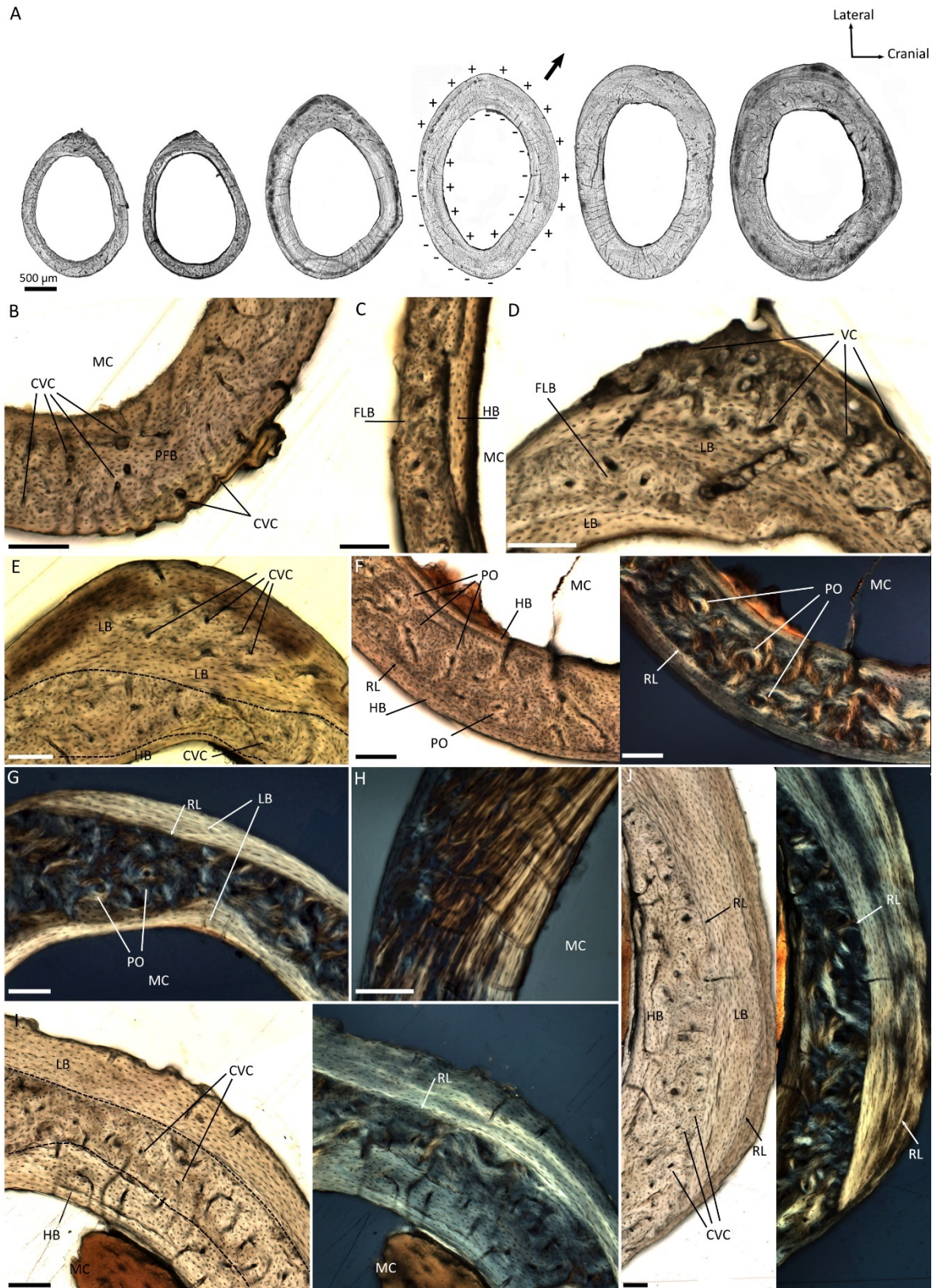


Fig. 8-9 Histological cross-section of right femora of *Arvicola sapidus*. (A) Cross-section of all age classes (0-5). Juvenile to adult individuals from left to right. Scheme of the depositional (+) and resorptive (-) surface according to the characteristics described in the results, in order to reconstruct the predominance of the cortical drift direction (arrow). Scale bar: 500 μm. (B) Craniomedial cortex of a juvenile male (FOMAS84062308) composed by vascularized parallel-fibered bone. (C) Caudal cortex of a juvenile female

(F1FAS83091802) composed by fibrolamellar bone and limited by hybrid bone. (D) Lateral cortex of a juvenile male (F0MAS84062801) showing primary osteons between layers of lamellar bone. Subperiosteal deposition by vascular canals. (E) Lateral cortex of an older juvenile female (F2FAS83121901) showing circular vascular canals within the lamellar bone and disorganized bone region (DBR) composed by vascular canals and calcified cartilage areas. (F) Conventional transmitted light image (left) and circularly polarized light image (CPL) (right) of the caudal cortex of an older juvenile male (F2MAS84041501). Conventional transmitted light image shows the distribution of vascular canals and primary osteons in the cortex, between hybrid bone. Circularly polarized light image shows the convulsion pattern in DBR. (G) Circularly polarized light image of the lateral cortex of a subadult female (F3FAS84120702) showing an isotropic orientation in DBR. (H) Circularly polarized light image of the caudolateral cortex of a subadult male individual (F3MAS84022002) showing lamellar bone running in circumferential swaths. (I) Conventional transmitted light image (left) and CPL image (right) of the craniolateral cortex of an adult male (F4MAS83012302). Conventional transmitted light image shows the distribution of vascular canals in the cortex within DBR, periosteal lamellar bone and endosteal hybrid bone. Circularly polarized light image shows a resorption line between endosteal lamellar bone and the DBR. (J) Conventional transmitted light image (left) and CPL image (right) of the cranial cortex of an adult male (F5MAS84030902). Conventional transmitted light image shows a DBR with a dense vascular zone between endosteal hybrid bone and periosteal lamellar bone. Circularly polarized light image shows the convulsion pattern caused by the DBR. Abbreviations: CVC, circular vascular canal; FLB, fibrolamellar bone; HB, hybrid bone; LB, lamellar bone; MC, medullary cavity; PFB, parallel-fibered bone; PO, primary osteons; RL, resorption lines (or reversal lines); VC, vascular canals; TB, trabecular bone. Dashed line delimited the DBR. Scale bar for B–J: 150  $\mu\text{m}$ .

## 8.4. DISCUSSION

Since previous geometric morphometric analysis showed notable differences in the macrostructure of limb long bones between *A. sapidus* and *A. scherman*, associated in part with lifestyle (Durão et al., 2020, 2022), a strong need exists to understand whether interspecific differences associated with function are also observed at the microstructural level. In addition, an ontogenetic histological study allows us a better understanding of the bone growth and how the tissues microstructures properties interact with mechanical forces to establish the adult form of the bone (Goldman et al., 2009; Gosman et al., 2013). Here, we have determined the histological changes in the midshaft of the humerus and femur during postweaning ontogeny of *A. sapidus* and *A. scherman*. As hypothesized, common histological features were found both between species and long bones, as well as divergencies in matrix composition and in modelling process. These results suggest that lifestyle play an important role in microstructural variation of these bones in water voles, as reported for other rodent species (e.g., Montoya-Sanhueza & Chinsamy, 2017; Montoya-Sanhueza et al., 2020; Singh et al., 1974).

### 8.4.1. Histology

Long bones of both species are composed of a wide variety of tissue types (so called histodiversity), including woven, parallel-fibered, hybrid and lamellar bones, as well as composite tissues such as fibrolamellar bone. As we move through ontogenetic stages, the long bones of water voles show a more organized matrix related to a decrease in histodiversity. Woven bone and well-vascularized parallel-fibered bone are observed in juveniles while lamellar and hybrid

bones occupy mostly the cortex of older ontogenetic stages. According to Amprino's rule, variation in the type of primary tissue and its vascularization reflect variation in the bone deposition rate during ontogeny, which in turns reflects different bone growth rate (Amprino, 1947; de Margerie et al., 2002, 2004; de Ricqlès et al., 1991; Francillon-Viellot et al., 1990). Thus, change of tissue types from woven bone or vascularized parallel-fibered bone to lamellar bones manifest a decrease in growth velocity (Amprino, 1947; de Ricqlès et al., 1991). In long bones of mammals (e.g. Goldman et al., 2009; McFarlin et al., 2016; Smith, 1960, Warshaw, 2008), namely rodents (e.g. Enlow, 1962; Montoya-Sanhueza & Chinsamy, 2017; Montoya-Sanhueza et al., 2020; Sontag, 1986) it is common to observe high rates of bone formation in the early stages of life and the emergence of bone tissues with lower rates of osteogenesis as bone matures in the subadult and adult stages (Amprino, 1947; de Ricqlès et al., 1991; Francilon-Viellot et al., 1990). Consistent with the literature, the cortical bone growth of the humerus and femur of *A. scherman* and *A. sapidus* follows a similar pattern to other mammals. This change in bone organization throughout ontogeny appears to be related to somatic growth rates (such as increased body mass) (Kuehn et al., 2019; Lee & O'Connor, 2013), since woven bone has lower biomechanical properties compared to lamellar tissue (Currey, 2002; Martin, 1991).

In the two long bones analysed here, *A. scherman* showed a slower transition from tissues with lower to higher ontogenesis rates than *A. sapidus*. In other words, while juvenile and subadult specimens of *A. scherman* have woven, fibrolamellar and well-vascularized parallel-fibred bones, *A. sapidus* from age class 2 already exhibits a cortex formed practically by hybrid and lamellar bones. The difference in tissue composition between species in juvenile and subadult individuals suggests different rates of bone growth (Amprino, 1947; de Margerie et al., 2002). The density of vascular canals and the existence of fibrolamellar bone tissue in the cortex of older juvenile and subadult specimens of *A. scherman* seems to correspond to relative periods of rapid growth, since both histological features are related to high deposition rates (de Margerie, 2002). The emergence of these histological features could be associated with biomechanical changes of both bones. Throughout ontogeny of *A. scherman*, a slight difference between both bones was detected in the cortical composition, with the femur showing more fast-growing tissues in the early ontogenetic stage than the humerus.

In humerus and femur of both species, most of the endosteal bone tissue deposition has a laminar organization. Humerus show a caudal extension, while femur a more medial one. These expansions reflect the direction of cortical drift in these bones. Except for the humerus of *A. sapidus*, the endosteal bone tissue tends to decrease through ontogeny, being limited to restricted areas of the perimedullary region, feature seen in other mammals (Goldman et al., 2009; McFarlin et al., 2016). We interpreted the trabecular zones observed in the perimedullary region as areas

of recent resorption related to cortical drift. Nevertheless, mineralization density studies are needed to corroborate this observation.

Interestingly, in both species a disorganized bone region (DBR) with calcified cartilage inside was detected in the intracortical region of both bones. This histological feature has been previously described in the femur of mice and rats, (Bach-Gansmo et al., 2013; Ip et al., 2016; Shipov et al., 2013), however, to our knowledge, this is the first time that it has been described in the humerus of rodent species. The observation of this region in the cortex of *Arvicola* is probably due to the absence of bone remodelling and therefore, the preservation of bone formation residues throughout ontogeny. The resorption rate plays a key role in the maintaining of these tissues during ontogeny, since the higher the resorption rate, the lower the possibility of identifying these residual tissues. This is easily visible, for example, in the humerus of *A. scherman*, in which the reduction of the disorganized region throughout ontogeny occurs due to the high resorption rate, reaching a remnant in some adult specimens. In the femur, the marked presence of DBR is similar to that previously described in other rodent species; an asymmetric band distributed along the femur cross-section (Bach-Gansmo et al., 2013; Ip et al., 2016; Shipov et al., 2013; Sontag, 1986). This distribution in the cortex is due to the combination of longitudinal growth of the femur and cortical drift (Ip et al., 2016; Sontag, 1986b, 1992).

Calcified cartilage is presumed to remain from endochondral ossification acting as a framework for rapid bone growth, as it allows rapid disorganized deposition (Shipov et al., 2013). Thus, it would be expected to observe DBR from the early ontogenetic stage. Although it was detected in several juvenile individuals of age class 1, it was not in individuals of age class 0. This fact may be related to longitudinal bone growth, since this occurs from the epiphyseal growth-plates and, therefore, as the bone grows, the most distal point becomes the midpoint (Ip et al., 2016). Another interesting result was the increase of DBR in the femur throughout ontogeny in *A. sapidus*. A similar result had already been reported in mice, which has been related to the existence of distinct DBR content along the bone diaphysis (Ip et al., 2016). Analyses of different locations of both the femur and humerus are needed to understand the non-appearance of this region in younger juvenile voles and the DBR increase in adult ones.

Although calcified cartilage is observed in large quantities in junction regions (Evans & Pitsillides, 2022), little information about the biomechanical effect of this tissue on the cortical bone is found in the literature. However, a correlation between calcified cartilage and the decrease in maximal force and bending stress has been detected in mice (Ip et al., 2016), resulting from the high stiffness of calcified cartilage in relation to the surrounding bone (Bach-Gansmo et al., 2013; Shipov et al., 2013). Moreover, the stiffness of the calcified cartilage seems to be important in the accumulation of microdamage, since in areas of articulation the calcified cartilage is the first zone of fracture when trauma occurs (Keinan-Adamsky et al., 2005). Additional, calcified cartilage areas

were described to be surrounded by lines known as bone cartilage interface, similar to reversal/arrest line and cement line, presenting a high mineralization (Bach-Gansmo et al., 2013). By analogy to what happens with the cement lines around secondary osteons, Bach-Gansmo et al. (2013) suggested that the bone-cartilage interface leads to a decrease in longitudinal toughness and an increase in transversality. The presence of DBR in the long bones of adult specimens of *A. scherman* and *A. sapidus* may be due to a biomechanical advantage, playing an important role in stabilizing of the cortex.

#### 8.4.2. *Histology and macrostructure*

As mentioned in the previous section, younger juvenile individuals of both species have a matrix composed mainly of well-vascularized parallel-fibered bone. Although this tissue type is an intermediate between woven and lamellar bones (Newell-Morris & Sirianni, 1982), its porosity and high vascularity contribute to a decrease in bone strength (Liebermann & Pearson, 2001; Martin, 1991). Furthermore, juvenile voles (mainly of *A. scherman*) have a thin cortical wall. This characteristic, together with the decrease in the biomechanical properties of the bone, increases the propensity for fractures in young individuals (e.g., Cabtree et al., 2001; Main & Biewener, 2006). Structural properties such as the diameter and thickness of the cortex have been showing a great influence in bone mass and bone biomechanical integrity (Turner, 2002). Particularly in relation to the external diameter, it has been demonstrated that it can predict up to ~55% of the variation in bone strength (Hart et al., 2017, and references therein). Previous works, on long bones of *A. sapidus* and *A. scherman* have shown that, regardless of the type of locomotion, bones of juvenile individuals are more robust than in adult water voles (Durão et al, 2020, 2022). In this context, the results of the present study broadly support the hypothesis that external robust limb long bones in young water voles must reflect a compensatory response to minimize the risk of fractures during initial locomotor efforts (Durão et al, 2020, 2022).

#### 8.4.3. *Bone microstructure*

##### ***Cortical thickness throughout ontogeny***

During ontogeny, the increase in cortical thickness in humerus and femur in *A. scherman* and *A. sapidus* may be due in part to increased body mass. Structural properties of bones such as bone mass, architectural structure (both macro and microscopic), and mechanical quality of the material (the composition of bone tissue), influence the mechanical properties of bones (Caeiro et al., 2013; Currey, 2002; Ferreti et al., 2003; Hart et al., 2017). The cortical thickness showed a positive relationship with bone strength (Turner, 2002). According to the "bone mechanostat" hypothesis (Frost, 1987, 2003), bone is optimized through the permanent redistribution of



mineralized tissue, stimulated by normal stresses of bone tissues (detected by osteocytes) which are induced by gravitational forces (body mass) and by contractions of regional muscles. With age, both body mass and muscle mass increase. Thus, it is expected that the long bones such as the femur and humerus, which support the animal's body, increase their mass, and adapt their mechanical properties in order to satisfy the demands imposed by growth. This increase in cortical thickness is gradual throughout ontogeny. Similar characteristics have been described in other rodent species, such as the cape dune mole-rat (*Bathyergus suillus*) and the naked mole-rat (*Heterocephalus gaber*), both typical fossorial species (Montoya-Sanhueza & Chinsamy, 2017; Montoya-Sanhueza et al., 2020). It has been suggested that the gradual increase in cortical thickness of long bones during postnatal ontogeny is a generalized growth pattern in diggers (Montoya-Sanhueza & Chinsamy, 2017, 2020). Although the cortical areas were not quantified, our results seem to corroborate the existence of a positive allometry during cortical thickness ontogeny and reinforce the possibility of a growth pattern, not only in fossorial species, but also in species with another lifestyle. Anyhow, more ontogenetic studies must be performed to determine if these results reflect a generalized growth pattern, at least in rodents.

It is well known that the growth and maintenance of the mammalian skeleton is influenced by the hormonal environment (e.g., see Gasser & Kneissel, 2017 and references therein), namely sex hormones (e.g., Compston, 2001; Khosla et al., 2012; Narla & Ott, 2018). For instance, gonadal androgens are thought to increase cortical size by stimulating periosteal apposition (Turner et al., 1990) and that oestrogen levels have an important implication during sexual maturation in bone resorption and formation (Khosla et al., 2012; Martin, 1993; Turner et al., 1992). Thus, the variation in cortical thickness observed of the humerus and femur of *A. scherman* and *A. sapidus*, especially in subadult individuals, may be related, at least in part to a hormonal effect.

### ***Cortical thickness between species***

In both long bones, *A. sapidus* has always greater cortical thickness than *A. scherman*, which may be related to a functional issue. In general, the cross-section of both long bones of *A. scherman* adult is characterized by a moderately thick compact cortex, and a large medullary cavity, similar to those reported for terrestrial mammals (Laurin et al., 2011). The fact that *A. scherman* does not show a thick cortical wall is not concordant to what is observed in other fossorial rodent species (Casinos et al., 1993; Heck et al., 2019; Legendre & Botha-Brink, 2018; Montoya-Sanhueza & Chinsamy, 2017; Montoya-Sanhueza et al., 2020; Straehl et al., 2013; Walker et al., 2020), since the thick cortical wall has been considered an adaptive feature to the fossorial lifestyle (Montoya-Sanhueza & Chinsamy, 2017). The relatively thin cortical wall of *A. scherman* could be attributed to its body mass (66-183g) (Ventura, 2007). Meier et al. (2013) compared the global compactness (amount of bone present on a surface) of humerus between fossorial talpids and non-fossorials

talpids and detected no difference between functional groups. These authors suggested that their results are related to the possibility that the microanatomical structure of the humerus in small mammals already have all needs to cope with the biomechanical strains of digging activity (Meier et al., 2013). So, the Wolff's Law doesn't fit well to this group of vertebrates (Dawson, 1980). However, high cortical thickness has already been reported for two small fossorial rodent species, the cape dune mole-rat (*Bathyergus suillus* - 780g) and the naked mole-rat (*Heterocephalus glaber* - 20-80g), contradicting this statement. Since most of the fossorial species studied are scratch-diggers (i.e., the claws of the hand are used to break the ground), the absence of a very thick cortical wall in *A. scherman* may be due to that this species is a chisel-tooth digger. *Heterocephalus glaber*, another fossorial rodent that use its incisors to break the ground, could be the exception rather than the rule since it is one of the most peculiar mammals in the world (Montoya-Sanhueza et al., 2020). Somehow, this result indicates that the humerus of *A. scherman* doesn't need greater resistance of the bone to stress and strain to face the mechanical demands of the humerus in the digging process.

Compared to other semiaquatic small mammal species (*Ondatra zibethicus*; *Galemys pyrenaicus*) (Laurin et al., 2011), *A. sapidus* has a relatively similar cortical thickness. It is possible that the increase in cortical thickness of the Southwestern water vole in relation to *A. scherman* is in part a functional response. Previous comparative morphological studies of long bones in these species have observed that *A. sapidus* exhibits slender bones compared to *A. scherman* (Durão et al., 2020, 2022). Considering that thinner bones tend to have greater cortical thickness than robust bones to compensate for the reduced dimensions of cross-sectional areas and cross-sectional moment of inertia (Hart et al., 2017 and references therein), it is possible that increasing cortical thickness is an adaptive response to obtain additional stiffness at the expense of ductility and toughness (Hart et al., 2017 and references therein). This could be the explanation of the results here obtained for water voles.

#### 8.4.4. Bone modelling

*Arvicola scherman* and *A. sapidus* show notable differences in the humerus midshaft modelling pattern during postnatal ontogeny. During early ontogeny (age class 0 and 1) both species share a similar modelling process, with a cortex formed mainly by periosteal tissue and high endosteal resorption. This is concordant with the process described for other mammalian species (Enlow, 1962; Montoya-Sanhueza & Chinsamy, 2017; Montoya-Sanhueza et al., 2020). In *A. scherman* this growth pattern is maintained during postnatal ontogeny, with craniomedial expansion of periosteal tissue and extensive endosteal resorption, producing a large medullary cavity, as described in other rodent species (Ferguson et al., 2003; Smith, 1960). Unlike *A. scherman*, the increase of the cortical section size in *A. sapidus* occurs essentially in most juvenile individuals,

reaching in older juvenile ones a cross-section size similar to subadult voles, which indicates a constant periosteal expansion throughout the juvenile stage. This dynamic coincides with increased bone elongation of the humerus (Ventura, 1988), which is subject to environmental and genetic effects (Sanger et al., 2011). However, in previous works using linear measurements, the increase of the midshaft diameter had been reported in a more progressive way throughout the postnatal ontogeny (Ventura, 1988). At this point, older juvenile individuals of *A. sapidus* have a cross-section size comparable to subadult voles but with less cortical thickness, with endosteal bone tissue formation playing an important role in bone augmentation. Subadult and adult individuals of *A. sapidus* show a positive bone modelling balance, with deposit of endosteal and periosteal tissue. As a result, peak bone mass in *A. sapidus* seems to start with a continuous periosteal bone apposition in juvenile voles and endosteal and periosteal tissue apposition in subadult and adult individuals' ones.

Contrary to humerus, the growth pattern of the femur midshaft between species is very similar with a slight difference in the adult stage. Both taxa have a relatively large medullary cavity with a cranio-lateral growth of periosteal tissue. From early postnatal ontogeny stage periosteal and endosteal tissue are identified by resorption lines. Throughout growth, both water voles show an increase in cross-section size as well as in cortical thickness. As in the humerus, cross-section growth is more uniform in *A. scherman* than in *A. sapidus*, where a large increase it is seen between older juvenile individuals and subadult ones. The tissues matrix composition is quite similar to that observed in other rodents (Bach-Gansmo et al., 2013, Ip et al., 2016, Shipov et al., 2013).

Several recent articles have shown that bone microstructural characters include genetic information, and therefore, that certain taxon-specific patterns may be identified in the cortex (e.g., Canoville & Laurin, 2010; Castanet et al., 2001; de Ricqlès et al., 1991; Houssaye et al., 2013; Rensberger & Watabe, 2000, Warshaw, 2008). Despite the existence of a phylogenetic component (Cubo et al., 2005), several authors assume that the shared similarities between different species may be due to the convergence of bone microstructures as a result of adaptations to biomechanical constraints (e.g., Currey, 2002; de Margerie et al., 2004; Laurin et al., 2004). Given that, the species here studied belong the same genus, the similarities found in the modelling process, as well as in histology features may reflect the existence of phylogenetic preservation. Likewise, as they show distinct modes of locomotion, the macroscopic and histological differences observed, mainly in the humerus, can be attributed, at least in part, to functional factors.

In the case of *A. scherman*, the modelling process of the humerus is in accordance with what have been described for long bones in terrestrial mammals (Goldman et al., 2009; McFarlin et al., 2016; Sontag, 1986; Smith, 1960). Namely, the increase in cross-section size, periosteal replacement by new bone and expansion of the medullary cavity in adult individuals coincide with the characteristics described for C57BL/6J mice (Ferguson et al., 2003). However, considering that

*A. scherman* is a digger, it would be expected that its bone modelling would be more akin to that reported for other fossorial species (Montoya-Sanhueza & Chinsamy 2017; Montoya-Sanhueza et al., 2020; Legendre & Botha-Brink, 2018), i.e., with a continuous periosteal bone apposition in early voles and endosteal bone formation in older individuals, with consequent reduction of the medullary cavity. The absence of this bone modelling pattern in *A. scherman* may be because it is a chisel-tooth digger and, although the humerus plays an important role in the digging activity, this is not the main bone structure in this activity. Thus, considering that the structure most involved in the chisel-tooth is the mandible, it would be interesting to analyse this structure at the histological level, and to compare it with other fossorial species with different digging modes.

In functional terms, the increase in the medullary cavity decreases bone weight by saving bone mass. This saving of weight in the diaphysis results in a reduction in the energy cost of running, which can have important implications for accelerating and decelerating with each stride (Currey & Alexander, 1985). Although montane water voles spend most of their life underground, they perform short displacements (30 to 50m) above the ground (Airoldi, 1978), where they play a fundamental role as prey for several predators (Girandoux et al., 2020; Rodriguez et al., 2020; Weber et al., 2002). Thus, since a larger medullary cavity is an advantage for running, and the cortical thickness of the humerus seems to cope with the mechanical demands in the digging process (see section Cortical thickness between species), maintaining a large medullary cavity in *A. scherman* could be associated with the ability to move on the surface.

Since semiaquatic species move between land and water, it is expected that bone microstructure reflects a compromise between terrestrial and aquatic locomotion (e.g., Stein, 1989). The humerus bone growth in *A. sapidus* may reflect this compromise. Increased compact bone deposition in the appendicular skeleton has been referred as a way in which semiaquatic mammals are able to increase their density to overcome buoyancy (Houssay et al., 2009; Stein, 1989; Wall, 1983). In particular, an increase in bone mass has been observed in less active swimmers (Houssay, 2009). Furthermore, a comparative study of humeral microanatomy of terrestrial, semiaquatic, and aquatic carnivorans showed a decrease in bone resorption in limb bones in semiaquatic animals compared to terrestrial animals, meaning a progressive aquatic adaptation (Nakajima & Endo, 2013). Thus, the modelling process observed in the humerus of *A. sapidus*, i.e., continuous bone apposition and reduced bone resorption, together with the fact that Southwestern water vole is an excellent swimmer and diver, seems to suggest a progressive adaptation to the aquatic environment. The fact that no major differences were observed in femur cross-section microstructures between *A. scherman* and *A. sapidus* seems to be in line with other comparative studies between terrestrial and semiaquatic animals, with the hindlimbs appearing to be slightly less informative in functional terms than the forelimbs (Canoville & Laurin, 2010; Houssay et al., 2016; Houssay & Botton-Divet, 2018; Laurin et al., 2011).

#### 8.4.5. *Cross-section shape*

Based on Wolff's law (bone tissue responds dynamically to stress and strain, optimizing itself to the mechanical environment), several studies have used bone cross-sectional geometry to draw behavioural inferences in several species (e.g., Canoville & Laurin, 2010; Carlson, 2005; Demes et al., 1991; Houssaye et al., 2013; Meier et al., 2013; Montoya-Sanhueza & Chinsamy, 2018; Sparacello et al., 2010). The cross-sectional shape is one of the bone cross-sectional geometry variables used to correlate long bone's mechanical loading history (Jepson et al., 2015).

During the postnatal ontogeny of *A. scherman* the cross-section of the humeral midshaft changes its shape from circular in younger juvenile individuals to rounded triangular shape in older juvenile ones, maintaining this shape during later ontogeny. This change in the cross-section shape of humeral midshaft could result from a combination of mechanobiological factors (e.g., weight and locomotion) and periosteal pressures. Due to the pressure that the belly of the muscles exerts on the bone, the bone surfaces that contact with them are usually flattened (Carpenter & Carter, 2008). Adjacent to the medial side is the coracobranchialis muscle (flexor and adductor of the forelimb), and the medial head of triceps branchialis muscle (important in all extensions of the forelimb). Therefore, it is possible that the flat shape in the medial side that contributes to the triangular shape in the humerus is due in part to the pressure exerted by the belly of these muscles. This would explain the slight medial resorption and perimedullary asymmetry observed in subadult, since increased pressure on the periosteal surface can lead to periosteal resorption and inhibition or deposition of endosteal bone tissue (Carpenter & Carter, 2008).

An expansion with vascularization on the lateral side of the humerus was observed in individuals of age classes 4 and 5 of *A. scherman*. Raised crests appear to be related to the ligament of muscles (Carpenter & Carter, 2008). This lateral expansion observed in fossorial water voles could be due to the insertion of the deltoid muscle in the deltoid crest, a location that coincides with its lateral side. Conversely, the cross-section of the humerus of *A. sapidus* changes its shape from circular in younger juvenile voles to elliptical in older juvenile ones, shape that is maintained throughout the rest of the ontogeny. In general, a circular shaped cross-section is associated with variable loading regime, such as, bending and torsion in multiple planes, while the elliptical shape is typically interpreted to better resist bending loads in a specific plane or direction, (e.g., Carlson, 2005; de Margerie et al., 2005; Marelli & Simons, 2014). The elliptical cross-section shape in *A. sapidus* is most likely due to increased bending forces related to uniform locomotor behaviour during forepaw kinematic development. Similar to what occurs in *A. scherman*, adult individuals of *A. sapidus* show a crest in the lateral side of the humerus. This expansion affects the morphology of the midshaft cross-section changing from an elliptical in subadults to a drop shape in adults.

Something that deserved attention in this region in both species was the alteration in the orientation of osteocytes and collagen fibres, as well as the presence of large primary osteons compared to those visible along the cortex. It is known that osteocytes respond early to mechanical stimulation (e.g., Quin et al., 2020; Takano-Yamamoto, 2014; Uda et al., 2017) and that the orientation and distribution of collagen fibres have a biomechanical significance, aligning themselves in the direction of stress (Bromage et al., 2003). Furthermore, size and orientation of osteons have an influence on mechanical properties of bone (Ritchie et al., 2005; Camelli et al., 2013). Therefore, and together with the fact that the presence of regional histological variations corresponds to functional demands on different regions of the same bone (Enlow, 1963, 1968), these alterations observed in both species seem to indicate that the lateral side may be under different mechanical loads than the rest of the bone.

In general, in *A. scherman* and *A. sapidus* the cross-sectional shape of the femur does not change much during postnatal ontogeny, showing an elliptical shape in all age classes. Although differences were observed in both cortical thickness and femur strength between these species (Durão et al., 2022) in response to the loads (see section Cortical thickness between species section), no difference was observed between the cross-sections shape. This indicates that the different mechanical stresses to which the *A. scherman* and *A. sapidus* are exposed during digging and swimming activity, respectively, are not so strong to produce important interspecific shape changes in the midshaft of the femur.

#### 8.4.6. Ontogenetic trajectories

In previous studies based on geometric morphometrics, the phenotypic trajectories during the postnatal ontogeny of humerus (Durão et al., 2020) and femur (Durão et al., 2022) in *A. scherman* and *A. sapidus* were compared. This analysis quantifies the variation of different attributes (size, orientation, and shape) of the trajectory between points (age classes) for each species (group) and compares these attributes between groups via permutation (Adams & Collyer, 2009). In humerus (Durão et al., 2020), significant differences in all attributes of the phenotypic trajectories analysis were detected between fossorial and semiaquatic water voles; specifically, the ontogenetic trajectories showed different directions (orientation), the magnitude of shape change was greater in *A. scherman* than in *A. sapidus* (size) and, the trajectory shape was different. The ontogenetic trajectory in *A. scherman* showed changes in its direction between age classes 0 - 2 (juveniles), and maintained a constant path until age class 4, where a sharp change occurs when compared with age class 5. In *A. sapidus* the direction of the trajectory changes substantially from age class 2 onwards (Fig. 8-10). In the femur (Durão et al., 2022) the only interspecific difference observed in the phenotypic trajectories was in the orientation. In both species, the shape of the trajectories was constant (Fig. 8-11).

Histologically, the humerus of *A. scherman* shows a similar growth pattern throughout ontogeny, with craniomedial expansion of periosteal tissue and extensive endosteal resorption. Geometrically, fossorial water voles change the femur shape from circular in younger juvenile to rounded triangular shape in older ones, as a result of a marked deposit of fast-growing tissue. From age class 2 forward, a slowing of osteogenesis rates and an increase in cortical thickness and medullary cavity was observed. These results seem to coincide with the humerus ontogenetic trajectory of *A. scherman*, in which the turning point occurs in the juvenile stage, remaining afterwards constant. In turn, the humerus of *A. sapidus* has a variable growth pattern, with continuous periosteal bone apposition in juvenile voles (age classes 0-2) and endosteal and periosteal tissue apposition in subadult and adult individuals. This change in bone modelling process coincides with the substantial changes' direction of the trajectory between age class 2 and 3 observed in the ontogenetic trajectory of this bone (Fig. 8-10). In both species, the transition from juvenile to adult stage is where major macrostructural changes were reported (Durão et al., 2020), coinciding with the main microstructural changes observed in the present study. The fact that these changes occur earlier in *A. scherman* than in *A. sapidus* may be due that juvenile voles exhibit a digging behaviour similar to adult ones (Airoldi et al., 1976). Although the histological analysis was restricted to a single cut in the middle of the diaphysis and the study of ontogenetic trajectories was obtained from data of the entire humerus, the microstructural interspecific differences here reported, such as the bone growth pattern, cross-section shape and histodiversity (greater in *A. scherman* than in *A. sapidus*) is concordant with the results observed at the macrostructural level (Durão et al., 2020). Thus, the functional demands caused by digging and swimming activities are also reflected in the histology of the humerus.

During postnatal ontogeny, the femur of both species is histologically and geometrically quite similar, coinciding with the constant direction of the ontogenetic trajectories (Fig. 8-11). The only marked interspecific difference was found in the transition from tissues with lower to higher osteogenesis rates, with juvenile specimens of *A. scherman* showing a cortex composed of woven, fibrolamellar, and well-vascularized parallel-fibred bones, while older juveniles of *A. sapidus* show a cortex formed practically by hybrid and lamellar bones. This interspecific difference in tissue composition suggests a different rate of bone growth between species. This result may somehow reinforce the fact that *A. scherman* and *A. sapidus* have shown different orientation in phenotypic trajectories.

As initially hypothesized, during postnatal ontogeny the humerus shows more marked microstructural changes than the femur both in *A. scherman* and *A. sapidus*, coinciding with the prominent action of this bone in the digging activity and with the fact that it is an activity of high biomechanical demand.

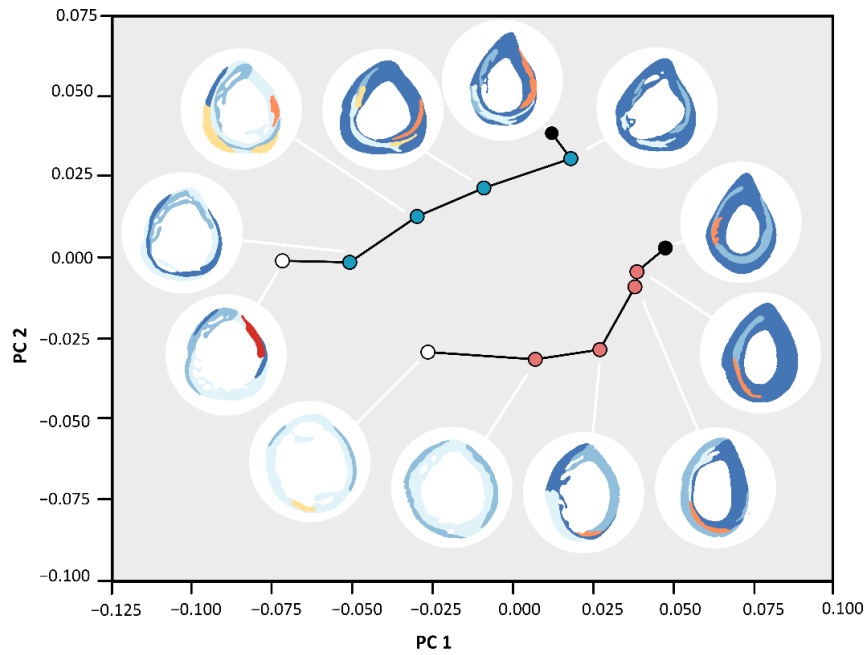


Fig. 8-10 Ontogenetic phenotypic trajectories of the humerus of *Arvicola scherman* (line with blue dots) and *Arvicola sapidus* (line with red dots) derived from the phenotypic trajectory analysis (adapted from Durão et al., 2020). Each dot corresponds to an age class; white dots represent the beginning (age class 0) and the black dots the end (age class 5) of the trajectories. The lines define the trajectories and the larger dots to the mean of each age class. The images from the dots are Illustrative maps of the areas occupied by the different bone tissues. Each image was chosen taking into account the specimen that best characterizes the histological pattern defined in this age class. For an easier comparison, all images are the same size.

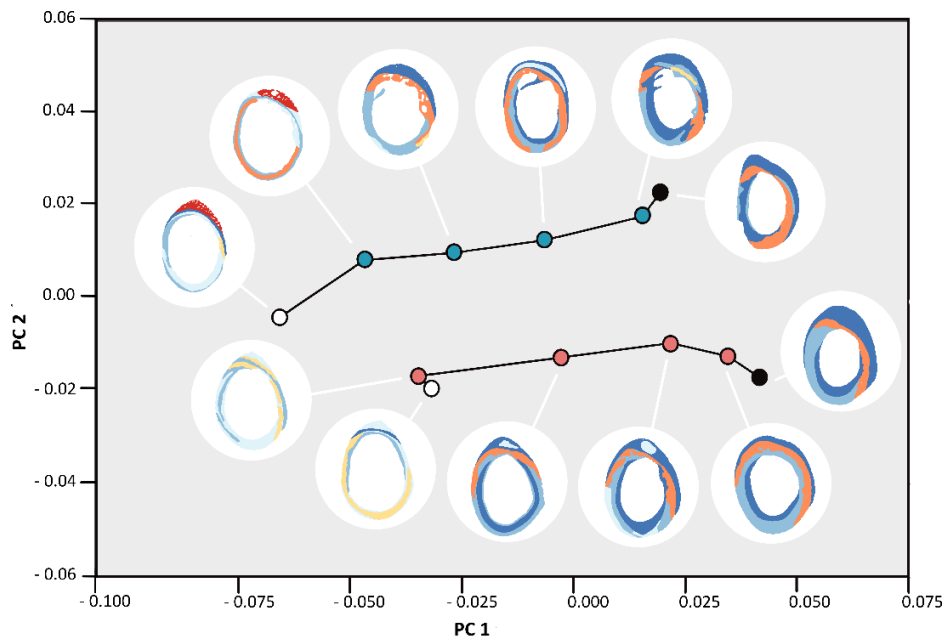


Fig. 8-11 Ontogenetic phenotypic trajectories of the femur of *Arvicola scherman* (line with blue dots) and *Arvicola sapidus* (line with red dots) derived from the phenotypic trajectory analysis (adapted from Durão et al., 2022). Each dot corresponds to an age class; white dots represent the beginning (age class 0) and the black dots the end (age class 5) of the trajectories. The lines define the trajectories and the larger dots to the mean of each age class. The images from the dots are Illustrative maps of the areas occupied by the different bone tissues. Each image was chosen taking into account the specimen that best characterizes the histological pattern defined in this age class. For an easier comparison, all images are the same size.



## 8.5. CONCLUSIONS

To our knowledge, the present work is the first comparative histological study of postnatal growth of limb bones (humerus and femur) between phylogenetically close species (of the same genus) with different modes of locomotion (fossorial and semiaquatic). Analysis of the diaphyseal midshaft revealed that *A. scherman* and *A. sapidus* exhibit a typical pattern of bone growth, in which high rates of bone formation in early stages of life decrease during adulthood. Nevertheless, several interspecific histological differences were found associated in part with the corresponding lifestyles. These divergences were more marked in the humerus than in the femur, highlighting the involvement of each bone in the different type of locomotion. The descriptions and comparisons performed in the present study, complement the knowledge of the postnatal growth of these bones obtained from geometric morphometric analysis. However, despite the limitations of the present work, such as, the sample size that restricted qualitative descriptions, the finding here reported contribute to the knowledge of bone modelling throughout ontogeny and how it may affect the adult form. In addition, it constitutes a baseline for future comparative studies between semiaquatic and fossorial species. It would be interesting in future works to involve quantitative assessments, as well as to include more *Arvicola*, populations that vary their ecology depending on the population density and/or environmental factors.

8.6. SUPPLEMENTARY INFORMATION

Table S8-1 Sample composition.

Species	Number	Age class	Sex	Ontogenetic stage	H	F
<i>Arvicola sapidus</i>	83071202	0	F	Juvenile	■	■
	84062308	0	M		■	■
	84062801	0	M		■	■
	84062405	0	M		■	■
	84062702	0	M		■	■
	83091802	1	F		■	■
	83121901	2	F		■	■
	84011301	2	F		■	■
	84111101	2	F		■	■
	84041403	2	M		■	■
	84041501	2	M		■	■
	83101305	3	F		Subadult	■
	84120702	3	F	■		■
	84080401	3	F	■		■
	83012306	3	M	■		■
	83111601	3	M	■		■
	84022002	3	M	■		■
	83012303	4	F	Adult		■
	83022001	4	F		■	■
	84031004	4	F		■	■
	84061601	4	F		■	■
	83043003	4	M		■	■
	83012302	4	M		■	■
	84111002	4	M		■	■
	83011302	5	F		■	■
	84011405	5	F		■	■
	83091801	5	F		■	■
	83111701	5	F		■	■
	83091803	5	M		■	■
	84011402	5	M	■	■	
	83012305	5	M	■	■	
	84030902	5	M	■	■	

Abbreviations: H, humerus; F, femur

COMPARATIVE HISTOLOGY OF THE HUMERUS AND THE FEMUR

Table S8-1 Sample composition (continued).

Species	Number	Age class	Sex	Ontogenetic stage	H	F	
	84042907	0	F	Juvenile			
	84052709	0	F				
	84083013	0	M				
	84052614	0	M				
	83081106	1	F				
	83112628	1	F				
	83092620	1	F				
	83112703	1	F				
	83072920	1	M				
	83092725	1	M				
	83092727	1	M				
	83081117	2	F				
	83081012	2	F				
	83112708	2	F				
	83072914	2	M				
	83081114	2	M				
	83102806	2	M				
	83072804	3	M		Subadult		
	83072827	3	F				
	83092802	3	F				
<i>Arvicola scherman</i>	83092706	3	F				
	83092613	3	M				
	83081008	3	M	Adult			
	83122310	4	F				
	83122321	4	F				
	83122308	4	F				
	84072804	4	F				
	83122413	4	M				
	83122414	4	M				
	83112709	4	M				
	83112603	5	F				
	84021210	5	F				
	84042908	5	F				
	84021207	5	M				
	84042917	5	M				
	83092717	5	M				

Abbreviations: H, humerus; F, femur

---

# CHAPTER 9

## GENERAL DISCUSSION



## CHAPTER 9. GENERAL DISCUSSION

---

### 9.1. GENERAL CONTEXT

Several studies on rodents have shown that species from different groups may share physical characteristics related to the mode of locomotion, which suggests that it is an important factor in shaping morphological traits (e.g., Hildebrand, 1985; Lessa et al., 2008; Samuels & Valkenburgh, 2008). Furthermore, it has been observed that external forces, such as functional and biomechanical constraints, can cause changes in the ontogenetic pattern of the corresponding structures (e.g., Adams & Nistri, 2010). Understanding which factors can shape phenotypic variation is fundamental to expanding knowledge about the development of an organism and its evolutionary implications. In this way, comparative studies between phylogenetically close species with different type of locomotion should permit to understand how function can affect the different stages of development. The genus *Arvicola* has two ecotypes, fossorial and semiaquatic, so that it constitutes an excellent model to study this topic. Besides, previous works on this taxon have shown remarkable morphological variations related, at least in part, to locomotion (Ventura & Casado-Cruz, 2011; Cubo et al., 2006; Ventura, 1993). In this sense, the main aim of the current research has been to determine to which extent phylogenetic and functional factors are involved in the phenotypic differences that could exist in the form (size and shape) of several bones involved in locomotion between typical fossorial and semiaquatic morphotypes of *Arvicola*. Specifically, the postweaning ontogenetic patterns of mandible (see Chapter 4), humerus (see Chapter 6) and femur (see Chapter 7) in *A. scherman* (fossorial) and *A. sapidus* (semiaquatic) were determined and the corresponding ontogenetic trajectories were compared by using the geometric morphometric method. Since the mandible of *Arvicola* is a relatively flat structure and studies have shown a considerable agreement in 2D and 3D results on the variation pattern of its form (Cardini, 2014; Navarro & Maga, 2016), in the present study, 2D geometric morphometrics was applied on this bone (see Chapter 4). In the case of the humerus and femur, 3D geometric morphometrics was used due to their important three-dimensional component of these bones (see Chapter 6 and 7). Even though many works have already applied 3D analysis in bones of diverse mammalian species, few have been done on wild rodent populations. This may be related to the high cost of the devices precise enough to obtain 3D data from small structures. Thus, as an alternative to existing methods, a procedure based on photogrammetry to obtain 3D models of limb long bones from small mammals was developed (see Chapter 5). To assess the usefulness of this protocol for geometric morphometric studies, the form variation of the humerus in a sample of adult individuals of *A. scherman* and *A. sapidus* was examined. The results here obtained are consistent with those already described in the literatures (Laville et al., 1989), which support the

reliability of the method. This protocol may have many positive implications for shape analysis in skeletal structures of small mammals due to its simple procedure and low-cost.

Since the analyses here performed revealed notable differences in the external morphology of the humerus and femur between *A. scherman* and *A. sapidus*, associated in part with their lifestyle, the need arises to determine to which extent interspecific differences exist at the microstructural level. Comparative histological studies on mammal species have been carried out with an emphasis on function and the possibility of bone microstructures offering information on growth patterns, physiological and biomechanical adaptations (Enlow, 1962, 63; Currey, 2002; de Ricqlès, 1993). The complementarity of morphometric and histological results provides unique pieces of information for a better understanding of the extent of the effect of phylogenetic and functional factors on morphological variation. Results presented in this research constitute, to our knowledge, the first contribution on this topic in two phylogenetically close species with very different lifestyles and mode of locomotion.

### **9.2. COMMON ONTOGENETIC PHENOTYPIC CHANGES IN THE MANDIBLE, HUMERUS, AND FEMUR OF SEMIAQUATIC AND FOSSORIAL WATER VOLES**

According to our results obtained in geometric morphometric analyses, *A. scherman* and *A. sapidus* show a similar growth pattern of the mandible, humerus, and femur during postnatal ontogeny. The long bones of juvenile voles of both species were more robust than adult ones. These results match with those observed in *Ctenomys talarum* (Echeverría et al., 2014) and *Bathyergus suillus* (Montoya-Sanhueza et al., 2019). Histologically, humerus and femur of both *Arvicola* species show a similar cortical bone growth with high rates of bone formation in early growth stages and low rates of osteogenesis in older age classes. This pattern has been previously described in other mammals (e.g., Enlow, 1962; Sontag, 1986; McFarlin et al., 2016). Similarities were also found in the modelling process, with the same cortical drift being identified in these bones of both species. These results indicate that the changes in the cortex found in juvenile individuals are similar in *A. scherman* and *A. sapidus*. A very interesting histological feature detected in the humerus and femur of these species was a disorganized region with calcified cartilage inside (see Chapter 8). Although this had been previously reported for the femur of mice and rats (Bach-Gansmo et al., 2013; Ip et al., 2016; Shipov et al., 2013), to our knowledge, this is the first time that this trait has been described in the humerus of a rodent species. The presence of this characteristic throughout ontogeny seems to be related to the absence of bone remodelling observed in these water vole species.

The complementary use in the present research of geometric morphometric and histological analyses contributes to a better understanding the morphological variation of humerus and femur

throughout ontogeny. As mentioned above, geometric morphometric analyses revealed that, regardless of locomotion mode, juvenile individuals of both *Arvicola* species share more robust bones than adult ones. The fact that the former exhibited a thinner wall bone and higher intracortical porosity than adult voles, features that confer low biomechanical properties to the bone (Liebermann & Pearson, 2001; Martin, 1991), could explain the increase of its external robustness in juvenile individuals. This probably minimizes the fracture risk during initial locomotion efforts.

### 9.3. DIFFERENCES IN THE POSTWEANING GROWTH OF THE MANDIBLE, HUMERUS, AND FEMUR BETWEEN SEMIAQUATIC AND FOSSORIAL WATER VOLES

In addition to the common characteristics detected between *A. scherman* and *A. sapidus* results obtained here also revealed that both species show significant differences associated with their lifestyle. Consistent with the size relation between them (Cubo et al., 2006; Ventura 1993), all bones analysed here were smaller in *A. scherman* than in *A. sapidus*. The size of fossorial water vole seems to be linked with an adaptative response to the hypogeal life (Cubo et al., 2006). Actually, the digging activity requires a high energy cost (Vleck, 1979), and therefore, the decrease in body size is advantageous for fossorial animals due the decrease in their burrow construction cost (Vleck, 1979, White, 2005). So, the comparatively smaller body size of *A. scherman*, and consequently of their mandible, humerus, and femur, is likely related with a reduction of the energy devoted to burrowing.

Studies on ontogenetic allometry have shown that changes in the attributes of ontogenetic patterns (orientation and magnitude) can influence evolutionary processes (e.g., Klingenberg, 1998; Wilson & Sánchez-Villagra, 2010). In our comparative analysis, the direction of the vectors of the allometric coefficients of the mandible, humerus and femur showed significant interspecific differences. This indicates that the shape changes associated with size in these bones are significantly different between *A. scherman* and *A. sapidus*. The angle between the vectors of the allometric coefficients of the two species was quite similar in the three bones, albeit in the femur it was slightly lower. Considering that phylogenetically close species tend to differ little in the angle between the vectors of the allometric coefficients which implies parallel or overlapping trajectories (Esquerré et al., 2017), the angles here obtained were unexpectedly high. However, several studies have shown that allometric trajectories can evolve (e.g., Adams & Nistri, 2010; Gray et al., 2019), contrary to what was initially suggested (Gould, 1966; Voje et al., 2013). In this context, our results add to the growing literature that changes in the direction of the allometric slopes are not so rare. Significant interspecific differences in the length of allometric trajectory (i.e., amount of shape changes per size unit) of the mandible and humerus, suggest that functional



## GENERAL DISCUSSION

pressures on these bones act differently in *A. scherman* and *A. sapidus*. In both bones, the former species showed greater vector length than *A. sapidus*, indicating a higher rate of allometric shape changes along postweaning ontogeny in fossorial water voles. Functional pressure causes fast and important morphological changes in the mandible and the humerus since they play an important role in digging. Species belonging to the same genus tend to differ little in the length of their allometric trajectory due to a strong phylogenetic effect (Esquerré et al., 2017). Since the femur did not reveal significant differences in the length of the vectors in *A. scherman* and *A. sapidus*, the magnitude of the shape changes associated with size are not significantly different between these species. This result may also be related with the strong phylogenetic effect. In fact, in both taxa juvenile individuals show a similar behaviour to adult ones from an early age (Airoldi et al., 1976; J. Ventura, personal observations), which can promote a quick adaptative response of the femur in both species. Although *A. scherman* and *A. sapidus* moves in different environments, digging and swimming can represent a similar functional pressure on this bone (Salton & Sargis, 2009; Samuels et al., 2013; Samuels & Valkenburgh, 2008; Smith & Savage, 1956), which determines shape changes associated with size of similar magnitude in both species.

The direction of the phenotypic trajectories of *A. sapidus* and *A. scherman* were different in the mandible, humerus, and femur, indicating that their shape changes occurring during ontogeny are different in these species. The fact that the angles obtained in the phenotypic and allometric trajectories were similar suggests that in all cases the shape variation observed is essentially allometric. Contrary to the mandible and the femur, the humerus showed interspecific differences in the length (greater in *A. scherman* than *A. sapidus*) and in shape of the phenotypic trajectories. In this case, length of phenotypic trajectory was lower than allometric vectors indicating that most shape changes across ontogeny are related to size. Histological analyses of the limb long bones seem to corroborate the results concerning the phenotypic trajectories. Remarkable differences in modelling pattern of the humerus between *A. scherman* and *A. sapidus* were found. Both species revealed a similar growth pattern in juvenile individuals with craniomedial expansion of periosteal tissue and high endosteal resorption. In *A. scherman* these changes remained constant throughout ontogeny causing large medullary cavities. In subadult *A. sapidus*, an endosteal and periosteal tissue apposition was observed, thus causing an increase in cortical thickness. This divergence in the growth process may be related to an adaptation to the biomechanical constraints produced by the different modes of locomotion, despite the existence of a phylogenetic heritage (Cubo et al., 2005). Additionally, both humerus and femur show a slower transition from tissues with lower to higher ontogenesis rates in fossorial than in semiaquatic water voles. Since variation in tissue composition reflects variation in bone deposition rate during ontogeny (e.g., Amprino, 1947; de Margerie et al., 2002, 2004), differences between *A. scherman* and *A. sapidus* in the deposit rates may indicate that both species have different rates of bone growth.

The phenotypic trajectories of the mandible and the femur showed a constant direction of change across the shape space both in *A. scherman* and *A. sapidus*, indicating that shape variations occurring in these bones through ontogeny are more or less constant in both taxa. However, a sharp shift in the direction of shape changes was observed in the humerus of both species. In *A. scherman* it remained constant until the adult stage, varying the direction between age classes 4 and 5. In *A. sapidus* a substantial shift in the direction of shape changes was observed at age class 2, remaining more or less constant from this age class onwards. Both in the femur and in the humerus, the histological pattern seems to coincide with that observed in the ontogenetic trajectories of each species. In the case of humerus, both at the macro and microstructural level, the greatest modifications occur between the transition from the juvenile phase to the adult one. In fossorial water voles, the main variation occurs between younger and older juvenile individuals, with a change of the cross-section shape, from circular in younger juvenile voles to rounded triangular shape in older juvenile ones. In *A. sapidus* humerus, this shift appears between the juveniles and subadult individuals age classes with alteration in the modelling process. The fact that changes occur earlier in *A. scherman* than in *A. sapidus* may be related to the early juvenile individuals mimicking the digging behaviour of adult ones (Airoidi et al., 1976), resulting in an adaptive response to a functional demand. In the femur, the microstructural characteristics are quite similar between the two species, coinciding with the constant direction of the ontogenetic trajectories.

A previous work on postweaning ontogeny of the mandible in *A. scherman* (Ventura & Casado-Cruz, 2011) detected morphological differences between age classes 4 and 5, suggesting that the mechanical stress caused by the persistence of digging affects the shape of this bone during adulthood. This explanation was not supported by either the ontogenetic trajectory of the mandible nor the Procrustes distances between species in age classes 4 and 5. However, the allometric regression revealed an important mandible shape variation not associated with size between these age groups. This could be related to age class variability or to a shape change in older individuals. A similar pattern was also detected in the allometric regression of the humerus. In this bone, a distancing between phenotypic trajectories was also observed in age class 5, consistent with a greater Procrustes distance between species in this group than in age class 4. Moreover, the angle of the allometric coefficient vectors calculated only with age classes 4 and 5 was greater than that obtained considering all age groups. These results seem to indicate that the pattern of shape variation observed between these classes 4 and 5 in both structures is attributed to shape changes in adulthood. In short, shape changes in adults were more pronounced in the humerus than in the mandible. This may be because the humerus is implicated in all steps of the digging process (see section 1.5.1 Fossorial locomotion), which make this bone more prone to shape modifications related to the mechanical stress produced by burrowing. At histological level,

## GENERAL DISCUSSION

no difference was observed in the humerus of *A. scherman* between individuals of age classes 4 and 5. Specifically, both groups share a similar variation pattern: an increase in the periosteal perimeter and medullary cavity with a consequent decrease in cortical thickness. These characteristics had already been described for other long bones of other rodent species in individuals older than 1 year (Ferguson et al., 2003, Sontag, 1986). As suggested in these works, the increase in the periosteal perimeter can be a compensation for thin cortical thickness (Ferguson et al., 2003) and loss of flexibility that occurs with age (Sontag, 1986).

Morphological distances between *A. scherman* and *A. sapidus* were significant in all age classes in all bone structures analysed, both using shape and non-allometric shape data. In general, morphological distances were greater in the non-allometric shape data than shape data, which reveal that these taxa share part of allometric shape changes. Comparing the adult shape of mandible, humerus, and femur between both water vole species several differences were found. Most of them are associated with expansion of the area on the skeleton for greater muscular origin and insertion, allowing an increase in the force generated by the bone, an advantageous characteristic for the fossorial species. Several features here reported for *A. scherman* had already been described for scratch-diggers (e.g., Echeverría et al., 2014; Lessa et al., 2008; Salton & Sargis, 2009), such as enlargement of the deltopectoral crest (humerus), epicondylar expansion (humerus), larger lesser trochanter (femur) or greater robustness of the third trochanter (femur), among others. Despite the presence of these traits in fossorial water voles they are less marked than in scratch-diggers, which is coincident with the different implications of the forelimbs in different digging modes. Although aquatic life can promote morphological changes to cope with hydrodynamic challenges (e.g., Fish, 2016), these seem to be related to time and the activities carried out by the animal in the water (Dunstone, 1979; Stein, 1988). In this line, the only specific feature associated with aquatic locomotion detected in *A. sapidus* was the slight medial-cranial extension of the greater trochanter, which could be associated with improving locomotor performance and stability (Fish & Stein, 1991). Surprisingly, at the histological level, both the humerus and the femur of *A. scherman* do not show typical fossorial characteristics, such as high cortical thickness (Montoya-Sanhueza & Chinsamy, 2017). Conversely, results revealed that during postnatal growth both bones showed greater cortical thickness in *A. sapidus* than in *A. scherman*. The absence of this characteristic in fossorial water voles may be related to the fact that these limb bones do not need further microstructural changes to cope with the mechanical demands caused by burrowing. Conversely, increased cortical thickness in *A. sapidus* may correspond to an adaptive response to increase bone stiffness (Hart et al., 2017). The modelling process of long bones in *A. scherman* do not coincide with that described for other fossorial rodent species (Montoya-Sanhueza & Chinsamy, 2017; Montoya-Sanhueza et al., 2020, Legendre & Botha-Brink, 2018). In fact, it is more similar to that described for limb long bones of other terrestrial

mammals (Goldman et al., 2009; McFarlin et al., 2016; Sontag, 1986; Smith, 1960): the increase in cross-section size, periosteal replacement by new bone and expansion of the medullary cavity. Enlarging the medullary cavity saves bone mass, which reduces the running cost (Currey & Alexander, 1985). Thus, the increase in the medullary cavity in *A. scherman* could be related to the displacement on the surface. Contrary to that found in the morphological analyses, in which no features associated with swimming were detected, at the microstructural level, *A. sapidus* shows a modelling process with reduced bone resorption, trait probably linked with this mode of locomotion (Nakajami & Endo, 2013).

Altogether, the results obtained in the present research revealed that, as for the bone analyses, many differences between *A. scherman* and *A. sapidus* are due to the functional pressure exerted by the type of locomotion, being particularly intense in burrowing. However, in both species, bone morphology seems to reflect a balance between the functional pressures of digging (*A. scherman*) or swimming (*A. sapidus*) and the terrestrial locomotion (walking and running) existing in both species. The results obtained also reveal that the functional pressures do not act in the same way in all structures. The role that each bone plays in the locomotion activity seems to be related to whether shape changes over ontogeny are more or less pronounced. As hypothesized, of the bones here analysed, the humerus shows the most marked shape changes during postnatal ontogeny. This is probably due that although the mandible is essential in burrowing, through the insertion of the incisors to break the earth, the humerus is involved in more phases of the digging process (Laville, 1989b).

Traditionally, the emergence of external morphological characteristics linked to the invasion of a hypogeal habitat has been attributed to a genetic regulation (e.g., Cubo et al., 2006; Echeverría et al., 2014). Namely Cubo et al. (2006), suggest that the appearance of this features in the skull and limb long bones in *A. scherman* are the result of a direct expression of genetic changes. In concordance with previous studies (Cubo et al., 2006; Ventura, 1993; Ventura & Casado-Cruz, 2011), results here obtained revealed that juvenile individuals of *A. scherman* have skeletal traits associated with the fossorial mode of locomotion. Nevertheless, since juvenile fossorial water voles show an identical digging behaviour to adult ones (Airoldi et al., 1976) it is not possible to determine if these features correspond to a plastic response during postnatal ontogeny to burrowing or whether they are genetically fixed in the developmental patterns of the species. Increasingly studies have evidenced that mechanical stimuli may play an important role in prenatal morphogenesis and ossification (e.g., Sharir et al., 2011). In this way, it is possible that the emergence of new characteristics is more complex than initially thought. Howsoever, this question in *A. scherman* remains to be solved.

Results presented here constitute a significant contribution to the understanding of how function can affect ontogenetic patterns of bones involved in locomotion and the relationship

## GENERAL DISCUSSION

between external morphological features and cortical properties of these bones throughout postnatal growth. In addition, results reinforce the importance of carrying out comparative studies on the ontogeny of these structures between phylogenetically close species with different locomotion modes, in order to detect functional and phylogenetic signals in the bone development. As initially predicted, the combination of geometric morphometrics and histological results has been essential to acquire a global view of the relationships between morphology and function during the postnatal ontogeny of the skeletal structures analysed. It is important to note that the museum material used in the present research was essential to analyse these topics. In fact, a large sample of limb long bones that include a good representation of juvenile, subadult and adult specimens from wild rodent populations is difficult to find in collections. In this way, for example, the analyses of shape variation of bone structures during growth by means of geometric morphometrics method requires a relatively large sample size (Cardini & Elton, 2007). As for histological analyses, although the sample here used was not appropriate for quantitative statistical analysis, the number of individuals of each age class was enough to obtain important information of the microstructural changes that occur during ontogeny. The analysis of several specimens of the same age class has been fundamental to determine the growth pattern and histological features inherent to each of these groups.

## FUTURE PERSPECTIVES

The lack of microanatomical information on limb long bones of *A. scherman* and *A. sapidus*, was a compelling reason to perform histological analysis of these structures. In fact, the present research constitutes the first study that describes and compares the histological variation during postnatal growth of the middle diaphyseal section of the humerus and femur in rodent species of the same genus with fossorial and semiaquatic lifestyles. Results obtained have not only provided a holistic approach to bone changes related to locomotion but also constitute the starting point to perform similar comparative studies on other bones. It would be interesting, for example, to analyse the histological variation of the mandible along the ontogeny, and to compare and contextualize it with the results of geometric morphometrics here presented. It would also be useful to have wide knowledge of the issues studied to compare the growth patterns of the bones involved in burrowing with those of other fossorial rodent species that show other digging modes. Likewise, it would be welcome future works based on wide samples that permitted to perform quantitative assessments at the histological level. As mentioned in the Introduction (see section 1.5. Structures involved in *Arvicola* locomotion), several bones play a role, more or less important, in digging or swimming. Bearing in mind that certain evolutionary changes in the form of the skull, ulna and tibia have been reported in *Arvicola* by using linear measurements (Cubo et al., 2006), it would be also interesting to perform in these structures of *A. sapidus* and *A. scherman* further

comparative morphometrical and histological analyses similar to those conducted here. Taking into account their involvement in the digging process, other bones that would be appealing to analyse are the scapula and atlas (Airoldi et al., 1976; Laville, 1989; Laville et al., 1989). Finally, extending the analysis done in the present investigation to other fossorial and semiaquatic populations of *Arvicola*, as well as populations that change their type of locomotion according to climatic characteristics, reproductive cycles and/or population density (e.g., Kratochvíl & Grulich, 1961; Stewart et al., 2019; Telfer et al., 2003) would be a valuable contribution to the knowledge of the morphological variation patterns of the locomotor skeleton during the postnatal growth, not only in water voles but also in rodents in general.



---

# CHAPTER 10

## GENERAL CONCLUSIONS





## CHAPTER 10. GENERAL CONCLUSIONS

---

1. The 3D models of limb long bones of water voles obtained with photogrammetric techniques are appropriate for landmark-based geometric morphometric analyses. Thus, photogrammetry can be considered an appropriate and affordable way to obtain 3D models of limb long bones of small mammals.
2. The patterns of shape variation of the mandible, the humerus and the femur that occur during the postnatal ontogeny are similar in fossorial (*Arvicola scherman*) and semiaquatic (*A. sapidus*) water voles. Both species also share the growth pattern of the cortex of limb long bones during postnatal ontogeny. These similarities are probably due to their close phylogenetic relationship.
3. Shape variations and differences in allometric and phenotypic trajectories of the mandible, the humerus and the femur, as well as differences in the histological characteristics of the long bones between *A. scherman* and *A. sapidus* are associated with their corresponding locomotion mode.
4. The main morphological differences between these species, especially in the mandible, and the humerus shapes are due to the fossorial locomotion of *A. scherman*. This is concordant with the fact that digging is biomechanically and energetically more demanding than swimming.
5. Form differences between *A. scherman* and *A. sapidus* associated with the locomotion mode already appear in the juvenile stage. However, these differences become more marked throughout growth.
6. The morphological features of the bones involved in burrowing observed in *A. scherman* are similar to those described for other fossorial mammals, namely scratch-diggers. However, these characteristics are less pronounced in the water vole species, what is concordant with the implication of these bones in the different digging modes.
7. The cortical thickness and modelling process observed in the humerus and the femur of *A. scherman* are similar to those described in other terrestrial mammals, regardless of the type of locomotion. In *A. sapidus* these microanatomical features seems to be related to swimming.
8. The external robustness of long bones in juvenile voles is probably a compensatory response to the thin cortical wall and the high intracortical porosity of the bone cortex to reduce the fracture risk during the initial efforts of locomotion.
9. Of all bones analysed, the humerus shows the most marked shape changes during postnatal ontogeny, coinciding with the preponderant role it plays in the digging activity. It follows that

## GENERAL CONCLUSIONS

functional pressure on a particular bone depends on its implication in the particular type of locomotion.

10. In *A. scherman* and *A. sapidus* the type of locomotion is an important modeler of the ontogenetic trajectories of the mandible, the humerus and the femur. This indicates that function has the potential to affect morphological evolution of these species by inducing changes in their respective growth patterns.

11. The combination of geometric morphometrics and histological analyses in the study of limb long bones provides a holistic view and contribute to a deeper understanding of their morphological variation during growth and the corresponding relationships between form and function.

---

# CHAPTER 11

REFERENCES



## CHAPTER 11. REFERENCES

---

- Adams, D. C., & Collyer, M. L. (2007). Analysis of character divergence along environmental gradients and other covariates. *Evolution*, *61*, 510–515.
- Adams, D. C., & Collyer, M. L. (2009). A general framework for the analysis of phenotypic trajectories in evolutionary studies. *Evolution*, *63*, 1143–1154.
- Adams, D. C., Collyer, M. L., Kaliontzopoulou, A., & Sherratt, E. (2017). Geomorph: Software for geometric morphometric analyses. R package version 3.0.5.
- Adams, D. C., & Otárola-Castillo, E. (2013). Geomorph: An R package for the collection and analysis of geometric morphometric shape data. *Methods in Ecology and Evolution*, *4*, 393–399.
- Adams, D. C., & Nistri, A. (2010). Ontogenetic convergence and evolution of foot morphology in European cave salamanders (Family: Plethodontidae). *BMC Evolutionary Biology*, *10*, 216.
- Airoidi, J. P. (1976). Le terrier de la forme fousseuse du campagnol terrestre (*Arvicola terrestris scherman* Shaw) (Mammalia, Rodentia). *Zeitschrift für Säugetierkunde*, *41*, 23–42.
- Airoidi, J. P. (1978). Etude par capture et recapture d'une population de Campagnols terrestres, *Arvicola terrestris scherman* Shaw (Mammalia, Rodentia). *Terre Vie*, *32*, 3–45.
- Airoidi, J. P., Altrocchi, R., & Meylan, A. (1976). Le comportement fousseur du campagnol terrestre, *Arvicola terrestris scherman* Shaw (Mammalia, Rodentia). *Revue Suisse Zoologie*, *83*, 282–286.
- Airoidi, J. P., & de Werra, D. (1993). The burrow system of the fossorial form of the water vole (*Arvicola terrestris scherman* Shaw) (Mammalia, Rodentia): An approach using graph theoretical methods and simulation models. *Mammalia*, *57*, 423–433.
- Álvarez, A., Perez, S.I., & Verzi, H. V. (2011). Ecological and phylogenetic influence on mandible shape variation of South American caviomorph rodents (Rodentia: Hystricomorpha). *Biological Journal of the Linnean Society*, *102*, 828–837.
- Amprino, R. (1947). La structure du tissu osseux envisagée comme expression des différences dans la vitesse de l'accroissement. *Archives de Biologie*, *58*, 315–330.
- Anderson, R. A., Mcbrayer, L. D., & Herrel, A. (2008). Bite force in vertebrates: Opportunities and caveats for use of a nonpareil whole-animal performance measure. *Biological Journal of the Linnean Society*, *93*, 709–720.
- Anderson, P. S., Renaud, S., & Rayfield, E. J. (2014). Adaptive plasticity in the mouse mandible. *BMC Evolutionary Biology*, *14*, 85.
- Anderson, M. J. & terBraak, C. J. F. (2003). Permutation tests for multi-factorial analysis of variance. *Journal of Statistical Computation and Simulation*, *73*, 85–113.
- Anemone, R. L., & Covert, H. H. (2000). New skeletal remains of *Omomys* (Primates, Omomyidae): Functional morphology of the hindlimb and locomotor behavior of a Middle Eocene primate. *Journal of Human Evolution*, *38*, 607–633.

## REFERENCES

- Argot, C. (2002). Functional-adaptive analysis of the hindlimb anatomy of extant marsupials and the paleobiology of the Paleocene marsupials *Mayulestes ferox* and *Pucadelphys andinus*. *Journal of Morphology*, 256, 76–108.
- Arias-Martorell, J., Potau, J. M., Bello-Hellegouarch, G., Pastor, J. F., & Pérez- Pérez, A. (2012). 3D geometric morphometric analysis of the proximal epiphysis of the hominoid humerus. *Journal of Anatomy*, 221, 394–405.
- Arístide, L., Soto, I.M., Mudry, M.D., & Nieves, M. (2014). Intra and Interspecific variation in cranial morphology on the southernmost distributed Cebus (Platyrrhini, Primates) species. *Journal of Mammalian Evolution*, 21, 349-355.
- Attanasio, C., Nord, A. S., Zhu, Y., et al. (2013). Fine tuning of craniofacial morphology by distant-acting enhancers. *Science*, 342, 6157.
- Bach-Gansmo, F. L., Irvine, S. C., Brüel, A., Thomsen, J. S., & Birkedal, H. (2013). Calcified cartilage islands in rat cortical bone. *Calcified Tissue International*, 92, 330-338.
- Bailey, R.C., & Byrnes, J. (1990). A new, old method for assessing measurement error in both univariate and multivariate morphometric studies. *Systematic Zoology*, 39, 124-130.
- Ball, A. D., Job, P. A., & Walker, A. E. L. (2017). SEM-microphotogrammetry, a new take on an old method for generating high-resolution 3D models from SEM images. *Journal of Microscopy*, 267, 214-226.
- Balmori-de la Puente, A., Ventura, J., Miñarro, M., Somoano, A., Hey, J. & Castresana, J. (2022). Divergence time estimation using ddRAD data and an isolation-with-migration model applied to water vole populations of *Arvicola*. *Scientific Reports*, 12, 4065.
- Barreto, G. R., & MacDonald, D. W. (2000). The decline and local extinction of a population of water voles, *Arvicola terrestris*, in southern England. *Zeitschrift Für Säugetierkunde*, 65, 110–120.
- Berendsen, A. D., & Olsen, B. R. (2015). Bone development. *Bone*, 80, 14–18.
- Bernard, J. (1961). A propos d'un croisement entre *Arvicola terrestris terrestris* L. et *A. t. scherman* Shaw. *Mammalia*, 25, 120–121.
- Biewener, A. A., & Patek, S. N. (2018). *Animal Locomotion* (2nd Eds). Oxford, England: Oxford University Press.
- Bookstein, F. L. (1991). *Morphometric tools for landmark data: Geometry and biology*. New York, NY: University Press.
- Borges, L. R., Maestri, R., Kubiak, B. B., Galiano, D., Fornel, R., & Freitas, T. R. O. (2017). The role of soil features in shaping the bite force and related skull and mandible morphology in the subterranean rodents of genus *Ctenomys* (Hystricognathi: Ctenomyidae). *Journal of Zoology*, 301, 108–117.
- Botton-Divet, L., Cornette, R., Fabre, A., Herrel, A., & Houssaye, A. (2016). Morphological analysis of long bones in semi-aquatic mustelids and their terrestrial relatives. *Integrative and*

- Comparative Biology*, 56, 1298–1309.
- Botton-Divet, L., Cornette, R., Houssaye, A., Fabre, A., & Herrel, A. (2017). Swimming and running: A study of the convergence in long bone morphology among semi-aquatic mustelids (Carnivora: Mustelidae). *Biological Journal of the Linnean Society*, 121, 38–49.
- Boulesteix, A., (2005). A note on between-group PCA. *International Journal of Pure and Applied Mathematics*, 19, 359–366.
- Bromage, T. G., Goldman, H. M., McFarlin, S. C., Warshaw, J., Boyde, A., & Riggs, C. M. (2003). Circularly polarized light standards for investigations of collagen fiber orientation in bone. *The Anatomical Record Part B The New Anatomist*, 274, 157–168.
- Brown, M. T., & Tinsley, H. E. A. (1983) Discriminant Analysis. *Journal of Leisure Research*, 15, 290–310.
- Burgin, C. J., Colella, J. P., Kahn, P. L. & Upham, N. S. (2018). How many species of mammals are there? *Journal of Mammalogy*, 99, 1–14.
- Buser, T. J., Sidlaukas, B. L., & Summers, A. P. (2017). 2D or Not 2D? Testing the utility of 2D vs. 3D landmark data in Geometric Morphometrics of the Sculpin Subfamily Oligocottinae (Pisces; Cottoidea). *The Anatomical Record*, 301, 806–818.
- Caeiro J., González P., & Guede D. (2013). Biomechanics and bone (& II): Trials in different hierarchical levels of bone and alternative tools for the determination of bone strength. *Revista de Osteoporosis y Metabolismo Mineral*, 5, 99–108.
- Calede, J. J., Samuels, J. X., & Chen, M. (2019). Locomotory adaptations in entoptychine gophers (Rodentia: Geomyidae) and the mosaic evolution of fossoriality. *Journal of Morphology*, 280, 879–907.
- Candela, A. M., & Picasso, B. J. (2008). Functional anatomy of the limbs of Erethizontidae (rodentia, caviomorpha): Indicators of locomotor behavior in Miocene porcupines. *Journal of Morphology*, 269, 552–593.
- Canoville, A. & Laurin, M. (2010). Evolution of humeral microanatomy and lifestyle in amniotes, and some comments on paleobiological inferences. *Biological Journal of the Linnean Society*, 100, 384–406.
- Cardini, A. (2014). Missing the third dimension in geometric morphometrics: How to assess if 2D images really are a good proxy for 3D structures? *Hystrix, the Italian Journal of Mammalogy*, 25, 73–81.
- Cardini, A. & Elton, S. (2007). Sample size and sampling error in geometric morphometric studies of size and shape. *Zoomorphology*, 126, 121–134.
- Cardini, A., O’Higgins, P. & Rohlf, F.J. (2019). Seeing distinct groups where there are none: Spurious patterns from between-group PCA. *Evolutionary Biology*, 46, 303–316.
- Cardini, A., & Polly, P. D. (2020). Cross-validated between group PCA scatterplots: A solution to



## REFERENCES

- spurious group separation? *Evolutionary Biology*, 47, 85-95.
- Cardini, A., & Tongiorgi, P. (2003). Yellow-bellied marmots (*Marmota flaviventris*) "in the shape space?" (Rodentia, Sciuridae): Sexual dimorphism, growth and allometry of the mandible. *Zoomorphology*, 122, 11-23.
- Carlson, K. (2005). Investigating the form-function interface in African apes: Relationships between principal moments of area and positional behaviors in femoral and humeral diaphyses. *American Journal of Physical Anthropology*, 127, 312-334.
- Carnelli, D., Vena, P., Dao, M., Ortiz, C., & Contro, R. (2013). Orientation and size dependent mechanical modulation within individual secondary osteons in cortical bone tissue. *Journal of The Royal Society Interface*, 10, 20120953.
- Carpenter, R. D. & Carter, D. R. (2008). The mechanobiological effects of periosteal surface load. *Biomechanics and Modeling in Mechanobiology*, 7, 227-242.
- Carrier, D. R. (1983). Postnatal ontogeny of the musculo-skeletal system in the black-tailed jack rabbit (*Lepus californicus*). *Journal of Zoology*, 201, 27-55.
- Casinos, A., Quintana, C., & Viladiu, C. (1993). Allometry and adaptation in the long bones of a digging group of rodents (Ctenomyiinae). *Zoological Journal of the Linnean Society*, 107, 107-115.
- Caskenette, D., Penuela, S., Lee, V., Barr, K., Beier, F., Laird, D. W., & Willmore, K. E. (2016). Global deletion of *Panx3* produces multiple phenotypic effects in mouse humeri and femora. *Journal of Anatomy*, 228, 746-756.
- Castanet, J., Cubo, J., & de Margerie, E. (2001). Signification de l'histodiversité osseuse: Le message de l'os. *Biosystema*, 19, 133-147.
- Caumul, R. & Polly, P. D. (2005). Phylogenetic and environmental components of morphological variation: Skull, mandible, and molar shape in marmots (*Marmota*, Rodentia). *Evolution*, 59, 2460-2472.
- Centeno-Cuadros, A., Delibes, M. & Godoy, J. A. (2009). Phylogeography of Southern water vole (*Arvicola sapidus*): Evidence for refugia within the Iberian glacial refugium? *Molecular Ecology*, 18, 3652-3667.
- Chevret, P., Renaud, S., Helvaci, Z., Ulrich, R. G., Quéré, J., & Michaux, J. R. (2020). Genetic structure, ecological versatility, and skull shape differentiation in *Arvicola* water voles (Rodentia, Cricetidae). *Journal of Zoology Systematics and Evolutionary Research*, 58, 1323-1334.
- Chiari, Y., Wang, B., Rushmeier, H., & Caccone, A. (2008). Using digital images to reconstruct three-dimensional biological forms: A new tool for morphological studies. *Biological Journal of the Linnaean Society*, 95, 425-436.
- Christiansen, P. (2012). The making of a monster: Postnatal ontogenetic changes in craniomandibular shape in the great Sabercat *Smilodon*. *PLoS One*, 7, 19-21.

- Collyer, M. L., & Adams, D. C. (2007). Analysis of two-state multivariate phenotypic change in ecological studies. *Ecology*, 88, 683–692.
- Collyer, M. L., & Adams, D. C. (2013). Phenotypic trajectory analysis: Comparison of shape change patterns in evolution and ecology. *Hystrix*, 24, 75–83.
- Collyer, M. L., & Adams, D. C. (2018). RRPP: An r package for fitting linear models to high-dimensional data using residual randomization. *Methods in Ecology and Evolution*, 9, 1772–1779.
- Collyer, M. L., Sekora, D. J., & Adams, D. C. (2015). A method for analysis of phenotypic change for phenotypes described by high-dimensional data. *Heredity*, 115, 357–365.
- Compston, J. E. (2001). Sex Steroids and Bone. *Physiological Reviews*, 81, 419–447.
- Cook, W.M., Timm, R.M., Hyman, D.E., 2001. Swimming ability in three Costa Rica dry forest rodents. *Revista de Biología Tropical*, 49, 1177–1181.
- Cornette, R., Baylac, M., Souter, T., & Herrel, A. (2013). Does shape covariation between the skull and the mandible have functional consequences? A 3D approach for a 3D problem. *Journal of Anatomy*, 223, 329–336.
- Cox, P. G. & Hautier, L. (2015). *Evolution of the rodents – Advances in phylogeny, functional morphology, and development*. Cambridge, England: Cambridge University Press.
- Cox, P. G., Rinderknecht, A., & Blanco, R. E. (2015). Predicting bite force and cranial biomechanics in the largest fossil rodent using finite element analysis. *Journal of Anatomy*, 226, 215–223.
- Crabtree, N., Loveridge, N., Parker, M., Rushton, N., Power, J., Bell, K. L., Beck, T. J., & Reeve, J. (2001). Intracapsular hip fracture and the region-specific loss of cortical bone: analysis by peripheral quantitative computed tomography. *Journal of Bone and Mineral Research*, 16, 1318–1328.
- Cubo J., Ponton F., Laurin M., de Margerie E., & Castanet J. (2005). Phylogenetic signal in bone microstructure of sauropsids, *Systematic Biology*, 54, 562–574.
- Cubo, J., Ventura, J., & Casinos, A. (2006). A heterochronic interpretation of the origin of digging adaptations in the northern water vole, *Arvicola terrestris* (Rodentia: Arvicolidae). *Biological Journal of the Linnean Society*, 87, 381–391.
- Currey J. (2002). *Bone, structure and mechanics*. Oxfordshire, England: Princeton University Press.
- Currey J., & Alexander R. (1985). The thickness of the walls of tubular bones. *Journal of Zoology*, 206, 453–468.
- Dagg, A. I., & Windsor, D. E. (1972). Swimming in northern terrestrial mammals. *Canadian Journal of Zoology*, 50, 117–130.
- Dawson D. L. (1980). Functional interpretations of the radiographic anatomy of the femora of *Myotis lucifugus*, *Pipistrellus subflavus*, and *Blarina brevicauda*. *American Journal of Anatomy*, 1980, 157, 1–15.
- de Margerie, E. (2002). Laminar bone as an adaptation to torsional loads in flapping flight. *Journal*

## REFERENCES

- of Anatomy*, 201, 521-526.
- de Margerie, E., Cubo, J., & Castanet, J., (2002). Bone typology and growth rate: Testing and quantifying 'Amprino's rule' in the mallard (*Anas platyrhynchos*). *Comptes Rendus Biologies*, 325, 221-230.
- de Margerie, E., Robin, J.-P., Verrier, D., Cubo, J., Groscolas, R., & Castanet, J. (2004). Assessing a relationship between bone microstructure and growth rate: A fluorescent labelling study in the king penguin chick (*Aptenodytes patagonicus*). *Journal of Experimental Biology*, 207, 869-879.
- de Margerie, E., Sanchez, S., Cubo, J., Castanet, J., (2005). Torsional resistance as a principal component of the structural design of long bones: Comparative multivariate evidence in birds. *The Anatomical Record Part A*, 282, 49-66.
- de Ricqlès, A. J. (1993). Some remarks on palaeohistology from a comparative evolutionary point of view. In G. Grupe, & A. N. Garland (Eds.), *Histology of Ancient Human Bone: Methods and Diagnosis*. Berlin: Springer.
- de Ricqlès, A. J. (2007). Fifty years after Enlow and Brown's comparative histological study of fossil and recent bone tissues (1956–1958): A review of Professor Donald H. Enlow's contribution to palaeohistology and comparative histology of bone. *Comptes Rendus Palevol*, 6, 591-601.
- de Ricqlès, A., & Buffrénil, V. (2001). Bone histology, heterochronies and the return of Tetrapods to life in water: Where are we? In J. Mazin, & V. Buffrénil (Eds.), *Secondary adaptation of Tetrapods to life in water* (pp 289-310). Verlag Dr Friedrich Pfeil.
- de Ricqlès, A., Meunier, F., Castanet, J., & Francillon-Vieillot, H. (1991). Comparative microstructure of bone. In: B. Hall (Ed.), *Bone - Volume 3: Bone Matrix and Bone Specific Products* (pp. 1–78). CRC Press.
- Demes, B., Jungers, W. L., & Selpien, K. (1991). Body size, locomotion, and long bone cross-sectional geometry in indriid primates. *American Journal of Physical Anthropology*, 86, 537-547.
- Dryden, I., & Mardia, K. V. (1998). *Statistical shape analysis*. Chichester, England: Wiley.
- Dunstone, N. (1979). Swimming and diving behavior of the mink (*Mustela vison* Schreber). *Carnivore*, 2, 56-61.
- Durão, A. F., Muñoz-Muñoz, F., Martínez-Vargas, J., & Ventura, J. (2018). Obtaining three-dimensional models of limb long bones from small mammals: A photogrammetric approach. In C. Rissech, L. Lloveras, J. Nadal, & J. M. Fullola (Eds.), *Geometric morphometrics. Trends in biology, paleobiology and archaeology* (pp. 125–138). Barcelona: SERP - Universitat Barcelona.
- Durão, A. F., Muñoz-Muñoz, F., & Ventura, J. (2020). Three-dimensional geometric morphometric analysis of the humerus: Comparative postweaning ontogeny between fossorial and semiaquatic water voles (*Arvicola*). *Journal of Morphology*, 281, 1679-1692.
- Durão A. F., Muñoz-Muñoz F. & Ventura J. (2022). Postnatal ontogeny of the femur in fossorial and semiaquatic water voles in the 3D-shape space. *The Anatomical Record*, 305, 1073-1086.

- Durão, A. F., Ventura, J., & Muñoz-Muñoz, F. (2019). Comparative post-weaning ontogeny of the mandible in fossorial and semiaquatic water voles. *Mammalian Biology*, 97, 95-103.
- Echeverría, A. I., Becerra, F., & Vassallo, I. (2014). Postnatal ontogeny of limb proportions and functional indices in the subterranean rodent *Ctenomys talarum* (Rodentia: Ctenomyidae). *Journal of Morphology*, 275, 902-913.
- Elissamburu, A., & de Santis, L. (2011). Forelimb proportions and fossorial adaptations in the scratch-digging rodent *Ctenomys* (Caviomorpha). *Journal of Mammalogy*, 92, 683-689.
- Elissamburu, A., & Vizcaíno, S. F. (2004). Limb proportions and adaptations in caviomorph rodents (Rodentia: Caviomorpha). *Journal of Zoology*, 262, 145-159.
- Enlow, D. H. (1962). A study of the post-natal growth and remodeling of bone. *American Journal of Anatomy*, 110, 79-101.
- Enlow, D. H. (1963). *Principles of bone remodeling: An account of post-natal growth and remodeling processes in long bones and the mandible*. Springfield, IL: Charles C. Thomas.
- Enlow, D. H. (1968). *The human face*. New York, NY: Harper and Row.
- Enomoto, A., Watahiki, J., Yamaguchi, T., Irie, T., Tachikawa, T., & Maki, K. (2010). Effects of mastication on mandibular growth evaluated by microcomputed tomography. *European Journal of Orthodontics*, 32, 66-70.
- EOS Systems Inc. (2015). Photomodeler Scanner. Version 2015.1.1. Vancouver: EOS Systems Inc.
- Esquerré, D., Sherratt, E., & Keogh, J. S. (2017). Evolution of extreme ontogenetic allometric diversity and heterochrony in pythons, a clade of giant and dwarf snakes. *Evolution*, 71, 2829-2844.
- Eulitz, M., & Reiss, G. (2015). 3D reconstruction of SEM images by use of optical photogrammetry software. *Journal of Structural Biology*, 191, 190-196.
- Evin, A., Horáček, I., & Hulva, P. (2011). Phenotypic diversification and island evolution of pipistrelle bats (*Pipistrellus pipistrellus* group) in the Mediterranean region inferred from geometric morphometrics and molecular phylogenetics. *Journal of Biogeography*, 38, 2091-2105.
- Evin, A., Souter, T., Hulme-Beaman, A., Ameen, C., Allen, R., Viacava, P., Larson, G., Cucchi, T., & Dobney, K. (2016). The use of close-range photogrammetry in zooarchaeology: Creating accurate 3D models of wolf crania to study dog domestication. *Journal of Archaeological Science: Reports*, 9, 87-93.
- Fadda, C., & Corti, M. (2001). Three-dimensional geometric morphometrics of *Arvicanthis*: Implications for systematics and taxonomy. *Journal of Zoological Systematics and Evolutionary Research*, 39, 235-245.
- Fadda, C., Faggiani, F., & Corti, M. (1997). A portable device for the three dimensional landmark collection of skeletal elements of small mammals. *Mammalia*, 61, 622-627.

## REFERENCES

- Falkingham, P. L. (2012). Acquisition of high resolution 3D models using free, open-source, photogrammetric software. *Palaeontologia Electronica*, 15, 1–15.
- Ferguson, V. L., Ayers, R. A., Bateman, T. A., & Simske, S. J. (2003). Bone development and age-related bone loss in male C57BL/6J mice. *Bone*, 33, 387–98.
- Fernandes, F. A., Fornel, R., Cordeiro-Estrela, P., & Freitas, T. R. O. (2009). Intra and interspecific skull variation in two sister species of the subterranean rodent genus *Ctenomys* (Rodentia, Ctenomyidae): Coupling geometric morphometrics and chromosomal polymorphism. *Zoological Journal of the Linnaean Society*, 155, 220-237.
- Fernández, M. E., Vassallo, A. I., & Zárata, M. (2000). Functional morphology and palaeobiology of the pliocene rodent *Actenomys* (Caviomorpha: Octodontidae): The evolution to a subterranean mode of life. *Biological Journal of the Linnean Society*, 71, 71–90.
- Ferretti, J. L., Cointry, G. R., Capozza, R. F., & Frost H. M. (2003). Bone mass, bone strength, muscle-bone interactions, osteopenias and osteoporoses. *Mechanisms of Ageing and Development*, 124, 269-79.
- Fish, F. E. (1993). Comparison of Swimming Kinematics between Terrestrial and Semiaquatic Opossums. *Journal of Mammalogy*, 74, 275–284.
- Fish, F. E. (2016). Secondary evolution of aquatic propulsion in higher vertebrates: Validation and prospect. *Integrative and Comparative Biology*, 56, 1285-1297.
- Fish, F. E., & Stein, B. R. (1991). Functional correlates of differences in bone density among terrestrial and aquatic genera in the family Mustelidae (Mammalia). *Zoomorphology*, 110, 339-345.
- Foote, J. (1913). The comparative histology of the femur. *Smithsonian Miscellaneous Collections*, 61, 1–9.
- Francillon-Vieillot, H., de Buffrénil, V., Castanet, J., Geraudie, J., Meunier, F. J., Sire, J. Y., Zylberberg, L., & de Ricqlès, A. (1990). Microstructure and mineralization of vertebrate skeletal tissues. In J. G. Carter (Eds.), *Skeletal biomineralization: Patterns, processes and evolutionary trends* (pp. 471–530.). New York, NY: Van Nostrand Reinhold.
- Frankino, W. A. (2005). Natural selection and developmental constraints in the evolution of allometries. *Science*, 307, 718–720.
- Freeman, P.W., Lemen, C.A., 2008. A simple morphological predictor of bite force in rodents. *Journal of Zoology*, 275, 418–422.
- Frost, H. M. (1987). Bone “mass” and the “mechanostat”: A proposal. *The Anatomical Record*, 219, 1-9.
- Frost, H. M. (2003). Bone’s Mechanostat: A 2003 Update, *The Anatomical Record Part A*, 275, 1081-1101.

- Fuchs, M., Geiger, M., Stange, M., & Sánchez-Villagra, M. R. (2015). Growth trajectories in the cave bear and its extant relatives: An examination of ontogenetic patterns in phylogeny. *BMC Evolutionary Biology*, 15, 1–10.
- Gajski, D., Solter, A., & Gašparovic, M., (2016). Applications of macro photogrammetry in Archaeology. *International Archives of the Photogrammetry, Remote Sensing and Spatial Information Sciences*, 41, 263-266.
- Gambaryan P. P. & Gasc J.-P. (1993). Adaptive properties of the musculoskeletal system in the mole-rat *Myospalax myospalax* (Mammalia, Rodentia): Cinefluorographical, anatomical, and bio-mechanical analyses of burrowing. *Zoologische Jahrbucher Anatomie*, 123, 363–401.
- García-Esponda, C. M., & Candela, A. M. (2016). Hindlimb musculature of the largest living rodent *Hydrochoerus hydrochaeris* (Caviomorpha): Adaptations to semiaquatic and terrestrial styles of life. *Journal of Morphology*, 277, 286–305.
- García-Martínez, R., Marín-Moratalla, N., Jordana, X. & Köhler, M. (2011). The ontogeny of bone growth in two species of dormice: Reconstructing life history traits. *Comptes Rendus Palevol*, 10, 489-498.
- García, G. J. M., & da Silva, J. K. L. (2006). Interspecific allometry of bone dimensions: A review of the theoretical models. *Physics of Life Reviews*, 3, 188–209.
- Garde, J. M. (1992). *Biología de la rata de agua Arvicola sapidus Miller, 1908 (Rodentia, Arvicolidae) en el sur de Navarra (España)*. Ph.D. thesis. Navarra: Universidad de Navarra.
- Garde, J. M., & Escala, M. C. (2000). The diet of the southern water vole, *Arvicola sapidus* in southern Navarra (Spain). *Folia Zoologica*, 49, 287-293.
- Garde, J., Escala, M. C., & Ventura, J. (1993). Determinación de la edad relativa en la rata de agua meridional, *Arvicolá sapidus* Miller, 1908 (Rodentia, Arvicolidae). *Doñana, Acta Vertebrata*, 20, 266–276.
- Gasser, J. A., & Kneissel, M. (2017). Bone Physiology and Biology. In S. Smith, A. Varela, & R. Samadfam (Eds.), *Bone toxicology - Molecular and integrative toxicology* (pp. 27-94). Cham, Switzerland: Springer.
- Gearty, W., McClain, C. R., & Payne, J. L. (2018). Energetic tradeoffs control the size distribution of aquatic mammals. *Proceedings of the National Academy of Sciences of the United States of America*, 115, 4194–4199.
- Gillis, G. B., & Blob, R. W. (2001). How muscles accommodate movement in different physical environments: Aquatic vs terrestrial locomotion in vertebrates. *Comparative Biochemistry and Physiology - Part A*, 131, 61–75.
- Gingerich, P. D. (2003). Land-to-sea transition in early whales: Evolution of Eocene Archaeoceti (Cetacea) in relation to skeletal proportions and locomotion of living semiaquatic mammals. *Paleobiology*, 29, 429–454.

## REFERENCES

- Giraudoux, P., Levret, A., Alfonso, E., Coeurdassier, M., & Couval, G. (2020). Numerical response of predators to large variations of grassland vole abundance and long-term community changes. *Ecology and Evolution*, 10, 14221-14246.
- Giraudoux, P., Delattre, P., Habert, M., Quéré, J. P., Deblay S., Defaut, R., Duhamel, R., Moissenet, M. F., Salvi, D., & Truchetet, D. (1997). Population dynamics of fossorial water vole (*Arvicola terrestris scherman*): A land use and landscape perspective. *Agriculture, Ecosystems & Environment*, 66, 47-60.
- Goldman H. M., McFarlin S. C., Cooper D. M. L. Thomas, C. D. L., & Clement, J. G. (2009) Ontogenetic patterning of cortical bone microstructure and geometry at the human mid-shaft femur. *The Anatomical Record*, 292, 48-64.
- Gomes-Rodrigues, H., Šumbera, R., & Hautier, L. (2016). Life in burrows channelled the morphological evolution of the skull in rodents: The case of African mole-rats (Bathyergidae, Rodentia). *Journal of Mammalian Evolution*, 23, 175-189.
- Goodall, C. (1991). Procrustes methods in the statistical analysis of shape. *Journal of the Royal Statistical Society*, 53, 285–339.
- Gosàlbez, J. (1987). Insectívors i rosegadors de Catalunya. Metodologia d'estudi i catàleg faunístic. Barcelona: Ketres.
- Gosman, J. H. (2012). Growth and development: morphology, mechanisms and abnormalities. In C. Crowder, & S. D. Stout (Eds.), *Bone histology: An anthropological perspective* (pp. 23-44). CRC Press.
- Gosman J. H, Hubbell Z. R., Shaw C. N., & Ryan T. M. (2013). Development of cortical bone geometry in the human femoral and tibial diaphysis. *The Anatomical Record*, 296, 774-87.
- Gould, F. D. H. (2014). To 3D or not to 3D, that is the question: Do 3D Surface analyses improve the ecomorphological power of the distal femur in placental mammals? *PLoS ONE*, 9, e91719.
- Gould, S. J. (1966). Allometry and size in ontogeny and phylogeny. *Biological Reviews*, 41, 587-640.
- Gray, J. A., Sherratt, E., Hutchinson, M. N., & Jones, M. E. H. (2019). Changes in ontogenetic patterns facilitate diversification in skull shape of Australian agamid lizards. *BMC Evolutionary Biology*, 19, 1–10.
- Haneberg, W. C. (2008). Using close range terrestrial digital photogrammetry for 3-D rock slope modeling and discontinuity mapping in the United States. *Bulletin of Engineering Geology and the Environment*, 67, 457-469.
- Hart, N. H., Nimphius, S., Rantalainen, T., Ireland, A., Sifrikas, A., & Newton, R. U. (2017). Mechanical basis of bone strength: Influence of bone material, bone structure and muscle action. *Journal of Musculoskeletal and Neuronal Interaction*, 17, 114–139.

- Hasset, B. R., Lewis-Bale, T. (2017). Comparison of 3D landmark and 3D dense cloud approaches to Hominin mandible morphometrics using structure-from-motion. *Archaeometry*, 59, 191-203.
- Heck, C. T., Varricchio, D. J., Gaudin, T. J., Woodward, H. N. & Horner, J.R. (2019) Ontogenetic changes in the long bone microstructure in the nine-banded armadillo (*Dasypus novemcinctus*). *PLoS One*, 14, e0215655.
- Hedrick, B. P., Dickson, B. V., Dumont, E. R. & Pierce, S. E. (2020). The evolutionary diversity of locomotor innovation in rodents is not linked to proximal limb morphology. *Scientific Reports*, 10, 717.
- Heffner, R. S., & Heffner, H. E. (1990). Vestigial hearing in a fossorial mammals, the pocket gopher (*Geomys bursarius*). *Hearing Research*, 46, 239–252.
- Herring, S. W. (2003). Ontogenetic integration of form and function. In B. K. Hall, W. M. Olson (Eds.), *Keywords and concepts in evolutionary developmental biology*. Cambridge: Harvard University Press.
- Hewitt, G.M. (1999). Post-glacial re-colonization of European biota. *Biological Journal of the Linnean Society*, 68, 87–112.
- Hildebrand, M. (1985). Digging of quadrupeds. In M. Hildebrand, D. M. Bramble, K. F. Liem, & D. B. Wake (Eds.), *Functional vertebrate morphology* (pp. 89–109). Cambridge: Belknap Press.
- Hildebrand, M. (1988). *Analysis of vertebrate structure*. New York, NY: Wiley.
- Hopkins, S. S. B., & Davis, E. B. (2009). Quantitative morphological proxies for fossoriality in small mammals. *Journal of Mammalogy*, 90, 1449–1460.
- Houssaye A. (2009). "Pachyostosis" in aquatic amniotes: A review. *Integrative Zoology*, 4, 325-340.
- Houssaye, A. & Botton-Divet, L. (2018). From land to water: Evolutionary changes in long bone microanatomy of otters (Mammalia: Mustelidae). *Biological Journal of the Linnean Society*, 125, 240–249.
- Houssaye, A., & Fish, F. E. (2016). Functional (secondary) adaptation to an aquatic life in vertebrates: An introduction to the symposium. *Integrative and Comparative Biology*, 56, 1266–1277.
- Houssaye A., Lindgren J., Pellegrini R., Lee A. H., Germain D., & Polcyn M. J. (2013). Microanatomical and histological features in the long bones of Mosasaurine mosasaurs (Reptilia, Squamata)-implications for aquatic adaptation and growth rates. *PLoS One*, 8, e76741.
- Houssaye, A., Sander, P. M., & Klein, N. (2016). Adaptive patterns in aquatic amniote bone microanatomy-more complex than previously thought. *Integrative and Comparative Biology*, 56, 1349-1369.
- Howell, A. B. (1930). *Aquatic mammals—Their adaptations to life in the water*. Springfield, IL: Charles C. Thomas.



## REFERENCES

- Ip V., Toth Z., Chibnall J., & McBride-Gagy S. (2016) Remnant woven bone and calcified cartilage in mouse bone: Differences between ages/sex and effects on bone strength. *PLoS ONE*, 11, e0166476.
- Jacobshagen, B. (1981). The limits of conventional techniques in anthropometry and the potential of alternative approaches. *Journal of Human Evolution*, 10, 633-637.
- Jepsen K. J., Silva M. J., Vashishth D., Guo X. E., & van der Meulen M. C. (2015). Establishing biomechanical mechanisms in mouse models: Practical guidelines for systematically evaluating phenotypic changes in the diaphyses of long bones. *Journal of Bone and Mineral Research*, 30, 951-66.
- Jolliffe, I. T. (1986). *Principal component analysis*. New York, NY: Springer.
- Jolliffe, I. (2005). Principal Component Analysis. In B. S. Everitt, & D. C. Howell (Eds.) *Encyclopedia of Statistics in Behavioral Science - Volume 3* (pp. 1580- 1584). Chichester: John Wiley & Sons, Ltd.
- Kamilari, M., Tryfonopoulos, G., Fraguedakis-Tsolis, S., & Chondropoulos, B. (2013). Geometric morphometrics on Greek house mouse populations (*Mus musculus domesticus*) with Robertsonian and all-acrocentric chromosomal arrangements. *Mammalian Biology*, 78, 241-250.
- Karantanis, N-E., Rychlik, L., Herrel, A. & Youlatos, D. (2017). Arboreal gaits in three sympatric rodents *Apodemus agrarius*, *Apodemus flavicollis* (Rodentia, Muridae) and *Myodes glareolus* (Rodentia, Cricetidae). *Mammalian Biology*, 83, 51–63.
- Katz, D., Friess, M. (2014). Technical note: 3D from standard digital photography of human crania - preliminary assessment. *American Journal of Physical Anthropology*, 154, 152-158.
- Keinan-Adamsky, K., Shinar, H., & Navon, G. (2005). The effect of detachment of the articular cartilage from its calcified zone on the cartilage microstructure, assessed by 2H-spectroscopic double quantum filtered MRI. *Journal of Orthopaedic Research*, 23, 109-17.
- Kesner, M. H. (1980). Functional morphology of the masticatory musculature of the rodents subfamily Microtinae. *Journal of Morphology*, 165, 205–222.
- Khosla, S., Oursler, M. J., & Monroe, D. G. (2012). Estrogen and the skeleton. *Trends in Endocrinology & Metabolism*, 23, 576-81.
- Kilbourne, B. M. (2017). Selective regimes and functional anatomy in the mustelid forelimb: Diversification toward specializations for climbing, digging, and swimming. *Ecology and Evolution*, 7, 8852–8863.
- Klingenberg, C. P. (1998). Heterochrony and allometry: The analysis of evolutionary change in ontogeny. *Biological Reviews*, 73, 79–123.
- Klingenberg, C. P. (2011). MorphoJ: An integrated software package for geometric morphometrics. *Molecular Ecology Resources*, 11, 353–357.

- Klingenberg, C. P. (2016). Size, shape, and form: Concepts of allometry in geometric morphometrics. *Development Genes and Evolution*, 226, 113-137.
- Klingenberg, C. P., Barluenga, M. & Meyer, A. (2002). Shape analysis of symmetric structures: Quantifying variation among individuals and asymmetry. *Evolution*, 56, 1909–1920.
- Klingenberg, C. P. & McIntyre, G. S. (1998). Geometric morphometrics of developmental instability: Analyzing patterns of fluctuating asymmetry with Procrustes methods. *Evolution*, 52, 1363-1375.
- Klingenberg, C. P., Mebus, K., Auffray, J. C. (2003). Developmental integration in a complex morphological structure: How distinct are the modules in the mouse mandible? *Evolution & Development*, 5, 522–531.
- Klingenberg, C. P. & Monteiro, L. R. (2005). Distances and directions in multidimensional shape spaces: Implications for morphometric applications. *Systematic Biology*, 54, 678-88.
- Kopp, R. (1993). *Étude de l'impact de la forme fouisseuse du Campagnol terrestre, Arvicola terrestris scherman (Shaw), sur la végétation d'une prairie*. Ph.D. thesis. Lausanne: Université de Lausanne.
- Kovarovic, K., Aiello, L. C., Cardini, A., & Lockwood, C. A. (2011). Discriminant function analyses in archaeology: are classification rates too good to be true? *Journal of Archaeological Science*, 38, 3006-3018.
- Kratochvíl, J. (1983). Variability of some criteria in *Arvicola terrestris* (Arvicolidae, Rodentia). *Acta scientiarum naturalium Academiae Scientiarum Bohemicae, Brno* 17, 1–40.
- Kratochvíl, J., & Grulich, I. (1961). On the distribution and habitat requirements in the water-vole *Arvicola terrestris*, in Czechoslovakia. *Zoologické Listy*, 10, 265-280.
- Kryštufek, B., Koren, T., Engelberger, S., Horváth, G. F., Purger, J. J., Arslan, A., Chişamera, G., Murariu, D., 2015. Fossorial morphotype does not make a species in water voles. *Mammalia*, 79, 293–303.
- Kuehn, A. L., Lee, A. H., Main, R. P., & Simons, E. L. R. (2019). The effects of growth rate and biomechanical loading on bone laminarity within the emu skeleton. *PeerJ*, 7, e7616.
- Laurin, M., Canoville, A., & Germain, D. (2011). Bone microanatomy and lifestyle: A descriptive approach. *Comptes Rendus Palevol*, 10, 381-402.
- Laurin, M., Girondot, M., & Loth, M.-M. (2004). The evolution of long bone microanatomy and lifestyle in lissamphibians. *Paleobiology*, 30, 589-613.
- Laville, E. (1989). Etude cinématique du fouissage chez *Arvicola terrestris scherman* (Rodentia, Arvicolidae). *Mammalia*, 53, 177–190.
- Laville, E. (1989b). Etude morphofonctionnelle comparative des structures osseuses impliquées dans le fouissage d'*Arvicola terrestris scherman* (Rodentia, Arvicolidae). *Canadian Journal of Zoology*, 68, 2437–2444.

## REFERENCES

- Laville, E., Casinos, A., Gasc, J. P., Renous, S., & Bou, J. (1989). Les mécanismes du fouissage chez *Arvicola terrestris* et *Spalax ehrenbergi*: Étude fonctionnelle et évolutive. *Anatomischer Anzeiger*, 169, 131–144.
- Lee, A. H. & O'Connor, P. M. (2013) Bone histology confirms determinate growth and small body size in the noasaurid theropod *Masiakasaurus knopfleri*. *Journal of Vertebrate Paleontology*, 33, 865-876.
- Legendre, L. J., & Botha-Brink, J. (2018). Digging the compromise: Investigating the link between limb bone histology and fossoriality in the aardvark (*Orycteropus afer*). *PeerJ*, 6, e5216.
- Lehmann, W. H. (1963). The forelimb architecture of some fossorial rodents. *Journal of Morphology*, 113, 59-76.
- Lessa, E. P., & Stein, B. R. (1992). Morphological constraints in the digging apparatus of pocket gophers (Mammalia: Geomyidae). *Biological Journal of the Linnean Society*, 47, 439-453.
- Lessa, E. P., Vassallo, A. I., Verzi, D. H., & Mora, M. S. (2008). Evolution of morphological adaptations for digging in living and extinct ctenomyid and octodontid rodents. *Biological Journal of the Linnean Society*, 95, 267-283.
- Lieberman, D. E., & Pearson, O. M. (2001). Trade-off between modeling and remodeling responses to loading in the mammalian limb. *Bulletin of the Museum of Comparative Zoology*, 156, 269–282.
- Maestri, R., Patterson, B. D., Fornel, R., Monteiro, L. R., & de Freitas, T. R. O., (2016). Diet, bite force and skull morphology in the generalist rodent morphotype. *Journal of Evolutionary Biology*, 29, 2191–2204.
- Maggiano, C. M. (2012). Making the mold: A microstructural perspective on bone modeling during growth and mechanical adaptation. In C. Crowder & D. D. Stout (Eds.), *Bone Histology: An Anthropological Perspective* (pp. 45-90). CRC Press.
- Mahmoudi, A., Maul, L. C., Khoshyar, M., Darvish, J., Aliabadian, M., & Kryštufek, B. (2020). Evolutionary history of water voles revisited: Confronting a new phylogenetic model from molecular data with the fossil record. *Mammalia*, 84, 171-184.
- Main R. P., & Biewener A. A. (2006). In vivo bone strain and ontogenetic growth patterns in relation to life-history strategies and performance in two vertebrate taxa: Goats and emu. *Physiological and Biochemical Zoology*, 79, 57-72.
- Mallison, H., & Wings, O. (2014). Photogrammetry in paleontology—A practical guide. *Journal of Paleontological Techniques*, 12, 1–31.
- Marcolini, F., Piras, P., Kotsakis, T., Claude, J., Michaux, J., Ventura, J., & Cubo, J. (2011). Phylogenetic signal and functional significance of incisor enamel microstructure in *Arvicola* (Rodentia, Arvicolinae). *Comptes Rendus Palevol*, 10, 479-487.

- Marcy, A. E., Hadly, E.A., Sherratt, E., Garland, K., & Weisbecker, V. (2016). Getting a head in hard soils: Convergent skull evolution and divergent allometric patterns explain shape variation in a highly diverse genus of pocket gophers (*Thomomys*). *BMC Evolutionary Biology*, 16, 207.
- Marelli C. A., & Simons E. L. (2014). Microstructure and cross-sectional shape of limb bones in Great Horned Owls and Red-tailed Hawks: How do these features relate to differences in flight and hunting behavior? *PLoS One*, 9, e106094.
- Martin T. J. (1993). Hormones in the coupling of bone resorption and formation. *Osteoporosis International*, 3, 121-125.
- Martin, R. B., (1991). Determinants of the mechanical properties of bones *Journal of Biomechanics*, 24, 79-88 [published erratum appears in 1992, *Journal of Biomechanics*, 25, 1251].
- Martin, R. B., Burr, D.B., & Sharkey, N.A. (1998). *Skeletal tissue mechanics*. New York, NY: Springer.
- Martínez-Abadías, N., Holmes, G., Pankratz, T., Wang, Y., Zhou, X., Jabs, E. W., & Richtsmeier, J. T. (2013). From shape to cells: Mouse models reveal mechanisms altering palate development in Apert syndrome. *Disease Models and Mechanisms*, 6, 768-779.
- Martinez-Maza, C., Montes, L., Lamrous, H., Ventura, J., & Cubo, J. (2012). Postnatal histomorphogenesis of the mandible in the house mouse. *Journal of Anatomy*, 220, 472-483.
- Martínez-Vargas, J., Muñoz-Muñoz, F., Martínez-Maza, C., Molinero, A., & Ventura, J. (2017). Postnatal mandible growth in wild and laboratory mice: Differences revealed from bone remodeling patterns and geometric morphometrics. *Journal of Morphology*, 278, 1058-1074.
- Marziali, S., Dionisio, G., 2017. Photogrammetry and macro photography. The experience of the MUSINT II Project in the 3D digitization of small archaeological artifacts. *Studies in Digital Heritage*, 1, 298-309.
- Mate, I., Barrull, J., Salicrú, M., Ruiz-Olmo, J., & Gosàlbez, J. (2013). Habitat selection by southern water vole (*Arvicola sapidus*) in riparian environments of Mediterranean mountain areas: A conservation tool for the species. *Acta Theriologica*, 58, 25-37.
- Mavropoulos, A., Ammann, P., Bresin, A., & Kiliaridis, S. (2005). Masticatory demands induce region-specific changes in mandibular bone density in growing rats. *The Angle Orthodontist*, 75, 625-630.
- Mavropoulos, A., Bresin, A., Kiliaridis, S. (2004). Morphometric analysis of the mandible in growing rats with different masticatory functional demands: Adaptation to an upper posterior bite block. *European Journal Oral Science*, 112, 259-266.
- McFarlin, S. C., Terranova, C. J., Zihlman, A. L., & Bromage, T. G. (2016). Primary bone microanatomy records developmental aspects of life history in catarrhine primates. *Journal of Human Evolution*, 92, 60-79.

## REFERENCES

- McGowan, C. P., & Collins, C. E. (2018). Why do mammals hop? Understanding the ecology, biomechanics and evolution of bipedal hopping. *Journal of Experimental Biology*, 221, jeb161661.
- McIntosh, A.F., & Cox, P. G. (2016a). The impact of digging on craniodental morphology and integration. *Journal of Evolutionary Biology*, 29, 2383-2394.
- McIntosh, A. F., Cox, P. G. (2016b). The impact of gape on the performance of the skull in chisel-tooth digging and scratch digging mole-rats (Rodentia: Bathyergidae). *Royal Society Open Science*, 3, 160568.
- Meier, P. S., Bickelmann, C., Scheyer, T. M., Koyabu, D., & Sánchez-Villagra, M. R. (2013). Evolution of bone compactness in extant and extinct moles (Talpidae): Exploring humeral microstructure in small fossorial mammals. *BMC Evolutionary Biology*, 13, 55.
- Menegaz, R.A., Ravosa, M.J., 2017. Ontogenetic and functional modularity in the rodent mandible. *Zoology*, 124, 61–72.
- Meylan, A. (1977). Fossorial forms of the water vole, *Arvicola terrestris* (L.), in Europe. *EPPO Bulletin*, 7, 209–221.
- Michaux, J., Chevret, P., Renaud, S., 2007. Morphological diversity of Old World rats and mice (Rodentia, Muridae) mandible in relation with phylogeny and adaptation. *Journal of Zoological Systematics Evolutionary Research*, 45, 263–279.
- Mitteroecker, P., & Bookstein, F. (2011). Linear discrimination, ordination, and the visualization of selection gradients in modern morphometrics. *Evolutionary Biology*, 38, 100–114.
- Mitteroecker, P., & Gunz, P. (2009). Advances in geometric morphometrics. *Evolutionary Biology*, 36, 235-247.
- Monteiro, L. (1999). Multivariate regression models and geometric morphometrics: The search for causal factors in the analysis of shape. *Systematic Biology*, 48, 192–199.
- Monteiro, L.R., Duarte, L.C., & dos Reis, S.F. (2003). Environmental correlates of geographical variation in skull and mandible shape of the punare rat *Thrichomys apereoides* (Rodentia: Echimyidae). *Journal of Zoology*, 261, 47-57.
- Montgomery, W. I. (1980). The use of arboreal runways by the woodland rodents, *Apodemus sylvaticus* (L.), *A. flavicollis* (Melchior) and *Clethrionomys glareolus* (Schreber). *Mammal Review*, 10, 189-195.
- Montoya-Sanhueza G., Bennett, N. C., Oosthuizen, M. K., Dengler-Crish, C. M., & Chinsamy A. (2020). Long bone histomorphogenesis of the naked mole-rat: Histodiversity and intraspecific variation. *Journal of Anatomy*, 238, 1259-1283.
- Montoya-Sanhueza, G., & Chinsamy, A. (2017) Long bone histology of the subterranean rodent *Bathyergus suillus* (Bathyergidae): Ontogenetic pattern of cortical bone thickening. *Journal of Anatomy*, 230, 203-233.

- Montoya-Sanhueza, G., & Chinsamy, A. (2018) Cortical bone adaptation and mineral mobilization in the subterranean mammal *Bathyergus suillus* (Rodentia: Bathyergidae): Effects of age and sex. *PeerJ*, 6, e4944.
- Montoya-Sanhueza, G., Wilson, L. A. B., & Chinsamy, A. (2019). Postnatal development of the largest subterranean mammal (*Bathyergus suillus*): Morphology, osteogenesis and modularity of the appendicular skeleton. *Developmental Dynamics*, 248, 1101-1128.
- Morel J. (1981) *Le campagnol terrestre, Arvicola terrestris (L.) en Suisse: Biologie et systématique (Mammalia, Rodentia)*. Ph.D. thesis. Lausanne: University of Lausanne.
- Morgan, C.C., Álvarez, A., 2013. The humerus of South American caviomorph rodents: Shape, function and size in a phylogenetic context. *Journal of Zoology*, 290, 107-116.
- Morgan, C. C., & Verzi, D. H. (2006) Morphological Diversity of the Humerus of the South American Subterranean Rodent *Ctenomys* (Rodentia, Ctenomyidae). *Journal of Mammalogy*, 87, 1252–1260.
- Morgan, C. C., Verzi, D. H., Olivares, A. I., Vieytes, E. C. (2017). Craniodental and forelimb specializations for digging in the South American subterranean rodent *Ctenomys* (Hystricomorpha, Ctenomyidae). *Mammalian Biology*, 87, 118-124.
- Moyano, S. R., & Giannini, N. P. (2017). Comparative cranial ontogeny of *Tapirus* (Mammalia: Perissodactyla: Tapiridae). *Journal of Anatomy*, 231, 665–682.
- Muñoz-Muñoz, F., Quinto-Sánchez, M., & González-José, R. (2016). Photogrammetry: A useful tool for three-dimensional morphometric analysis of small mammals. *Journal of Zoological Systematics and Evolutionary Research*, 54, 318-325.
- Musser, G. G., & Carleton, M. C. (2005). *Arvicola* Lacépède, 1799; *Arvicola amphibius* (Linnaeus, 1758); *Arvicola sapidus* Miller, 1908; *Arvicola scherman* (Shaw, 1801). In D. E. Wilson, & D. M. Reeder (Eds.), *Mammal species of the world. A taxonomic and geographic reference* (pp. 963–966). Baltimore, MA: Johns Hopkins University Press.
- Nakajima, Y., & Endo, H. (2013). Comparative humeral microanatomy of terrestrial, semiaquatic, and aquatic carnivores using micro-focus CT scan. *Mammal Study*, 38, 1-8.
- Narla, R. R., & Ott, S. M. (2018). Bones and the sex hormones. *Kidney International*, 94, 239-242.
- Navarro, N., & Maga, A. M. (2016). Does 3D phenotyping yield substantial insights in the genetics of the mouse mandible shape? *G3: Genes/Genome/Genetics*, 6, 1153–1163.
- Nevo, E. (1979). Adaptive convergence and divergence of subterranean mammals. *Annual Review of Ecology and Systematics*, 10, 269–308.
- Newell-Morris L. & Sirianni J. E. (1982). Parameters of bone growth in the fetal and infant macaque (*Macaca nemestrina*) humerus as documented by trichromatic bone labels. *Progress in clinical and biological research*, 101, 243-258.

## REFERENCES

- Nowak, R. M. (1999). *Walker's mammals of the world (Vol. 1, 6th ed.)*. Baltimore, MA: Johns Hopkins University Press.
- O'Higgins, P., & Jones, N. (1998). Facial growth in *Cercocebus torquatus*: An application of three-dimensional geometric morphometric techniques to the study of morphological variation. *Journal of Anatomy*, 193, 251-272.
- Ödman, A., Mavropoulos, A., & Kiliaridis, S. (2008). Do masticatory functional changes influence the mandibular morphology in adult rats. *Archives of Oral Biology*, 53, 1149-1154.
- Ord, T. J., & Summers, T. C. (2015) Repeated evolution and the impact of evolutionary history on adaptation. *BMC Ecology and Evolution*, 15,137.
- Palmer, A.R., & Strobeck, C. (1986). Fluctuating asymmetry: Measurement, analysis, patterns. *Annual Reviews in Ecology, Evolution and Systematics*, 17, 391-421.
- Panteleyev, P. A. (2001). *The water vole. Mode of species*. Moscow: Nauka.
- Pardiñas U. F. J., Myers P., León-Paniagua L., Ordóñez-Garza N., Cook J. A., Kryštufek B., Haslauer R., Bradley R. D., Shenbrot G. I. & J. L. Patton. (2017). Family Cricetidae (True Hamsters, Voles, Lemmings and New World Rats and Mice). In D. E. Wilson, T.E. Jr. Lacher, & Mittermeier R. A. (Eds.). *Handbook of the mammals of the world. Vol. 7. Rodents II* (pp. 204-535). Barcelona: Lynx Edicions.
- Parfitt, A. M. (1994). The two faces of growth: Benefits and risks to bone integrity. *Osteoporosis International*, 4, 382-398.
- Pearson, O. M., & Lieberman, D. E. (2004). The aging of Wolff's "law": Ontogeny and responses to mechanical loading in cortical bone. *American Journal of Physical Anthropology*, 39, 63-99.
- Pérez, M. J., Barquez, R. M., & Díaz, M. M. (2017). Morphology of the limbs in the semi-fossorial desert rodent species of *Tympanoctomys* (Octodontidae, Rodentia). *ZooKeys*, 710, 77-96.
- Perez, S. I., Diniz-Filho, J. A. F., Rohlf, F. J., & Dos Reis, S. F. (2009). Ecological and evolutionary factors in the morphological diversification of South American spiny rats. *Biological Journal of the Linnean Society*, 98, 646-660.
- Piertney, S. B., Stewart, W. A., Lambin, X., Telfer, S., Aars, J., & Dallas, J. F. (2005). Phylogeographic structure and postglacial evolutionary history of water voles (*Arvicola terrestris*) in the United Kingdom. *Molecular Ecology*, 14, 1435-1444.
- Polly, P. D. (2007). Limbs in mammalian evolution. In B. K. Hall (Ed.), *Fins into limbs—Evolution, development, and transformation* (pp. 245-283). Chicago, IL: The University of Chicago Press.
- Potapov, M. A., Nazarova, G. G., Muzyka, V. Y., Potapova, O. F., & Evsikov, V. I. (2012). Extrinsic and intrinsic factors of regulations of reproductive potential in the water vole (*Arvicola amphibius*) population from western Siberia. In A. Triunverí & D. Scalise (Eds.), *Rodents - Habitats, pathology and environmental impact* (pp. 23-41). New York, NY: Nova Science Publishers.

- Qin, L., Liu, W., Cao, H., & Xiao, G. (2020). Molecular mechanosensors in osteocytes. *Bone Research*, 8, 23.
- Quéré, J. P. (2009). Position systematique et éléments de la biologie du campagnol terrestre. In: P. Delattre, & P. Giraudoux (Eds.), *Le campagnol terrestre. Prévention et contrôle des populations* (pp. 27–30). Versailles: Éditions Quæ.
- Quéré, J., & Le Louarn, H. (2011). *Les rongeurs de France. Faunistique et biologie*. Versailles: Éditions Quæ.
- Quinto-Sánchez, M., Muñoz-Muñoz, F., Gomez-Valdes, J., et al., 2018. Developmental pathways inferred from modularity, morphological integration and fluctuating asymmetry patterns in the human face. *Scientific Reports*, 8, 963.
- R Development Core Team (2016). R: A language and environment for statistical computing. Version 3.5.1. Vienna: R Foundation for Statistical Computing Retrieved from [www.R-project.org](http://www.R-project.org)
- Reichstein, H. (1963). Beitrag zur systematischen Gliederung des Genus *Arvicola Lacépède* 1799. *Zeitschrift für Zoologische Systematik und Evolutionsforschung*, 1, 155–204.
- Reichstein, H. (1982). Gattung *Arvicola Lacépède* 1799 Schermäuse. In: J. Niethammer & F. Krapp (Eds.). *Handbuch der Säugetiere Europas Vol. 2/1* (pp. 209–252). Wiesbaden: Akademische Verlagsgesellschaft.
- Reig, S., Daniels, M. J., Macdonald, D. W. (2001). Craniometric differentiation within wild-living cats in Scotland using 3D morphometrics. *Journal of Zoology*, 253, 121-132.
- Renaud, S., Auffray, J.-C., & de la Porte, S. (2010). Epigenetic effects on the mouse mandible: Common features and discrepancies in remodeling due to muscular dystrophy and response to food consistency. *BMC Evolutionary Biology*, 10, 28.
- Renaud, S., Chevret, P. & Michaux, J. (2007), Morphological vs. molecular evolution: Ecology and phylogeny both shape the mandible of rodents. *Zoologica Scripta*, 36, 525-535.
- Rensberger, J. M., & Watabe, M. (2000). Fine structure of bone dinosaurs, birds and mammals. *Nature*, 406, 619-623.
- Rice, W. R. (1989). Analyzing tables of statistical tests. *Evolution*, 43, 223–225.
- Richtsmeier, J. T., Corner, B. D., Grausz, H. M., Cheverud, J. M., & Danahey, S. E. (1993). The role of postnatal growth pattern in the production of facial morphology. *Systematic Biology*, 42, 307–330.
- Rigaux, P., Vaslin, M., Noblet, J. F., Amori, G., & Palomo, L. J. (2008). *Arvicola sapidus*. The IUCN Red List of Threatened Species 2008. Retrieved from <https://www.iucnredlist.org/species/2150/9290712>



## REFERENCES

- Ritchie, R. O., Kinney, J. H. Kruzic, J. J. & Nalla, R. K. (2005). A fracture mechanics and mechanistic approach to the failure of cortical bone. *Fatigue & Fracture of Engineering Materials & Structures*, 28, 345-371.
- Robling, A. G., & Turner, C. H. (2009). Mechanical signaling for bone modeling and remodeling. *Critical Review in Eukaryotic Gene Expression*, 19, 319–338.
- Rodrigues, H.G., Šumbera, R., & Hautier, L. (2016). Life in burrows channelled the morphological evolution of the skull in rodents: The case of African mole-rats (Bathyergidae, Rodentia). *Journal of Mammalian Evolution*, 23, 175–189.
- Rodríguez, A., Urra, F., Jubete, F., Román, J., Revilla, E., & Palomares, F. (2020). Spatial segregation between red foxes (*Vulpes vulpes*), european wildcats (*Felis silvestris*) and domestic cats (*Felis catus*) in pastures in a livestock area of northern Spain. *Diversity*, 12, 268.
- Rohlf, F. J. (2010). TpsDig2: Digitize coordinates of landmarks and capture outlines. New York, NY: Department of Ecology and Evolution, <http://life.bio.sunysb.edu/morph/index.htm>
- Rohlf, F. J., & Slice, D. (1990). Extensions of the Procrustes method for the optimal superimposition of landmarks. *Systematic Zoology*, 39, 40–59.
- Rose, K. D., & Emry, R. J. (1983). Extraordinary fossorial adaptations in the Oligocene palaeonodons *Epoicotherium* and *Xenocranium* (Mammalia). *Journal of Morphology*, 175, 33–56.
- Sahd, L., Bennett, N. C., & Hotzé, S. H. (2019). Hind foot drumming: Morphological adaptations of the muscles and bones of the hind limb in three African mole-rat species. *Journal of Anatomy*, 235, 811–824.
- Salazar-Ciudad I. (2006). Developmental constraints vs. variational properties: How pattern formation can help to understand evolution and development. *Journal of Experimental Zoology Part B: Molecular and Developmental Evolution*, 306, 107-25.
- Salton, J. A., & Sargis, E. J. (2009). Evolutionary morphology of the tenrecoidea (Mammalia) hindlimb skeleton. *Journal of Morphology*, 270, 367-387.
- Samuels, J. X., & Valkenburgh, B. V. (2008). Skeletal indicators of locomotor adaptations in living and extinct rodents. *Journal of Morphology*, 269, 1387–1411.
- Samuels, J. X., & Valkenburgh, B. V. (2009). Craniodental adaptations for digging in extinct burrowing beavers. *Journal of Vertebrate Paleontology*, 29, 254–268.
- Samuels, J. X., Meachen, J. A., & Sakai, S. A. (2013). Postcranial morphology and the locomotor habits of living and extinct carnivorans. *Journal of Morphology*, 274, 121–146.
- Sanfelice, D., & Freitas, T. R. O. (2007). The ontogeny of shape disparity in three species of Otariids (Pinnipedia: Mammalia). *LAJAM*, 6, 139–154.

- Sanger, T. J., Norgard, E. A., Pletscher, L. S., Bevilacqua, M., Brooks, V. R., Sandell, L. J., & Cheverud, J. M. (2011). Developmental and genetic origins of murine long bone length variation. *Journal of Experimental Zoology. Part B, Molecular and Developmental Evolution*, 316, 146-161.
- Sans-Fuentes, M. A., Ventura, J., López-Fuster, M. J., & Corti, M. (2009). Morphological variation in house mice from the Robertsonian polymorphism area of Barcelona. *Biological Journal of the Linnaean Society*, 97, 555-570.
- Santori, R. T., Vieira, M.V., Rocha-Barbosa, O., Magnan-Neto, J.A., & Gobbi, N. (2008). Water absorption of the fur and swimming behavior of semiaquatic and terrestrial oryzomine rodents. *Journal of Mammalogy*, 89, 1152-1161.
- Sargis, E. J. (2002). Functional morphology of the hindlimb of Tupaiids (Mammalia, Scandentia) and its phylogenetic implications. *Journal of Morphology*, 254, 149-185.
- Satoh, K. (1997). Comparative functional morphology of mandibular forward movement during mastication of two murid rodents, *Apodemus speciosus* (Murinae) and *Clethrionomys rufocanus* (Arvicolinae). *Journal of Morphology*, 231, 131-141.
- Saucy, F. (1999). *Arvicola sapidus* Miller, 1908. In A. J. Mitchell-Jones, G. Amori, W. Bogdanowicz, B. Kryštufek, P. J. H. Reijnders, F. Spitzenberger, M. Stubbe, J. B. M. Thissen, V. Vohralík, & J. Zima (Eds.), *The atlas of European mammals* (pp. 220-221). London: T&AD Poyser Ltd.
- Saucy, F., & Schneider, B. (1998). Juvenile dispersal in the vole, *Arvicola terrestris*, during rainy nights: A preliminary report. *Bulletin de la Société Vaudoise des Sciences Naturelles*, 84, 33-345.
- Schmidt, A. & Fischer, M. S. (2011). The kinematic consequences of locomotion on sloped arboreal substrates in a generalized (*Rattus norvegicus*) and a specialized (*Sciurus vulgaris*) rodent. *Journal of Experimental Biology*, 214, 2544-59.
- Scott, N., Neubauer, S., Hublin, J. J., Gunz, P. (2014). A shared pattern of postnatal endocranial development in extant hominoids. *Evolutionary Biology*, 41, 572-594.
- Seeman E. (2009). Bone modeling and remodeling. *Critical Reviews™ in Eukaryotic Gene Expression*, 19, 219-33.
- Serrat, M. A., Lovejoy, C. O., & King, D. (2007). Age- and site specific decline in insulin-like growth factor-I receptor expression is correlated with differential growth plate activity in the mouse hindlimb. *The Anatomical Record: Advances in Integrative Anatomy and Evolutionary Biology*, 290, 375-381.
- Seymour, R. S., Withers, P. C., & Weathers, W. W. (1998). Energetics of burrowing, running, and free-living in the Namib Desert golden mole (*Eremitalpa namibensis*). *Journal of Zoology*, 244, 107-117.
- Sharir, A., Stern, T., Rot, C., Shahar, R., & Zelzer, E. (2011). Muscle force regulates bone shaping for optimal-bearing capacity during embryogenesis. *Development*, 138, 3247-3259.

## REFERENCES

- Sheets, H. D., & Zelditch, M. L. (2013). Studying ontogenetic trajectories using resampling methods and landmark data. *Hystrix*, 24, 67–73.
- Shipov A., Zaslansky P., Riesemeier H., Segev G., Atkins A., & Shahar R. (2013). Unremodeled endochondral bone is a major architectural component of the cortical bone of the rat (*Rattus norvegicus*). *Journal of Structural Biology*, 183, 132–40.
- Singh, I., Tonna, E., & Gandel, C. (1974) A comparative histological study of mammalian bone. *Journal of Morphology*, 144, 421-437.
- Smith, J. W. (1960) Collagen fibre patterns in mammalian bone. *Journal of Anatomy*, 94, 329-344.
- Smith, J. M., & Savage, R. J. G. (1956). Some locomotory adaptations in mammals. *Zoological Journal of the Linnean Society*, 42, 603–622.
- Sontag, W. (1986). Quantitative measurements of periosteal and cortical-endosteal bone formation and resorption in the midshaft of male rat femur. *Bone*, 7, 63–70.
- Sontag W. (1986b) Quantitative measurements of periosteal and cortical-endosteal bone formation and resorption in the midshaft of female rat femur. *Bone*, 7, 55–62.
- Sontag W. (1992) Age-dependent morphometric alterations in the distal femora of male and female rats. *Bone*, 13, 297–310.
- Sparacello, V. S., & Pearson, O. M. (2010). The importance of accounting for the area of the medullary cavity in cross-sectional geometry: A test based on the femoral midshaft. *American Journal of Physical Anthropology*, 143, 612-24.
- StatSoft. (2014). Statistica (data analysis software system). Version 12. Tulsa: StatSoft Inc.
- Stein, B. R. (1988). Morphology and allometry in several genera of semiaquatic rodents (*Ondatra*, *Nectomys*, and *Oryzomys*). *Journal of Mammalogy*, 69, 500-511.
- Stein, B. R. (1989). Bone density and adaptation in semiaquatic mammals. *Journal of Mammalogy*, 70, 467-476.
- Stein, B. R. (1993). Comparative hind limb morphology in Geomyine and Thomomyine pocket gophers. *Journal of Mammalogy*, 74, 86–94.
- Stein, B. R. (2000). Morphology of subterranean rodents. In E. A. Lacey, J. L. Patton, & G.N. Cameron (Eds.), *Life underground: The biology of subterranean mammals* (pp. 19–61). Chicago, IL: University of Chicago Press.
- Stewart, R. A., Jarrett, C., Scott, C., White, S. A., & McCafferty, D. J. (2019). Water vole (*Arvicola amphibius*) abundance in grassland habitats of Glasgow. *The Glasgow Naturalist*, 27, 10–19.
- Strachan, R., Moorhouse, T., & Gelling, M. (2011). *Water vole—Conservation handbook (3th ed.)*. Oxford: Wild Conservation Research Unit.
- Straehl, F. R., Scheyer, T. M., Forasiepi, A. M., MacPhee, R. D. & SánchezVillagra, M. R. (2013) Evolutionary patterns of bone histology and bone compactness in xenarthran mammal long bones. *PLoS One*, 8, e69275.

- Szalay, F. S., & Sargis, E. J. (2001). Model-based analysis of postcranial osteology of marsupials from the Palaeocene of Itaboraí (Brazil) and the phylogenetics and biogeography of Metatheria. *Geodiversitas*, 23, 139–302.
- Taberlet, P., Fumagalli, L., Wust-Saucy, A. G., & Cosson, J. F. (1998). Comparative phylogeography and postglacial colonization routes in Europe. *Molecular Ecology*, 7, 453–464.
- Takano-Yamamoto T. (2014). Osteocyte function under compressive mechanical force. *Japanese Dental Science Review*, 50, 29–39.
- Tanaka, E., Sano, R., Kawai, N., Langenbach, G. E. J., Brugman, P., Tanne, K., & van Eijden, T. M. G. J. (2007). Effect of food consistency on the degree of mineralization in the rat mandible. *Annals of Biomedical Engineering*, 35, 1617–1621.
- Taylor, M. E. (1976). The functional anatomy of the hindlimbs of some African Viverridae (Carnivora). *Journal of Morphology*, 148, 227–254.
- Telfer, S., Dallas, J. F., Aars, J., Piertney, S. B., Stewart, W. A., & Lambin, X. (2003). Demographic and genetic structure of fossorial water voles (*Arvicola terrestris*) on Scottish islands. *Journal of Zoology*, 259, 23–29.
- Thewissen, J. G. M., & Taylor, M. A. (2007). Aquatic adaptations in the limbs of amniotes. In B. K. Hall (Ed.), *Fins into limbs - Evolution, development, and transformation* (pp. 310–322). Chicago, IL: The University of Chicago Press.
- Thorington, R. W., & Santana, E. M. (2007). How to Make a Flying Squirrel: *Glaucomys* Anatomy in Phylogenetic Perspective. *Journal of Mammalogy*, 88, 882–896.
- Toledo, N., Bargo, M. S., & Vizcaíno, S. F. (2015). Muscular reconstruction and functional morphology of the hind limb of santacrucian (Early Miocene) sloths (Xenarthra, Folivora) of Patagonia. *The Anatomical Records*, 298, 842–864.
- Turner, C. H. (1998). Three rules for bone adaptation to mechanical stimuli. *Bone*, 23, 399–407.
- Turner, C. H. (2002). Biomechanics of bone: Determinants of skeletal fragility and bone quality. *Osteoporosis International*, 13, 97–104.
- Turner, R. T., Backup, P., Sherman, P. J., Hill, E., Evans, G. L., & Spelsberg, T. C. (1992) Mechanism of action of estrogen on intramembranous bone formation: Regulation of osteoblast differentiation and activity. *Endocrinology*, 131, 883–889.
- Turner, R. T., Colvard, D. S., & Spelsberg, T. C. (1990). Estrogen inhibition of periosteal bone formation in rat long bones: Down-regulation of gene expression for bone matrix proteins. *Endocrinology*, 127, 1346–1351.
- Uda, Y., Azab, E., Sun, N., Shi, C., & Pajević, P. D. (2017). Osteocyte Mechanobiology. *Current Osteoporosis Reports*, 15, 318–325.
- Urošević, A., Ljubisavljević, K., & Ivanović, A., 2013. Patterns of cranial ontogeny in lacertid lizards: Morphological and allometric disparity. *Journal of Evolutionary Biology*, 26, 399–415.

## REFERENCES

- Vassallo, A. I. (1998). Functional morphology, comparative behaviour, and adaptation in two sympatric subterranean rodents genus *Ctenomys* (Caviomorpha: Octodontidae). *Journal of Zoology*, 244, 415–427.
- Vassallo, A. I., Becerra, F., Echeverría, A. I. & Casinos, A. (2016). Ontogenetic integration between force production and force reception: A case study in *Ctenomys* (Rodentia: Caviomorpha). *Acta Zoologica (Stockholm)*, 97, 232–240.
- Ventura, J. (1988). *Contribución al conocimiento del género Arvicola Lacépède, 1799, en el nordeste de la Península Ibérica*. Ph.D. thesis. Barcelona: Universidad de Barcelona.
- Ventura, J. (1990). Datos biométricos sobre los huesos largos y la escapula de *Arvicola sapidus* Miller, 1908 (Rodentia, Arvicolidae). *Boletín de la Real Sociedad Española de Historia Natural (Sección Biológica)*, 86, 85–64.
- Ventura, J. (1992). Morphometric data on the scapula and limb long bones of *Arvicola terrestris* (Linnaeus, 1758) (Rodentia, Arvicolidae). *Revue Suisse Zoologie*, 99, 629–636.
- Ventura, J. (1993). Crecimiento relativo de *Arvicola terrestris monticola* (Rodentia, Arvicolidae). *Miscellania Zoológica*, 17, 237–248.
- Ventura, J. (2001). Characteristics of the southwestern water vole, *Arvicola sapidus* Miller, 1908. In P. A. Panteleyev (Ed.), *The water vole Arvicola terrestris. Mode of the species* (pp. 163–172). Moscow: Nuaka.
- Ventura, J. (2007). *Arvicola sapidus* Miller, 1908. Ficha Libro Rojo. In L. J. Palomo, J. Gisbert & J. C. Blanco (Eds.), *Atlas y Libro Rojo de los Mamíferos Terrestres de España* (pp. 405-407). Madrid: Dirección General para la Biodiversidad -SECEM-SECEMU.
- Ventura, J. (2007). *Arvicola terrestris* (Linnaeus, 1758). Rata topera. In L. J. Palomo, J. Gisbert & J. C. Blanco (Eds.), *Atlas y Libro Rojo de los Mamíferos Terrestres de España* (pp. 401-404), Madrid: Dirección General para la Biodiversidad -SECEM - SECEMU.
- Ventura, J., & Casado-Cruz, M. (2011). Post-weaning ontogeny of the mandible in fossorial water voles: Ecological and evolutionary implications. *Acta Zoologica*, 92, 12–20.
- Ventura, J., & Gosàlbez, J. (1992). Criterios para la determinación de la edad relativa en *Arvicola terrestris monticola* (Rodentia, Arvicolidae). *Miscel·lània Zoològica*, 16, 197-206.
- Verde Arregoitia L. D., Fisher, D. O., & Schweizer, M. (2017). Morphology captures diet and locomotor types in rodents. *Royal Society Open Science*, 4, 160957.
- Verzi, D. H., Álvarez, A., Olivares, A. I., Morgan, C. C. & Vassallo, A. I. (2010). Ontogenetic trajectories of key morphofunctional cranial traits in South American subterranean ctenomyid rodents. *Journal of Mammalogy*, 91, 1508–1516.
- Viscosi, V., & Cardini, A. (2011) Leaf Morphology, Taxonomy and Geometric Morphometrics: A Simplified Protocol for Beginners. *PLoS ONE* 6, e25630.

- Vleck, D. (1979). The energy cost of burrowing by the pocket gopher *Thomomys bottae*. *Physiological Zoology*, 52, 122–136.
- Voje, K. L., Hansen, T. F., Egset, C. K., Bolstad, G. H., & Pélabon, C. (2013). Allometric constraints and the evolution of allometry. *Evolution*, 68, 866–885.
- Walker, M. M., Louys, J., Herries, A. I. R., Gilbert, J. P. & Miszkiewicz, J. J. (2020) Humerus midshaft histology in a modern and fossil wombat. *Australian Mammalogy*, 43, 30-39.
- Wall, W. P. (1983) The correlation between high limb-bone density and aquatic habits in recent mammals. *Journal of Paleontology*, 57, 197-207.
- Warshaw, J. (2008) Comparative primate bone microstructure: Records of life history, function, and phylogeny. In E. Sargis, & M. Dagosto (Eds.), *Mammalian Evolutionary Morphology. A Tribute to Frederick S. Szalay. Vertebrate Paleobiology and Paleoanthropology Series* (pp. 385-424). Netherlands: Springer.
- Warshaw, J., Bromage, T. G., Terranova, C. J., & Enlow, D. H. (2017). Collagen fiber orientation in primate long bones. *The Anatomical Record*, 300, 1189-1207.
- Webb, P. W., & Blake, R. W. (1985). Swimming. In M. Hildebrand, D. M. Bramble, K. F. Liem, & D. B. Wake (Eds.), *Functional vertebrates morphology* (pp. 110–128). Cambridge: Harvard University Press.
- Weber, J. M., Aubry, S., Ferrari, N., Fischer, C., Lachat-Feller, N., Meia, J. S., & Meyer, S. (2002). Population changes of different predators during a water vole cycle in a central european mountainous habitat. *Ecography* 25, 95-101.
- White, C. R. (2005). The allometry of burrow geometry. *Journal of Zoology*, 265, 395–403.
- White, C. R., Matthews, P. G. D., & Seymour, R. S. (2006). Balancing the competing requirements of saltatorial and fossorial specialisation: Burrowing costs in the spinifex hopping mouse, *Notomys alexis*. *Journal of Experimental Biology*, 209, 2103–2113.
- Wilson, L. A. B. (2013). Geographic variation in the greater Japanese shrew-mole, *Urotrichus talpoides*: Combining morphological and chromosomal patterns. *Mammalian Biology*, 78, 267-275.
- Wilson, L. A. B. (2018). The evolution of ontogenetic allometric trajectories in mammalian domestication. *Evolution*, 72, 867–877.
- Wilson, L. A. B., & Geiger, M. (2015). Diversity and evolution of femoral variation in Ctenohystrica. In P. G. Cox & L. Hautier (Eds.), *Evolution of the rodents: Advances in phylogeny, functional morphology, and development* (pp. 510–538). Cambridge, MA: Cambridge University Press.
- Wilson, L. A. B., & Sánchez-Villagra, M. R. (2010). Diversity trends and their ontogenetic basis: An exploration of allometric disparity in rodents. *Proceedings of The Royal Society*, 277, 1227-1234.

## REFERENCES

- Wilson L. A. B., & Sánchez-Villagra, M. R. (2011) Evolution and phylogenetic signal of growth trajectories: The case of chelid turtles. *Journal of Experimental Zoology Part B: Molecular and Developmental Evolution*, 316, 50-60.
- Wölfer J., Aschenbach T., Michel J. & Nyakatura J. A. (2021) Mechanics of arboreal locomotion in Swinhoe's striped squirrels: A potential model for early Euarchontoglires. *Frontiers in Ecology and Evolution*, 9, 636039.
- Yamada, K., Kimmel, D. B. (1991). The effect of dietary consistency on bone mass and turnover in the growing rat mandible. *Archives of Oral Biology*, 36, 129-138.
- Yanagi, H., & Chikatsu, H. (2010). 3D Modelling of small objects using macro lens in digital very close range photogrammetry. *International Archives of Photogrammetry, Remote Sensing and Spatial Information Sciences*, 38, 617-622.
- Yazdi, F. T., & Adriaens, D. (2013). Cranial variation in *Meriones tristrami* (Rodentia: Muridae: Gerbillinae) and its morphological comparison with *Meriones persicus*, *Meriones vinogradovi* and *Meriones libycus*: A geometric morphometric study. *Journal of Zoological Systematics and Evolutionary Research*, 51, 239-251.
- Young, N. M. (2008). A comparison of the ontogeny of shape variation in the anthropoid scapula: Functional and phylogenetic signal. *American Journal of Physical Anthropology*, 136, 247-264.
- Young, J. W., Fernández, D., & Fleagle, J. G. (2010). Ontogeny of long bone geometry in capuchin monkeys (*Cebus albifrons* and *Cebus apella*): Implications for locomotor development and life history. *Biology Letters*, 6, 197-200.
- Zagorodniuk, I. V., 2001. Nomenclature and system of genus *Arvicola*. In P. A. Panteleyev (Ed.), *The water vole. Mode of the species* (pp. 174-192). Moscow: Nauka.
- Zelditch, M. L., Calamari, Z. T., & Swiderski, D. L. (2016). Disparate postnatal ontogenies do not add to the shape disparity of infants. *Evolutionary Biology*, 43, 188-207.
- Zelditch, M. L., Swiderski, D. L. & Sheets, H. D. (2012). *Geometric morphometrics for biologists* (2nd Eds.) (pp. 23-50). Elsevier.
- Zelditch, M. L., Swiderski, D. L., Sheets, H. D., & Fink, W. L. (2004). *Geometric Morphometrics for Biologists. A Primer*. San Diego: Elsevier Academic Press.
- Zoetis, T., Tassinari, M.S., Bagi, C., Walthall, K., & Hurtt, M. E. (2003). Species comparison of postnatal bone growth and development. *Birth Defects Research Part B: Developmental and Reproductive Toxicology*, 68, 86-110.

---

# APPENDIXES





## APPENDIXES

---

### APPENDIX 1

Specimens provisionally deposited in the collection of the Mammalian Biology Research Group of the Universitat Autònoma de Barcelona (UAB, Bellaterra, Spain):

*Arvicola scherman* - Age class 0, females: 83112706; 84052616. Age class 0, males: 84052602;84052614; 84082909. Age class 1, females: 83112628; 83112703; 84092902. Age class 1, males: 83072920; 83092719; 83092725; 83092727; 83102833. Age class 2, females: 83081012; 83081113; 83081117; 83092703; 83102804; 83102814; 83102827; 83102830; 84052708. Age class 2, males: 83072914; 83081114; 83081118; 83102806; 83102810; 83102822; 83102915; 83102920; 83112704; 83122324; 84063016. Age class 3, females: 83072827; 83072833; 83092706; 83112602; 83112605; 83112707; 84063020; 84082901; 84083003; 84083009. Age class 3, males: 83072804; 83081005; 83081008; 83092612; 83092613; 83092704; 83092707; 83112502; 83112720; 83122314; 84072807. Age class 4, females: 83122306; 83122308; 83122310; 83122321; 84072801; 84072804; 84072806; 84072901; 84072902; 84072909; 84073002. Age class 4, males: 83122323; 83122413; 83122414; 84012201; 84042801; 84042905; 84043001; 84043004; 84043008; 84072811. Age class 5, females: 83072704; 83072918; 83081004; 83081112; 83112603; 83112617; 84021210; 84042908; 84042909; 84042911; 84052701; 84052702; 84052704; 84052705; 84052711. Age class 5, males: 83072808; 83072834; 83092710; 83092717; 83112601; 84021207; 84042805; 84042904; 84042906; 84042912; 84042914; 84042917; 84092806.

*Arvicola sapidus* - Age class 0, males: 83051701; 84062308; 84062801. Age class 1, female: 83061101; 83091802; 84120701; 85071302. Age class 2, female: 83043002; 83101402; 83121901; 84011301; 84111101. Age class 2, male: 84041501; 84061502. Age class 3, female: 83101305; 84022103; 84031001; 84080401; 84120702. Age class 3, male: 83012306; 83043008; 83111601; 84022002; 84062203; 84062204; 84062309; 84071901; 84091401; 84091501. Age class 4, female: 83012303; 83022001; 83043007; 83101301; 83101303; 83101304; 84022102; 84031004; 84051201; 84051302; 84061601; 84091602. Age class 4, male: 83012302; 83031301; 83043003; 83121801; 84011501; 84022001; 84041301; 84041401; 84071701; 84071801; 84091502; 84091603. Age class 5, female: 83091801; 84011302; 84011405; 84061602. Age class 5, female: 83012305; 83041601; 83043001; 83043005; 83071201; 83091803; 84011402; 84011403; 84022101; 84030902; 84041402; 84111102.

Collection of the Museo de Ciencias of the Universidad de Navarra (UNAV, Pamplona, Spain):

## APPENDICES

***Arvicola sapidus*** - Age class 0, females: 168396; 168398; 168399; 168402. Age class 0, males: 168397; 168401. Age class 1, females: 168414; 168415. Age class 1, males: 168406; 168408; 168410; 168411; 168413; 168416. Age class 2, females: 168370; 168373; 168382; 168383; 168384; 168394. Age class 2, males: 168367; 168369; 168371; 168375; 168378; 168380; 168381; 168386; 168388.

## **APPENDIX 2**

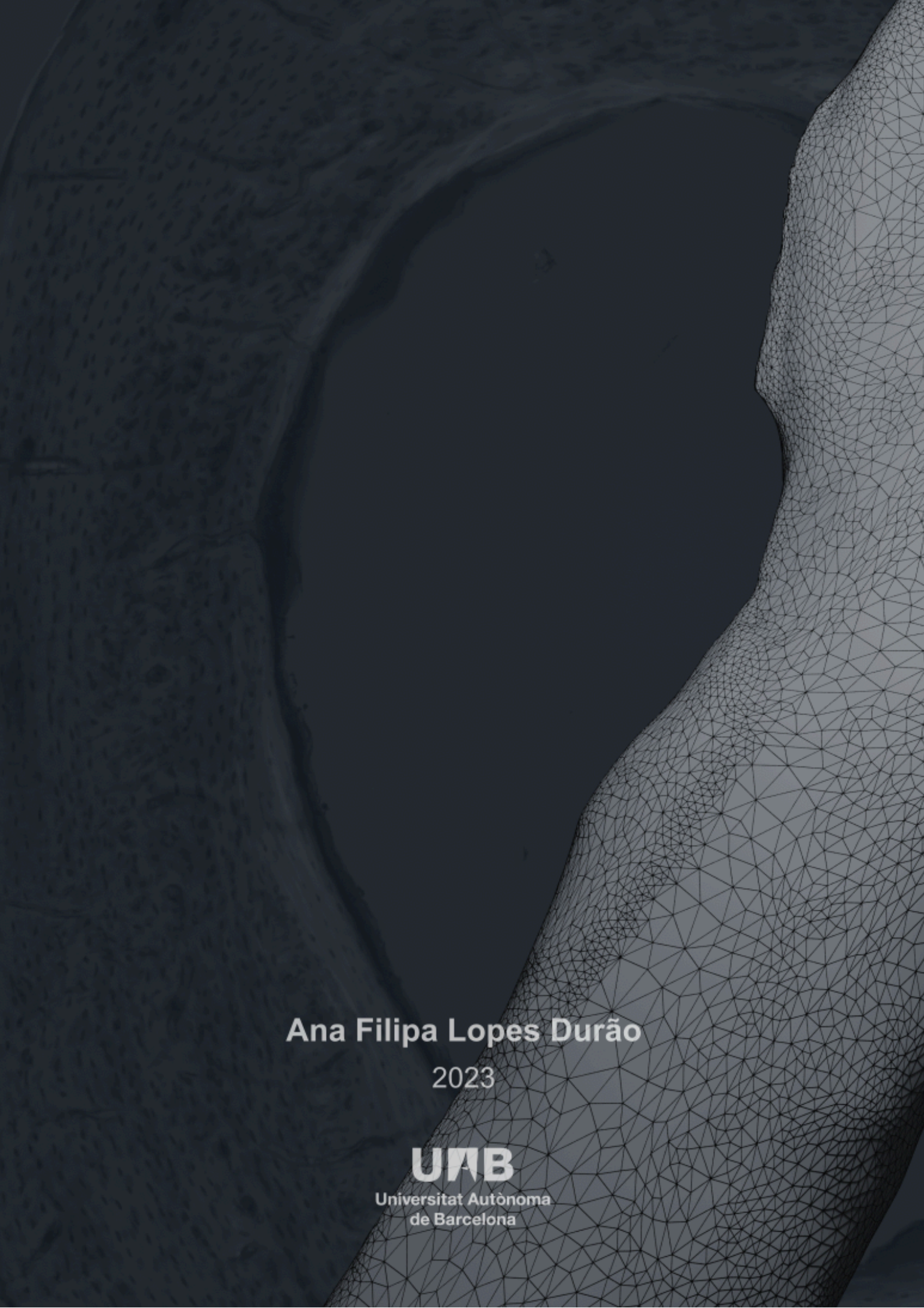
Specimens provisionally deposited in the collection of the Mammalian Biology Research Group of the Universitat Autònoma de Barcelona (UAB, Bellaterra, Spain):

***Arvicola scherman*** – Age class 0, females: 83112706; 84052709; Age class 0, males: 84052602; 84052614; 84082909; 84083113; Age class 1, female: 83081106; 83092620; 83112703; 84052617; 84092902; Age class 1, male: 83072920; 83092727; Age class 2, female: 83081009; 83081012; 83081113; 83081117; 83092703; 83092810; 83102814; 83102827; 83102830; 83112708; Age class 2, male: 83072914; 83081114; 83081118; 83102806; 83102810; 83102822; 83102915; 83102920; 83122324; 84052603; Age class 3, female: 83072827; 83072833; 83092706; 83092802; 83111602; 83112605; 83112707; 84063020; 84082901; 84083003; Age class 3, male: 83072804; 83081008; 83092612; 83092613; 83092704; 83092707; 83112502; 83112609; 83112616; 83122724; Age class 4, female: 83122306; 83122308; 83122310; 83122321; 84072801; 84072804; 84072901; 84072902; 84072909; 84072913; Age class 4, male: 83112709; 83122323; 83122413; 83122414; 84012201; 84042801; 84042905; 84043001; 84043004; 84043008. Age class 5, female: 83072918; 83081112; 83112603; 83112617; 84021210; 84042908; 84042909; 84042911; 84052701; 84052702. Age class 5, male: 83072704; 83072808; 83072834; 83081013; 83092709; 83092710; 83092717; 83112601; 84021207; 8404280.

***Arvicola sapidus*** – Age class 0, males: 84062308; 84062405; 84062702. Age class 1, female: 83061101; 83091802. Age class 2, female: 83121901; 84011301; 84111101. Age class 2, male: 84041501. Age class 3, female: 84022103; 84080401; 84120702. Age class 3, male: 83012306; 83043008; 83111601; 83111602; 84022002; 84032903; 84062203; 84062204; 84062309; 84062901. Age class 4, female: 83101301; 83101303; 84022102; 84031004; 84051201; 84051302; 84061601; 84091602; 84120801. Age class 4, male: 83012302; 83031301; 83043003; 84011501; 84022001; 84041401; 84091603; 84111002; 84120803. Age class 5, female: 83111701; 84011302; 84011405; 84061602. Age class 5, male: 83012305; 83041601; 83043001; 83043005; 83071201; 83081701; 83121801; 84030902; 84041302; 84111003; 84111102; 84120703.

Collection of the Museo de Ciencias of the Universidad de Navarra (UNAV, Pamplona, Spain):

***Arvicola sapidus*** – Age class 0, females: 168400; 168404. Age class 1, female: 168405; 168414; 168415; 168417; 168426; 168428; 168429; 168430. Age class 1, male: 168406; 168408; 168410; 168412; 168413; 168416; 168419; 168422; 168425; 168427. Age class 2, female: 168373; 168376; 168382; 168383; 168390; 168394. Age class 2, male: 168369; 168372; 168375; 168378; 168388; 168391; 168392



Ana Filipa Lopes Durão

2023

**UAB**

Universitat Autònoma  
de Barcelona